

Mixing in the Presence of Non-Monotonicity

Joseph Douglas Myers Hill

Supervisors:

Dr. Rob Sturman

Dr. Mark C. T. Wilson

Submitted in accordance with the requirements for the degree of:

Doctor of Philosophy



The University of Leeds

Centre for Doctoral Training in Fluid Dynamics

School of Computing

September 2022

To my parents, I hope you enjoy the pictures . . .

Intellectual Property

The candidate confirms that the work submitted is his own, except where work which has formed part of jointly authored publications has been included. The contribution of the candidate and the other authors to this work has been explicitly indicated below. The candidate confirms that appropriate credit has been given within the thesis where reference has been made to the work of others.

Parts of this thesis have appeared in two publications. Firstly *A family of non-monotonic toral mixing maps* (Myers Hill et al., 2022b) published in *Journal of Nonlinear Science*, secondly *Exponential mixing by orthogonal non-monotonic shears* (Myers Hill et al., 2022a) published in *Physica D: Nonlinear Phenomena*. For both publications the candidate was the first author, with R. Sturman and M.C.T. Wilson as co-authors. The candidate derived the analysis for each and wrote, submitted, and revised the manuscripts. The co-authors provided conceptualisation, supervision, and suggested edits. R. Sturman further contributed the introduction to Myers Hill et al. (2022b). Anonymous reviewers provided helpful feedback, improving the quality of the publications and by extension this thesis.

A breakdown of published material from this thesis is as follows. Analysis from section 3.5 appeared in Myers Hill et al. (2022b), as did sections 4.1, 4.2, and Appendix A. The supplementary material quoted throughout these sections is available on the publisher's website. Sections 4.3, 5.3.2, and 6.2 appeared in Myers Hill et al. (2022a).

This copy has been supplied on the understanding that it is copyright material and that no quotation from the thesis may be published without proper acknowledgement.

Acknowledgements

I thank my supervisors Rob and Mark for being so generous with their time, always providing valuable feedback, and encouraging me to develop my own research agenda. I particularly thank Rob for his guidance post PhD and support at conference, and Mark for imparting his fluids intuition and patience during the more technical detours.

I thank EPSRC for funding* and the Leeds Centre for Doctoral Training in Fluid Dynamics, for support throughout and the opportunity to pursue this PhD in the first place. My office mates in the CDT have made the last few years much more enjoyable, particularly my cohort: Greg, Imran, Jen, Josh, Michael, Molly.

I extend my thanks to friends outside of university, for climbs at the Lab and days out on the grit, giving welcome breaks from work. Finally I thank Glenis for her care and kindness, and my parents Monica and Don for support and encouragement throughout.

*Grant Reference EP/L01615X/1.

Abstract

Non-monotonic velocity profiles are an inherent feature of mixing flows obeying no-slip boundary conditions. Here we consider simple ‘stretching and folding’ models of laminar fluid mixing, composing orthogonal shears on the two dimensional torus, and study the effect of imposing non-monotonic, piecewise linear shears. We give conditions under which non-mixing regions (elliptic islands) emerge and the factors which determine their size. We further study examples where no islands form, proving (measure theoretic) mixing properties over open parameter windows.

Over the variety of systems considered, we encounter both uniformly and non-uniformly hyperbolic examples (with singularities). This is reflected in their mixing rates, exponential and polynomial respectively, which we establish using results from the chaotic billiards literature. We put these systems in the context of similar laminar mixing models, linked twist maps and a map of Cerbelli and Giona. Finally we consider a broader range of mixing protocols, rigorously comparing their efficiency, and discuss the challenges of relaxing piecewise linearity.

Contents

1	Background	1
1.1	Motivation	1
1.2	Modelling	2
1.3	Measure theory	2
1.4	Basic hyperbolic dynamics, ergodic theory	3
1.5	Proving mixing properties	9
2	Applications and Modern Advancements	11
2.1	Link to physical systems	11
2.2	Mixing properties of stretching and folding models	12
2.3	Establishing mixing rates	20
3	Mixing by Piecewise Linear Shears	24
3.1	Guide for the following chapters	24
3.2	Alternating shear maps framework	24
3.3	Visualisation of piecewise linear ASMs	26
3.4	Island structure analysis	27
3.5	Establishing hyperbolicity	31
4	Proving Mixing Results - Bounded Return Times	36
4.1	Mixing properties of H_η	36
4.1.1	Establishing ergodicity	36
4.1.2	Establishing the Bernoulli property	45
4.2	Mixing properties of H_ε	46
4.2.1	Establishing hyperbolicity	46
4.2.2	Establishing ergodicity	47
4.2.3	Establishing the Bernoulli property	53
4.2.4	Remarks	53
4.3	Mixing properties of $H_{(\xi,\eta)}$	53
4.3.1	Hyperbolicity of $H_{(\eta,\eta)}$	55
4.3.2	Ergodicity of $H_{(\eta,\eta)}$	55
4.3.3	Mixing properties of $H_{(\eta,\eta)}$	58
4.3.4	The full parameter space	59
4.4	Summary	63
5	Proving Mixing Results - Unbounded Return Times	66
5.1	Introduction	66
5.2	Mixing properties of non-monotonic LTMs	67
5.2.1	Map definition	67
5.2.2	Establishing non-uniform hyperbolicity	67

5.2.3	Establishing the Bernoulli property	69
5.2.4	Remarks	75
5.3	Mixing properties of the OTM	76
5.3.1	Introduction	76
5.3.2	Establishing non-uniform hyperbolicity	77
5.3.3	Nature of local manifolds	83
5.3.4	Growth lemma	83
5.3.5	Establishing the Bernoulli property	91
5.3.6	Remarks	92
6	Rates of Mixing	93
6.1	Introduction	93
6.2	Exponential mixing rates	95
6.3	Polynomial mixing rates	97
6.3.1	Bernoulli property	97
6.3.2	Invariant cones	100
6.3.3	Structure of the singularity set	101
6.3.4	One-step expansion	102
6.3.5	Decay of correlations	109
6.4	Summary	111
7	Wider Protocols, Summary & Outlook	112
7.1	Mixing protocols	112
7.1.1	Introduction	112
7.1.2	Ergodic properties	113
7.1.3	Bounds on Lyapunov exponents	114
7.1.4	Analysis of $E = 3$ protocols	115
7.1.5	Analysis of $E = 4$ protocols	118
7.1.6	Remarks	120
7.2	Summary & outlook	121
	Appendices	127
A	Bounds from the proof of Lemma 4.6	128
A.1	Establishing the lower bound $\mathcal{B}_1(\varepsilon)$	128
A.2	Expanding the expression for $\mathcal{B}_1(\varepsilon)$	131
A.3	$\mathcal{B}_1(\varepsilon)\mathcal{B}_2(\varepsilon)$ is monotone increasing	132
B	Mapping behaviour of a non-monotonic LTM	134
C	Two-step expansion calculations from section 6.3.4	135
C.1	Calculations for Proposition 6.3	135
C.2	Two-step expansion near P_1	135
	Bibliography	138

List of Tables

3.1	A collection of non-monotonic ASMs $H = G \circ F$	25
5.1	Minimum expansion factors $K_{\pm}(M) = \inf_{v \in \mathcal{C}_{\pm}} \ Mv\ /\ v\ $ for each $M \in \mathcal{M}$ over the cones \mathcal{C}_{\pm}	86
6.1	Possible values of the Jacobian DH_{σ} at z if $z \in \sigma_i$ (rows) and $z' = H_{\sigma}(z) \in \sigma_j$ (columns). Exponent k takes values in \mathbb{N} , dashes are shown if no transition is possible, e.g $H_{\sigma}(\sigma_1) \cap \sigma_2 = \emptyset$	101

List of Figures

1.1	Classical examples of viscous laminar flow between two infinitely long plates. Poiseuille flow is shown in (a), driven by a horizontal pressure gradient ∇p and restricted by no-slip boundary conditions at the plates. Couette flow is shown in (b), instead driven by one plate moving with velocity V , no pressure gradient.	2
1.2	Part of an orbit $f^n(x)$ near a hyperbolic fixed point at the origin.	4
1.3	Action of the cat map on the torus. Horizontal then vertical shears map the unit square to a parallelogram in $[0, 2] \times [0, 3]$, split into 4 regions by the lines $x, y \in \mathbb{Z}$. Modding out by 1 then places these regions onto the original square.	5
1.4	Mixing behaviour of the Cat Map on two initially regions. The orthogonal shears stretch out the regions into thin filaments which are then interwoven by the periodic boundaries. The eigenvectors v^u, v^s of the defining matrix M give the directions of expansion and contraction.	7
2.1	Mixing behaviour of the Sawtooth Map at parameter value $\alpha = 0.6$. The forward images of discontinuity line are plotted in the fifth frame, showing regions that have been ‘cut and placed’. The magnified section illustrates regions where this has aided mixing, aligning red next to blue, and others where it has not.	13
2.2	A linked twist map $H = G \circ F$ on the region $R = P \cup Q \subset \mathbb{T}^2$. The boundary ∂R is drawn in red, noting the periodic boundaries of \mathbb{T}^2	14
2.3	Mixing behaviour of the co-rotating piecewise linear linked twist map shown in Figure 2.2.	15
2.4	Mixing behaviour of a counter-rotating piecewise linear linked twist map over 2,4,6,24 iterates.	16
2.5	Cerbelli and Giona’s map toral map H : (a) map definition, (b) effect on a three element partition of the torus.	18
2.6	Mixing behaviour of Cerbelli and Giona’s map over 1,2,...5 iterates. Dashed arrows show the effect of H^2 on the red-blue interface in B , solid arrows show v^u in $A \cup B$ and $DH_0 v^u$ in C	18
3.1	(a) Orbits of a grid of points over 3000 iterates of H_η at $\eta = 2/5$. (b) FTLE field for the same map over a uniform grid of 1000×1000 points, 2000 iterates considered.	27
3.2	Mixing behaviour of H_η at $\eta = 2/5$ on two initially segregated regions coloured red and blue.	28
3.3	Approximate total island measure for H_η over $0.3 \leq \eta \leq 0.45$ using finite time Lyapunov exponents over 2000 iterates. An analytical lower bound $h(\eta)$ is shown as the solid line.	31
3.4	Illustration of a cone \mathcal{C} (shaded) with axis L and opening α . Similarly defined as the cone bounded by v_\pm containing some vector v parallel to L	32
3.5	Partition of the torus for H , establishing return times to A in $\{1, 2, 3\}$. Case illustrated $\eta = \frac{1}{4}$, the image of the partition is also shown with consistent shading.	34

4.1	A partition of the torus based on returns to \mathbf{a} under H^{-1} and its image under H^{-1} . Case illustrated $\eta = \frac{1}{4}$	37
4.2	Left: a partition of \mathbf{a} into three parts \mathbf{a}_i , where i is the return time of points in \mathbf{a}_i to \mathbf{a} . A line segment Γ is shown which has simple intersection with \mathbf{a}_3 and non-simple intersection with \mathbf{a}_2 . Right: the equivalent plot for A , considering return times under H^{-1}	39
4.3	Case (I). A quadrilateral $\mathcal{Q}_3 \subset \mathbf{a}_3$ and its image in \mathbf{a}_1 under H^5 . Any line segment Γ which joins the sloping boundaries of \mathbf{a}_3 will join the sloping boundaries of \mathcal{Q}_3 , and hence $H^5(\Gamma \cap \mathcal{Q}_3)$ is a v -segment.	41
4.4	Geometry of line segments satisfying case (II).	41
4.5	Case (II) for η either side of the critical value $\eta_0 = 1 - \frac{1}{\sqrt{2}}$	42
4.6	Two quadrilaterals $Q_2 \subset A_2$ and $Q_3 \subset A_3$ which map into A_1 under H^{-3} and H^{-5} respectively. Their long boundaries map into the sloping boundaries of A_1 , so segments Γ which join these long boundaries map into h -segments. Case illustrated $\eta = \frac{1}{4}$	43
4.7	Case (II) for $\eta > \eta_0$. Any Γ satisfying case (II) must intersect the A_1A_3 boundary on L and the A_2A_3 boundary on L^* . This gives a lower bound on x^* on the x -coordinate of this intersection so that if $x^* > x'$, then Γ joins the parallel sides of Q'_2	44
4.8	Two quadrilaterals Q^+, Q^- in A_1 which map into A_1 under H and H^{-1} respectively. Any v -segment must join the dotted sides of Q^+ , hence maps into another v -segment. Similar for h -segments and Q^-	45
4.9	Part (a) gives partition of A based on return time to A under iterations of H^{-1} . Part (b) shows a subdivision $A_4 \cup A_5 = A_2$, with the boundary between these sets defined as the segment joining the points Q_1, Q_2 . Case illustrated $\varepsilon = 0.05$	47
4.10	Left: Two regions $\mathfrak{D} \subset \mathfrak{b}$ and $D \subset B$, bounded by the piecewise linear curves ω, ζ and α, β respectively. Right: Their images in A_1 under H^{-4} and H^4 respectively, establishing h - and v -segments.	52
4.11	Shown behaviour of $H_{(\xi, \eta)}$ over the parameter space $0 < \xi, \eta < 1$	54
4.12	A partition of the torus into four rectangles R_j , and their images A_j under F_η^{-1} , A'_j under G_ξ . The smallest partition elements A_4 and A'_4 are left unlabelled. Case illustrated $\xi = \eta = 0.2$	54
4.13	Four pairs of line segments ja, jb on the boundaries of A_j , and their images ja', jb' under H on the boundaries of A'_j . A line segment Γ is shown which satisfies case (2). Its image $H(\Gamma) \subset A'_2$ connects $2a'$ to $2b'$, necessarily satisfying case (3).	58
4.14	Four pairs of line segments jA', jB' on the boundaries of A'_j , and their images jA, jB under H^{-1} on the boundaries of A_j	59
4.15	Diagram showing that if a segment Γ connects $3a'$ to $3b'$ through A'_3 , then $H(\Gamma)$ must satisfy case (2).	60
4.16	Plot of analytical results over \mathcal{P} . The curves c_1 and c_2 define \mathcal{P}' , c_3 defines $\mathcal{B} \subset \mathcal{P}'$, on which H is respectively hyperbolic, mixing. Note that c_3 meets c_2 at the point (η_1, η_1)	62
4.17	Left: a discretised parameter space \mathcal{P} . FTLE fields are calculated at each parameter value (pixel), coloured red in the case of elliptic islands, blue where the dynamics appear ergodic. The black lines highlight a strip where a key matrix is non-hyperbolic. Right: proven behaviour over \mathcal{P} in this chapter; islands (red), hyperbolicity (light blue), Bernoulli (blue). Notable maps on the periphery are also labelled.	64

5.1	A pair of orthogonal non-monotonic shears F (a) and G (b), parameterised by $0 < \beta < 1$ and $0 < \eta < 1 - \beta$, which act on the annuli P and Q respectively. Their composition leaves the complement R^c of $R = P \cup Q$ invariant.	67
5.2	A partition of S into four squares S_j . Each S_j are then partitioned based on return time to S under the map (a) F , (b) G , (c) F^{-1} , (d) G^{-1} . For sets with specific labels (e.g. A_j^k) the subscript j refers to the parent set S_j and the superscript k is the return time.	71
5.3	The upper section of S_1 with sets of constant return time A_1^k highlighted. The length L_6 shows the maximum height of a line segment satisfying case (A1.2) which does not traverse A_1^6 . The length h_7 is the minimum height of a line segment which traverses A_1^7 , defined using the cone boundary $\mathbf{v}^+ = (2 - \sqrt{3}, 1)^T$. The gradients in the magnified region have been altered to ease viewing.	73
5.4	Line segments l_j satisfying $H : l_1 \leftrightarrow l_2, l_3 \leftrightarrow l_4$. Each are periodic with period 2, their union is invariant under H	77
5.5	A partition of the torus into four rectangles S_j , and their preimages A_j, A'_j under F, G^{-1}	77
5.6	Left: Two subsets V (blue) and U_1 (red) of S_3 , each composed of two quadrilaterals. Right: The image $U_2 = \mathcal{H}(U_1 \cap V)$ in S_3 , the dashed lines show the boundary of V	79
5.7	Partitions of the return sets σ, σ' (white) for H, H^{-1} into four sets $\sigma_j \subset H(A_j), \sigma'_j \subset H^{-1}(A'_j)$	80
5.8	Part (a) shows the portions of σ (red, blue) with return time 1 to σ . Points in the white region have return times of 2 or more. Part (b) shows the singularity set \mathcal{S} for the return map H_σ . Red dashed lines denote the shared boundaries of the σ_j	81
5.9	Partitions of the region A_3 . Part (a) shows a partition into sets A^k where k is the escape time. Part (b) shows a subdivision into sets $A_{j,3}^k \subset A^k$ where j is such that $H^k(A_{j,3}^k) \subset A_j$. Red lines in each A^k are the preimages of the $A_1 A_2$ boundary under H^k	82
5.10	Part (a) shows the singularity curves dividing up $\sigma_1 \cup \sigma_3$ with some key partition elements labelled. The elements $A_{3,2}^1, A_4 \cap \sigma$ split $\sigma_1 \cup \sigma_3$ into six subsets $\sigma_{1a}, \dots, \sigma_{3b}$, any two of which are either disjoint or have intersection given by $A_4 \cap \sigma$ or one of the three subsets which make up $A_{3,2}^1$, see part (b). \mathcal{R} denotes the set $\sigma_{3a} \cap \sigma_{3b}$	84
5.11	The singularity set of H_σ over σ_{1a} . Unlabelled sets are given by $A_{4,2}^k$ for $k \geq 5$ which limit onto the point $(0, 1/4)$ in the obvious fashion. The dashed red line is $\partial P(\varepsilon)$, useful for establishing (KS1) for H_σ	85
5.12	The singularity set of H_σ over the lower part of σ_{1b} with the top portion of $A_4 \cap \sigma_1$ omitted. Unlabelled sets are given by $A_{4,3}^k$ for $k \geq 2$ which limit onto the point $(1/4, 1/2)$ in the obvious fashion. The segment \mathcal{P} is the preimage under H of the segment joining $(1/2, 3/4)$ to $(1, 1)$ in S_4 . The length L_0 denotes maximum height of any segment in σ_{1b} bounded by \mathcal{P} and $y = 1/2$	88
5.13	Behaviour of H_σ over $\sigma_{3b} \setminus \varsigma_3$ and H_σ^2 over ς_3 , shaded in blue.	90
5.14	Gray: lin-log and log-log plots of the estimated autocorrelation function $ C_n $ over $n = 1, \dots, 64$ iterates for the OTM. Red: rolling average over two elements.	92
6.1	Plot of analytical results over \mathcal{P} . The curves c_1 and c_2 define \mathcal{P}' , c_3 defines $\mathcal{B} \subset \mathcal{P}'$, c_3 and c_4 define $\mathcal{E} \subset \mathcal{B}$, on which H is respectively hyperbolic, mixing, and exhibits exponential decay of correlations.	96
6.2	The set σ' superimposed on σ , their intersection left white. A \mathfrak{h} -segment (red) and a \mathfrak{h}' -segment (blue) are plotted in \mathcal{R} and \mathcal{R}' respectively.	98

6.3	Left: The upper part $\Gamma_1 \subset A_1$ of a v -segment in $\sigma_3 \setminus (H(\sigma_2) \cap \sigma_3)$ and its images $F(\Gamma_1)$ (dashed), $H(\Gamma_1) \cap S_1$. Right: A right part $\Gamma_2 \subset A_1$ of $H(\Gamma_1)$ and its images $F(\Gamma_2)$, $H(\Gamma_2) \cap S_1$. This image necessarily contains a line segment Γ_3 traversing $A_{3,2}^1$.	99
6.4	Unstable and stable cone fields $\mathcal{C}_j, \mathcal{C}_j^s$ over the subsets $\sigma_j \subset \sigma$ for the return map H_σ . Also shown in red are the gradients of the line segments which make up the boundary $\partial\sigma$ which lie outside of all cone fields.	100
6.5	Part (a) shows an unstable curve W passing near to the accumulation point $(1/4, 1/2)$, split into W_\star below $y = 1/2$ and the collection $W_k \subset A_{4,3}^k$. Part (b) shows the image $U_k = H_\sigma(W_k) \subset H_\sigma(A_{4,3}^k)$, which for odd k lies near the accumulation point $(1/2, 3/4)$ and contains subcurves $U_{k,l} \subset A_{1,3}^l$.	104
7.1	Comparison of normalised Lyapunov exponents $\hat{\chi}$ for a selection of $E = 3$ protocols over the ergodic parameter space $0 < \eta < 1/5$. Crosses show numerically estimated $\hat{\chi}$, shaded region shows analytical upper and lower bounds. Order of protocols in the legend matches that of the plot.	117
7.2	Part (a) shows ranking of all $E = 4$ protocols into groups \mathcal{P}_p by (A), then further ranked by variance (B). Same colour signifies equivalent ranking, error bars show analytical bounds where available. Part (b) considers a tertiary ranking (C).	119
7.3	Plot of proven mixing behaviour over the full $0 \leq \xi, \eta \leq 1$ parameter space for $H_{(\xi, \eta)}$, i.e. including the limiting maps H_η and its symmetries. Notable maps are highlighted, alongside an atypical example marked with \times .	121
7.4	Three trajectories, one chaotic (black) and two elliptic (red, blue) for the map $H_{(\xi, \eta)}$ at $\xi = 0.286, \eta = 1/2$. Zoomed image shows a closeup on the ‘island’ centred at a period two point on the singularity set.	122
7.5	Comparison of mixing dynamics between (a) the OTM and (b) the PSM on two initially segregated regions coloured red and blue.	124
7.6	Convergence of FTLEs $\chi_n(z)$ for the PSM, iterates shown: $n = 2^2, \dots, 2^7$. Lighter colour corresponds to higher values of $\chi_n(z)$.	124
7.7	Shrinking of the region exhibiting low FTLEs. Noting the log-log scaling, the decay appears polynomial in nature.	125
7.8	Tail end of the (estimated) autocorrelations $ C_n $ for the PSM, same observable as Figure 5.14. Log-log scaling suggests a polynomial law.	125
A.1	A close-up on the lower portion of A_2 , $\varepsilon = 0.05$. Part (a) shows the lines which bound the regions A_4 and A_5 . Part (b) shows the curve (thickest line) across A_2 which minimises (4.10), crossing L_1 at Q_3 . Also shown is the segments S_4 which provides a lower bound for its diameter in A_4 . Segments S'_4 and S'_5 are defined to give further bound on (4.10) with minimal ε dependence.	129

Chapter 1

Background

1.1 Motivation

Mixing is a ubiquitous feature of fluid flows across all length scales, ranging from planetary atmospheres to small scale industrial processes. In this latter context, optimising the homogenisation of two initially segregated fluids for energy and time efficiency is a rich and expansive field of research. A traditional approach to mixing relies on turbulence and diffusion as the primary mechanisms. Consider two initially segregated fluids subject to a turbulent flow. As energy is transferred from the large scales to the small, small scale flow structures develop which rapidly interweave the two fluids. The boundary between the two fluids becomes progressively more intricate and is then smoothed by molecular diffusion, resulting in a homogeneous mixture. While effective, the high energy input required to maintain a high Reynolds number flow makes this an inefficient mixing strategy when considering small length scales or highly viscous fluids. In microfluidics, this approach is impractical. *Chaotic advection*, essentially stirring, aims to arrive at the same state of intricately interwoven fluid sheets by more direct means than simply relying on turbulence. It achieves this through a repetitive process of stretching and folding. The first step stretches fluid parcels into thin filaments, expanding in some direction u and contracting in some transverse direction u^\perp . The second step aligns these filaments next to each other and the process can begin once more. Repetition causes the thickness of each filament to shrink finer and finer until length scales are small enough for diffusion to dominate, smoothing the fluid interface to result in a homogeneous mixture. Chaotic advection dates back to the work of Aref (1984); for textbook references see Ottino (1989b) and Sturman et al. (2006). A review of more recent developments is found in Aref et al. (2017).

Factors such as the nature of the vessel surrounding the fluid and the particular stirring protocol employed can have a dramatic effect on mixing quality and the rate at which we approach homogeneity. Imposing no-slip boundary conditions on the walls bounding the fluid naturally gives rise to *non-monotonic* velocity profiles, characterised by zero motion at the boundaries and one or more peaks in flow over the fluid bulk. An example is sketched in Figure 1.1(a), showing viscous fluid forming a parabolic shaped profile when driven between two stationary plates by a pressure gradient. In contrast, Figure 1.1(b) shows the *monotonic* flow profile driven not by pressure, but by one of the plates moving horizontally with velocity V . Non-monotonic flow profiles lead to non-uniform stretching around the domain, in terms of both the magnitude and axes (i.e. directions) of stretching and contraction. This can potentially lead to an ‘unstirring’ effect where a parcel of fluid is stretched in some direction u , only to be transported to the other side of the domain where u is the direction of contraction and the stretch is undone. In many fluid mixing applications non-monotonic flow profiles are unavoidable. It is therefore desirable to understand the potential effects of non-monotonicity on mixing quality and mixing rates.

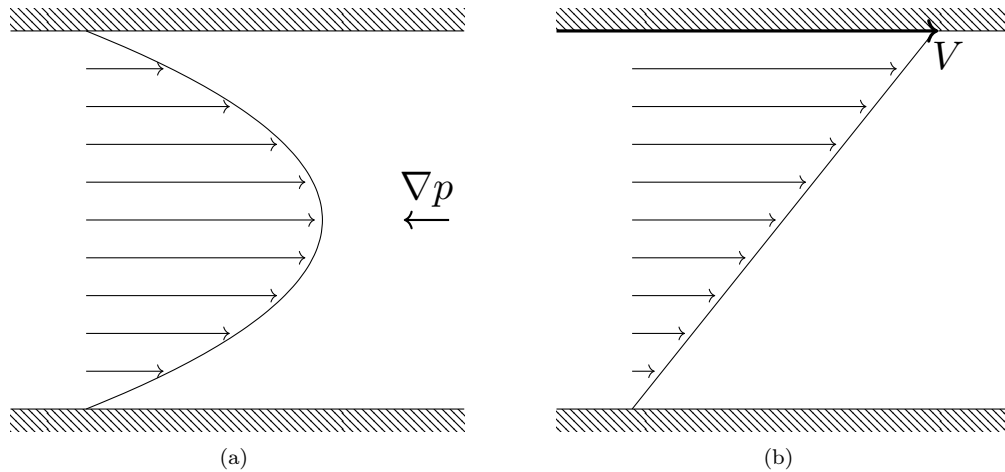


Figure 1.1: Classical examples of viscous laminar flow between two infinitely long plates. Poiseuille flow is shown in (a), driven by a horizontal pressure gradient ∇p and restricted by no-slip boundary conditions at the plates. Couette flow is shown in (b), instead driven by one plate moving with velocity V , no pressure gradient.

1.2 Modelling

Mixing in some domain X by chaotic advection concerns the study of time dependent fluid flows $\mathbf{v}(x, t)$, where $x \in X$ and $t \geq 0$. Typically we assume these flows to be time T periodic $\mathbf{v}(x, t+T) = \mathbf{v}(x, t)$ where T is the time taken to complete a single stretch and fold cycle or *stir*. This defines a map $f : X \rightarrow X$ which sends the initial position of a particle x to its position $f(x)$ after the stir, i.e. after being subjected to the flow for time T . The long term behaviour of the flow \mathbf{v} on X is then described by repeated iterations of the map f . These flows are referred to as *blinking flows* (see §1.5 of Sturman et al., 2006 for a variety of examples) and the maps $f : X \rightarrow X$ as *stroboscopic maps* (Cerbelli and Giona, 2005).

One can similarly arrive at a discrete time map f by relying on some spatial periodicity. For fluid moving through a cylindrical pipe (r, θ, z) with stirrers spaced periodically at $z = L, 2L, \dots$, we could take f to be the map taking the initial position of a particle $x = (r, \theta)$ on the cross-section $z = 0$ to its intersection with the next cross-section $z = L$ when subjected to the flow \mathbf{v} . Such a mapping is referred to as a *Poincaré map* which, in this example, reduces a three dimensional flow to a two dimensional mapping which encodes much (but not necessarily all) of the mixing dynamics. Studies of such systems can be found in Khakhar et al. (1987), Mezić et al. (1999).

The assumption that these flows are *incompressible*, $\nabla \cdot \mathbf{v} = 0$, tells us that f should preserve volume. That is, no fluid is created nor destroyed during a stir and the density of the fluid remains constant. Measure theory provides the mathematical framework for a rigorous study of volume and allows us to encode this assumption into the model.

1.3 Measure theory

We provide a basic introduction here, a more detailed treatment is provided in e.g. Halmos (1976).

Definition 1.1. Let X be a set. We say that a collection of subsets $\mathcal{A} \subset \mathcal{P}(X)$ is a σ -algebra if

1. $X \in \mathcal{A}$,
2. If $A \in \mathcal{A}$ then $X \setminus A \in \mathcal{A}$,
3. If (A_n) is a sequence of sets in \mathcal{A} then $\bigcup_{n \geq 1} A_n \in \mathcal{A}$.

To study the measures of length, area, volume etc. we consider X to be a metric space and consider the *Borel σ -algebra*, the smallest such σ -algebra which contains all open sets of X . We call the pair (X, \mathcal{A}) a *measurable space*.

Definition 1.2. A *measure* on (X, \mathcal{A}) is a mapping $\mu : \mathcal{A} \rightarrow [0, \infty]$ such that

1. $\mu(\emptyset) = 0$,
2. If (A_n) is a sequence of sets in \mathcal{A} with each $A_i \cap A_j = \emptyset$ for $i \neq j$, then $\mu\left(\bigcup_{n \geq 1} A_n\right) = \sum_{n \geq 1} \mu(A_n)$.

The triple (X, \mathcal{A}, μ) is called a *measure space*. In short $A \in \mathcal{A}$ are the subsets of X to which we can assign a measure $\mu(A)$. Throughout this thesis we will be concerned with *finite measures* $\mu(X) < \infty$, which we may normalise to $\mu(X) = 1$ to give a *probability space*. The broad definition of a measure allows for a wide range of ways to compare the size of sets. We are primarily concerned with the *Lebesgue measure* (see e.g. Halmos, 1976 for definition) which coincides with the traditional notions of length, area, volume. For example, letting ν, μ be the Lebesgue measures on \mathbb{R}, \mathbb{R}^2 , the measure of an interval $I = [a_1, a_2]$ is $\nu(I) = a_2 - a_1$ and the measure of rectangle $R = [a_1, a_2] \times [b_1, b_2]$ is $\mu(R) = (a_2 - a_1)(b_2 - b_1)$. We define *Lebesgue null sets* to be those $A \in \mathcal{A}$ with $\mu(A) = 0$. By the above we see that line segments $I \times \{0\}$ (taking $b_1 = b_2$) are Lebesgue null with respect to μ . One can show that the countable union of Lebesgue null sets also has measure 0. We say that a property holds for *almost every (a.e.)* $x \in X$ if it holds over some full measure set $X' \subset X$, i.e. with Lebesgue null complement $\mu(X \setminus X') = 0$. Generally we treat zero measure sets as negligible, proving results over a.e. $x \in X$. With the application of fluid mixing in mind, this assumption is reasonable as fluid parcels of negligible volume do not impact the global mixing statistics.

Definition 1.3. Let (X, \mathcal{A}, μ) be a measure space, $f : X \rightarrow X$. We say that f is *measure preserving* if $\mu(f(A)) = \mu(A)$ for all $A \in \mathcal{A}$.

Many reference texts will state this definition using preimages, $\mu(f^{-1}(A)) = \mu(A)$, as invertibility of the map f is not assumed. All maps considered in this thesis are invertible so we adopt the above definition. Given a measure space (X, \mathcal{A}, μ) and a self map $f : X \rightarrow X$ which preserves μ , we call the quadruple (X, \mathcal{A}, μ, f) a *measure preserving dynamical system*. We now have a correspondence

$$\text{The flow } \mathbf{v} \text{ is incompressible } (\nabla \cdot \mathbf{v} = 0) \quad \leftrightarrow \quad f : X \rightarrow X \text{ preserves the Lebesgue measure}$$

which directs our analysis. To understand the mixing dynamics of laminar incompressible flows \mathbf{v} on some domain X , we study the Lebesgue measure preserving dynamical system (X, \mathcal{A}, μ, f) . Ergodic theory describes the long term statistical behaviour of such systems.

1.4 Basic hyperbolic dynamics, ergodic theory

We provide a brief overview of classical ergodic theory here. A natural starting place is the following:

Definition 1.4. Let (X, \mathcal{A}, μ, f) be a measure preserving dynamical system, $\mu(X) = 1$. We say that f is *ergodic* if any invariant set $f(A) = A$ satisfies $\mu(A) = 0$ or $\mu(A) = 1$.

In ergodic systems, then, invariant sets are either negligibly small or large enough to be essentially indistinguishable from the whole domain. Intuitively, if our system is mixing we expect it to be ergodic, for if f admitted an invariant set A with $0 < \mu(A) < 1$ we could split the domain into

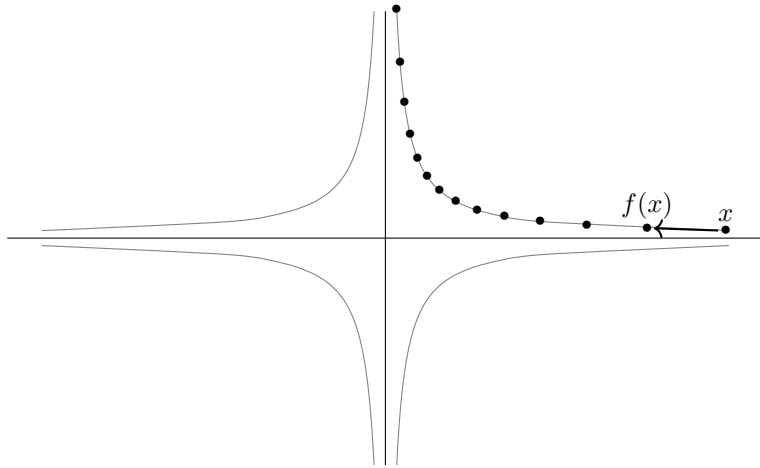


Figure 1.2: Part of an orbit $f^n(x)$ near a hyperbolic fixed point at the origin.

two invariant disjoint sets $A, X \setminus A$ which never mix and cannot be neglected as $\mu(A) < 1$ implies $\mu(X \setminus A) > 0$. Moreover, ergodicity implies another property we expect mixing systems to satisfy.

Definition 1.5. A dynamical system $f : X \rightarrow X$ on a metric space X is *topologically transitive* if for every pair of open sets $U, V \subset X$ there exists n such that $f^n(U) \cap V \neq \emptyset$.

Noting that all non-empty open sets have positive Lebesgue measure, topological transitivity implies that any non-negligible set U visits every region of the domain as we iterate f . Ergodicity, then, is a necessary condition for mixing behaviour, but it does not constitute a full definition.

Consider the following classical example. Let X be the unit circle $S^1 = [0, 1]$ with $0 \sim 1$. Let $f(x) = x + \alpha \pmod{1}$ where α is irrational, which preserves the induced Lebesgue measure μ on X . It is not too hard to show that f is ergodic (see e.g. Brin and Stuck, 2002) but it is certainly not mixing. Indeed if we segregate the domain into two, $X = X_1 \cup X_2 := [0, 1/2) \cup [1/2, 1)$, and iteratively apply f we see that the interface between the subsets does not become progressively more intricate, nor are the subsets interwoven. For f to be mixing, we should expect each subset to be spread ‘evenly’ around the domain, i.e. for positive measure sets $A, B \in \mathcal{A}$ we expect that the fraction of B which ends up in A approaches the proportion of A to the whole domain X . That is,

$$\frac{\mu(f^n(B) \cap A)}{\mu(B)} \rightarrow \frac{\mu(A)}{\mu(X)}.$$

Now for $\mu(X) = 1$,

Definition 1.6. We say that $f : X \rightarrow X$ is (*strong*) *mixing* if

$$\lim_{n \rightarrow \infty} \mu(f^n(B) \cap A) = \mu(A)\mu(B).$$

As mentioned in section 1.1, mixing by chaotic advection relies on an iterative *stretching* process, an idea we now make more precise. First we recall some basic dynamical systems terminology. Let X be a Riemannian manifold, assume (for now) that $f : X \rightarrow X$ is a diffeomorphism with Jacobian Df_x at $x \in X$. If f preserves the Lebesgue measure on X , necessarily this matrix has determinant 1. Given a point $x \in X$, we define its *orbit* as the bi-infinite sequence $\dots, f^{-n}(x), \dots, f^{-1}(x), x, f(x), \dots, f^n(x), \dots$. We say that x is periodic with period m if $\{f^n(x) \mid n \in \mathbb{Z}\}$ is finite with cardinality m . *Fixed points* are those $x \in X$ with $f(x) = x$, i.e. periodic with period 1. If at such an x the Jacobian Df_x has eigenvalues off the unit circle, we call it a *hyperbolic fixed point*.

A simple example is given by $f : \mathbb{R}^2 \rightarrow \mathbb{R}^2$, $f(x_1, x_2) = (x_1/\Lambda, \Lambda x_2)$ where $\Lambda > 1$ is a constant. It admits a single fixed point $p = (0, 0)$ on which the Jacobian has eigenvalues $\Lambda^{\pm 1}$. Part of an

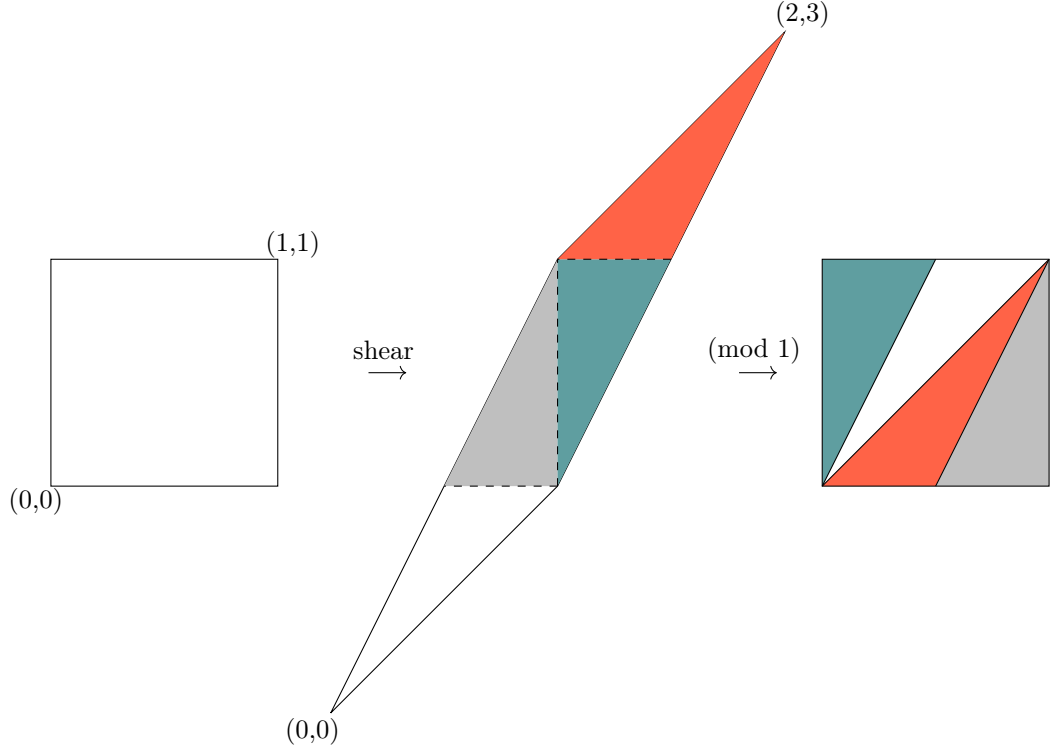


Figure 1.3: Action of the cat map on the torus. Horizontal then vertical shears map the unit square to a parallelogram in $[0, 2] \times [0, 3]$, split into 4 regions by the lines $x, y \in \mathbb{Z}$. Modding out by 1 then places these regions onto the original square.

orbit $f^n(x)$ near p is plotted in Figure 1.2. As time progresses, the point is drawn towards the x_2 -axis and repelled from the x_1 -axis, sketching out the hyperbola $x_1 x_2 = \text{const.}$ which passes through x . Note that the axes are invariant under f , with $Df = \begin{pmatrix} 1/\Lambda & 0 \\ 0 & \Lambda \end{pmatrix}$ expanding the x_2 -axis: $Df(0, 1)^T = (0, \Lambda)^T$ and contracting the x_1 -axis: $Df(1, 0)^T = (1/\Lambda, 0)^T$. Conversely in backwards time Df^{-1} contracts $(0, 1)^T$ and expands $(1, 0)^T$. We call these the *unstable and stable directions* respectively, which generate vector subspaces $E^u = \langle (0, 1)^T \rangle$, $E^s = \langle (1, 0)^T \rangle$. Note that the tangent space at p splits as $\mathcal{T}_p \mathbb{R}^2 = E^s \oplus E^u$; this trait defines (uniform) hyperbolicity beyond a single fixed point. Given an orbit $f^n(x)$, we define the associated *cocycle* as the product of Jacobians

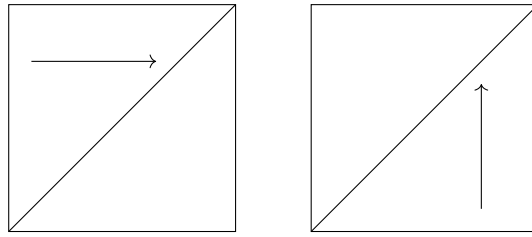
$$Df_x^n = Df_{f^{n-1}(x)} \cdot \dots \cdot Df_{f(x)} \cdot Df_x.$$

Definition 1.7 (Sturman et al., 2006). A diffeomorphism $f : M \rightarrow M$ of a compact Riemannian manifold M is *Anosov* if there exists constants $c > 0$, $0 < \lambda < 1$ and a continuous splitting of the tangent space $\mathcal{T}_x M = E_x^s \oplus E_x^u$ at each $x \in M$ such that

- $Df_x E_x^s = E_{f(x)}^s$,
- $Df_x E_x^u = E_{f(x)}^u$,
- $\|Df_x^n v\| \leq c \lambda^n \|v\|$ for $v \in E_x^s$,
- $\|Df_x^{-n} v\| \leq c \lambda^n \|v\|$ for $v \in E_x^u$.

The fact that the constants c, λ can be defined globally (i.e. independent of x) such systems are referred to as *uniformly hyperbolic*. A canonical example is the *Cat Map* (Arnol'd and Avez, 1968), which composes orthogonal shears on the two dimensional torus \mathbb{T}^2 , taken as the unit square $[0, 1]^2 \bmod 1$. Shearing provides a measure preserving mechanism for stretching out fluid parcels into thin filaments. The periodic boundaries of \mathbb{T}^2 then interweave these filaments, making this

a natural model of stretching and folding in a bounded domain. Parameterising \mathbb{T}^2 by $(x, y) \in (\mathbb{R}/\mathbb{Z})^2$, the map $H = G \circ F : \mathbb{T}^2 \rightarrow \mathbb{T}^2$ can be expressed pictorially as



or in matrix form as

$$\begin{pmatrix} x \\ y \end{pmatrix} \mapsto \underbrace{\begin{pmatrix} 1 & 0 \\ 1 & 1 \end{pmatrix}}_{DG} \underbrace{\begin{pmatrix} 1 & 1 \\ 0 & 1 \end{pmatrix}}_{DF} \begin{pmatrix} x \\ y \end{pmatrix} \pmod{1} = \underbrace{\begin{pmatrix} 1 & 1 \\ 1 & 2 \end{pmatrix}}_M \begin{pmatrix} x \\ y \end{pmatrix} \pmod{1},$$

where DF , DG denote the Jacobians of the maps F , G and $DH = M$. The action of H is shown in Figure 1.3. One can verify that the pair of shears together with the periodic boundaries gives an area preserving diffeomorphism on \mathbb{T}^2 . The fact that H can be defined using a single hyperbolic matrix M allows for straightforward proofs of its ergodic properties (see e.g., Brin and Stuck, 2002). Figure 1.4 gives a visualisation of its mixing behaviour, showing the forward images of two initially segregated regions over 4 iterates. Letting $\lambda = (3 - \sqrt{5})/2$, the matrix M has eigenvalues $\lambda^s = \lambda < 1$ and $\lambda^u = 1/\lambda > 1$ with corresponding eigenvectors v^s , v^u . As M contracts v^s and expands v^u we refer to these as the stable and unstable eigenvectors respectively. The vector subspaces generated by these eigenvectors give the splitting described in Definition 1.7, as M is constant the unstable and stable directions are the same at every point on the torus, as are the rates of stretching and contraction. This is reflected in the striation width of the red and blue strips of Figure 1.4, decaying like λ^n in the direction v^s . As we iterate H the laminate structure becomes finer and finer, spreading each region increasingly evenly around the domain, and the mixing property follows. The length of the interface between the two regions grows as λ^{-n} , starting initially parallel to $(0, 1)^T$ and tending towards v^u as we iteratively apply H .

While the regimented mixing resulting from uniform hyperbolicity may be desirable, it is far from realistic in physical laminar mixing systems where the rates and directions of stretching, contraction are typically non-uniform. Lyapunov exponents help us characterise more general hyperbolicity in these systems.

Definition 1.8. Given $f : X \rightarrow X$, the *Lyapunov exponent* $\chi(x, v)$ at the point $x \in X$ in the direction v is defined as

$$\chi(x, v) = \lim_{n \rightarrow \infty} \frac{1}{n} \log \|Df_x^n v\|.$$

Lyapunov exponents measure the average exponential rate of expansion over vectors $v \in \mathcal{T}_x X$ under the cocycle associated with the orbit $f^n(x)$.

Definition 1.9 (Chernov and Markarian, 2006). A point $x \in X$ is said to be *hyperbolic* if Lyapunov exponents exist at x and none of them equals 0.

A map $f : X \rightarrow X$ is said to be *hyperbolic* if almost every point $x \in X$ is hyperbolic.

Existence of Lyapunov exponents follows from Oseledets' theorem (Oseledets, 1968). Paraphrasing from Viana (2014), a general form in two dimensions is as follows. Let $\log^+(\cdot) = \max\{\log(\cdot), 0\}$ and write the operator norm as $\|\cdot\|_{\text{op}}$. For $p \geq 1$ denote by L^p the space of measurable functions $f : X \rightarrow \mathbb{R}$ such that $\|f\|_p = (\int |f|^p d\mu)^{1/p} < \infty$.

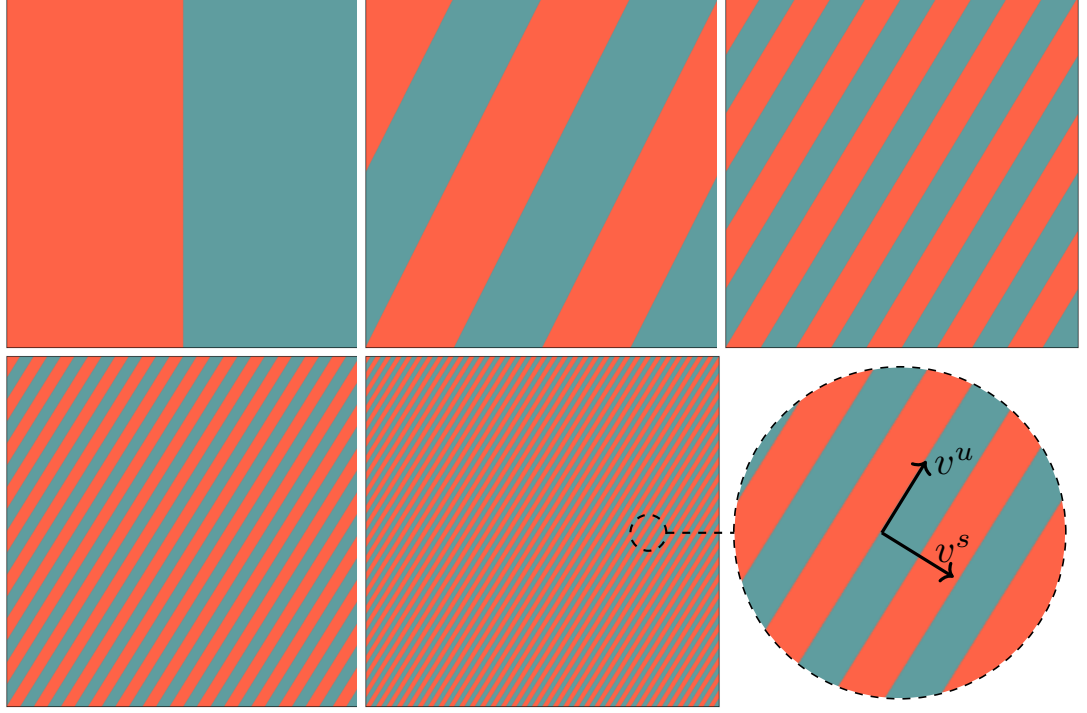


Figure 1.4: Mixing behaviour of the Cat Map on two initially regions. The orthogonal shears stretch out the regions into thin filaments which are then interwoven by the periodic boundaries. The eigenvectors v^u, v^s of the defining matrix M give the directions of expansion and contraction.

Theorem 1.1 (Oseledets, Viana). *Let $F : X \times \mathbb{R}^2 \rightarrow X \times \mathbb{R}^2$ be given by $F(x, v) = (f(x), A(x)v)$ for some μ -preserving map f on a 2-dimensional manifold X and some measurable function $A : X \rightarrow \text{GL}(2)$. Suppose $\log^+ \|A^{\pm 1}\|_{\text{op}} \in L^1$ and define*

$$\lambda_+(x) = \lim_{n \rightarrow \infty} \frac{1}{n} \log \|A^n(x)\|_{\text{op}}, \quad \lambda_-(x) = \lim_{n \rightarrow \infty} \frac{1}{n} \log \|(A^n(x))^{-1}\|_{\text{op}}^{-1},$$

where $A^n(x) = A(f^{n-1}(x)) \cdot \dots \cdot A(f(x)) \cdot A(x)$. Then for almost every $x \in X$,

1. either $\lambda_-(x) = \lambda_+(x)$ and

$$\lim_{n \rightarrow \infty} \frac{1}{n} \log \|A^n(x)v\| = \lambda_{\pm}(x) \quad \forall v \in \mathbb{R}^2 \setminus \{0\}$$

2. or $\lambda_+(x) > \lambda_-(x)$ and there exists a vector line $E_x^s \subset \mathbb{R}^2$ such that

$$\lim_{n \rightarrow \infty} \frac{1}{n} \log \|A^n(x)v\| = \begin{cases} \lambda_-(x) & \text{for } v \in E_x^s \setminus \{0\}, \\ \lambda_+(x) & \text{for } v \in \mathbb{R}^2 \setminus E_x^s. \end{cases}$$

Corollary 1.1. *Further assuming that A takes values in $\text{SL}(2)$ gives $\lambda_-(x) = -\lambda_+(x)$. Hence if at some x there exists $v_0 \in \mathbb{R}^2$ with $\lim_{n \rightarrow \infty} \frac{1}{n} \log \|A^n(x)v_0\| \neq 0$, then $\lim_{n \rightarrow \infty} \frac{1}{n} \log \|A^n(x)v\| \neq 0$ for all non-zero vectors v .*

Applying this corollary to the cocycle generated by derivatives Df_x gives an efficient scheme for establishing non-zero Lyapunov exponents. Let $A^n(x) = Df_x^n$, which takes values in $\text{SL}(2)$ when f preserves the Lebesgue measure. If there exists v_0 such that $\|Df_x^n v_0\|$ grows exponentially with n , Corollary 1.1 gives $\chi(z, v) \neq 0$ for all $v \neq 0$. Note that the choice of norm is unimportant here, norm independence of Definition 1.8 follows from equivalence of norms on finite dimensional vectors spaces and the fact that $\frac{1}{n} \log c \rightarrow 0$ for any constant $c > 0$. Similarly the magnitude of

the starting vector v is unimportant: $\chi(x, cv) = \chi(x, v)$ for any $c \neq 0$.

For the Cat Map, it is straightforward to show (see e.g. Sturman et al., 2006) that Lyapunov exponents are non-zero everywhere and are given by

$$\chi(x, v) = \begin{cases} \log \lambda^s & \text{for } v \in \langle v_s \rangle \setminus \{0\}, \\ \log \lambda^u & \text{for } v \in \mathbb{R}^2 \setminus \langle v_s \rangle. \end{cases}$$

The rest of this chapter describes conditions under which hyperbolic systems are ergodic and mixing. First, though, we conclude this section with some defining features of ergodic and mixing systems. Define *observables* as measurable functions $\varphi : X \rightarrow \mathbb{R}$. With fluid mixing applications in mind these could represent measurements such as temperature or concentration, but we keep their definition more general. Studying the effect of f on φ , i.e. comparing the measurements $\varphi \circ f^n$ and φ , gives an alternate functional framework for understanding the mixing dynamics of f . We call an observable φ *essentially invariant* if $\varphi \circ f = \varphi$ almost everywhere.

Proposition 1.1. *The following are equivalent:*

- (1) (X, \mathcal{A}, μ, f) is ergodic.
- (2) Every essentially invariant observable is constant.
- (3) For each $\varphi \in L^1$ and a.e. $x \in X$,

$$\hat{\varphi}(x) = \lim_{n \rightarrow \infty} \frac{1}{n} \sum_{k=0}^{n-1} \varphi(f^k(x)) = \int \varphi d\mu. \quad (1.1)$$

- (4) For all $A, B \in \mathcal{A}$,

$$\lim_{n \rightarrow \infty} \frac{1}{n} \sum_{k=0}^{n-1} \mu(f^k(B) \cap A) = \mu(A)\mu(B).$$

Proofs of the above are standard, found in e.g. Petersen (1983), Brin and Stuck (2002). Each can be taken as definitions of ergodicity and can potentially offer a more efficient path to establishing the property, for example the functional approach of (2) may be easier than dealing with measurable sets. Property (3) follows from the Birkhoff ergodic theorem (see Brin and Stuck, 2002) and states that in ergodic systems, time averages $\hat{\varphi}$ and space averages are equal for L^1 observables. Taking φ as the indicator function

$$\chi_A(x) = \begin{cases} 1 & x \in A, \\ 0 & \text{otherwise,} \end{cases}$$

for measurable A , a useful corollary is that the proportion of time an orbit spends in A approaches $\mu(A)$ as we consider more and more iterates. We will make use of this in section 7.1. Statement (4) clarifies the link between ergodic and mixing properties, which we may also express in functional form:

Proposition 1.2. *The following are equivalent:*

- (1) (X, \mathcal{A}, μ, f) is mixing.
- (2) $|C_n(\varphi, \psi, f, \mu)| \rightarrow 0$ as $n \rightarrow \infty$ for all L^2 observables φ, ψ where

$$C_n(\varphi, \psi, f, \mu) = \int (\varphi \circ f^n) \psi d\mu - \int \varphi d\mu \int \psi d\mu.$$

We refer to C_n as the *correlation function* and consider results on its decay rate in section 2.3.

1.5 Proving mixing properties

We give a brief outline here, aiming to describe the relevant theorems in the context of laminar mixing rather than providing a detailed historic overview. Such an overview can be found in Chernov and Markarian (2006). When proving mixing properties in later chapters, our approach will be to apply a theorem of Katok and Strelcyn (1986) which gives conditions under which a broad class of hyperbolic systems (in particular those with singularities) are mixing. To state it we require some preliminary definitions.

The first of these is the *Bernoulli property*. Roughly speaking, a system (X, \mathcal{A}, μ, f) being Bernoulli (equivalently ‘having the Bernoulli property’) implies that it behaves as randomly as possible. Its name derives from Bernoulli trials, the random process of repeatedly flipping a fair coin. For our purposes, we do not require a precise definition. A more detailed treatment, with systems relevant to fluid mixing applications in mind, is provided in Sturman et al. (2006) and Springham (2008). Its relevance to our applications is that Bernoulli systems are automatically strong mixing. Indeed we have

$$\text{Bernoulli} \implies \text{strong mixing} \implies \text{ergodic},$$

referred to as the *ergodic hierarchy* for measure preserving systems.

When studying the Cat Map, we saw that the hyperbolic behaviour in the tangent space manifested itself in the dynamics of H on the torus itself. The Hadamard-Perron theorem describes this link for general Anosov systems. Given a metric space (M, d) , let $B_r(x)$ denote the *ball* of points y such that $d(x, y) < r$.

Theorem 1.2 (Hadamard-Perron, Sturman et al., 2006). *Let $f : M \rightarrow M$ be an Anosov diffeomorphism. Then for each $x \in M$ there exist local stable and unstable manifolds*

$$\gamma_s(x) = \{y \in B_{r(x)}(x) \mid d(f^n(y), f^n(x)) \rightarrow 0 \text{ as } n \rightarrow \infty\}$$

$$\gamma_u(x) = \{y \in B_{r(x)}(x) \mid d(f^{-n}(y), f^{-n}(x)) \rightarrow 0 \text{ as } n \rightarrow \infty\}$$

of the same dimension as, and tangent to, the subspaces E_x^s and E_x^u respectively. The local manifolds $\gamma_s(x)$ and $\gamma_u(x)$ are as smooth as f (so in particular, they are differentiable, since f is a diffeomorphism). The size of the local stable and unstable manifolds at x is given by the radius $r(x)$ of the ball $B_{r(x)}(x)$, and moreover there is a uniform bound $r(x) \geq r' > 0$ for all $x \in M$.

For the Cat Map, it is easy to see that at every x , the local manifolds are the line segments passing through x parallel to v^s, v^u . Analogous constructions hold for non-uniformly hyperbolic diffeomorphisms f , in particular at points $x \in X$ with non-zero Lyapunov exponents (see Pesin, 1977). A key difference is that the size of these manifolds is no longer uniformly bounded away from 0; they can be arbitrarily small. Pesin also shows that nonuniform hyperbolicity ensures the existence of an *ergodic partition*. Let Λ denote the set of points x with non-zero Lyapunov exponents $\chi(x, v) \neq 0$ for all vectors $v \neq 0$.

Theorem 1.3 (Pesin, 1977). *There are sets $\Lambda_i \subset \Lambda$, $i = 0, 1, 2, \dots$ such that*

1. $\Lambda_i \cap \Lambda_j = \emptyset$, $i \neq j$, $\bigcup_{i \geq 0} \Lambda_i = \Lambda$,
2. $\mu(\Lambda_0) = 0$, $\mu(\Lambda_i) > 0$ for $i > 0$,
3. $f(\Lambda_i) = \Lambda_i$,
4. *The restricted map $f|_{\Lambda_i} : \Lambda_i \rightarrow \Lambda_i$ is ergodic for $i > 0$.*

We now wish to connect up these positive measure components, showing that their union forms one large (full measure) ergodic component. The classical technique to achieve this is the construction of a *Hopf chain* (originally Hopf, 1939, 1940, see also Coudène, 2016; Wilkinson, 2009) of local stable and unstable manifolds. In short, time averages are constant on both local manifolds and the ergodic components so if any Λ_i can be connected to any other Λ_j via a chain of local manifolds, time averages agree over all components and are therefore constant almost everywhere. Ergodicity then follows by (3) of Proposition 1.1. In practice, since in non-Anosov systems local manifolds can be arbitrarily small, a Hopf chain may be difficult to construct in the non-uniformly hyperbolic setting. Assuming the Λ_i , $i > 0$, are open (see Pesin, 1977), topological transitivity would also suffice to extend local ergodicity over the components Λ_i to their union.

Pesin further describes a countable partition into Bernoulli components. This was then generalised in Katok and Strelcyn (1986) to a wider class of maps $f : X \rightarrow X$, so called ‘smooth maps with singularities’. Paraphrasing Sturman et al. (2006),

Theorem 1.4 (Katok and Strelcyn). *Let (X, \mathcal{F}, μ, f) be a measure preserving dynamical system such that f is C^2 smooth outside of a singularity set S . Suppose that the Katok-Strelcyn conditions hold:*

(KS1): $\exists a, C_1 > 0$ s.t. $\forall \epsilon > 0, \mu(B_\epsilon(S)) \leq C_1 \epsilon^a$.

(KS2): $\exists b, C_2 > 0$ s.t. $\forall x \in X \setminus S, \|D_x^2 f\| \leq C_2 d(x, S)^{-b}$.

(KS3): *Lyapunov exponents exist and are non-zero almost everywhere.*

Then at almost every x we can define local unstable and stable manifolds $\gamma_u(x)$ and $\gamma_s(x)$. Suppose that the manifold intersection property holds:

(M): *For almost any $x, x' \in X, \exists m, n$ s.t. $f^m(\gamma_u(x)) \cap f^{-n}(\gamma_s(x')) \neq \emptyset$.*

Then f is ergodic. Furthermore the Bernoulli property holds, provided we can show the repeated manifold intersection property:

(MR): *For almost any $x, x' \in X$ there exists M, N such that for all $m > M$ and $n > N, f^m(\gamma_u(x)) \cap f^{-n}(\gamma_s(x')) \neq \emptyset$.*

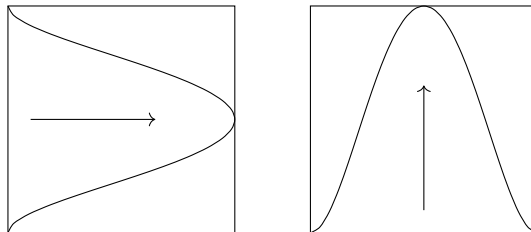
We will rely on this theorem to prove mixing properties in later chapters so it is worth taking a moment to dissect its contents and give some context with laminar mixing applications in mind. **(KS1-2)** are technical conditions on the influence of the singularity set, ensuring that it is sufficiently small with respect to the measure μ **(KS1)** and that the second derivative of f doesn’t ‘blow-up’ too fast in its vicinity **(KS2)**. For spaces X of dimension 2 and above, what we mean by the second derivative requires a technical definition, see for example the appendix of Przytycki (1983). We simply remark here that **(KS2)** is trivially satisfied by piecewise linear transformations. **(KS3)** is the hyperbolicity assumption which, together with **(KS1-2)**, guarantee the existence of local manifolds and a partition of X into Bernoulli components. The final conditions **(M)**, **(MR)** say that these components can be linked via images of these manifolds, giving global ergodic and Bernoulli properties. In a fluids context, local stable and unstable manifolds roughly describe the characteristic local flow direction in backwards and forwards time respectively (see for example Beigie et al., 1994). The way in which parcels of fluid are stretched and spread across the domain is then described well by the images of these local manifolds, and mixing properties follow from intersection conditions on these images: **(M)** says that fluid parcels are spread all around X (achieving topological transitivity), the stronger condition **(MR)** then guarantees that they remain spread over subsequent stirs.

Chapter 2

Applications and Modern Advancements

2.1 Link to physical systems

The Cat Map, and similar systems which alternate orthogonal shears, serve as a simple model for hand mixers where a pair of blades rotate in opposite directions, shearing a common fluid domain horizontally, vertically, horizontally, and so on. That no material is lost in the mixing process is modelled by the periodic boundaries of the torus. Dubbed ‘eggbeater flows’ (Ottino, 1989a), these time dependent (i.e. *unsteady*) flows possess a necessary phenomenon for good mixing in two dimensions: *streamline crossing*. In steady two dimensional flows mixing is necessarily poor (Franjone and Ottino, 1992) with fluid parcels forever confined to their streamlines. Alternating between two flows with intersecting streamline patterns provides a way of escaping this confinement. An example of a simple eggbeater flow is sketched below.



Franjone and Ottino (1992) provide numerical illustrations of the dynamics typical to eggbeater flows, defining symmetries which simplify their theory and may be exploited to optimise mixing quality. Physical implementations of these flows are explored, including three dimensional pipe flows with immediate engineering applications.

A more direct implementation is considered in Hertzsch et al. (2007), where mixing in a DNA hybridisation chamber is achieved using alternating flows between ‘source-sink’ pairs. The depth of the cylindrical chamber is assumed small enough that vertical variations in velocity are negligible and a Hele-Shaw cell approximation holds. The flow induced by each pair is then well modelled by that of fluid moving around a disk D with no-slip boundary conditions at its boundary ∂D . Given a source-sink pair $z_+, z'_- \in D$, the streamline pattern consists of families of curves joining z_+ to z_- , foliating D right up to its boundary, near which the contours limit onto near circular arcs. When fluid reaches z_- it is immediately reinjected at z_+ along the same streamline, achieved in practice by a pumping mechanism. As before, alternating between two sink-source pairs allows fluid parcels to escape their starting streamlines and spread around D . The resulting system can be linked to the eggbeater flows described above, achieved by ‘pinching together’ the sides of the

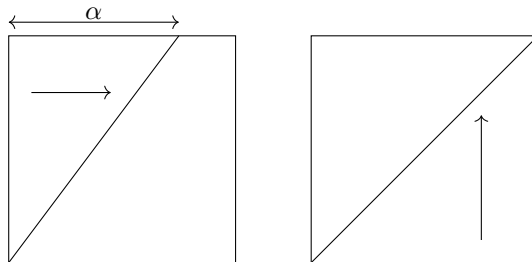
torus perpendicular to the flow direction.

The location of the pairs in D and their ‘pump times’ (the time duration each pair is activated) give control parameters for maximising mixing quality. Their analogues in the eggbeater model are the *foci* of the shears (where the shears peak, half way along the domain the illustration above) and their *strength* (the magnitude of the shear peak). Numerical simulations reveal mixing to be poorest near the boundary ∂D where streamline patterns for each pair are barely transversal, both limiting onto the outer circular boundary in a similar fashion. Mixing can be improved in these regions by placing the source-sink pairs closer to the boundary, resulting in stronger local transversality. The analogue to this in the eggbeater model is to push the foci of the shears away from the centre, resulting in shears that are nearly monotonic over their domain, barring some thin strip towards the edge. As a result the shears more closely resemble those of the Cat Map, with known excellent mixing behaviour.

2.2 Mixing properties of stretching and folding models

In this section we review the application of ergodic theory techniques to prove mixing properties of simple stretching and folding models. Many of the systems can be thought of as ‘Cat Map variants’, similarly composing orthogonal shears on the torus but incorporating some feature which mimics a phenomenon found in laminar mixing applications. Typically this breaks the Anosov property, introducing singularities or non-uniform hyperbolicity.

Our first example is the *Sawtooth Map*, studied in Vaienti (1992). Letting $\alpha > 0$, it takes the form $H = G \circ F : \mathbb{T}^2 \rightarrow \mathbb{T}^2$ where $F(x, y) = (x + \alpha y, y)$, $G(x, y) = (x, x + y)$ so that setting $\alpha = 1$ recovers the Cat Map. We sketch the map for $\alpha < 1$ below.



More generally, when $\alpha \in \mathbb{N}$ the map H is a hyperbolic toral automorphism, uniformly hyperbolic with easily provable mixing properties. When α is not integer valued, the map is discontinuous. Action of the map on two initially segregated regions is shown in Figure 2.1. Comparing with the same visualisation of the Cat Map (Figure 1.4) we see similar behaviour, with the stretching and folding action mixing the domain, however not in such a uniform fashion. This is due to the discontinuity over $\mathcal{D} = \{(x, y) \mid y = 0\}$ causing a ‘cutting and placing’ effect. The images of this discontinuity $\mathcal{D}_4 = \cup_{k=1}^4 H^k(\mathcal{D})$ are plotted in the fifth frame, showing the regions which have been cut and realigned under H, \dots, H^4 . Towards the edges of the magnified section we see that this can aid mixing; when \mathcal{D}_4 lies on the red-blue interface, it means that each region has been cut and placed alongside the other, resulting in thinner striations. In contrast, towards the top right of the magnified section we see that a blue region has been cut only to be realigned next to another blue region, so mixing is not enhanced. These situations together give non-uniform decay of striation widths and non-uniform mixing as a result.

Cutting together with stretching and folding forms the basis for the design of several laminar mixing devices, e.g. the partitioned pipe mixer (Khakhar et al., 1987; Mezić et al., 1999) and the Kenics static mixer (Galaktionov et al., 2003). For a more detailed review of mixing by discontinuous maps see Sturman (2012), Kreczak (2019).

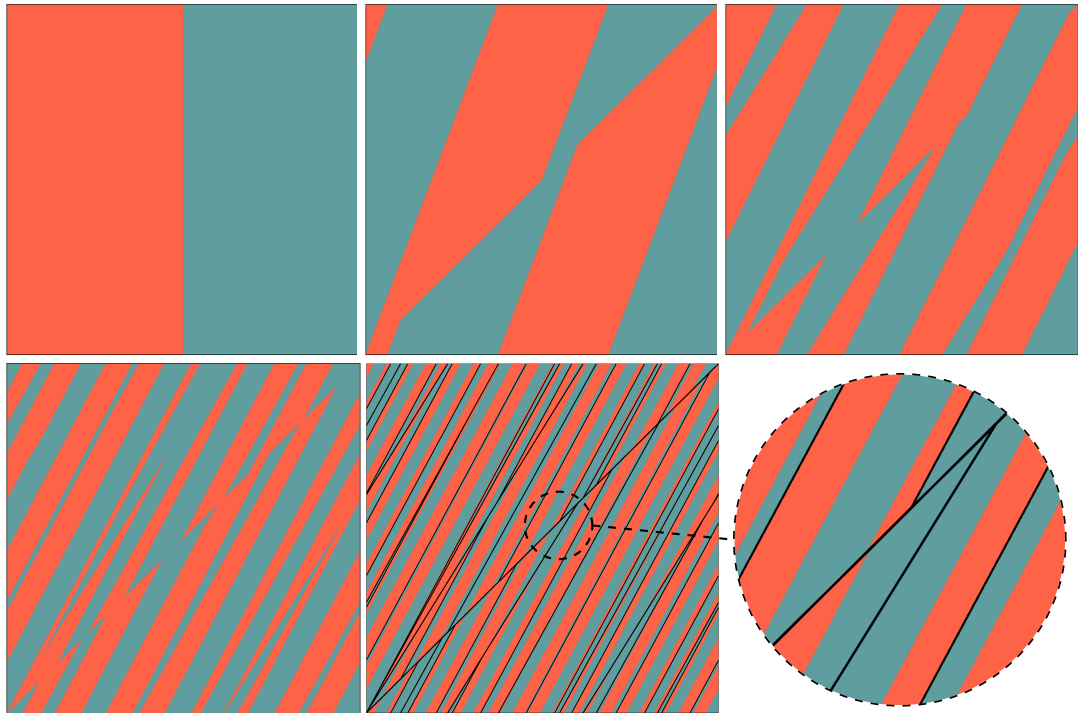


Figure 2.1: Mixing behaviour of the Sawtooth Map at parameter value $\alpha = 0.6$. The forward images of discontinuity line are plotted in the fifth frame, showing regions that have been ‘cut and placed’. The magnified section illustrates regions where this has aided mixing, aligning red next to blue, and others where it has not.

Returning to H , we may define Lyapunov exponents outside of the set $\mathcal{D}_\infty = \bigcup_{k \in \mathbb{Z}} H^k(\mathcal{D})$, i.e. the points x whose orbit never lands on \mathcal{D} , so the associated cocycle is well defined. As $\mu(\mathcal{D}) = 0$, so too is $\mu(\mathcal{D}_\infty)$ and Lyapunov exponents exist almost everywhere. They are non-zero, analogous to the Cat Map, by hyperbolicity of the constant Jacobian DH . The set \mathcal{D} trivially satisfies **(KS1-2)**, so \mathbb{T}^2 partitions into a countable collection of ergodic components. Vaienti constructs a Hopf chain, linking up the components via local manifolds to establish ergodicity (and stronger mixing properties, following the work of Wojtkowski, 1981). While (like the Cat Map) the geometry of these manifolds is quite simple, being parallel to the eigenvectors of DH , they are cut up into arbitrarily small pieces by \mathcal{D}_∞ which aggravates analysis. The construction uses the method of regular coverings, developed to prove ergodicity in billiards systems of hard balls. See §6.1 of Chernov and Markarian (2006) and the references therein for an overview. Billiards often serve as motivating examples for the development of new techniques to study statistical properties of hyperbolic systems. They are, in general, far more complicated than the toral maps considered here but their analysis shares many common attributes: encoding the dynamics in a Poincaré map, showing that expansion via hyperbolicity dominates the cutting up effect of singularities, studying recurrence to regions of strong hyperbolicity. We explore this relationship further in section 2.3, looking first at a system where this ‘recurrence’ is central to its mixing behaviour.

As alluded to in section 1.1, see also Gouillart et al. (2008, 2007), walls bounding a fluid domain impact finite time mixing quality and the rate of mixing within. Incorporating this behaviour into simple stretching and folding models, Linked Twist Maps (hereafter LTMs) serve as a paradigm for chaotic mixing in the presence of a boundary. Encompassing a broad class of maps, LTMs can be defined on two dimensional manifolds beyond the torus, including the 2-sphere (Springham, 2008) and the plane (Springham and Wiggins, 2010). Here we restrict our focus to toral LTMs, which are directly related to the maps studied in subsequent chapters. For $(x, y) \in \mathbb{T}^2$, consider horizontal and vertical annuli $P = \{(x, y) \mid y_0 \leq y \leq y_1\}$ and $Q = \{(x, y) \mid x_0 \leq x \leq x_1\}$. Write

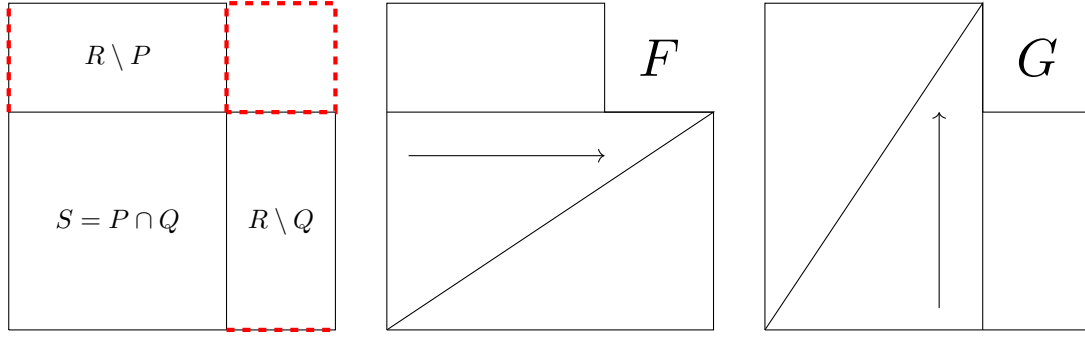


Figure 2.2: A linked twist map $H = G \circ F$ on the region $R = P \cup Q \subset \mathbb{T}^2$. The boundary ∂R is drawn in red, noting the periodic boundaries of \mathbb{T}^2 .

their intersection as $S = P \cap Q$, union as $R = P \cup Q$. Define a horizontal shear $F : R \rightarrow R$ by

$$(x, y) \mapsto \begin{cases} (x + f(y), y) & (x, y) \in P, \\ (x, y) & \text{otherwise,} \end{cases}$$

where $f : [y_0, y_1] \rightarrow \mathbb{R}$ is a C^2 function satisfying

- $f(y_0) = 0$,
- $f(y_1) = k$ for some $k \in \mathbb{Z}$,
- $f'(y) \neq 0$ for $y_0 < y < y_1$ (monotonicity).

We call f a *twist function*. Similarly define vertical shears $G : R \rightarrow R$,

$$(x, y) \mapsto \begin{cases} (x, y + g(x)) & (x, y) \in Q, \\ (x, y) & \text{otherwise,} \end{cases}$$

for twist functions $g : [x_0, x_1] \rightarrow \mathbb{R}$, $g(x_1) = l \in \mathbb{Z}$. It follows that the composition $H = G \circ F : R \rightarrow R$ is continuous, preserves the normalised Lebesgue measure μ on R , and leaves the rectangle ∂R invariant. Imposing

$$f'(y_0) = f'(y_1) = g'(x_0) = g'(x_1) = 0 \quad (2.1)$$

ensures that H is a diffeomorphism. Otherwise it satisfies the conditions to be a smooth map with singularities (Katok and Strelcyn, 1986). When the twist functions are piecewise linear, so too is H . The relative signs of the twist functions f, g significantly impact the dynamics. We class LTMs as *co-rotating* if the twists have the same sign ($kl > 0$), *counter-rotating* if they have different signs ($kl < 0$). We focus first on co-rotating LTMs; an example is sketched in Figure 2.2 with $f(t) = g(t) = 3t/2$, $x_0 = y_0 = 0$, $x_1 = y_1 = 2/3$.

We remark that taking $x_0 = y_0 = 0$, $x_1, y_1 \rightarrow 1$ shrinks the complement $X \setminus R$ and we recover the Cat Map for $f = g = \text{Id}$. For $x_1, y_1 < 1$ the invariant set ∂R forms the ‘boundary’ of the model on which, barring the corner points, we shear in only one of the two orthogonal directions. This behaviour extends into the fluid bulk, giving regions P_n, Q_n on which H^n is given by F^n, G^n respectively. These are clearly visible in the visualisation of Figure 2.3, contained within the persistent unmixed red and blue regions respectively. For $(x, y) \in P_n$ for example, the behaviour in the tangent space over these n iterates is determined by

$$DH^n = DF^n = \begin{pmatrix} 1 & f'(y) \\ 0 & 1 \end{pmatrix}^n = \begin{pmatrix} 1 & nf'(y) \\ 0 & 1 \end{pmatrix},$$

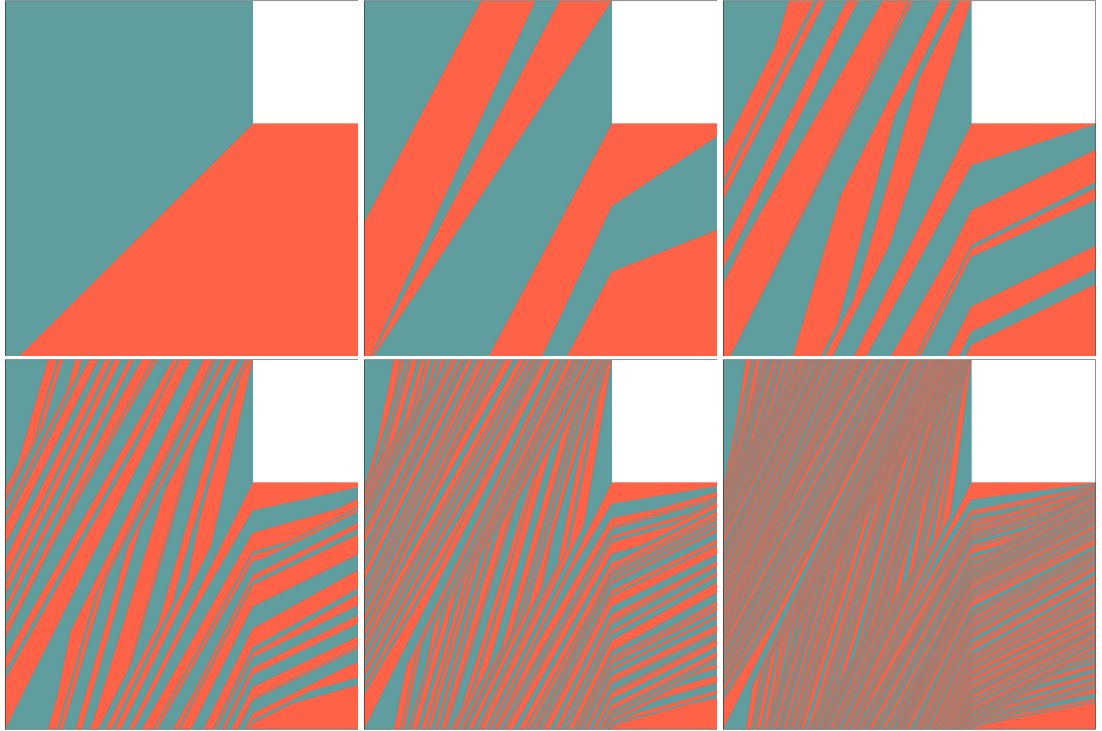


Figure 2.3: Mixing behaviour of the co-rotating piecewise linear linked twist map shown in Figure 2.2.

which is non-hyperbolic. Eventually, though, $F^n(x, y)$ will hit $S = P \cap Q$ (Burton and Easton, 1980) and is subsequently sheared vertically some $m \geq 1$ times by G until it lands in S once more. The cocycle $DG^m DF^n$ associated with this mapping $(x', y') = H^{n+m-1}(x, y)$ is necessarily hyperbolic. We may decompose any orbit in this way, logging returns to S , splitting the associated cocycle into hyperbolic blocks $DG^m DF^n$. This forms the basis for establishing hyperbolicity in co-rotating LTMs. Importantly, since each block will stretch and contract in different directions, we must check that expansion from one block is not immediately undone by contraction from the next. Cones are the standard tool for ensuring this does not occur, which we define formally in Chapter 3. They ensure that all the blocks have roughly similar directions of stretching and contraction, so no ‘unstirring’ occurs. Figure 2.3 illustrates this. We see that on successive returns to S , fluid parcels are stretched in varying directions but we could bound these directions by a fairly small gradient range. Existence of such a cone rests, in this case, on the twist functions being co-rotating and monotonic.

Indeed if we flip the sign of g , (essentially considering the map $H = G^{-1} \circ F$ with F and G as given in Figure 2.2) no such invariant cone exists and unstirring occurs. Figure 2.4 illustrates this, showing the effect of H^2, H^4, H^6, H^{24} on two initially segregated regions. The wide range in gradients of the line segments making up the red-blue interface in S highlight the inconsistent directions of stretching and contraction. As more and more iterates are considered, a heterogeneous phase space emerges with non-mixed ‘island’ structures interspersed within a well mixed ‘sea’. Together these island structures form an invariant positive measure set, so H is non-ergodic and by extension non-mixing. We cover island structures more rigorously in Chapter 3, establishing conditions under which they exist and what determines their measure.

We now give a brief summary of proven (measure theoretic) mixing results for toral LTMs. For an account of earlier planar LTMs, topological mixing results, and more details see Sturman et al. (2006) and Springham (2008). In Burton and Easton (1980), existence of an ergodic partition is shown for smooth (i.e. twists satisfying equation 2.1) co-rotating toral LTMs. A geometric

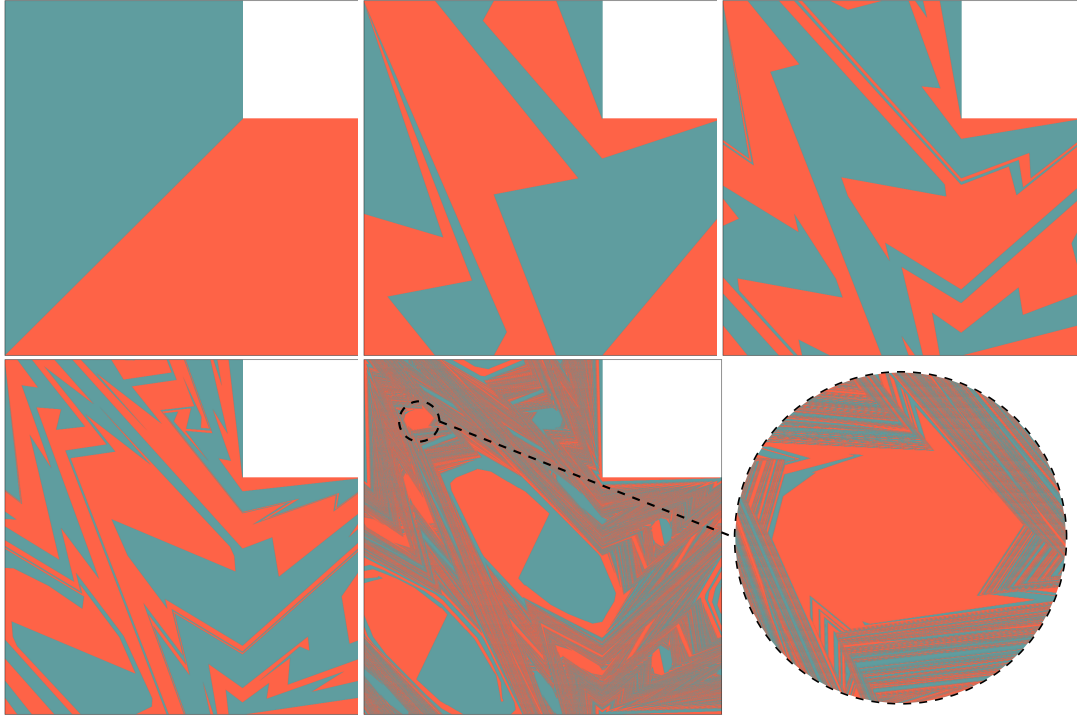


Figure 2.4: Mixing behaviour of a counter-rotating piecewise linear linked twist map over 2,4,6,24 iterates.

argument sketches out how this extends to the global Bernoulli property. Wojtkowski (1980) considers linear twist functions, showing the Bernoulli property* for $kl > 0$ (co-rotating) and the existence of an ergodic partition for $kl < -4$, where the twists are strong enough to form an invariant cone. Przytycki (1983) then follows the Katok and Strelcyn approach, giving conditions under which counter-rotating LTMs with linear twists satisfy **(MR)** and are therefore Bernoulli. Noting the monotonicity condition for twist functions f and g , we may define their non-zero (signed) *strengths* as

$$\alpha = \begin{cases} \inf_{y_0 \leq y \leq y_1} f'(y) & \text{if } k > 0, \\ \sup_{y_0 \leq y \leq y_1} f'(y) & \text{if } k < 0, \end{cases} \quad \beta = \begin{cases} \inf_{x_0 \leq x \leq x_1} g'(x) & \text{if } l > 0, \\ \sup_{x_0 \leq x \leq x_1} g'(x) & \text{if } l < 0. \end{cases}$$

Przytycki shows that $\alpha\beta < -C_0 \approx -17.244$ and $|k|, |l| \geq 2$ are sufficient conditions to prove **(MR)**. The key step is showing that the images of local manifolds $H^n(\gamma_u), H^{-n}(\gamma_s)$ grow exponentially in diameter, a necessary requirement to establish an intersection given that (by non-uniform hyperbolicity) the local manifolds may be arbitrarily small. In the co-rotating case this is straightforward, $H^n(\gamma_u)$ is piecewise linear monotonic curve whose diameter is the sum of the diameters of its constituent line segments. Exponential growth can then be deduced by considering returns to S and bounds on expansion factors derived from the invariant cone. In the counter-rotating case diameter growth is not so straightforward. While the overall *length* of $H^n(\gamma_u)$ may grow exponentially by a similar cone construction, monotonicity is no longer assured. This means that the curve may repeatedly fold in on itself, staying confined to a small region of the domain, and never meeting $H^{-n}(\gamma_s)$. Such a ‘doubling back’ effect is illustrated clearly in the acute angles of Figure 2.4, akin to the sharp kinks we would see in forward images of local unstable manifolds. To establish sufficient diameter growth, then, we require that some individual line segment in $H^n(\gamma_u)$ grows

*Wojtkowski actually shows the K-mixing property which sits between mixing and Bernoulli in the ergodic hierarchy. The Bernoulli property then follows from Chernov and Haskell (1996).

exponentially in diameter and we disregard the rest. Przytycki gives a concise argument for the existence of such a line segment, relying on periodicity specific to linear toral LTMs. We will return to toral LTMs in section 2.3, first covering some other Cat Map variants.

The Katok Map (Katok, 1979) breaks the uniform hyperbolicity of the Cat Map by slowing down trajectories near the fixed point $(0, 0)$ until this point becomes neutral. We do not state its lengthy definition here, see either the original work or Barreira and Pesin (2002). The key aspect of this ‘slow down’ is that it preserves features of the original map (e.g. smoothness), indeed they are topologically conjugate. A Pesin theory approach can be followed to establish mixing properties. Maps of this form can be thought of as *almost Anosov*, hyperbolic outside of some finite set of neutral points. Sitting at the edge of uniform hyperbolicity, they are typically more approachable than other non-uniformly hyperbolic maps.

A further Cat Map variant is found in Liverani (2004). Making a change of coordinates, we can think of the map T_ε as the Cat Map $H = G \circ F$ with F replaced by the shear $(x, y) \mapsto (x + f(y), y)$ where $f(y) = y - \frac{1+\varepsilon}{2\pi} \sin(2\pi y)$, $\varepsilon \geq -1$. At $\varepsilon = -1$ we recover the Cat Map and any perturbation $\varepsilon > -1$ gives a shear that is non-linear and smooth. The map is Anosov for $-1 < \varepsilon < 0$ and non-uniformly hyperbolic at $\varepsilon = 0$; mixing properties at this parameter value follow from the existence of an invariant cone. Outside of this parameter range, the map admits elliptic islands, so is non-mixing. We note that this mixing window corresponds to the parameter range over which f is non-decreasing. Indeed, in all of the models above, monotonicity of the Cat Map shears has been preserved and has been relied upon to establish mixing properties.

The diverse behaviour possible from removing the monotonicity condition is best illustrated by the Chirikov Standard Map (Chirikov, 1971). Defined as Liverani’s example above but with $f(y) = \frac{K}{2\pi} \sin(2\pi y)$, the map is integrable at $K = 0$ and nonlinear for $K > 0$. As such it serves as a classic example of ‘transition to chaos’. Analysis of the system is famously challenging with many open questions still remaining, e.g. are there values of K for which the map is ergodic? See Giorgilli and Lazutkin (2000) for a more detailed discussion. Simpler examples have been constructed where analysis is tractable using known techniques. A piecewise linear version of the standard map was studied in Bullett (1986); Wojtkowski (1981), where $f(y) = A(|y - 1/2| - 1/4)$, and shown for certain parameter values to be hyperbolic ($A \geq 4$) and mixing ($A > A_0 \approx 4.0329$). Similar to Przytycki (1983), hyperbolicity (and by extension the mixing property using a similar approach to Wojtkowski, 1980) are achieved by taking stronger and stronger shears. For $A < 4$ the map exhibits island structures surrounded by a chaotic sea. Over a countable parameter subset $S \subset [2, 4)$ a single polygonal island forms on which the map is periodic, rather than the quasi-periodicity seen in ellipse shaped islands for generic parameters $A \notin S$. Over S , Wojtkowski establishes hyperbolicity outside of this island structure, relying on cone constructions. Strong mixing properties over this chaotic domain follows from the work of Liverani and Wojtkowski (1995), see their §14B. Smaller positive parameter values $A \approx 0$ are the focus of Wojtkowski (1982); coexistence of elliptic and chaotic behaviour is similarly observed, hyperbolicity shown over a domain shrinking in measure (asymptotically) like $\frac{A}{16} \ln \frac{1}{A}(1 + o(1))$ as $A \rightarrow 0$.

A further non-monotonic toral map is considered in Cerbelli and Giona (2005), retaining the linear vertical shear of the Cat Map but replacing its horizontal shear by a ‘tent’ shaped profile, see Figure 2.5(a). The map can be expressed as $H : (x, y)^T \mapsto DH \cdot (x, y)^T \bmod 1$, where

$$DH = \begin{cases} DH_1 = \begin{pmatrix} 1 & 2 \\ 1 & 3 \end{pmatrix} & 0 < y < \frac{1}{2}, \\ DH_0 = \begin{pmatrix} 1 & -2 \\ 1 & -1 \end{pmatrix} & \frac{1}{2} < y < 1. \end{cases}$$

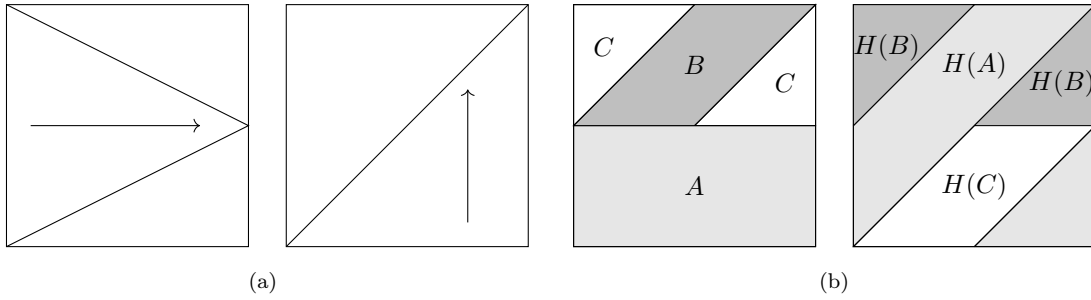


Figure 2.5: Cerbelli and Giona's map toral map H : (a) map definition, (b) effect on a three element partition of the torus.

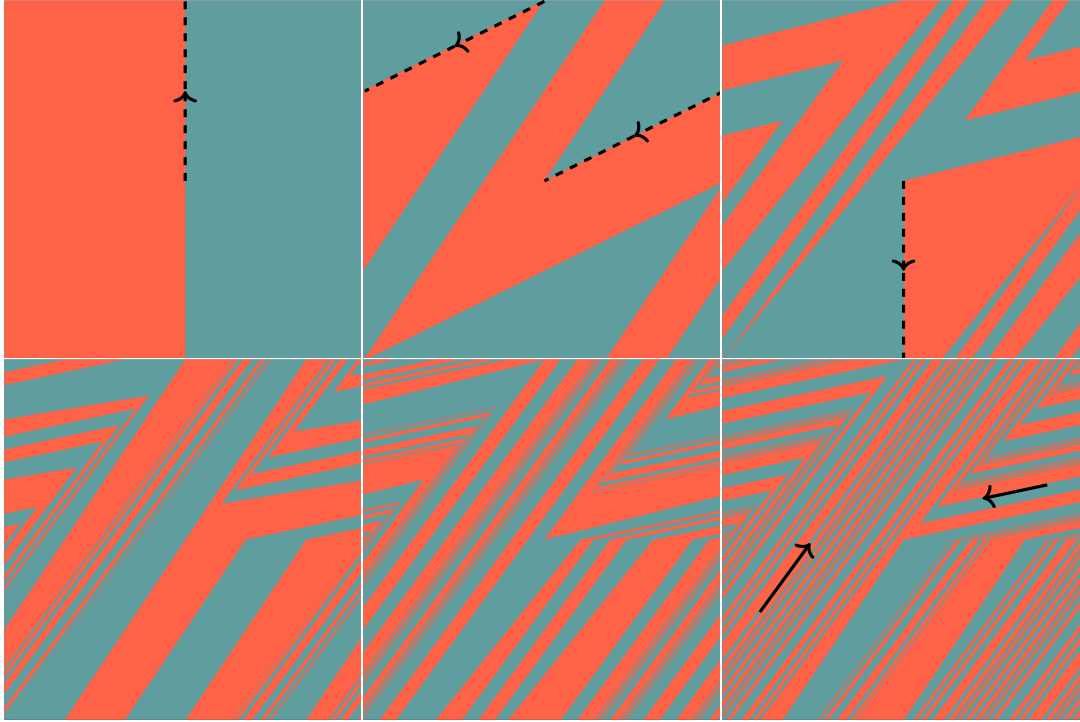


Figure 2.6: Mixing behaviour of Cerbelli and Giona's map over 1,2,...5 iterates. Dashed arrows show the effect of H^2 on the red-blue interface in B , solid arrows show v^u in $A \cup B$ and $DH_0 v^u$ in C .

Taking a phase shift $y \rightarrow y + 1/2 \pmod{1}$ retrieves Wojtkowski's example at $K = 2$. Note that DH_1 is hyperbolic whereas DH_0 is elliptic. One may expect, a priori, that this would be detrimental to mixing (indeed Wojtkowski's example is non-mixing at $K = 2$). For if H admits any periodic orbit in the upper annulus $0 < y < 1/2$, one or more elliptic islands would necessarily form within it. However H possesses unique mapping behaviour which prohibits this. Consider the ABC partition of \mathbb{T}^2 shown in Figure 2.5(b). One can show that $H(A) \subset A \cup B$, $H(B) = C$, and $H(C) \subset A$ so that orbits entering the upper annulus necessarily escape after two iterates of H . Further, the behaviour in the tangent space during this escape is characterised by $DH_0 DH_0 = \begin{pmatrix} -1 & 0 \\ 0 & -1 \end{pmatrix}$ so that any cocycle can essentially be expressed as $DH_z^n = (-1)^l DH_1^m$ for some $l, m \in \mathbb{Z}$, perhaps pre-/post-multiplied by DH_0 . Hyperbolicity follows as a straightforward consequence and mixing properties can be deduced by more direct means than following the Katok-Strelcyn approach.

A visualisation of its mixing behaviour is given in Figure 2.6. Comparing the first and third panes, the sign flipping effect of H^2 on B is apparent with the dashed line segment $(1/2, y)$, $1/2 < y < 1$ on the red-blue interface mapping to $(-1/2, -y) \pmod{1} \equiv (1/2, 1 - y) \pmod{1}$, i.e. the segment $(1/2, y)$, $0 < y < 1/2$. Considering more and more iterates of H (and by extension

more and more stretches by DH_1) the interface limits onto two distinct directions v^u and DH_0v^u , where v^u is the unstable eigenvector of DH_1 . Similar to the Cat Map, in terms of the local directions of stretching and contraction, the mixing is quite regimented. Indeed, the gradients of local unstable manifolds are easily found to be parallel to v^u in $A \cup B$ and DH_0v^u in C , defining a simple invariant unstable foliation. Globally, however, the mixing is non-uniform, owing to some regions being stretched multiple times upon its return to A and others just once. Analogously, the images of local manifolds spread around the domain in a non-uniform fashion. The so called w -measure μ_w (Giona and Adrover, 1998) quantifies this space filling behaviour and is observed to be singular (and possess multifractal properties, see Cerbelli and Giona, 2008). From a fluid mixing perspective, μ_w provides an asymptotic invariant distribution of interface length between stretched out fluid parcels. Using the visualisation of Figure 2.6, peaks in μ_w form where the striation widths are finest, highlighting the regions where diffusion would play a significant role. For the Cat Map (and other Anosov systems conjugate to it by a differentiable conjugacy) we would expect the measure to be non-singular. Note that this excludes Liverani’s example T_ε over $-1 < \varepsilon < 0$, for which the conjugacy is only C^0 (see §5 of Cerbelli and Giona, 2005).

The authors define another property of H , further distancing it from Anosov maps. The *alternating-sign* property states that given an oriented line segment, its forward images intersect every ε -ball (topological transitivity) and cross them in both directions. For H , this follows from the tight folding behaviour around the fixed points $(0, 0)$ and $(0, 1/2)$. MacKay (2006) revises this definition to the non-orientability of the invariant foliations. As no Anosov map can hold this property (including Liverani’s example above) the authors propose it to be the ‘watershed’ between uniform and non-uniform chaotic maps. Subsequent literature surrounding Cerbelli and Giona’s map has approached it in the context of so called *pseudo-Anosov* maps, first introduced by Thurston (1988). We do not provide details here (none of the maps in subsequent chapters appear to possess the property); for a full definition and properties of pseudo-Anosov maps see Boyland (1994). MacKay (2006) proves the pseudo-Anosov property for H , immediately showing many of the properties which Cerbelli and Giona proved from first principles. The proof involves the construction of a finite *Markov partition* for the map, encoding much of the dynamics of H in a much simpler system, represented as a *subshift of finite type* on symbol sequences. See Robinson (1995) for an introduction; Wright (2018) also studies specific Markov partitions for H .

Several perturbations and generalisations to H have been proposed. Demers and Wojtkowski (2009) define a countable family of maps preserving the pseudo-Anosov property, constructing Markov partitions and analysing the associated symbolic dynamics. Perturbations which ‘smooth’ the singularities of the tent shaped shear are commented on in Cerbelli and Giona (2008); MacKay (2006). While certain aspects of the dynamics may be preserved[†], numerical experiments suggest that mixing with respect to the Lebesgue measure is not one of them. We observe, therefore, that non-monotonic toral maps with proven mixing properties are quite rare. They fit into two categories: maps such as Wojtkowski’s where the mixing property follows only from taking stronger and stronger shears, or maps such as Cerbelli and Giona’s where precise mapping behaviour and properties of the Jacobian align to produce a pseudo-Anosov transformation. In an industrial mixing context, these examples correlate to (potentially unnecessary) increased energy expenditure or systems whose mixing dynamics are potentially too sensitive to perturbations. This motivates our first research question:

(Q1): Can we perturb Cerbelli and Giona’s map, and still retain mixing with respect to the Lebesgue measure?

More precisely, we try to answer whether elliptic islands necessarily form under continuous (i.e. pa-

[†]Following from proven results on perturbations to pseudo-Anosov maps, see MacKay (2006) and the references therein. Cerbelli and Giona (2008) provide numerical evidence of preserved properties under their smooth perturbation.

parameterised with a real parameter) perturbations to H as we destroy the pseudo-Anosov structure. With the aim of modelling realistic flow profiles in both shears, our next question asks:

(Q2): Can we construct mixing systems incorporating *two* non-monotonic shears?

This would move us closer to the egg-beater type flows considered in section 2.1. Global mixing has been observed numerically in such systems, but measure theoretic mixing in the sense of Definition 1.6 has not yet been established. Finally, we explore:

(Q3): What are typical mixing rates in these systems?

That is, what is the rate of decay of $|\mu(f^n(B) \cap A) - \mu(A)\mu(B)|$ with n ? Such questions are answered in the language of ‘decay of correlations’, we review results on this topic in the following section.

2.3 Establishing mixing rates

Recall from section 1.4 that $f : X \rightarrow X$ preserving μ is mixing if $|C_n(\varphi, \psi, f, \mu)|$ decays to 0 for all L^2 observables φ, ψ . So far we have only been concerned with whether $|C_n|$ converges to 0, now we turn our attention to the *rate* of convergence. That is, what is the rate at which we approach homogeneity? What is the *mixing rate*? The decay of $|C_n|$ relates to classical questions on the statistical properties of dynamical systems, such as the nature of the convergence (1.1). For a dynamical system (X, \mathcal{A}, μ, f) and observable $\varphi : X \rightarrow \mathbb{R}$, $\int \varphi d\mu = 0$, we say that the *central limit theorem* (CLT) holds if the random variable

$$x \rightarrow \frac{1}{\sqrt{n}} \sum_{i=0}^{n-1} \varphi \circ f^i(x)$$

(x distributed according to the measure μ) converges in law[‡] to a normal distribution $\mathcal{N}(0, \sigma^2)$ (see Baladi, 2001). The variance σ^2 is related to autocorrelations $C_n(\varphi, \varphi, f, \mu)$ by $\sigma^2 = \sum_{n=-\infty}^{\infty} C_n$ (Chernov and Markarian, 2006) so a prerequisite for the CLT is the summability of C_n . Mixing ($C_n \rightarrow 0$) therefore does not imply the CLT, we require stronger conditions on its decay:

Definition 2.1. We say that $f : X \rightarrow X$ preserving μ enjoys exponential decay of correlations if there exists constants $0 < \theta < 1$ and $c(\varphi, \psi) > 0$ such that

$$|C_n(\varphi, \psi, f, \mu)| \leq c\theta^n.$$

Similarly we say that f enjoys polynomial decay of correlations if there exists $\alpha > 0$ and $c(\varphi, \psi) > 0$ such that

$$|C_n(\varphi, \psi, f, \mu)| \leq cn^{-\alpha}.$$

It is easy to see that correlations are summable in the exponential case but this condition generally fails in the polynomial case for $\alpha \leq 1$. In non-uniformly hyperbolic systems, polynomial decay of correlations is typical (Hu, 2001) and so the CLT may fail with the standard \sqrt{n} scaling. This slow decay can aggravate numerical studies, e.g. calculating Lyapunov exponents, whose convergence is observed to follow a similar law. In the discussion above we have imposed minimal conditions on the observable φ , merely that it is real valued. Typically we state an explicit function space $\Phi(X)$ and say e.g. that correlations decay exponentially for f for $\varphi \in \Phi(X)$.

Definition 2.2. Let $a > 0$. We say that $\varphi : X \rightarrow \mathbb{R}$ is *Hölder continuous* with exponent a if there exists $C > 0$ such that $|\varphi(x) - \varphi(x')| \leq Cd(x, x')^a$ for all $x, x' \in X$.

[‡]Equivalently ‘converges in distribution’.

The space of Hölder continuous functions is a common choice for $\Phi(X)$ and, unless explicitly stated otherwise, can be assumed for the rest of this section. With fluid mixing observables in mind (e.g. temperature, concentration) imposing this regularity on φ is reasonable as such observables are assumed to be smooth or at least piecewise smooth.

For linear, uniformly hyperbolic systems like the Cat Map, correlations decay exponentially for Hölder continuous observables and superexponentially for C^∞ observables (Baladi, 2001). Early approaches to these and more general Anosov systems employed spectral methods, establishing a spectral gap for the transfer operator. Finite Markov partitions were key here, the symbolic representation linking their dynamics to classical one dimensional models of statistical mechanics whose theory (thermodynamic formalism) could be drawn upon and expanded. For more information see Bowen (1975); Ruelle (1978).

Development of methods for establishing correlation decay rates in more general hyperbolic systems was driven by studies of dispersing billiards[§]. Here the tools developed to deal with Anosov systems weren't effective as Markov partitions for the billiards maps were no longer finite, rendering the symbolic representation inefficient (Chernov and Markarian, 2006). Other efforts (Bunimovich et al., 1991) yielded suboptimal bounds on decay rates until the seminal work of Young whose construction (commonly referred to as a *Young tower*) established exponential decay of correlations for certain dispersing billiards, first using the traditional transfer operator (Young, 1998) then image coupling methods (Young, 1999). The approach is tractable for a wider class of hyperbolic systems with singularities, including maps of relevance to us, so we provide some details. For a measure preserving system (X, \mathcal{A}, μ, f) and positive measure $A \in \mathcal{A}$, the Poincaré recurrence theorem says that the *return time* function $r_A : A \rightarrow \mathbb{N}$, $x \mapsto \inf\{n > 0 \mid f^n(x) \in A\}$ is well defined for almost every $x \in A$. Young considers a reference set Δ_0 with *hyperbolic product structure*: the intersection of continuous families of unstable and stable manifolds $\{\gamma^u\}$ and $\{\gamma^s\}$, with each γ^u meeting each γ^s transversally at a single point (see Young, 1998 for a precise definition). Correlation decay is then linked to recurrence on Δ_0 as follows. If there exists $C > 0$ and $\theta < 1$ such that

$$\mu(\{x \in \Delta_0 \mid R(x; f, \Delta_0) > n\}) < C\theta^n, \quad (2.2)$$

then correlations of f decay exponentially for Hölder observables. Here $R(x; f, \Delta_0)$ denotes the return time to Δ_0 under f with additional technical constraints; see the original papers for details. The revised approach of Young (1999) also allowed slower mixing rates to be addressed: If there exists $C > 0$ and $\alpha > 0$ such that

$$\mu(\{x \in \Delta_0 \mid R(x; f, \Delta_0) > n\}) < Cn^{-\alpha}, \quad (2.3)$$

then correlations of f decay polynomially for Hölder observables. In some systems Δ_0 may be simple to construct and the return time distribution straightforward to bound, see e.g. Chernov and Young (2000) where the scheme is applied to the Cat Map. In general, however, the manifold structure may be too complicated to explicitly construct Δ_0 . Even if this were possible, we would have to deal with all the iterates of f to understand its recurrence, a similarly prohibitive condition. Extensions to the theory thus focused on methods which avoided explicitly constructing Δ_0 and reduced to checking simple conditions on one iterate of the map f (or perhaps some finite number of iterates f^m). This resulted, after the work of Chernov (1999); Markarian (2004) in the following scheme of Chernov and Zhang (2005). They assume a number of conditions (**CZ1-7**) on a map $f : M \rightarrow M$ with singularity set S . We state these explicitly later in Chapter 6, jumping forwards now to their main theorem. Given a curve W , denote its length by $|W|$ and its connected components

[§]Poincaré maps of these billiards fall into the category of 'smooth maps with singularities' as defined in section 1.4

of $W \cap (M \setminus \mathcal{S})$ by W_i .

Theorem 2.1 (Chernov and Zhang, 2005, Theorem 10 with $m = 1$). *Let f be defined on a 2D manifold M and satisfy the requirements (CZ1-7). Suppose*

$$\liminf_{\delta \rightarrow 0} \sup_{W: |W| < \delta} \sum_i \lambda_i^{-1} < 1, \quad (2.4)$$

where the supremum is taken over unstable manifolds W and λ_i denotes the minimal expansion factor on W_i . Then the map $f : M \rightarrow M$ enjoys exponential decay of correlations.

The final key requirement (2.4) states that the cutting up of forward images of local manifolds by S is dominated by expansion in their lengths via hyperbolicity. In many systems, expansion factors vary widely depending on the location of W in M and may be weak in certain regions. If we expect expansion to dominate *eventually*, i.e. once W is mapped to regions of stronger expansion, condition (2.4) may be replaced by a multi-step expansion condition comparing the expansion under f^m to the cutting by $S_m = \cup_{i=0}^{m-1} H^{-i}(S)$.

Alongside giving (relatively) straightforward to verify conditions for exponential mixing, the scheme can be used to deduce non-exponential mixing rates as follows. Suppose $H : X \rightarrow X$ has suspected polynomial decay of correlations. We discuss the case $\alpha = 1$ here, motivated by the Poincaré map of the Bunimovich stadium (originally Bunimovich, 1974, for an overview see Chernov and Zhang, 2005) and linked twist maps. Choosing a subset $M \subset X$ where hyperbolicity appears ‘strong’, we define the first return map $H_M(x) = H^{r_M(x)}(x)$, using its strong hyperbolic properties over one (or several) iterates to satisfy (2.4). It follows, taking $f = H_M$ in the above theorem, that $H_M : M \rightarrow M$ exhibits exponential decay of correlations and admits a Young tower with base $\Delta_0 \subset M$ and exponential tail distribution

$$\mu(\{x \in M \mid R(x; H_M, \Delta_0) > n\}) < C\theta^n. \quad (2.5)$$

Suspicion of polynomial decay of correlations normally follows from observing

$$\mu(\{x \in X \mid R(x; H, M) > n\}) < Cn^{-1}, \quad (2.6)$$

which we extend, making use of (2.5), to return time statistics to the subset $\Delta \subset M$:

$$\mu(\{x \in X \mid R(x; H, \Delta_0) > n\}) < Cn^{-1}. \quad (2.7)$$

Comparing with (2.3), we may then directly appeal to the results of Young and polynomial decay of correlations follows. The step between (2.6) and (2.7) is non-trivial and typically relies on utilising unique mapping behaviour of H_M . Early efforts, see Chernov and Zhang (2005); Markarian (2004), established weaker bounds $|C_n| < c(\ln n)^2/n$ for the stadium map. Chernov and Zhang (2008) saw the improvement of these bounds to the expected $\mathcal{O}(1/n)$ law, we revisit this work later in Chapter 6. Springham and Sturman (2014) applied the above theory to linked twist maps, in particular the example sketched in Figure 2.2 with $x_0 = y_0 = 0$, $x_1 = y_1 = 1/2$. Similar to the method of establishing the mixing property, they appealed to the good hyperbolic behaviour over returns to $P \cap Q$ and established a two-step expansion for the return map. Recovering (2.7) relied on a unique feature of the map, that long returns to $P \cap Q$ were ‘isolated’, i.e. immediately succeeded and preceded by immediate returns. A geometric argument (Sturman and Springham, 2013) gave an optimal lower bound on correlations, establishing $|C_n| = \mathcal{O}(1/n)$.

Recalling condition (KS1) from Theorem 1.4, a modification was made to the one-step expansion condition in Chernov and Zhang (2009) to deal with systems satisfying (KS1) but only with $a < 1$. In such systems, the unstable manifold $|W|$ may be cut up by S into an arbitrarily

large number of pieces W_n . If the expansion factors satisfy $\lambda_n \sim cn$ then achieving the bound (2.4) is challenging, indeed the sum may even diverge. Note that the linked twist map[¶] studied in Springham and Sturman (2014) is of type $a < 1$ but, again, isolation of long return times gave sufficient geometric information to reduce (2.4) to a finite summation. The new one-step expansion condition requires some $q \in (0, 1]$ such that

$$\liminf_{\delta \rightarrow 0} \sup_{W:|W|<\delta} \sum_i \left(\frac{|W|}{|V_i|} \right)^q \frac{|W_i|}{|W|} < 1, \quad (2.8)$$

where the supremum is taken over all unstable curves, W_i are the components of W split by the singularity set for f , $V_i = f(W_i)$. In essence, (2.8) ensures that components of the images of short unstable curves grow on average (see Chernov and Zhang, 2009). This, together with some adjustments to the **(CZ1-7)** conditions, gives exponential decay of correlations for Hölder observables.

[¶]More precisely the return map, on which most of the analysis is based, is of type $a < 1$.

Chapter 3

Mixing by Piecewise Linear Shears

3.1 Guide for the following chapters

The rest of this thesis is organised as follows. We begin by defining a general framework of *alternating shear maps*, encompassing all the systems studied in later chapters. We explore their typical dynamics with some numerical visualisations and establish conditions under which they exhibit non-hyperbolic or hyperbolic behaviour, characterised by elliptic islands or non-zero Lyapunov exponents a.e. respectively. We apply these results to a family of maps which limits onto the Cat Map and Cerbelli and Giona’s map, establishing parameter windows of hyperbolicity and elliptic behaviour. In Chapter 4 we prove mixing properties over subsets of the hyperbolic windows, motivated by **(Q1)**. We next consider a two-parameter family of maps composing two non-monotonic shears, addressing **(Q2)**. Chapter 5 considers the situation of unbounded return times in a non-monotonic system, which poses an inherent challenge to proving mixing properties. We explore how it may be overcome, proving mixing properties of a non-monotonic linked twist map and a new map, the orthogonal tents map (OTM), the natural generalisation of Cerbelli and Giona’s map with two non-monotonic shears. We show that this map has a polynomial mixing rate in Chapter 6, in contrast to the exponential mixing rate seen elsewhere in the parameter space. Finally in Chapter 7 we study a broader range of mixing protocols, summarise our work in terms of **(Q1-3)**, and suggest natural extensions.

3.2 Alternating shear maps framework

Let $0 \leq a_i < b_i \leq 1$ and $f_i : [a_i, b_i] \rightarrow \mathbb{R}$ be differentiable, we call f_i a *twist function*. Given a collection of twist functions f_i , $i = 1, \dots, N$ with mutually disjoint domains satisfying $\cup_i [a_i, b_i] = [0, 1)$, we define a *horizontal shear* $F : \mathbb{T}^2 \rightarrow \mathbb{T}^2$ piecewise by $F(x, y) = (x + f_i(y), y) \bmod 1$ for $y \in [a_i, b_i)$. We remark that F is continuous if for each $i = 1, \dots, N - 1$ we have $\lim_{y \rightarrow b_i} f_i(y) = f_{i+1}(a_i) \bmod 1$ and $\lim_{y \rightarrow b_i} f_N(y) = f_1(a_i) \bmod 1$. We say that F is *non-monotonic* if there exists an open interval on which some f_i satisfies $f'_i > 0$ and another on which some f_j satisfies $f'_j < 0$.

We define *vertical shears* as piecewise functions $G(x, y) = (x, y + g_i(x)) \bmod 1$ for collections of twists g_i . An *alternating shear map* (ASM) $H : \mathbb{T}^2 \rightarrow \mathbb{T}^2$ is a composition of vertical and horizontal shears $H = G \circ F$. Table 3.1 gives the parameterised families of ASMs considered in subsequent chapters. Application of the map H models performing a single ‘stir’ on the domain and iteratively applying H gives the simplest possible stirring protocol of alternating F, G, F, G, \dots . The majority of this thesis will be restricted to analysis of this simple stirring protocol as the key aspects of the mixing dynamics are captured by repeated iteration of ASMs and typically this choice of protocol maximises stretching and folding behaviour over a fixed number of shear applications. We make

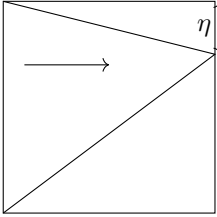
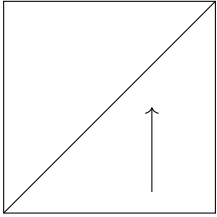
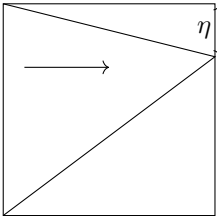
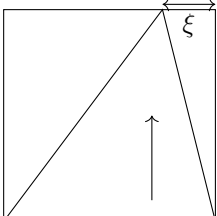
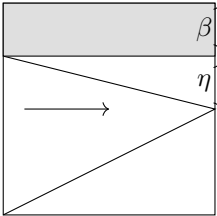
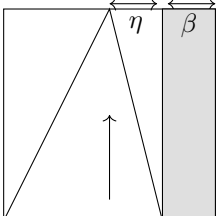
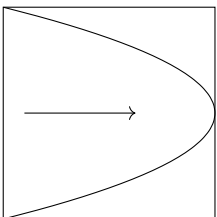
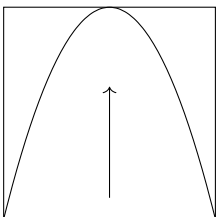
Map	F	G	Twist functions	Comments
H_η			$f_1 : [0, 1 - \eta) \rightarrow \mathbb{R},$ $y \mapsto y/(1 - \eta)$ $f_2 : [1 - \eta, 1) \rightarrow \mathbb{R},$ $y \mapsto (1 - y)/\eta$ $g_1 : [0, 1) \rightarrow \mathbb{R},$ $x \mapsto x$	Piecewise linear. Gives Cerbelli and Giona's map at $\eta = 1/2$. Limits pointwise onto the Cat Map as $\eta \rightarrow 0$.
$H_{(\xi, \eta)}$			$f_1 : [0, 1 - \eta) \rightarrow \mathbb{R},$ $y \mapsto y/(1 - \eta)$ $f_2 : [1 - \eta, 1) \rightarrow \mathbb{R},$ $y \mapsto (1 - y)/\eta$ $g_1 : [0, 1 - \xi) \rightarrow \mathbb{R},$ $x \mapsto x/(1 - \xi)$ $g_2 : [1 - \xi, 1) \rightarrow \mathbb{R},$ $x \mapsto (1 - x)/\xi$	Piecewise linear. Limits pointwise onto H_η as $\xi \rightarrow 0$. Gives the Orthogonal Tents Map (OTM) at $\xi = \eta = 1/2$.
$H_{\eta, \beta}$			See section 5.2.1	Piecewise linear. Limits pointwise onto a class of LTMs as $\eta \rightarrow 0$. Limits pointwise onto the map $H_{(\eta, \eta)}$ as $\beta \rightarrow 0$.
PSM			$f_1 : [0, 1) \rightarrow \mathbb{R},$ $y \mapsto 4y(1 - y)$ $g_i = f_i$	Continuous, nonlinear Parabolic velocity profile modelling Poiseuille flow.

Table 3.1: A collection of non-monotonic ASMs $H = G \circ F$.

this idea more concrete in Chapter 7 when we consider a wider variety of stirring protocols.

All ASMs considered will be non-monotonic, that is, composed of one or more non-monotonic shears. As a starting point towards a general theory of non-monotonic ASMs we will largely restrict our analytical work to piecewise linear ASMs, i.e. with linear twist functions. An ergodic theory analysis of these systems is tractable and piecewise linear ASMs still exhibit a variety of dynamics typical to laminar fluid mixing. We relax the piecewise linearity condition in Chapter 7 and perform a numerical analysis of the Parabolic Shears Map (PSM). We begin with a qualitative look at the typical mixing dynamics resulting from iterating a piecewise linear non-monotonic ASM.

3.3 Visualisation of piecewise linear ASMs

Consider the map H_η at $\eta = 2/5$. Figure 3.1 gives two visualisations of the mixing dynamics. The first (a) shows the orbits of a grid of 400 equally spaced points under repeated application of H_η . It is a Poincaré section of the underlying continuous time dynamics (alternating periodically between horizontal and vertical shear flows), sampled at the end of each ‘stir’. The phase space clearly splits into regions of regular and chaotic behaviour, with elliptic islands about the period three orbits $z_k \in \{(2/3, 13/15), (0, 13/15), (1/3, 1/5)\}$, $\zeta_k \in \{(1/3, 11/15), (0, 11/15), (2/3, 2/5)\}$ surrounded by a chaotic sea. Points starting within an island trace out ellipses around the periodic orbit, forming invariant subspaces which act as a barrier to mixing. Behaviour outside of these islands appears ergodic and chaotic, with the orbits eventually hitting every positive measure subset in the sea and neighbouring orbits separating at an exponential rate. As a visualisation tool for ASMs, Poincaré sections provide a computationally cheap way of assessing mixing quality by highlighting regions of regular behaviour. A disadvantage, however, is that small or particularly thin islands can often become lost in the noise of the surrounding chaotic sea. Such analysis is also purely qualitative, making effective comparison of mixing quality over a family of ASMs challenging.

An alternative is to study finite time Lyapunov exponent (FTLE) fields across a uniform grid of points. For any two points z, z' within an island, separated by a vector $v \neq 0$, the distance between their images $H^n(z), H^n(z')$ behaves as $\|DH_z^n v\|$ and is always bounded above by maximum island diameter. This uniform bound gives $\lim_{n \rightarrow \infty} \frac{1}{n} \ln \|DH_z^n v\| \leq 0$. Note that since H preserves the Lebesgue measure, DH_z^n takes values in $SL(2)$. By Oseledec’s theorem (Theorem 1.1), if some vector v gave $\chi(z, v) < 0$ then some other v' would give $\chi(z, v') = -\chi(z, v) > 0$. It follows that $\chi(z, v) = 0$ for all $v \neq 0$ so we expect small FTLEs within islands, decaying to 0 as we consider more and more iterates of the map. In the ergodic, chaotic region around these islands, we expect Lyapunov exponents to converge to some single non-zero quantity. An illustration of this is given in Figure 3.1(b) where the FTLE field has been calculated for a uniform grid of a million points over two thousand iterates. Alongside capturing the qualitative picture of the mixing dynamics, this data set quantifies the average rate of stretching in the chaotic sea and allows us to estimate the measure of the islands by simply counting FTLEs below a certain threshold. We can estimate to arbitrary precision by increasing the grid density and iterating for longer with tighter thresholds, albeit with increased computational cost. In systems exhibiting slower than exponential mixing rates, it may require very large n for $\frac{1}{n} \ln \|DH_z^n v\|$ to satisfy convergence criteria.

The visualisation methods described above both aim to describe asymptotic mixing behaviour. With applications in mind, it is also important to consider mixing efficiency of ASMs over a smaller number of iterates. We can make a qualitative assessment of this by splitting the domain into two subsets and simply iterate both forwards, essentially modelling the mixing behaviour of the underlying flow on two initially segregated fluids. We illustrate this in Figure 3.2 where the effect of H_η, \dots, H_η^5 is shown on two strips, coloured red and blue. Comparing with Figure 3.1 we note that the elliptic islands are still the primary barrier to mixing, alongside the non-uniform rates of

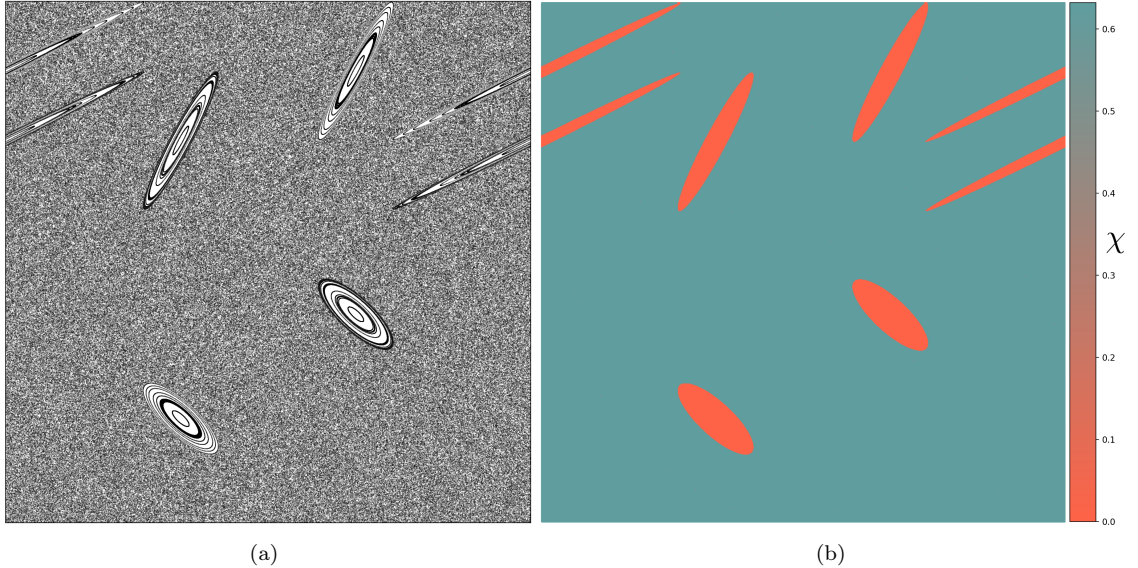


Figure 3.1: (a) Orbits of a grid of points over 3000 iterates of H_η at $\eta = 2/5$. (b) FTLE field for the same map over a uniform grid of 1000×1000 points, 2000 iterates considered.

stretching and contraction in the surrounding chaotic sea. For this reason, even when considering short time scale mixing, being able to predict and measure island structures is desirable. We explore the conditions under which island structures exist and what dictates their measure in the next section.

3.4 Island structure analysis

Let \mathcal{D} denote the singularity set for a piecewise linear ASM $H : \mathbb{T}^2 \rightarrow \mathbb{T}^2$. The set $S_n = \cup_{i=0}^{n-1} H^{-i}(\mathcal{D})$ then divides up the torus into regions A_j on which the cocycle DH_z^n is constant. That is, points $z \in A_j$ all experience the same stretching behaviour over the next n applications of H . If z is periodic with period n and DH_z^n is elliptic, then necessarily Lyapunov exponents $\chi(z, v)$ will be zero and we can expect $\chi(z', v) = 0$ for z' in some neighbourhood of z , dictated by the proximity of S_n to z . We make this precise with the following proposition.

Proposition 3.1. *Let $H : \mathbb{T}^2 \rightarrow \mathbb{T}^2$ be a piecewise linear, continuous, area-preserving map with singularity set \mathcal{D} . Suppose H admits an order n periodic orbit $\{z_1, z_2, \dots, z_n\}$ such that the associated cocycle $M = DH_{z_1}^n$ satisfies $|\text{tr}(M)| < 2$ and $\text{dist}(z_k, \mathcal{D}) > 0$ for $k = 1, \dots, n$. Then there exists an ellipse E centred at z_1 such that $H^n(E) = E$ and H is non-ergodic.*

Proof. Let $\overline{B(z, r)}$ denote the closed ball of radius r centred at z . Given that $\text{dist}(z_k, \mathcal{D}) > 0$ for $k = 1, \dots, n$, we can find $r^* > 0$ such that $H^k(\overline{B(z_1, r^*)}) \cap \mathcal{D} = \emptyset$ for $k = 0, \dots, n$. Letting $\|\cdot\|$ denote the operator norm, a lower bound on r^* is given by

$$(\|DH_{z_1}\| \cdot \|DH_{z_2}\| \cdot \dots \cdot \|DH_{z_n}\|)^{-1} \cdot \min_{k=1, \dots, n} \text{dist}(z_k, \mathcal{D}) > 0.$$

It follows that any point z in this ball also has derivative cocycle $DH_z^n = M$. Denote the complex conjugate of a point $\zeta = a + bi \in \mathbb{C}$ by $\bar{\zeta} = a - bi$. By the condition on its trace, M has distinct eigenvalues $\lambda, \bar{\lambda}$ on the unit circle with non-zero imaginary parts. Their associated complex eigenvectors will be of the form $(a \pm bi, 1)^T$. It is easily verified that $\text{Im}\lambda \neq 0$ implies $b \neq 0$ and we may assume without loss of generality that λ has associated eigenvector $(a + bi, 1)^T$ with $b > 0$.

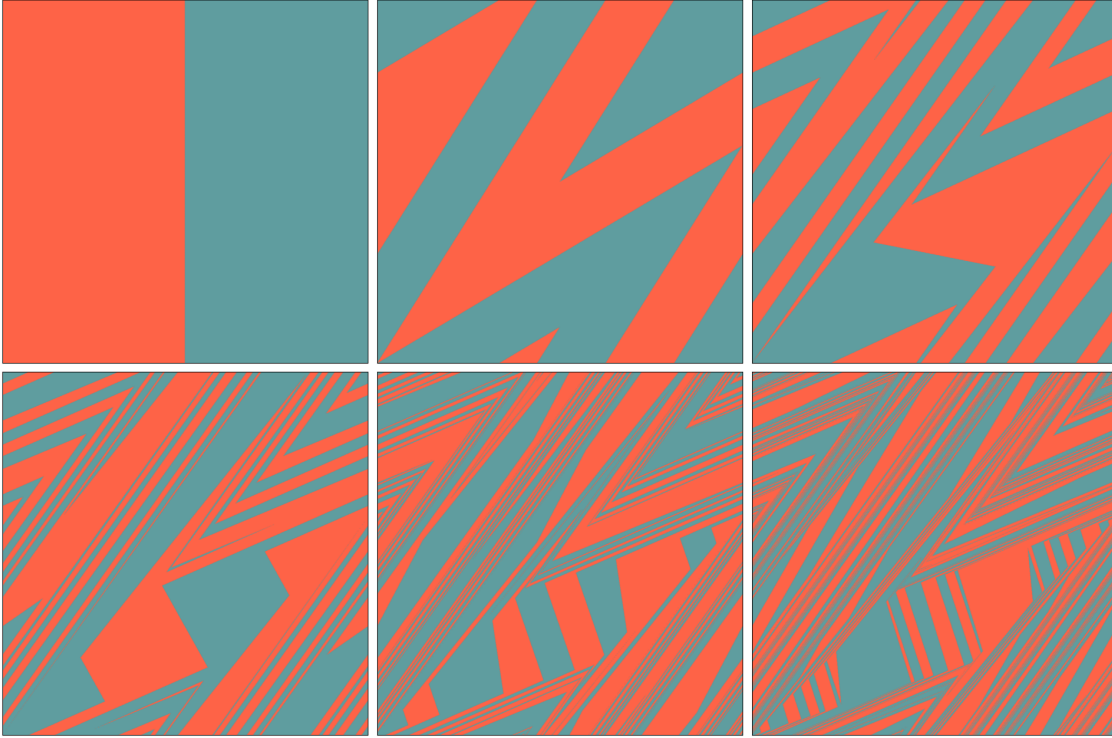


Figure 3.2: Mixing behaviour of H_η at $\eta = 2/5$ on two initially segregated regions coloured red and blue.

Writing the components of M as m_i , the system of equations is

$$\begin{aligned} m_1(a + bi) + m_2 &= \lambda(a + bi) \\ m_3(a + bi) + m_4 &= \lambda \end{aligned}$$

which, by equating real and imaginary parts, reduces to

$$m_1 = \operatorname{Re}\lambda + \frac{a}{b}\operatorname{Im}\lambda, \quad m_2 = -\left(b + \frac{a^2}{b}\right)\operatorname{Im}\lambda, \quad m_3 = \frac{1}{b}\operatorname{Im}\lambda, \quad m_4 = \operatorname{Re}\lambda - \frac{a}{b}\operatorname{Im}\lambda. \quad (3.1)$$

Define the matrices*

$$P = \begin{pmatrix} \sqrt{b} & \frac{a}{\sqrt{b}} \\ 0 & \frac{1}{\sqrt{b}} \end{pmatrix}, \quad R = \begin{pmatrix} \operatorname{Re}\lambda & -\operatorname{Im}\lambda \\ \operatorname{Im}\lambda & \operatorname{Re}\lambda \end{pmatrix}$$

which have unit determinants and satisfy

$$\begin{aligned} MP &= \begin{pmatrix} m_1 & m_2 \\ m_3 & m_4 \end{pmatrix} \begin{pmatrix} \sqrt{b} & \frac{a}{\sqrt{b}} \\ 0 & \frac{1}{\sqrt{b}} \end{pmatrix} = \frac{1}{\sqrt{b}} \begin{pmatrix} m_1b & m_1a + m_2 \\ m_3b & m_3a + m_4 \end{pmatrix} \\ &= \frac{1}{\sqrt{b}} \begin{pmatrix} b\operatorname{Re}\lambda + a\operatorname{Im}\lambda & a\operatorname{Re}\lambda - b\operatorname{Im}\lambda \\ \operatorname{Im}\lambda & \operatorname{Re}\lambda \end{pmatrix} \\ &= \frac{1}{\sqrt{b}} \begin{pmatrix} b & a \\ 0 & 1 \end{pmatrix} \begin{pmatrix} \operatorname{Re}\lambda & -\operatorname{Im}\lambda \\ \operatorname{Im}\lambda & \operatorname{Re}\lambda \end{pmatrix} = PR. \end{aligned}$$

Hence $P^{-1}MP$ is a rotation matrix and therefore preserves the unit circle: $P^{-1}MPS^1 = S^1$ where we define $S^1 = \{(u, v)^T \in \mathbb{R}^2 \mid u^2 + v^2 = 1\}$. It follows that $MPS^1 = PS^1$, so M preserves the set

*The idea to use the matrix P , which greatly simplifies our analysis, came from Gidea et al. (2011).

PS^1 . Let $(x, y)^T = P(u, v)^T$, then $(u, v)^T = P^{-1}(x, y)^T$ so that

$$\left(\frac{x}{\sqrt{b}} - \frac{ay}{\sqrt{b}}\right)^2 + (\sqrt{b}y)^2 = 1,$$

which simplifies to

$$x^2 - 2axy + (a^2 + b^2)y^2 - b = 0. \quad (3.2)$$

This is in the form of a general quadratic equation

$$Ax^2 + Bxy + Cy^2 + Dx + Ey + F = 0 \quad (3.3)$$

and represents an ellipse if $B^2 - 4AC < 0$. Indeed

$$\begin{aligned} B^2 - 4AC &= (-2a)^2 - 4(1)(a^2 + b^2) \\ &= -4b^2 < 0. \end{aligned}$$

Write the major and minor axes of this ellipse as r_1 and θr_1 respectively, where $0 < \theta \leq 1^\dagger$. If $a \neq 0$ then its major axis will make an angle α with the x -axis, where

$$\tan(2\alpha) = \frac{2ab}{b^2 - a^2 - 1}.$$

Write this ellipse centred at the origin as $E(0, r_1, \theta, \alpha)$. By linearity, M also preserves ellipses $E(0, r, \theta, \alpha)$ for $r > 0$. Taking $r = r^*$, we have that $E := E(z_1, r^*, \theta, \alpha) \subset \overline{B(z_1, r^*)}$. It follows that $H^n(E) = E$ as required. Let V be the region bounded by E and containing z_1 , then the set $U = \cup_{k=0}^{n-1} H^k(V)$ is invariant under H with measure $\mu(U) = n\pi\theta(r^*)^2 > 0$. If necessary we can take a smaller r^* to ensure that U does not have full measure, then H is not ergodic. \square

While the crude lower bound $n\pi\theta(r^*)^2$ on the unmixed region is enough to prove non-ergodicity, tighter bounds would help us assess the overall mixing quality. The above proof gives a collection of ellipses $\{E_k\}_{k=1, \dots, n}$ such that each E_k is centred at z_k and bounds a region V_k with $H(V_k) = V_{k+1 \bmod n}$. We now ask, how large can we make the regions V_k and still retain invariance? This amounts to scaling up the ellipses E_k until they touch the singularity set \mathcal{D} . We will then compare the measures of each V_k , finding an upper bound on how much we can scale up the ellipses by, which gives formula for the total measure of the unmixed region around the periodic orbit $\mu(U) = n \min_k \mu(V_k)$.

Fix k and lift \mathbb{T}^2 to the plane by $L: \mathbb{T}^2 \rightarrow \mathbb{R}^2$ so that $z_k \mapsto (0, 0)$. Let S_i denote the segments which make up $L(\mathcal{D})$, write the lines which contain them as $y = \beta_i x + \gamma_i$. Note that since points on the torus are at most a distance $1/\sqrt{2}$ apart, we need only consider the segments in the ball $B(0, 1/\sqrt{2})$. The image $\mathcal{E} = L(E_k)$ is now an ellipse centred at the origin and can be described by the equation

$$Ax^2 + Bxy + Cy^2 + F = 0$$

which bounds a region \mathcal{V} of measure

$$\mu(\mathcal{V}) = \frac{2\pi|F|}{\sqrt{4AC - B^2}}. \quad (3.4)$$

For each S_i , to ensure that $\mathcal{V} \cap S_i = \emptyset$ we require that $\mathcal{E} \cap S_i$ is empty or a single point. Solving the line intersection equations gives

$$Ax^2 + Bx(\beta_i x + \gamma_i) + C(\beta_i x + \gamma_i)^2 + F = 0$$

† We have equality when PS^1 is a circle, the case $a = 0, b = 1$.

or equivalently

$$(A + B\beta_i + C\beta_i^2)x^2 + (B\gamma_i + 2C\beta_i\gamma_i)x + (C\gamma_i^2 + F) = 0.$$

Single intersection implies that

$$(B\gamma_i + 2C\beta_i\gamma_i)^2 - 4(A + B\beta_i + C\beta_i^2)(C\gamma_i^2 + F) = 0$$

which is solved by

$$F_i := \frac{(B\gamma_i + 2C\beta_i\gamma_i)^2}{4(A + B\beta_i + C\beta_i^2)} - C\gamma_i^2.$$

Hence the largest such \mathcal{E} which avoids $L(\mathcal{D})$ bounds a region \mathcal{V} of measure

$$\mu(\mathcal{V}) = \inf_i \frac{2\pi|F_i|}{\sqrt{4AC - B^2}}.$$

Now $V_k = L^{-1}(\mathcal{V})$ so we have found an expression for $\mu(V_k) = \mu(\mathcal{V})$ as required. We now repeat this over each $k = 1, 2, \dots$ and compare to find $\mu(U) = n \min_k \mu(V_k)$. The values A, B, C for each ellipse E_k can be derived from the eigenvector of the cocycle $DH_{z_k}^n$ as described in the proof of Proposition 3.1. We carry out this procedure explicitly for the map H_η :

Proposition 3.2. *The map $H_\eta : \mathbb{T}^2 \rightarrow \mathbb{T}^2$ is non-ergodic for $1/3 < \eta < (9 - \sqrt{33})/8 \approx 0.407$. In particular it admits elliptic islands with total measure*

$$\mu(\mathcal{U}) \geq h(\eta) = \frac{\pi\eta(1-\eta)\sqrt{\alpha(\eta)}}{9\eta^2 - 21\eta + 9} \quad (3.5)$$

where $\alpha(\eta) = 36\eta^3 - 93\eta^2 + 54\eta - 9$.

Proof. The periodic orbits identified for H_η at $\eta = 2/5$ extend to general η and are given by

$$\dots \rightarrow z_1 = \left(\frac{2}{3}, 1 - \frac{\eta}{3}\right) \rightarrow z_2 = \left(0, 1 - \frac{\eta}{3}\right) \rightarrow z_3 = \left(\frac{1}{3}, \frac{1}{3} - \frac{\eta}{3}\right) \rightarrow \dots$$

and

$$\dots \rightarrow \zeta_1 = \left(\frac{1}{3}, 1 - \frac{2\eta}{3}\right) \rightarrow \zeta_2 = \left(0, 1 - \frac{2\eta}{3}\right) \rightarrow \zeta_3 = \left(\frac{2}{3}, \frac{2}{3} - \frac{2\eta}{3}\right) \rightarrow \dots$$

which are bounded away from \mathcal{D} . Starting with z_1 , the cocycle $DH_{z_1}^3$ is given by

$$DH_{z_1}^3 = \begin{pmatrix} 1 & \frac{1}{1-\eta} \\ 1 & \frac{2-\eta}{1-\eta} \end{pmatrix} \begin{pmatrix} 1 & -\frac{1}{\eta} \\ 1 & \frac{\eta-1}{\eta} \end{pmatrix}^2 = \begin{pmatrix} \frac{\eta^2-4\eta+2}{\eta(\eta-1)} & \frac{-3\eta^2+6\eta-2}{\eta^2(\eta-1)} \\ \frac{3\eta^2-7\eta+3}{\eta(\eta-1)} & \frac{\eta^2-7\eta^2+10\eta-3}{\eta^2(\eta-1)} \end{pmatrix}$$

and is elliptic for $1/3 < \eta < (9 - \sqrt{33})/8$. On this parameter range, its eigenvectors $(a \pm bi, 1)^T$ are complex with imaginary part

$$b = \frac{(1-\eta)\sqrt{\alpha}}{2\eta(3\eta^2 - 7\eta + 3)}. \quad (3.6)$$

It follows from Proposition 3.1 that H_η is non-ergodic on this parameter range and we proceed to calculate the measure of the elliptic islands using the procedure described above. Lifting to the plane and translating $z_1 \rightarrow (0, 0)$ sends the discontinuity lines $y = 1$ and $y = 1 - \eta$ to $y = \eta/3$ and $-2\eta/3$ so that $\beta_i = 0$ and $\gamma_i \in \{\eta/3, -2\eta/3\}$. Now F_i reduces to $(B\gamma_i)^2/(4A) - C\gamma_i^2$ which, combining with the values A, B, C from (3.2), gives $F_i = -b^2\gamma_i^2$. Hence the largest ellipse \mathcal{E}_1 about z_1 which avoids \mathcal{D} bounds an region \mathcal{V}_1 of measure

$$\mu(\mathcal{V}_1) = \inf_i \frac{2\pi|F_i|}{\sqrt{4AC - B^2}} = \frac{2\pi b^2 (\eta/3)^2}{\sqrt{4b^2}} = \frac{\pi\eta^2 b}{9}.$$

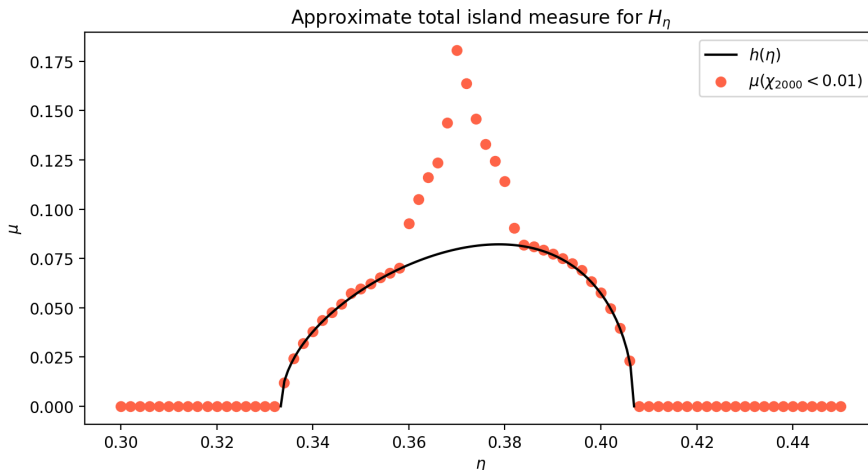


Figure 3.3: Approximate total island measure for H_η over $0.3 \leq \eta \leq 0.45$ using finite time Lyapunov exponents over 2000 iterates. An analytical lower bound $h(\eta)$ is shown as the solid line.

One can perform a similar calculation on z_2, z_3 and verify $\mu(\mathcal{V}_3) > \mu(\mathcal{V}_2) = \mu(\mathcal{V}_1)$ so that the total measure of the islands around the orbit z_k is $\pi\eta^2 b/3$. Performing the same calculation over the other periodic orbit ζ_k yields the same total island measure so that around both orbits we have islands of total measure

$$h(\eta) = \frac{2\pi\eta^2 b}{3} = \frac{2\pi\eta^2(1-\eta)\sqrt{\alpha}}{6\eta(3\eta^2 - 7\eta + 3)}.$$

The lower bound (3.5) then follows, noting that there may be other elliptic periodic orbits which we have not considered. \square

A comparison of this lower bound with approximate total island measure is shown in Figure 3.3. We consider the map H_η where η increases in fixed increments of 0.002 between 0.3 and 0.45. For each of these 76 parameter values, FTLEs are calculated over 2000 iterates on a grid of 350×350 points with those decaying below 0.01 classed as belonging to an island structure. The proportion of such points is then plotted against the analytical lower bound $h(\eta)$. We note that over $0.36 \leq \eta \leq 0.38$ the bound appears suboptimal, owing to the existence of other elliptic periodic orbits which appear and disappear over this narrow parameter window. Beyond the domain of $h(\eta)$ no island structures are captured by the numerics and the dynamics appear globally hyperbolic. That is, no orbits appear to get trapped in an elliptic cycle and each are characterised by non-zero Lyapunov exponents. We explore how to prove this in the next section.

3.5 Establishing hyperbolicity

Given a piecewise linear ASM $H : \mathbb{T}^2 \rightarrow \mathbb{T}^2$ with singularity set \mathcal{D} , let \mathcal{A}_j , $j \in J$ denote the connected components of $\mathbb{T}^2 \setminus \mathcal{D}$ on which the Jacobian DH is constant. Given a point z we define its *itinerary* as the sequence $\mathcal{A}_{j_0}, \mathcal{A}_{j_1}, \dots, \mathcal{A}_{j_n}$ where each j_k is the $j \in J$ is such that $H^k(z) \in \mathcal{A}_j$. This sequence is well defined for all $z \in \mathbb{T}^2 \setminus S_\infty$, where $S_\infty = \lim_{k \rightarrow \infty} S_k$. We may then write the cocycle DH_z^n as the product $\mathcal{M}_{j_{n-1}} \dots \mathcal{M}_{j_0}$ where M_j is DH on \mathcal{A}_j . A typical ASM may admit some \mathcal{M}_j which are hyperbolic and others which are not. A first step towards proving non-zero Lyapunov exponents is to show that any itinerary can be decomposed into blocks $I = \mathcal{A}_{j_k}, \dots, \mathcal{A}_{j_{k+l}}$ such that the corresponding cocycle block $M = \mathcal{M}_{j_{k+l}} \dots \mathcal{M}_{j_k}$ is hyperbolic. Index these cocycle blocks as M_i , $i \in I$, then any cocycle DH_z^n can be written as product of hyperbolic matrices $M_{i_m} \dots M_{i_1}$, perhaps pre-multiplied and post-multiplied by some matrices \mathcal{M}_j which do not form a complete block.

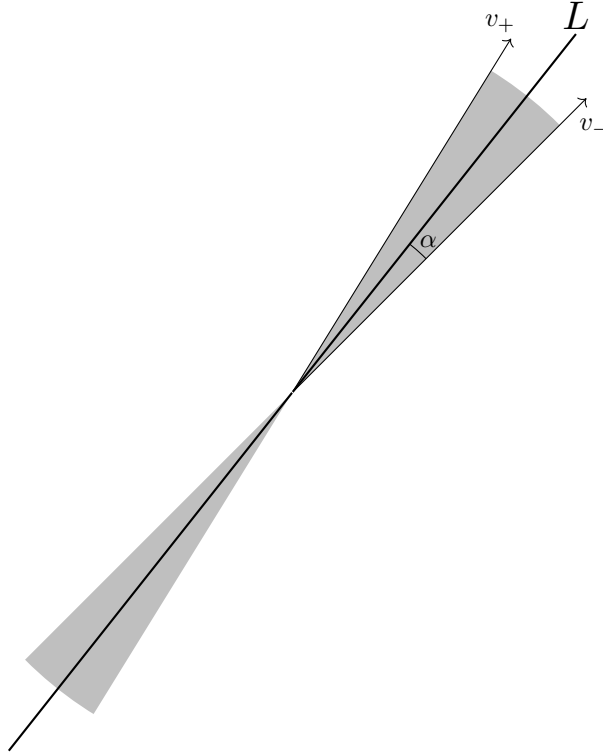


Figure 3.4: Illustration of a cone \mathcal{C} (shaded) with axis L and opening α . Similarly defined as the cone bounded by v_{\pm} containing some vector v parallel to L .

Now as we follow the orbit $H^n(z)$, completing itinerary blocks I_i , we see stretching and contraction of tangent vectors v by the hyperbolic matrices M_i . Note that this does not necessarily imply that $\chi(z, v) \neq 0$ (non-zero average stretching rate) as stretching from one matrix M_i may be immediately undone by contraction from the next. To avoid this situation, we establish *invariant expanding cones*. The use of cones to establish hyperbolicity dates back to the work of Alekseev (1969); a standard definition is as follows:

Definition 3.1 (Chernov and Markarian, 2006). Let $L \in \mathbb{R}^2$ be a line, $0 < \alpha < \pi/2$. A cone \mathcal{C} with axis L and opening α is the set of all vectors v which make an angle $\leq \alpha$ with L .

Note that \mathcal{C} does not include the zero vector. In practice it is often easier to define a cone using the bounding vectors v_{\pm} which make an angle α with L . This defines two cones (one containing L and another containing $L' \perp L$), \mathcal{C} is then uniquely defined by specifying a third vector $v \in \mathcal{C}$ not equal to v_{\pm} . An example illustration is given in Figure 3.4. We define two properties of cones:

Definition 3.2. Given a matrix M , we say that a cone \mathcal{C} is *invariant* under M if $Mv \in \mathcal{C}$ for all $v \in \mathcal{C}$. We say that \mathcal{C} is *expanding* with respect to a norm $\|\cdot\|$ if $\|Mv\| > \|v\|$ for all $v \in \mathcal{C}$.

Let M be a hyperbolic matrix with determinant 1. We seek easily verifiable conditions under which a cone is invariant and expanding under M with respect to a norm $\|\cdot\|$. Write the eigenvalues of M as $\lambda, 1/\lambda$ with $|\lambda| > 1$. Define its unstable, stable eigenvectors as v^u, v^s such that $Mv^u = \lambda v^u$ and $Mv^s = v^s/\lambda$. Normalise them so that $\|v^u\| = \|v^s\| = 1$.

Proposition 3.3. A cone \mathcal{C} , bounded by vectors v_{\pm} , is invariant and expanding under a hyperbolic matrix M if $v^u \in \mathcal{C}$, $v^s \notin \mathcal{C}$, and $\|Mv_{\pm}\| > \|v_{\pm}\|$.

Proof. As M is hyperbolic, $\{v^u, v^s\}$ form a basis for \mathbb{R}^2 . If $v^u \in \mathcal{C}$, $v^s \notin \mathcal{C}$ vectors $v \in \mathcal{C}$ can be written as $v = \alpha v^u + \beta v^s$ where β/α lies in some interval $a \leq \beta/\alpha \leq b$ containing 0 with v_{\pm} parallel to $v^u + av^s$ and $v^u + bv^s$. Applying the transformation gives $Mv = \lambda\alpha v^u + \beta v^s/\lambda$, we verify that

if $\beta/\alpha \in [a, b]$ then $(\beta/\lambda)/(\lambda\alpha) = \beta/(\lambda^2\alpha) \in [a/\lambda^2, b/\lambda^2] \subset [a, b]$ since $|\lambda| > 1$. Hence $Mv \in \mathcal{C}$, satisfying the invariance condition.

For expansion let $\text{ex}(v) := \|Mv\|/\|v\|$, then $\text{ex}(v^u) > 1$ and $\text{ex}(v^s) < 1$. As we rotate v from v^u to v^s , we pass through one of v_\pm and $\text{ex}(v)$ has at most one local minimum. If $\text{ex}(v_\pm) > 1$, then this minimum must lie between v_\pm and v^s , i.e. outside of the cone, so $\{\text{ex}(v) \mid v \in \mathcal{C}\}$ is minimal at one of its boundaries v_\pm . \square

Proposition 3.4. *Given a piecewise linear ASM $H : \mathbb{T}^2 \rightarrow \mathbb{T}^2$, suppose that for a.e. $z \in \mathbb{T}^2$ the cocycle DH_z^n can be split into blocks M_i , $i \in I$, of finite length. If this family of matrices admit a shared invariant expanding cone \mathcal{C} then Lyapunov exponents $\chi(z, v)$ are non-zero for $v \neq 0$.*

Proof. For each z , any $v_0 \in \mathcal{C}$ will remain trapped in the cone \mathcal{C} under premultiplication by the M_i and will be expanded each time by some factor $K_i > 1$. Letting N denote the maximum block length, the average expansion over each iterate is bounded below by $(\min_{i \in I} K_i)^{1/N}$, which is strictly greater than one for finite N . The norm $\|DH_z^n v_0\|$ therefore grows exponentially, producing a positive Lyapunov exponent $\chi(z, v_0) > 0$. The result then follows from Corollary 1.1 to Oseledets' theorem in two dimensions. \square

Establishing hyperbolicity, then, relies on finding suitable itinerary blocks I_i . For some systems these blocks may be obvious but for others, particularly those with many \mathcal{M}_j , the choice may be less clear with the number of possible itineraries over n iterates bounded above by $|J|^n$. As such there is no one-size-fits-all approach to this step but we can suggest some guiding principles. First we must identify the components \mathcal{A}_j on which the \mathcal{M}_j are non-hyperbolic and ensure that a.e. point $z \in \mathcal{A}_j$ escapes, that is, there exists $n \geq 1$ such that $H^n(z) \notin \mathcal{A}_j$. This provides a collection of blocks $M = \mathcal{M}_{j'} M_j^n$ on which we can test the cone conditions. An ideal situation is for all itinerary blocks to terminate on a common component \mathcal{A}_l , with \mathcal{M}_l hyperbolic, as then tangent vectors are pulled towards its unstable eigenvector v_l^u at the end of the block, suggesting invariance in some cone surrounding v_l^u . In practice, establishing such precise mapping behaviour to a single \mathcal{A}_l may be challenging and result in (for large $|J|$) an unwieldy number of long blocks M_i . In such a situation it may be easier to establish mapping behaviour to some family of components \mathcal{A}_j , $j \in J' \subset J$ for which the associated unstable eigenvectors v_j^u of the \mathcal{M}_j are close enough to each other to ensure an invariant cone.

Again, the map H_η serves as a straightforward example for illustrating this process.

Proposition 3.5. *H_η admits non-zero Lyapunov exponents $\chi(z, v) \neq 0$ for almost every $z \in \mathbb{T}^2$, $v \neq 0$, when $0 < \eta < \frac{1}{3}$.*

We give the same argument provided in Myers Hill et al. (2022b), making some minor notational changes.

Proof. To ease notation write $H = H_\eta$. Its Jacobian is given by

$$\mathcal{M}_0 = \begin{pmatrix} 1 & -\frac{1}{\eta} \\ 1 & \frac{\eta-1}{\eta} \end{pmatrix}$$

for over $\mathcal{A}_0 : 1 - \eta < y < 1$, and

$$\mathcal{M}_1 = \begin{pmatrix} 1 & \frac{1}{1-\eta} \\ 1 & \frac{2-\eta}{1-\eta} \end{pmatrix}$$

over $\mathcal{A}_1 : 0 < y < 1 - \eta$. We remark that \mathcal{M}_0 is elliptic for $\eta > 1/4$.

Figure 3.5 gives a partition of \mathbb{T}^2 into three sets $A = \mathcal{A}_1$ and $B, C \subset \mathcal{A}_0$. One can show that $H(A) \subset A \cup B$, $H(B) \subset A \cup C$, $H(C) \subset A$ so that orbits leaving A return after spending one or

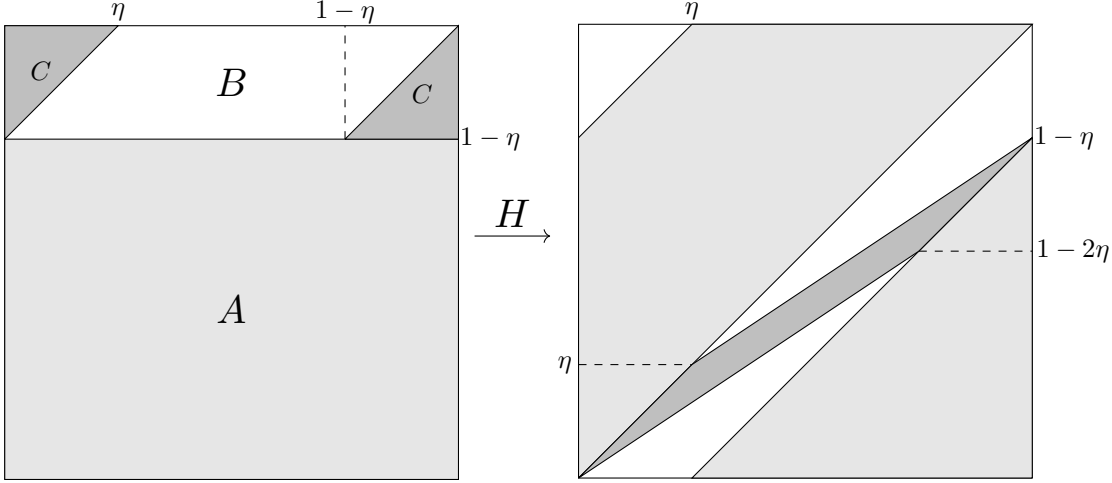


Figure 3.5: Partition of the torus for H , establishing return times to A in $\{1, 2, 3\}$. Case illustrated $\eta = \frac{1}{4}$, the image of the partition is also shown with consistent shading.

two iterations in $B \cup C$. Hence we may form itinerary blocks

$$I_1 = \mathcal{A}_1, \quad I_2 = \mathcal{A}_0 \mathcal{A}_1, \quad I_3 = \mathcal{A}_0 \mathcal{A}_0 \mathcal{A}_1,$$

with corresponding matrices

$$M_1 = \mathcal{M}_1, \quad M_2 = \mathcal{M}_1 \mathcal{M}_0, \quad M_3 = \mathcal{M}_1 \mathcal{M}_0^2,$$

all of which are hyperbolic over $0 < \eta < 1/3$. By Proposition 3.4, it is sufficient to show that these matrices share an invariant expanding cone. Given a vector $v = (v_1, v_2)^T$, define its *gradient* as $g = v_2/v_1$. Starting with invariance, one can verify that the gradients g_i^u, g_i^s of the unstable, stable eigenvectors of M_i satisfy

$$g_1^s(\eta) < g_2^s(\eta) < g_3^s(\eta) < g_3^u(\eta) < g_2^u(\eta) < g_1^u(\eta),$$

for all $0 < \eta < 1/3$ so that the cone bounded by the unstable eigenvectors of M_1 and M_3 is invariant. Explicit expressions for these gradients is available as supplementary material[‡].

It is clear, then, that it is possible to construct an invariant cone and, in fact, we have multiple options. The minimal cone is the smallest gradient range we can take to include all the unstable eigenvectors, defined at each parameter value. This will be a particularly useful construction in section 4.1 as it gives good bounds on the gradients of local unstable manifolds. Its η -dependence, however, makes the expansion factor calculations quite tedious. Given that $g_3^s(\eta) < \inf_{\eta} g_3^u(\eta)$ across $0 < \eta < \frac{1}{3}$, the cone bounded by the vectors v_{\pm} with gradients $g^+ = \sup_{\eta} g_1^u(\eta) = \frac{2}{\sqrt{5}-1}$ and $g^- = \inf_{\eta} g_3^u(\eta) = 1$ is invariant. Write this η -independent cone as $\bar{\mathcal{C}}$; it is sketched explicitly in Figure 3.4. To simplify the calculations take $\|\cdot\|$ to be the $\|\cdot\|_{\infty}$ norm (recall from section 1.4 that we have a free choice of norm) then $\|(v_1, v_2)^T\| = |v_2|$ for all vectors in the cone, since within $\bar{\mathcal{C}}$ we always have $|v_2| \geq |v_1|$. Normalise the cone boundaries as $v_{\pm} = \left(\frac{1}{g^{\pm}}, 1\right)^T$; we calculate:

- $\|M_1(1, 1)^T\| = \frac{2\eta-3}{\eta-1} > 3$
- $\|M_2(1, 1)^T\| = \frac{3\eta^2-7\eta+3}{\eta(1-\eta)} > \frac{9}{2}$
- $\|M_3(1, 1)^T\| = 4 - \frac{10}{\eta} + \frac{3}{\eta^2} > 1$

[‡]See doi.org/10.1007/s00332-022-09790-0

- $\|M_1 \left(\frac{\sqrt{5}-1}{2}, 1 \right)^T\| = \frac{(1+\sqrt{5})(\eta-1)-2}{2(\eta-1)} > \frac{3+\sqrt{5}}{2}$
- $\|M_2 \left(\frac{\sqrt{5}-1}{2}, 1 \right)^T\| = \frac{2\sqrt{5}\eta^2-3\sqrt{5}\eta-5\eta+6}{2\eta(1-\eta)} > \frac{39-7\sqrt{5}}{4}$
- $\|M_3 \left(\frac{\sqrt{5}-1}{2}, 1 \right)^T\| = \frac{(3\sqrt{5}-1)\eta^3-(7\sqrt{5}+7)\eta^2+(3\sqrt{5}+17)\eta-6}{2\eta^2(\eta-1)} > \frac{31-9\sqrt{5}}{4}$

for all $0 < \eta < \frac{1}{3}$, so that the cone is expanding across the parameter range. The result then follows from Proposition 3.4. \square

As a finite collection of lines, the singularity set $\mathcal{D} = \{(x, y) \mid y = 0, 1 - \eta\}$ of the piecewise linear map H_η easily satisfies the assumptions of Katok and Strelcyn's Theorem. As such, much of the work is complete towards showing the mixing property for H_η over $0 < \eta < 1/3$. We pursue this in the following chapter, where we also consider the parameter space $(9 - \sqrt{33})/8 < \eta < 1/2$ and extend our analysis to the map $H_{(\xi, \eta)}$ composing two non-monotonic shears.

Chapter 4

Proving Mixing Results - Bounded Return Times

4.1 Mixing properties of H_η

In this section we establish mixing properties for $H = H_\eta$ over a subset of the hyperbolic range $0 < \eta < 1/3$. In particular, we show:

Theorem 4.1. *H has the Bernoulli property for $0 < \eta < \eta_1 \approx 0.324$.*

This proof was the subject of Myers Hill et al. (2022b). We present the same argument here, making minor notational and organisational changes. Recalling Theorem 1.4, the Bernoulli property follows from condition **(MR)** which requires understanding the mapping behaviour of H and its inverse H^{-1} . The action of H on the ABC partition of Figure 3.5 and the invariant cone \mathcal{C} provide sufficient information about the behaviour of H on \mathbb{T}^2 and DH on the tangent space. We seek similar constructions for H^{-1} . As $H^{-1} = F^{-1} \circ G^{-1}$, the inverse map is differentiable over $z \in \mathbb{T}^2 \setminus G(\mathcal{D})$, with constant Jacobian over the sets $G(\mathcal{A}_0)$, $G(\mathcal{A}_1)$ given by \mathcal{M}_0^{-1} , \mathcal{M}_1^{-1} . Figure 4.1 shows the partition for returns to the set $\mathfrak{a} := G(\mathcal{A}_1)$, passing through $\mathfrak{b} \cup \mathfrak{c} \subset G(\mathcal{A}_0)$. Itineraries follow the same pattern: \mathfrak{a} , \mathfrak{ba} , and \mathfrak{bca} , giving blocks

$$I = G(\mathcal{A}_1), \quad I_2 = G(\mathcal{A}_0)G(\mathcal{A}_1), \quad I_3 = G(\mathcal{A}_0)G(\mathcal{A}_0)G(\mathcal{A}_1),$$

with corresponding matrices \mathfrak{M}_1 , \mathfrak{M}_2 , and \mathfrak{M}_3 respectively. The eigenvectors of each of these matrices allow us to construct an invariant expanding cone \mathcal{C}' . Let $\mathfrak{g}_i^s(\eta)$, $\mathfrak{g}_i^u(\eta)$ be the gradients of the stable, unstable eigenvectors of \mathfrak{M}_i . One can verify that

$$\mathfrak{g}_1^u(\eta) < \mathfrak{g}_2^u(\eta) < \mathfrak{g}_3^u(\eta) < \mathfrak{g}_3^s(\eta) < \mathfrak{g}_2^s(\eta) < \mathfrak{g}_1^s(\eta)$$

for $0 < \eta < \frac{1}{3}$ so that we can take our minimal backwards cone to be the cone bounded by the unstable eigenvectors of \mathfrak{M}_1 and \mathfrak{M}_3 . As before, taking the union of these cones over $0 < \eta < \frac{1}{3}$ gives an η -independent invariant expanding cone $\overline{\mathcal{C}'}$ for H^{-1} .

4.1.1 Establishing ergodicity

By **(KS1-3)** stable and unstable manifolds exist almost everywhere. These are line segments aligned with the subspace E_z^s as defined in Theorem 1.1, taking $f = H$ to find the stable direction, and $f = H^{-1}$ to find the unstable direction. The following lemma provides bounds on the gradients of these line segments.

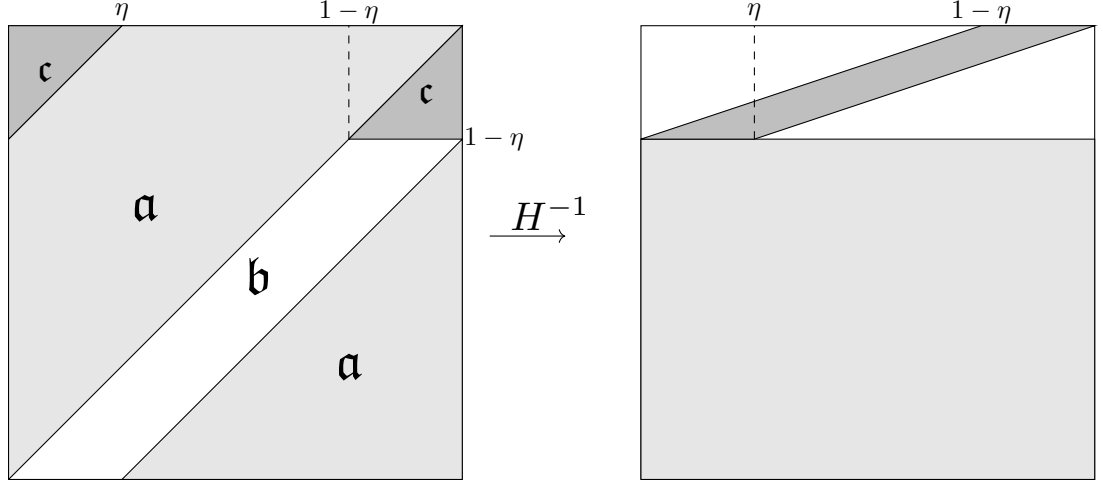


Figure 4.1: A partition of the torus based on returns to \mathbf{a} under H^{-1} and its image under H^{-1} . Case illustrated $\eta = \frac{1}{4}$.

Lemma 4.1. *Given local unstable, stable manifolds $\gamma_u(z)$, $\gamma_s(z)$ at $z \in X'$, let m_0, n_0 be the smallest non-negative integers such that $H^{m_0}(z) \in H(\mathbf{a})$, $H^{-n_0}(z) \in H^{-1}(\mathbf{a})$. Then*

- $H^{m_0}(\gamma_u(z))$ contains a segment γ aligned with some vector $v \in \mathcal{C}$,
- $H^{-n_0}(\gamma_s(z))$ contains a segment γ' aligned with some vector $v' \in \mathcal{C}'$.

Proof. We first note the link between the two minimal cones. Let $v_u(M_j)$, $v_s(M_j)$ be vector subspaces generated by the unstable and stable eigenvectors of some hyperbolic matrix M_j . Clearly $v_u(M_1) = v_s(M_1^{-1}) = v_s(\mathfrak{M}_1)$ and, in fact, we can always relate the stable, unstable eigenvectors of M_j to the unstable, stable eigenvectors of \mathfrak{M}_j . For $j = 2, 3$ these are given by

$$v_s(M_j) = \mathcal{M}_1 v_u(\mathfrak{M}_j) \quad (4.1)$$

and

$$v_u(M_j) = \mathcal{M}_1 v_s(\mathfrak{M}_j). \quad (4.2)$$

To see this, note that in the $j = 2$ case:

$$\begin{aligned} M_2^{-1} \cdot \mathcal{M}_1 v_u(\mathfrak{M}_2) &= \mathcal{M}_0^{-1} \mathcal{M}_1^{-1} \cdot \mathcal{M}_1 v_u(\mathfrak{M}_2) \\ &= (\mathcal{M}_1 \mathcal{M}_1^{-1}) \mathcal{M}_0^{-1} v_u(\mathfrak{M}_2) \\ &= \mathcal{M}_1 \mathfrak{M}_2 v_u(\mathfrak{M}_2) \\ &= c \mathcal{M}_1 v_u(\mathfrak{M}_2) \end{aligned}$$

for some c with $|c| > 1$. This implies $\mathcal{M}_1 v_u(\mathfrak{M}_2)$ is in the stable subspace of M_2 , showing (4.1). The same argument applied to the right hand side of (4.2) yields $|c| < 1$ as required. The case $j = 3$ is analogous.

Now let $\gamma_u(z)$ be the local unstable manifold at some $z \in X'$. By the partition construction, m_0 is in $\{0, 1, 2\}$. Now $H^{m_0}(\gamma_u(z))$ is a piecewise linear curve, the union of at most 3 line segments γ_j . Since z lies outside of the singularity set S , $H^{m_0}(z)$ lies in the interior of some γ_j , call it γ .

By definition, for any $\zeta, \zeta' \in \gamma_u(z)$

$$\text{dist}(H^{-n}(\zeta), H^{-n}(\zeta')) \rightarrow 0$$

as $n \rightarrow \infty$. By extension we have that

$$\text{dist}(H^{-n}(\xi), H^{-n}(\xi')) \rightarrow 0 \quad (4.3)$$

for any $\xi, \xi' \in \gamma$.

This means that $H^{-1}(\gamma) \subset H^{-1}(\mathfrak{a})$ must be aligned with some vector in the cone region \mathcal{C}_s bounded by $v_s(\mathfrak{M}_1)$ and $v_s(\mathfrak{M}_3)$, which includes $v_s(\mathfrak{M}_2)$. For if it falls outside of this region, it will be pulled into the invariant expanding cone $\overline{\mathcal{C}'}$ for H^{-1} , which contradicts (4.3). Now if we apply H to $H^{-1}(\gamma) \subset A$, γ must align with a vector in $\mathcal{M}_1 \mathcal{C}_s$. By (4.2), this is precisely the minimal cone for H . The argument for local stable manifolds is analogous, instead using (4.1). \square

The main result of this section is the following.

Proposition 4.1. *Condition (M) holds for H when $0 < \eta < \eta_1 \approx 0.324$.*

We will use the known behaviour of returns to $H(A)$ (resp. $H^{-1}(\mathfrak{a})$), and expansion during this return, to grow the images of local manifolds to the point where an intersection is certain in $A_1 = H(A) \cap H^{-1}(\mathfrak{a})$. This is a quadrilateral, shown in Figure 4.2. We call any line segment in A_1 which joins its upper and lower boundaries a v -segment. Similarly we call any line segment in A_1 which joins its left and right (sloping) boundaries a h -segment. Clearly v - and h -segments must always intersect. Given $z, z' \in X'$ our aim, then, is to find m, n such that $H^m(\gamma_u(z))$ contains a v -segment and $H^{-n}(\gamma_s(z'))$ contains a h -segment.

The key issue we have to overcome in the growth stage is that while the images of the segments may grow exponentially in total length, the alternating-sign property (as described in Cerbelli and Giona, 2005) means that they can repeatedly double back on themselves, meaning that their total diameter does not necessarily grow. We state some useful properties of line segments:

Definition 4.1. Let Γ be a line segment. We define the *height* of Γ as $\ell_v(\Gamma) = \nu(\{y \mid (x, y) \in \Gamma\})$, the *width* of Γ as $\ell_h(\Gamma) = \nu(\{x \mid (x, y) \in \Gamma\})$, where ν is the Lebesgue measure on \mathbb{R} .

Definition 4.2. Given a partition element A , we say that Γ has *simple intersection* with A if its restriction to A is empty or a single line segment. Conversely we say that Γ has *non-simple intersection* with A if its restriction to A contains more than one connected component. A sketch of these cases is given in Figure 4.2.

Due to vectors in \mathcal{C} having dominant vertical components and vectors in \mathcal{C}' having dominant horizontal components, $\ell_v(\cdot)$ (resp. $\ell_h(\cdot)$) measures the diameters of images of unstable (resp. stable) manifolds under H (resp. H^{-1}). Non-simple intersection ensures we have sufficient geometric information to establish v - and h -segments. We start with the method for growing unstable manifolds, partitioning $\mathfrak{a} = H(A)$ into three sets \mathfrak{a}_i , where the subscript i is the return time of its elements to \mathfrak{a} . This is shown in Figure 4.2. The growth stage involves iteratively applying the following lemma.

Lemma 4.2. *Let Γ_{p-1} be a line segment satisfying*

(C1) $\Gamma_{p-1} \subset \mathfrak{a}$,

(C2) Γ_{p-1} is aligned with some vector in the minimal invariant cone \mathcal{C} for H ,

and which has simple intersection with each of the \mathfrak{a}_i . Then there exists a line segment Γ_p satisfying (C1), (C2),

(C3) $\Gamma_p \subset H^i(\Gamma_{p-1})$ for a chosen $i \in \{1, 2, 3\}$, and

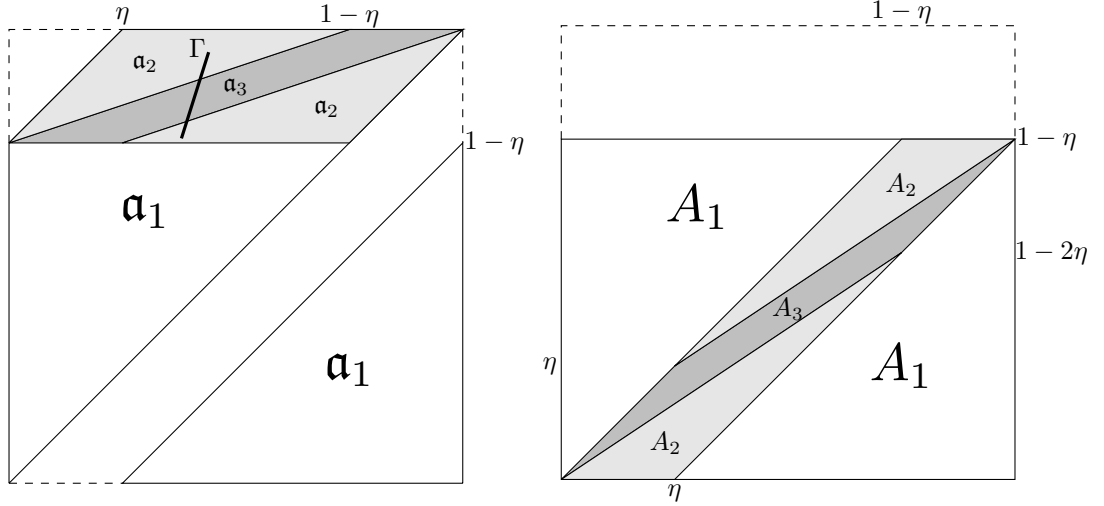


Figure 4.2: Left: a partition of \mathbf{a} into three parts \mathbf{a}_i , where i is the return time of points in \mathbf{a}_i to \mathbf{a} . A line segment Γ is shown which has simple intersection with \mathbf{a}_3 and non-simple intersection with \mathbf{a}_2 . Right: the equivalent plot for A , considering return times under H^{-1} .

(C4) $\ell_v(\Gamma_p) \geq (1 + \delta) \ell_v(\Gamma_{p-1})$ for some $\delta = \delta(\eta) > 0$, independent of Γ_{p-1} .

Proof. The process of generating Γ_p from Γ_{p-1} is as follows. Based on the location of Γ_{p-1} in \mathbf{a} , we will restrict Γ_{p-1} to one of the \mathbf{a}_i then map it forwards under H^i to give Γ_p , satisfying (C3). By definition of the \mathbf{a}_i , (C1) is satisfied. If Γ_{p-1} is aligned with some $v \in \mathcal{C}$, Γ_p is aligned with $M_i v$. By cone invariance, this is also in \mathcal{C} , so (C2) is satisfied.

The expansion in diameter can be bounded from below by

$$K_i(\eta) = \inf_{v \in \mathcal{C}} \frac{\|M_i v\|}{\|v\|}$$

where, again, we are using the $\|\cdot\|_\infty$ norm. Since we have already shown that the cone is expanding, if Γ_{p-1} is entirely contained within some \mathbf{a}_i then taking $\Gamma_p = H^i(\Gamma_{p-1})$ ensures expansion in diameter. Where it becomes more interesting is when Γ_p intersects multiple \mathbf{a}_i . Looking at each of the M_i across the invariant cone, at every parameter value M_1 has the smallest expansion on its eigenvector $v_u(M_1)$, M_2 and M_3 have the smallest expansion on the other cone boundary $v_u(M_3)$. Letting λ_i be the magnitude of the unstable eigenvalue of M_i , K_1 and K_3 are given by

$$K_1(\eta) = \lambda_1(\eta) = \frac{3 - 2\eta + \sqrt{5 - 4\eta}}{2(1 - \eta)}$$

and

$$K_3(\eta) = \lambda_3(\eta) = \frac{3 - 9\eta + 2\eta^2 + \sqrt{-36\eta^3 + 93\eta^2 - 54\eta + 9}}{2\eta^2}.$$

Next

$$K_2(\eta) = \frac{2\eta - 3}{1 - \eta} \frac{1}{g_3^u(\eta)} + \frac{3 - \eta}{\eta},$$

calculated using the lower elements of M_2 , the unit vector $\left(\frac{1}{g_3^u}, 1\right)^T$, and the fact that M_2 reverses the orientation of vectors in the cone.

Throughout, we assume that Γ_{p-1} has simple intersection with each of the \mathbf{a}_i . Suppose Γ_{p-1} intersects \mathbf{a}_1 and \mathbf{a}_2 , and write its restriction to these sets as Γ^1 and Γ^2 respectively. Since $K_1(\eta)$ and $K_2(\eta)$ are both greater than 2 for all $0 < \eta < \frac{1}{3}$, and one of Γ^1, Γ^2 has diameter greater than or equal to $\frac{1}{2}$, we can restrict to that segment Γ^i and expand under H^i to establish that Γ_p has larger

diameter than Γ_{p-1} . Now suppose Γ_{p-1} intersects \mathbf{a}_1 and \mathbf{a}_3 . If the proportion of the diameter of Γ_{p-1} in \mathbf{a}_1 is greater than $\frac{1}{K_1(\eta)}$, we can simply expand from there. Otherwise Γ^3 has diameter greater than or equal to $1 - \frac{1}{K_1(\eta)}$, and we can expand from \mathbf{a}_3 provided that

$$K_3(\eta) > \frac{1}{1 - \frac{1}{K_1(\eta)}}.$$

The above is satisfied for approximately $\eta < 0.332$. The case where Γ_{p-1} intersects \mathbf{a}_2 and \mathbf{a}_3 is similar and does not further restrict the parameter range.

Now suppose Γ_{p-1} intersects \mathbf{a}_1 , \mathbf{a}_2 , and \mathbf{a}_3 . By the same argument as before, we require

$$K_3(\eta) > \frac{1}{1 - \frac{1}{K_1(\eta)} - \frac{1}{K_2(\eta)}}.$$

Solving this numerically, the above inequality is satisfied for approximately $\eta < 0.327$. In any case, then, (C4) is satisfied. \square

The method for growing the backwards images of local stable manifolds is entirely analogous. We divide up $A = H^{-1}(\mathbf{a})$ into A_1, A_2, A_3 based on return time to A under H^{-1} (see Figure 4.2). The relevant hyperbolic matrices associated with the return map are \mathfrak{M}_i , which share an invariant, expanding cone \mathcal{C}' . We make minor adjustments to the (C) conditions to give:

Lemma 4.3. *Let Γ_{p-1} be a line segment satisfying*

$$(C1') \quad \Gamma_{p-1} \subset A,$$

$$(C2') \quad \Gamma_{p-1} \text{ is aligned with some vector in the minimal invariant cone } \mathcal{C}' \text{ for } H^{-1},$$

and which has simple intersection with each of the A_i . Then there exists a line segment Γ_p satisfying (C1'), (C2'),

$$(C3') \quad \Gamma_p \subset H^{-i}(\Gamma_{p-1}) \text{ for a chosen } i \in \{1, 2, 3\},$$

$$(C4') \quad \ell_h(\Gamma_p) \geq (1 + \delta) \ell_h(\Gamma_{p-1}) \text{ for some } \delta = \delta(\eta) > 0, \text{ independent of } \Gamma_{p-1}.$$

Proof. As before, define

$$\mathcal{K}_i(\eta) = \inf_{v \in \mathcal{C}'} \frac{\|\mathfrak{M}_i v\|}{\|v\|}.$$

All of the \mathfrak{M}_i see their minimum cone expansion on the cone boundary given by the unstable eigenvector of \mathfrak{M}_3 . The key calculation we have to make is the parameter value η_1 such that

$$\mathcal{K}_3(\eta) > \frac{1}{1 - \frac{1}{\mathcal{K}_1(\eta)} - \frac{1}{\mathcal{K}_2(\eta)}} \quad (4.4)$$

for $0 < \eta < \eta_1$. We can solve numerically, giving $\eta_1 \approx 0.324$. \square

Both of these lemmas hold, then, provided that $0 < \eta < \eta_1$. They ensure the exponential growth in diameter of the segments Γ_p up to some Γ_P which has non-simple intersection with some \mathbf{a}_i (or A_i for the stable case). At this point we will map directly into v - and h -segments.

Lemma 4.4. *For any line segment $\Gamma_P \subset \mathbf{a}$ which is aligned with a vector in \mathcal{C} and has non-simple intersection with some \mathbf{a}_i , $H^k(\Gamma_P)$ contains a v -segment for some $k \in \{0, 3, 5\}$.*

Proof. All non-simple intersections give useful geometric information about Γ_P . Suppose it has non-simple intersection with \mathbf{a}_3 . Then as a connected straight line segment, it must *traverse* \mathbf{a}_1 , that is, it connects the upper and lower boundaries of \mathbf{a}_1 , passing through \mathbf{a}_1 . By definition, this Γ_P contains a v -segment. Now suppose Γ_P has non-simple intersection with \mathbf{a}_2 . It follows that Γ_P

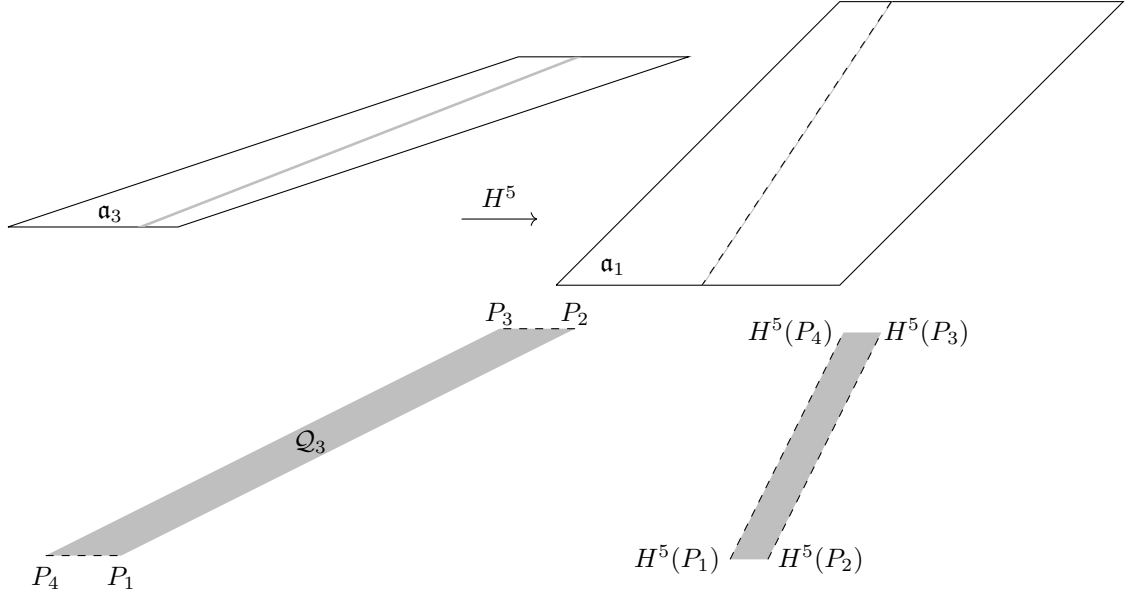


Figure 4.3: Case (I). A quadrilateral $\mathcal{Q}_3 \subset \mathfrak{a}_3$ and its image in \mathfrak{a}_1 under H^5 . Any line segment Γ which joins the sloping boundaries of \mathfrak{a}_3 will join the sloping boundaries of \mathcal{Q}_3 , and hence $H^5(\Gamma \cap \mathcal{Q}_3)$ is a v -segment.

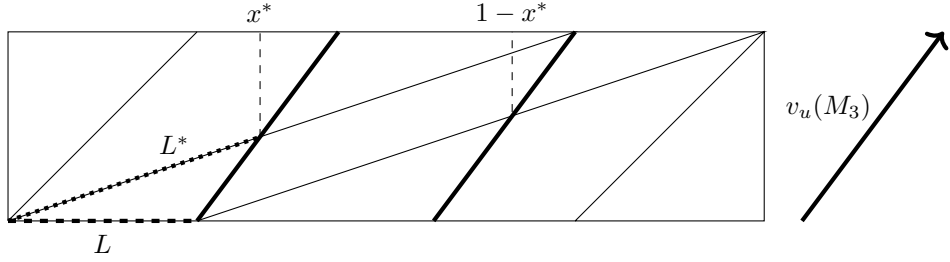


Figure 4.4: Geometry of line segments satisfying case (II).

traverses \mathfrak{a}_1 (v -segment) or Γ_P traverses \mathfrak{a}_3 , connecting its sloping boundaries. This is case (I). We will show that any such segment contains a v -segment in its 5th image. Finally assume that Γ_P has non-simple intersection with \mathfrak{a}_1 . It follows that we traverse \mathfrak{a}_3 , case (I), or the restriction to \mathfrak{a}_2 is sufficiently large that its 3rd image contains a v -segment, case (II).

We will start by showing case (I). Consider the quadrilateral $\mathcal{Q}_3 \subset \mathfrak{a}_3$, defined by the four points P_j , shown in Figure 4.3. Explicit coordinates for each of these points are given as part of the supplementary material. All of the points in the interior of \mathcal{Q}_3 share the same itinerary path under 5 iterations of H , $BCAAA$, so $H^5(\mathcal{Q}_3)$ is also a quadrilateral and any straight line segment contained within \mathcal{Q}_3 maps into a new straight line segment under H^5 . It is clear that any Γ_P which traverses \mathfrak{a}_3 , joining its sloping boundaries, must also traverse \mathcal{Q}_3 . The sloping boundaries of \mathcal{Q}_3 map into the upper and lower boundaries of \mathfrak{a}_1 under H^5 , so if Γ_P connects these sloping boundaries, $H^5(\Gamma_P)$ contains a v -segment.

Case (II) can be argued similarly. We assume that Γ_P has non-simple intersection with \mathfrak{a}_1 and that we do not traverse \mathfrak{a}_3 in such a way that we can argue as in case (I). We will concentrate first on the left portion of \mathfrak{a}_2 ; we shall soon see that the analysis for the right portion is analogous.

Since we assume Γ_P does not connect the sloping sides of \mathfrak{a}_3 , it must intersect the \mathfrak{a}_1 , \mathfrak{a}_3 boundary on L , shown in Figure 4.4. The solid thick line shown is aligned with clockwise bound on the invariant cone, with gradient g_3^u . The intersection of Γ_P with the \mathfrak{a}_3 , \mathfrak{a}_2 boundary must lie in L^* , whose x -range is bounded above by x^* .

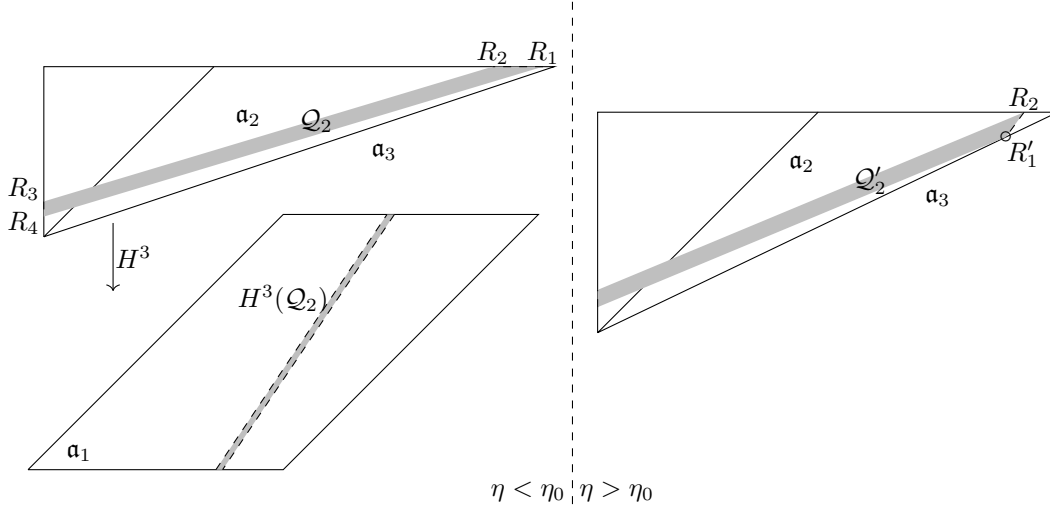


Figure 4.5: Case (II) for η either side of the critical value $\eta_0 = 1 - \frac{1}{\sqrt{2}}$.

Let Γ be the restriction to \mathfrak{a}_2 . We will show that Γ , constrained by the x^* , intersects a quadrilateral whose image under H^3 stretches across \mathfrak{a}_1 in much the same way we saw in case (I). For $\eta \leq \eta_0 = 1 - \frac{1}{\sqrt{2}} \approx 0.293$, such a quadrilateral \mathcal{Q}_2 exists and has all four corners on the lines $x = 0, y = 1$ (see left hand side of Figure 4.5). Starting with the top-right and cycling anti-clockwise, these corners have coordinates

$$R_1 = \left(\frac{-\eta^3 + 7\eta^2 - 13\eta + 7}{3\eta^2 - 10\eta + 8}, 1 \right), \quad R_2 = \left(\frac{2(2\eta^2 - 5\eta + 3)}{3\eta^2 - 10\eta + 8}, 1 \right),$$

$$R_3 = \left(0, \frac{5\eta^2 - 13\eta + 8}{\eta^2 - 7\eta + 8} \right), \quad \text{and} \quad R_4 = \left(0, \frac{-\eta^3 + 7\eta^2 - 14\eta + 8}{\eta^2 - 7\eta + 8} \right).$$

Any line segment joining the $\mathfrak{a}_2, \mathfrak{a}_3$ boundary to the $\mathfrak{a}_2, \mathfrak{a}_1$ boundary must connect the parallel boundaries of \mathcal{Q}_2 and therefore maps into a v -segment. At the critical value $\eta = \eta_0$ the point R_1 lies on the rightmost corner of \mathfrak{a}_2 , $(1 - \eta, 1)$. Now let $\eta > \eta_0$ and consider the quadrilateral \mathcal{Q}'_2 defined by the corners R_2, R_3, R_4 , and

$$R'_1 = (x', y') = \left(\frac{-\eta^2 + 2\eta - 1}{\eta(2\eta - 3)}, \frac{-2\eta^2 + 6\eta - 4}{2\eta - 3} \right). \quad (4.5)$$

This final corner also maps into $y = 1 - \eta$ under H^3 . Hence any line segment which joins the parallel sides of \mathcal{Q}'_2 maps into a v -segment. Certainly if $x^*(\eta) < x'(\eta)$ for $\eta_0 < \eta < \eta_1$, then Γ will connect the parallel sides of \mathcal{Q}'_2 . First we solve line equations to give

$$x^*(\eta) = \frac{\eta g_3^u(\eta)}{g_3^u(\eta) - \frac{\eta}{1-\eta}}$$

which is bounded from above by $x^*(\eta_1) \approx 0.5512$. Next by (4.5),

$$x'(\eta) = \frac{-\eta^2 + 2\eta - 1}{\eta(2\eta - 3)}$$

which is bounded from below by $x'(\eta_1) \approx 0.5998$, establishing the result.

The case where Γ traverses the other (right) part of \mathfrak{a}_2 is analogous. Note that we can transform one part of \mathfrak{a}_2 into the other by reflecting in the lines $y = 1 - \frac{\eta}{2}$ and $x = \frac{1}{2}^*$, written as $(S_x \circ S_y)(\mathfrak{a}_2) = \mathfrak{a}_2$. Now the images of \mathcal{Q}_2 and \mathcal{Q}'_2 under $S_x \circ S_y$ span across the right portion of \mathfrak{a}_2 in an analogous

*Since the lines are orthogonal, $S_x \circ S_y = S_y \circ S_x$.

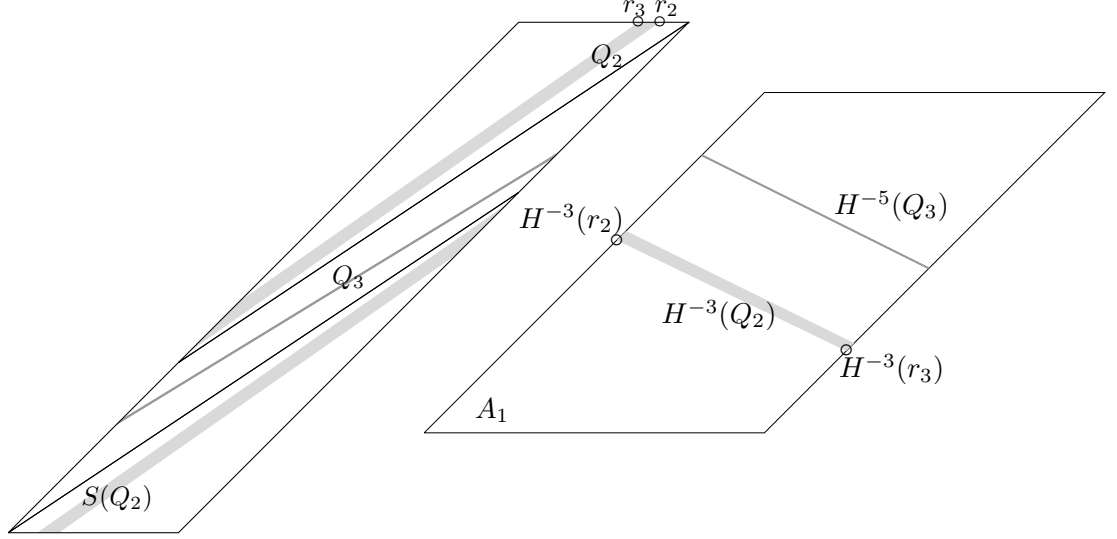


Figure 4.6: Two quadrilaterals $Q_2 \subset A_2$ and $Q_3 \subset A_3$ which map into A_1 under H^{-3} and H^{-5} respectively. Their long boundaries map into the sloping boundaries of A_1 , so segments Γ which join these long boundaries map into h -segments. Case illustrated $\eta = \frac{1}{4}$.

fashion to before and also map into v -segments under H^3 . Making the same assumption as before, that case (II) holds but case (I) does not, we know that Γ intersects the $\mathbf{a}_2, \mathbf{a}_3$ boundary at some point (x, y) with $x > 1 - x^*$ (see Figure 4.4). To ensure that Γ connects the parallel sides of $(S_x \circ S_y)(Q'_2)$, it remains to check that the x -coordinate of $(S_x \circ S_y)(x', y')$, $1 - x'$, is strictly less than $1 - x^*$ across $\eta_0 < \eta < \eta_1$. Indeed, $1 - x'(\eta) < 1 - x^*(\eta)$ follows from $x^*(\eta) < x'(\eta)$, established in the previous case. \square

Lemma 4.5. *For any line segment $\Gamma_P \subset A$ which is aligned with a vector in C' and has non-simple intersection with some A_i , $H^{-k}(\Gamma_P)$ contains a h -segment for some $k \in \{0, 3, 5\}$.*

Proof. The argument is similar to the forwards-time case. A partition of $H^{-1}(\mathbf{a}) = A$ by return time is shown in Figure 4.2. Case (I) assumes that Γ connects the two A_2, A_3 boundaries through A_3 , case (II) assumes that Γ joins the two sloping boundaries of A_1 through $A_2 \cup A_3$, but that case (I) does not hold. We will show that in case (I) $H^{-5}(\Gamma)$ contains a h -segment, and in case (II) $H^{-3}(\Gamma)$ contains a h -segment. Starting with Γ satisfying case (I), Figure 4.6 shows a quadrilateral $Q_3 \subset A_3$ with two short sides on the A_1, A_3 boundaries. It follows that Γ must connect a segment which joins the longer sides of Q_3 , through Q_3 . The argument is now the same as in the forwards time analysis, all points in Q_3 share the same itinerary under 5 iterations of H^{-1} , \mathbf{bcaaa} , so $H^{-5}(Q_3)$ is a quadrilateral in A . One can verify that it is wholly contained in $A_1 \subset A$ and that its longer sides map into its sloping boundaries (see right image in Figure 4.6). $H^{-5}(\Gamma)$ then contains a segment which connects these two boundaries through A_1 , that is, $H^{-5}(\Gamma)$ contains a h -segment. Explicit expressions for the corner coordinates of Q_3 and their images under H^{-5} will be given as supplementary material.

Moving onto Γ satisfying case (II) and first focusing on the upper portion of A_2 , for $\eta \leq \eta_0$ we can follow the same argument, defining a quadrilateral $Q_2 \subset A_2$ with itinerary \mathbf{baa} and $H^{-3}(Q_2) \subset A_1$ (see Figure 4.6). Its long sides must be joined by Γ , and map into the boundary of A_1 , so $H^{-3}(\Gamma)$ contains a h -segment. Starting with the bottom corner of Q_2 nearest the A_2, A_3 boundary and cycling anti-clockwise, label these points as r_1, \dots, r_4 , which have coordinates

$$r_1 = \left(\frac{\eta^3 - 4\eta^2 + 3\eta + 1}{3\eta^2 - 10\eta + 8}, \frac{\eta^3 - 4\eta^2 + 3\eta + 1}{3\eta^2 - 10\eta + 8} \right), \quad r_2 = \left(\frac{5\eta^3 - 20\eta^2 + 24\eta - 8}{4\eta^3 - 18\eta^2 + 23\eta - 8}, 1 - \eta \right),$$

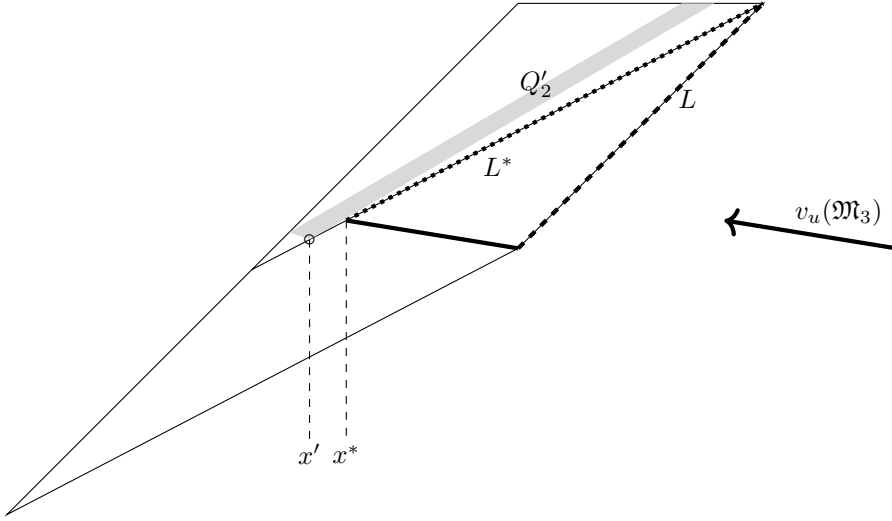


Figure 4.7: Case (II) for $\eta > \eta_0$. Any Γ satisfying case (II) must intersect the A_1A_3 boundary on L and the A_2A_3 boundary on L^* . This gives a lower bound on x^* on the x -coordinate of this intersection so that if $x^* > x'$, then Γ joins the parallel sides of Q'_2 .

$$r_3 = \left(\frac{-\eta^4 + 8\eta^3 - 23\eta^2 + 25\eta - 8}{4\eta^3 - 18\eta^2 + 23\eta - 8}, 1 - \eta \right), \text{ and } r_4 = \left(\frac{2 - \eta^2}{3\eta^2 - 10\eta + 8}, \frac{2 - \eta^2}{3\eta^2 - 10\eta + 8} \right).$$

For $\eta > \eta_0$ we consider the quadrilateral Q'_2 with corners r_2, r_3, r_4 and

$$r'_1 = \left(\frac{3\eta^2 - 5\eta + 1}{\eta(2\eta - 3)}, \frac{-2\eta^3 + 7\eta^2 - 6\eta + 1}{\eta(2\eta - 3)} \right).$$

This is shown in Figure 4.7, with the x -coordinate of r'_1 highlighted as $x'(\eta)$. Like in the forwards-time case, we need to check that $x'(\eta)$ is not so far along the A_2, A_3 boundary that any Γ satisfying case (II) does not connect the parallel sides of Q'_2 . Letting $\mathfrak{g}_3^u(\eta)$ be the gradient of the anti-clockwise invariant cone boundary for H^{-1} , this amounts to showing that $x'(\eta) < x^*(\eta)$ where (x^*, y^*) lies on the intersection of the lines

$$y = \eta + \frac{1 - 2\eta}{1 - \eta}(x - \eta)$$

(the A_2, A_3 boundary) and

$$y = 1 - 2\eta + \mathfrak{g}_3^u(\eta)(x - 1 + \eta),$$

shown as the solid bold line in Figure 4.7. Solving for x gives

$$x^*(\eta) = \frac{\eta^2 + 3\eta - 1 + \mathfrak{g}_3^u(\eta)(1 - \eta)^2}{\mathfrak{g}_3^u(\eta)(1 - \eta) - 1 + 2\eta}.$$

One can now verify that $x'(\eta) < x'(\eta_1) < x^*(\eta_1) < x^*(\eta)$ for all $\eta_0 < \eta < \eta_1$, establishing the result. To conclude case (II) we must extend the analysis to the other portion of A_2 . This process is entirely analogous to the forwards time case, taking reflections in $x = \frac{1}{2}$ and $y = \frac{1}{2} - \frac{\eta}{2}$. An example is shown in Figure 4.6, with the image of Q_2 under these reflections shown as $S(Q_2)$. \square

We are now ready to prove Proposition 4.1.

Proof of Proposition 4.1. Let $\gamma_u(z)$ be the local unstable manifold at some $z \in X'$. Let $m_0 \geq 0$ be the smallest integer such that $H^{m_0}(z) \in \mathfrak{a}$. Then by Lemma 4.1, $H^{m_0}(\gamma_u(z))$ contains a segment Γ_0 in \mathfrak{a} , aligned with some vector in the invariant cone \mathcal{C} . We can then iteratively apply Lemma 4.2 to generate a sequence of line segments with exponentially increasing diameter $(\Gamma_p)_{0 \leq p \leq P}$ with each

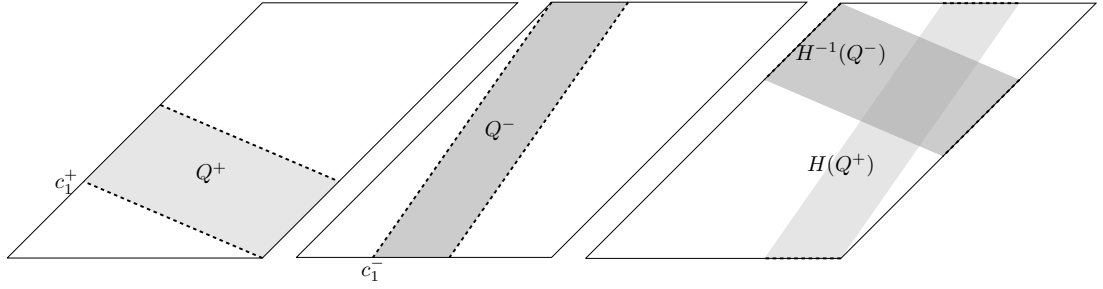


Figure 4.8: Two quadrilaterals Q^+, Q^- in A_1 which map into A_1 under H and H^{-1} respectively. Any v -segment must join the dotted sides of Q^+ , hence maps into another v -segment. Similar for h -segments and Q^- .

$\Gamma_P \subset H^{m_0+m_P}(\gamma_u(z))$ for some $m_P > 0$. Since the sequence has exponentially increasing diameter, after some finite number of steps P , the line segment Γ_P must have non-simple intersection with one of the a_i . Lemma 4.4 then tells us that $H^k(\Gamma_P)$ contains a v -segment for some $k \in \{0, 3, 5\}$. It follows that $H^m(\gamma_u(z))$ contains a v -segment where $m = m_0 + m_P + k$. Similarly given $z' \in X'$, we can apply Lemmas 4.1, 4.3, and 4.5 to find n such that $H^{-n}(\gamma_s(z'))$ contains a h -segment. Since z and z' were arbitrary, condition **(M)** of Theorem 1.4 holds. \square

This establishes H as ergodic over $0 < \eta < \eta_1$. Stronger mixing properties can now be easily shown.

4.1.2 Establishing the Bernoulli property

Proposition 4.2. *Condition **(MR)** holds for H when $0 < \eta < \eta_1 \approx 0.324$.*

Proof. To establish **(MR)** it is sufficient to show that the image of a v -segment under H contains a v -segment, and the image of a h -segment under H^{-1} contains a h -segment. We can approach this in the same way as before, defining quadrilaterals which these segments must traverse and looking at their images. Define the quadrilateral Q^+ by the corners (starting from the leftmost and cycling anti-clockwise)

$$c_1^+ = \left(\frac{1 + \eta - \eta^2}{3 - 2\eta}, \frac{(1 - \eta)^2}{3 - 2\eta} \right), c_2^+ = (0, 0),$$

$$c_3^+ = \left(\frac{(1 - \eta)^2}{3 - 2\eta}, \frac{(1 - \eta)^2}{3 - 2\eta} \right), \text{ and } c_4^+ = \left(\frac{2 - \eta}{3 - 2\eta}, \frac{2(1 - \eta)^2}{3 - 2\eta} \right).$$

This is shown in the first diagram in Figure 4.8. Note that we have shifted the domain horizontally to more easily see A_1 as a quadrilateral. Any v -segment must join the dotted sides of Q^+ , which map into the upper and lower boundaries of A_1 , so v -segments map into v -segments. We can similarly define the quadrilateral Q^- by the corners (starting from the leftmost and cycling anti-clockwise)

$$c_1^- = \left(\frac{1 + \eta - \eta^2}{3 - 2\eta}, 0 \right), c_2^- = \left(\frac{2 - \eta}{3 - 2\eta}, 0 \right), c_3^- = \left(\frac{(1 - \eta)^2}{3 - 2\eta}, 1 - \eta \right), \text{ and } c_4^- = (0, 1 - \eta).$$

Again, h -segments must connect the dotted sides of Q^- , which map into the sloping boundaries of A_1 , hence h -segments map into h -segments. \square

We are now ready to prove the main theorem of this section.

Proof of Theorem 4.1. Noting that **(KS1)** and **(KS2)** were trivially satisfied, the Bernoulli property holds for H over $0 < \eta < \eta_1$ by Theorem 1.4 and Propositions 3.5, 4.1, and 4.2. \square

We now move our attention to the other part of the parameter range nearer Cerbelli and Giona's Map, establishing mixing properties in a subset of $(9 - \sqrt{33})/8 < \eta < 1/2$. As in Myers Hill et al. (2022b) we let $\varepsilon = 1/2 - \eta$ and consider H as an ε -perturbation from the CG map.

4.2 Mixing properties of H_ε

In this section we will show:

Theorem 4.2. H has the Bernoulli property for $\eta_2 \leq \eta < \eta_3$ where $\eta_2 \approx 0.415$ and $\eta_3 \approx 0.491$.

4.2.1 Establishing hyperbolicity

Proposition 4.3. We have non-zero Lyapunov exponents $\chi(z, v) \neq 0$ for almost every $z \in \mathbb{T}^2$, $v \neq 0$, when $0 < \varepsilon < \varepsilon_1 \approx 0.0931$.

Proof. The partition and possible itinerary paths I_j around the partition are the same as before. Define the corresponding matrices M_i using the derivative matrices

$$\mathcal{M}_0 = \begin{pmatrix} 1 & \frac{-2}{1-2\varepsilon} \\ 1 & \frac{-1-2\varepsilon}{1-2\varepsilon} \end{pmatrix} \text{ and } \mathcal{M}_1 = \begin{pmatrix} 1 & \frac{2}{1+2\varepsilon} \\ 1 & \frac{3+2\varepsilon}{1+2\varepsilon} \end{pmatrix}.$$

Again, M_3 is the matrix which dictates our parameter range. It is hyperbolic for $\varepsilon < \varepsilon_1$, where $\varepsilon_1 = \frac{\sqrt{33}-5}{8} \approx 0.0931$. M_2 is hyperbolic for ε strictly greater than 0.

Following Proposition 3.4, it remains to define an invariant cone and show that it is expanding. Defining g_j^u and g_j^s as before, one can verify that

$$g_3^s(\varepsilon) < g_1^s(\varepsilon) < g_2^s(\varepsilon) < g_2^u(\varepsilon) < g_1^u(\varepsilon) < g_3^u(\varepsilon)$$

for $0 < \varepsilon < \frac{1}{\sqrt{3}} - \frac{1}{2} \approx 0.0774$, and

$$g_1^s(\varepsilon) < g_2^s(\varepsilon) < g_2^u(\varepsilon) < g_1^u(\varepsilon) < g_3^u(\varepsilon) < g_3^s(\varepsilon)$$

for $\frac{1}{\sqrt{3}} - \frac{1}{2} < \varepsilon < \varepsilon_1$. Hence the cone \mathcal{C} , bounded by and including the unstable eigenvectors of M_2 and M_3 , is the minimal invariant cone. The common cone $\bar{\mathcal{C}}$ is then defined as the open region bounded by the unstable eigenvector of M_2 at $\varepsilon = 0$ and the unstable eigenvector of M_3 at $\varepsilon = \varepsilon_1$. Under the $\|\cdot\|_\infty$ norm, these are the unit vectors $(1, 1)^T$ and $\left(\frac{\sqrt{33}-3}{6}, 1\right)^T$ respectively. One can show that

- $\|M_1(1, 1)^T\| > \frac{\sqrt{33}+9}{4}$
- $\|M_1\left(\frac{\sqrt{33}-3}{6}, 1\right)^T\| > \frac{9+5\sqrt{33}}{12}$
- $\|M_2(1, 1)^T\| > 1$
- $\|M_2\left(\frac{\sqrt{33}-3}{6}, 1\right)^T\| > 7 - \frac{2\sqrt{33}}{3}$
- $\|M_3(1, 1)^T\| > \frac{9+\sqrt{33}}{6}$
- $\|M_3\left(\frac{\sqrt{33}-3}{6}, 1\right)^T\| > 1$

for all ε in our range, so that our cone is expanding. \square

This establishes non-uniform hyperbolicity. As before, the next section shows ergodicity.

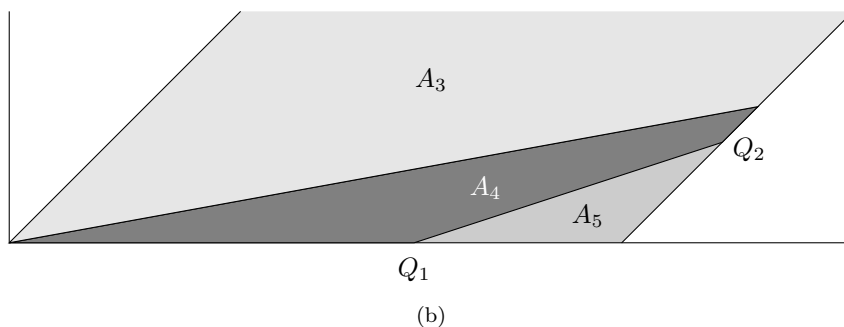
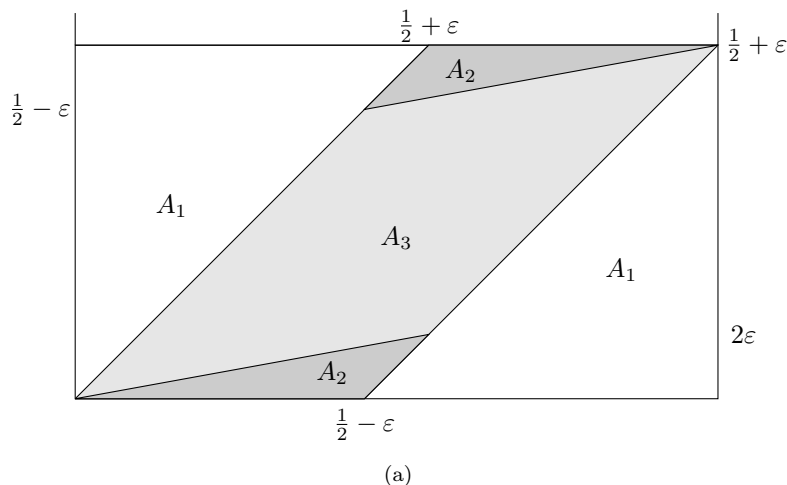


Figure 4.9: Part (a) gives partition of A based on return time to A under iterations of H^{-1} . Part (b) shows a subdivision $A_4 \cup A_5 = A_2$, with the boundary between these sets defined as the segment joining the points Q_1, Q_2 . Case illustrated $\varepsilon = 0.05$.

4.2.2 Establishing ergodicity

Proposition 4.4. *Condition (M) holds for H over $\varepsilon_0 < \varepsilon \leq \varepsilon_2$, where $\varepsilon_0 \approx 0.00925$ and $\varepsilon_2 \approx 0.0850$.*

The overall method for establishing (M) is unchanged. The key constructions are the partitions of $H(A)$ and $H^{-1}(a)$ given in section 4.1.1, and the invariant cones \mathcal{C} for H (given above) and \mathcal{C}' for H^{-1} . Defining the \mathfrak{M}_j as before, \mathcal{C}' is defined at each ε as the cone bounded by (and including) the unstable eigenvectors of \mathfrak{M}_2 and \mathfrak{M}_3 , i.e. the non-zero vectors with gradient $\mathfrak{g}_3^u < \mathfrak{g} < \mathfrak{g}_2^u$. One can show (by the same method as before) that \mathcal{C}' is invariant and expanding.

For the sake of brevity, we will only describe the process of growing the backwards images of local stable manifolds. The process for unstable manifolds is entirely analogous and, due to \mathcal{C} covering a smaller gradient range than \mathcal{C}' , results in less stringent bounds on the parameter range.

While for the η -perturbation the growth stage was relatively straightforward and the h -segment mappings more involved, the opposite is true for the ε -perturbation. If we were to follow the same method as before, reducing the parameter range to satisfy equations like (4.4), we would be left with just a fragment of the parameter range. Our way around this necessitates growing piecewise linear curves rather than line segments. To ensure that we can find the diameter of a curve by summing the diameters of its constituent line segments, we require that a curve *does not double back on itself*, that is, the projection to the x -axis is injective. The lemma for the growth stage is as follows:

Lemma 4.6. *Let Γ_{p-1} be a piecewise linear curve satisfying*

(C0') Γ_{p-1} *does not double back on itself,*

(C1') $\Gamma_{p-1} \subset A$,

(C2') Each line segment in Γ_{p-1} is aligned with some vector in the minimal invariant cone \mathcal{C}' for H^{-1} ,

and which has simple intersection with each of the A_i . Then there exists a piecewise linear curve Γ_p satisfying (C0'), (C1'), (C2'),

(C3') $\Gamma_p \subset H^{-i}(\Gamma_{p-1})$ for a chosen $i \in \{1, 2, 3\}$,

(C4') $\ell_h(\Gamma_p) \geq (1 + \delta) \ell_h(\Gamma_{p-1})$ for some $\delta = \delta(\varepsilon) > 0$, independent of Γ_{p-1} .

Proof. Figure 4.9(a) shows the return time partition of $A = H^{-1}(\mathbf{a})$ under H^{-1} . Define $\mathcal{K}_j(\varepsilon)$ for $j = 1, 2, 3$ as before. Both \mathfrak{M}_1 and \mathfrak{M}_2 see their minimum expansion over \mathcal{C}' on the unstable eigenvector of \mathfrak{M}_2 . As does \mathfrak{M}_3 for $\varepsilon < \varepsilon^* \approx 0.07735$, then on its own unstable eigenvector for $\varepsilon > \varepsilon^*$. Since \mathcal{C}' is expanding, each of the $\mathcal{K}_j(\varepsilon)$ are strictly greater than 1 across our parameter range.

First suppose Γ_{p-1} lies entirely within one of the A_j . Each of its constituent line segments $L(x_i, v_i)$ can be defined by an end point x_i and the vector v_i taking x_i to the other end point, with $v_i \in \mathcal{C}'$. Satisfying (C3') we let $\Gamma_p = H^{-j}(\Gamma_{p-1})$, then each $L(x_i, v_i)$ is mapped to a new segment $L(H^{-j}(x_i), \mathfrak{M}_j v_i)$ which lies in A , is aligned in \mathcal{C}' and has expanded in diameter by a factor of at least $\mathcal{K}_j(\varepsilon)$.

As the union of these new line segments, Γ_p satisfies (C1') and (C2'). It does not double back on itself since \mathfrak{M}_j will have the same orientation preserving (or reversing) effect on each of the v_i . This satisfies (C0') and tells us that the diameter of Γ_p is the sum of the diameters of the new line segments[†], meaning its diameter has expanded by at least the factor $\mathcal{K}_j(\varepsilon)$, satisfying (C4').

The above is the simplest case we will consider. The picture becomes more complicated as we allow intersections with multiple A_j . First assume that Γ_{p-1} intersects A_1 and one of A_2 or A_3 . We proceed by restricting to one of the A_j , $\Gamma^j := \Gamma_{p-1} \cap A_j$, and expanding from there, $\Gamma_p = H^{-j}(\Gamma^j)$. By the same reasoning given for the η -perturbation, we require

$$\mathcal{K}_2(\varepsilon) > \frac{1}{1 - \frac{1}{\mathcal{K}_1(\varepsilon)}} \quad (4.6)$$

and

$$\mathcal{K}_3(\varepsilon) > \frac{1}{1 - \frac{1}{\mathcal{K}_1(\varepsilon)}}. \quad (4.7)$$

Solving (4.6) gives $\varepsilon > \varepsilon_0 \approx 0.00925$, the lower bound on our parameter range. Solving (4.7) gives $\varepsilon < \varepsilon_3 \approx 0.0885$, slightly larger than the upper bound on our parameter range ε_2 .

Next assume that Γ_p intersects A_1 , A_2 , and A_3 . The case where Γ_p intersects A_2 and A_3 but not A_1 follows as a trivial consequence and will be addressed at the end of the proof. Clearly if the proportion of the diameter in A_1 exceeds $\mathcal{K}_1(\varepsilon)^{-1}$,

$$\frac{\ell_h(\Gamma^1)}{\ell_h(\Gamma_{p-1})} > \frac{1}{\mathcal{K}_1(\varepsilon)},$$

then we can take $\Gamma_p = H^{-1}(\Gamma^1)$ to satisfy (C0'-5'). Otherwise we have to expand from some subset of $\Gamma^2 \cup \Gamma^3$, giving Γ_p such that

$$\ell_h(\Gamma_p) > \frac{1}{1 - \frac{1}{\mathcal{K}_1(\varepsilon)}} \ell_h(\Gamma^2 \cup \Gamma^3).$$

[†]Assuming its not 1, at which point Γ_p has non-simple intersection with some A_j

To reduce the ε dependence of the problem and simplify the equations, we will take

$$c = \sup_{\varepsilon_0 < \varepsilon \leq \varepsilon_2} \frac{1}{1 - \frac{1}{\mathcal{K}_1(\varepsilon)}} \approx 1.4765$$

and show

$$\ell_h(\Gamma_p) > c \ell_h(\Gamma^2 \cup \Gamma^3). \quad (4.8)$$

We will give an argument for expanding Γ_{p-1} which intersects the lower portion of A_2 . The argument for the upper portion is entirely analogous due to the 180° rotational symmetry of both the partition of A and the invariant cone.

Consider the subdivision of A_2 into points which remain in A for a further iteration of H^{-1} after returning, A_4 , and those which do not, A_5 . This subdivision is shown in Figure 4.9(b). The labelled points are

$$Q_1 = \left(\frac{-4\varepsilon^3 - 2\varepsilon^2 + \varepsilon + \frac{1}{2}}{12\varepsilon^2 + 16\varepsilon + 1}, 0 \right) \quad \text{and} \quad Q_2 = \left(\frac{1 + 2\varepsilon}{2 + 2\varepsilon}, \frac{3\varepsilon + 2\varepsilon^2}{2 + 2\varepsilon} \right)$$

so that the segment L_1 along the A_4, A_5 boundary has gradient

$$k_1 = \frac{12\varepsilon^2 + 16\varepsilon + 1}{(2\varepsilon + 1)(2\varepsilon + 5)}.$$

The segment along the A_4, A_3 boundary has gradient

$$k_2 = \frac{4\varepsilon}{2\varepsilon + 1}.$$

Strictly speaking, at larger ε values A_4 contains an additional region in the lower part of A_5 near $(\frac{1}{2} - \varepsilon, 0)$. The only assumption we make about points in A_5 is that they return to A after two iterations, so treating this additional region as part of A_5 has no impact on our analysis.

The region A_4 has some useful properties. Firstly, like A_3 , segments contained within A_4 return to A after 3 iterations. This[‡] means we can take $\Gamma_p = H^{-3}(\Gamma_3 \cup \Gamma_4)$ and have a much larger initial curve to expand from. Secondly, diameter expansion is generally strong from A_4 . The itinerary path is **baa** with corresponding matrix

$$\mathfrak{M}_4 = \mathcal{M}_1^{-1} \mathcal{M}_1^{-1} \mathcal{M}_0^{-1}$$

which expands vectors at least as much as any of the other \mathfrak{M}_j : $\mathcal{K}_4(\varepsilon) > \mathcal{K}_j(\varepsilon)$ for all $\varepsilon_0 < \varepsilon \leq \varepsilon_2$, $j = 1, 2, 3$. Finally if Γ_{p-1} intersects A_5 , then it must traverse A_4 since, by assumption, it also intersects A_3 . The case where Γ_{p-1} does not intersect A_5 is trivial, reducing to the case where Γ_{p-1} only intersects A_1 and A_3 , since A_3 and A_4 both map into A under H^{-3} and $\mathcal{K}_4 > \mathcal{K}_3$.

Assume, then, that Γ_{p-1} intersects A_5 . Let $\Gamma_p = H^{-3}(\Gamma^3 \cup \Gamma^4)$. Our aim is to minimise $\ell_h(\Gamma_p)$, considering all possible curves Γ_{p-1} dictated by the invariant cone, and showing that it still satisfies (4.8). To arrive at the minimal case we can make several assumptions. Firstly, $\ell_h(\Gamma^3) = 0$. The condition that we intersect A_3 does not stipulate any minimum diameter in A_3 , it can be arbitrarily small. Since \mathfrak{M}_3 and \mathfrak{M}_4 have the same orientation reversing effect on vectors in the cone, assuming Γ_p does not have diameter 1 (at which point we have non-simple intersection with some A_j),

$$\ell_h(\Gamma_p) \geq \mathcal{K}_3(\varepsilon) \ell_h(\Gamma^3) + \mathcal{K}_4(\varepsilon) \ell_h(\Gamma^4).$$

Comparing with (4.8), taking $\ell_h(\Gamma^3) > 0$ grows the RHS of (4.8) by $c \ell_h(\Gamma^3)$, but grows the LHS of (4.8) by at least $\mathcal{K}_3(\varepsilon) \ell_h(\Gamma^3)$. Since $\mathcal{K}_3(\varepsilon) > c$ for every $\varepsilon_0 < \varepsilon \leq \varepsilon_2$, in the minimal case

[‡]Together with the fact that \mathfrak{M}_3 and \mathfrak{M}_4 have the same orientation reversing effect on the invariant cone

$\ell_h(\Gamma^3) = 0$. We note that the condition (4.8) now looks like

$$\ell_h(H^{-3}(\Gamma^4)) > c \ell_h(\Gamma^4 \cup \Gamma^5),$$

which is satisfied if

$$\mathcal{K}_4(\varepsilon) > c \frac{\ell_h(\Gamma^4) + \ell_h(\Gamma^5)}{\ell_h(\Gamma^4)}. \quad (4.9)$$

To show that this holds, we will put lower bounds on

$$\frac{\ell_h(\Gamma^4)}{\ell_h(\Gamma^4) + \ell_h(\Gamma^5)} \quad (4.10)$$

and $\mathcal{K}_4(\varepsilon)$, then compare their product with c .

By a purely geometric argument, comparing the admissible gradients given by the invariant cone with the lines which make up the partition boundaries, we have a lower bound

$$\frac{\ell_h(\Gamma^4)}{\ell_h(\Gamma^4) + \ell_h(\Gamma^5)} > \frac{(2\varepsilon + 1)(2\varepsilon + 1 - 2k_5^+)}{(2\varepsilon + 1)(-k_4^-(2\varepsilon + 3) - k_5^+(2\varepsilon + 5)) + 12\varepsilon^2 + 16\varepsilon + 1} := \mathcal{B}_1(\varepsilon)$$

where $k_5^+ = \sup_\varepsilon \mathfrak{g}_2^u(\varepsilon) \approx -0.08750$ and $k_4^- = \inf_\varepsilon \mathfrak{g}_3^u(\varepsilon) \approx -0.6688$. The calculation of this bound can be found in appendix A.

We will now put a lower bound on $\mathcal{K}_4(\varepsilon)$, the minimum expansion of \mathfrak{M}_4 over the minimal cone. This is on the anti-clockwise boundary, $v_u(\mathfrak{M}_2)$, which can be described as the vector $(1, k_5(\varepsilon))^T$ with

$$k_5(\varepsilon) = \frac{\varepsilon - \sqrt{\varepsilon(4\varepsilon^2 + 5\varepsilon + 1)}}{2\varepsilon + 1} < 0.$$

By calculating the matrix entries of \mathfrak{M}_4 and noting that \mathfrak{M}_4 reverses the orientation of vectors, one can show that

$$\mathcal{K}_4(\varepsilon) = \frac{3 + 46\varepsilon + 52\varepsilon^2 + 8\varepsilon^3}{1 + 2\varepsilon - 4\varepsilon^2 - 8\varepsilon^3} - \frac{12\varepsilon + 14}{1 - 4\varepsilon^2} k_5(\varepsilon).$$

Let $L(\varepsilon)$ be the linear approximation for $k_5(\varepsilon)$,

$$\begin{aligned} L(\varepsilon) &= \frac{\varepsilon - \varepsilon_0}{\varepsilon_2 - \varepsilon_0} (k_5(\varepsilon_2) - k_5(\varepsilon_0)) + k_5(\varepsilon_0) \\ &= \frac{\varepsilon - \varepsilon_0}{\varepsilon_2 - \varepsilon_0} (k_5^- - k_5^+) + k_5^+. \end{aligned}$$

One can verify that $\frac{d}{d\varepsilon} k_5 < 0$ and $\frac{d^2}{d\varepsilon^2} k_5 > 0$ for $\varepsilon_0 < \varepsilon \leq \varepsilon_2$, so that $L(\varepsilon) > k_5(\varepsilon)$ across this parameter range and is equal at its extremes. This implies

$$\mathcal{K}_4(\varepsilon) \geq \frac{3 + 46\varepsilon + 52\varepsilon^2 + 8\varepsilon^3}{1 + 2\varepsilon - 4\varepsilon^2 - 8\varepsilon^3} - \frac{12\varepsilon + 14}{1 - 4\varepsilon^2} L(\varepsilon) := \mathcal{B}_2(\varepsilon)$$

To show condition (4.9), and complete this final case, it is sufficient to show that

$$\mathcal{B}_1(\varepsilon)\mathcal{B}_2(\varepsilon) > c \approx 1.4765. \quad (4.11)$$

One can show that $\mathcal{B}_1(\varepsilon)\mathcal{B}_2(\varepsilon)$ is monotone increasing (see appendix A) over $\varepsilon_0 < \varepsilon \leq \varepsilon_2$ and therefore takes its minimal value at ε_0 . Plugging in this value gives

$$\mathcal{B}_1(\varepsilon_0)\mathcal{B}_2(\varepsilon_0) \approx 1.532235,$$

which establishes (4.11).

The case where $\ell_h(\Gamma^1) = 0$ follows as a trivial consequence. $\mathcal{B}_1(\varepsilon)$ is still a lower bound for the proportion of Γ_{p-1} in $A_3 \cup A_4$ so we only need to compare $\mathcal{B}_1(\varepsilon)\mathcal{B}_2(\varepsilon)$ against $c = 1$ in this

case. □

One can follow an entirely analogous argument to prove the equivalent lemma for growth in forwards time:

Lemma 4.7. *Let Γ_{p-1} be a piecewise linear curve satisfying*

(C0) Γ_{p-1} does not double back on itself,

(C1) $\Gamma_{p-1} \subset \mathbf{a}$,

(C2) Each line segment in Γ_{p-1} is aligned with some vector in the minimal invariant cone \mathcal{C} for H ,

and which has simple intersection with each of the \mathbf{a}_i . Then there exists a piecewise linear curve Γ_p satisfying (C0), (C1), (C2),

(C3) $\Gamma_p \subset H^i(\Gamma_{p-1})$ for a chosen $i \in \{1, 2, 3\}$,

(C4) $\ell_v(\Gamma_p) \geq (1 + \delta) \ell_v(\Gamma_{p-1})$ for some $\delta = \delta(\varepsilon) > 0$, independent of Γ_{p-1} .

We now give the argument for mapping into h -segments and v -segments, whose definitions we generalise to piecewise linear curves which connect the relevant boundaries of A_1 .

Lemma 4.8. *Let $\Gamma_P \subset A$ be a piecewise linear curve with each of its line segments aligned with a vector in \mathcal{C}' . If Γ_P has non-simple intersection with some A_i , then $H^{-k}(\Gamma_P)$ contains a h -segment for some $k \in \{0, 4\}$.*

Proof. In comparison with Lemma 4.5, we have fewer non-trivial cases to consider. We claim that any Γ_P which has non-simple intersection with A_2 contains a h -segment, that is, it can only connect A_2 to itself by traversing A_1 . Since if Γ_P were to connect the two parts of A_2 through A_3 , it would have to contain a segment with gradient

$$\mathbf{g} < \frac{\frac{1}{2} - \varepsilon - 2\varepsilon}{\frac{1}{2} - \varepsilon - (\frac{1}{2} + \varepsilon)} = -\frac{1 - 6\varepsilon}{4\varepsilon} =: h(\varepsilon),$$

the gradient of the line segment joining the points $(\frac{1}{2} - \varepsilon, \frac{1}{2} - \varepsilon)$ and $(\frac{1}{2} + \varepsilon, 2\varepsilon)$. However \mathbf{g} is bounded from below by $\mathbf{g}_3^u(\varepsilon)$ with

$$\mathbf{g}_3^u(\varepsilon) \geq \mathbf{g}_3^u(\varepsilon_2) \approx -0.6688$$

across $\varepsilon_0 < \varepsilon \leq \varepsilon_2$. Now

$$h(\varepsilon) \leq h(\varepsilon_2) \approx -1.4397$$

across the range, so that $\mathbf{g} > h(\varepsilon)$ at each ε . Hence if Γ_P has non-simple intersection with A_2 , it follows that it contains a h -segment. The same clearly holds if Γ_P has non-simple intersection with A_3 .

Assume, then, that Γ_P has non-simple intersection with A_1 . This implies that Γ_P connects the two sloping boundaries of A_1 through $\mathbf{b} = A_2 \cup A_3$. We will show that $H^{-4}(\Gamma_P)$ contains a h -segment. Figure 4.10 shows a region $\mathfrak{D} \subset \mathbf{b}$, bounded by two piecewise linear curves ω, ζ . These curves can be defined by their end points on $\partial\mathbf{b}$ and their turning points, whose full coordinates are given in the supplementary material. Label these points as ω_j, ζ_j , $j = 1, 2, 3, 4$ so that the x -coordinate increases with j . These curves (and hence \mathfrak{D}) are contained within \mathbf{b} for $\varepsilon \leq \varepsilon_2$, with ζ_2 limiting onto the right boundary of \mathbf{b} ($y = x - \frac{1}{2} + \varepsilon$) as $\varepsilon \rightarrow \varepsilon_2$. In particular $\varepsilon_2 \approx 0.08504$ is the positive solution to the cubic equation

$$8\varepsilon^3 + 20\varepsilon^2 + 10\varepsilon - 1 = 0.$$

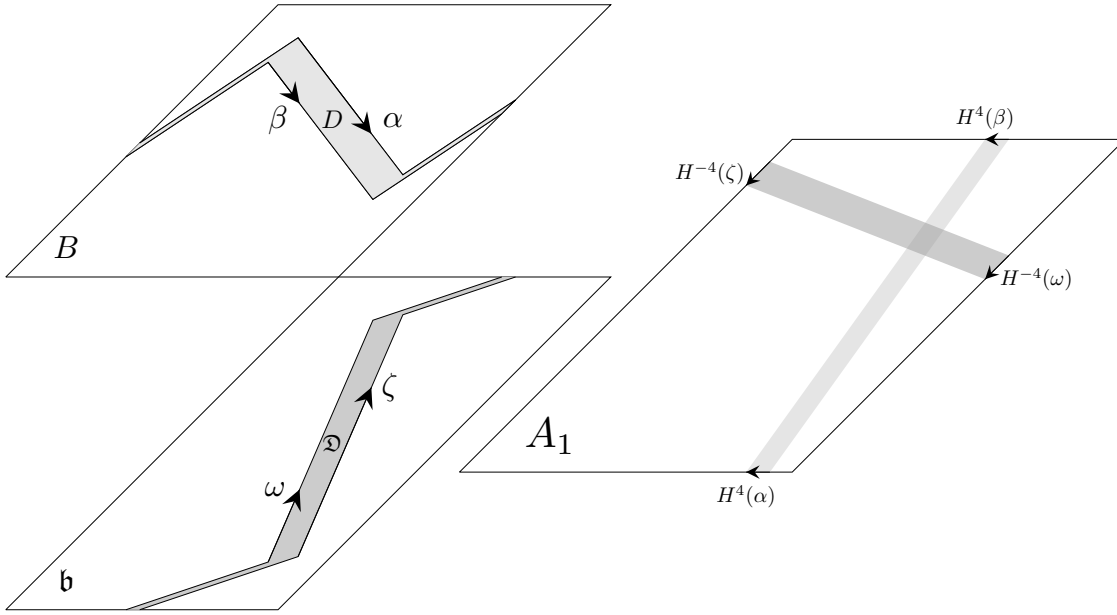


Figure 4.10: Left: Two regions $\mathfrak{D} \subset \mathfrak{b}$ and $D \subset B$, bounded by the piecewise linear curves ω, ζ and α, β respectively. Right: Their images in A_1 under H^{-4} and H^4 respectively, establishing h - and v -segments.

The argument for mapping into h -segments is roughly analogous to that given for the η -perturbation. Applying H^{-4} to \mathfrak{D} gives a quadrilateral in A_1 with sides on its left and right boundaries (the images of ζ and ω under H^{-4}). Clearly any Γ_P which joins the left and right sides of \mathfrak{b} must join ω and ζ through \mathfrak{D} . Let Γ be this part of the curve, then $H^{-4}(\Gamma)$ must be a piecewise linear curve joining $H^{-4}(\omega)$ and $H^{-4}(\zeta)$ through $H^{-4}(\mathfrak{D})$. That is, $H^{-4}(\Gamma)$ is a h -segment. \square

Lemma 4.9. *Let $\Gamma_P \subset \mathfrak{a}$ be a piecewise linear curve with each of its line segments aligned with a vector in \mathcal{C} . If Γ_P has non-simple intersection with some \mathfrak{a}_i , then $H^k(\Gamma_P)$ contains a v -segment for some $k \in \{0, 4\}$.*

Proof. Analogous to the previous lemma, non-simple intersection with \mathfrak{a}_2 or \mathfrak{a}_3 imply that Γ_P already contains a v -segment. To see this, note that if Γ_P connected the two parts of \mathfrak{a}_2 through \mathfrak{a}_3 , it would have to contain a segment with gradient

$$g(\varepsilon) > \frac{\frac{1}{2} - \varepsilon}{2\varepsilon} =: h(\varepsilon).$$

However $g(\varepsilon)$ is bounded from above by the anti-clockwise invariant cone boundary $g_3^u(\varepsilon)$ and

$$g_3^u(\varepsilon) \leq g_3^u(\varepsilon_2) \approx 1.669 < 2.440 \approx h(\varepsilon_2) \leq h(\varepsilon)$$

across $\varepsilon_0 < \varepsilon \leq \varepsilon_2$. As before, then, it remains to assess the case where Γ_P has non-simple intersection with \mathfrak{a}_1 . It follows that Γ_P joins the upper and lower boundaries of B through B . Figure 4.10 shows a region D bounded by ∂B and two piecewise linear curves α, β . These curves are contained within B across $\varepsilon_0 < \varepsilon \leq \varepsilon_2$, with α_2 limiting onto the line $y = 1$ as $\varepsilon \rightarrow \varepsilon_2$. Applying H^4 to D gives a quadrilateral spanning across A_1 , with sides $H^4(\alpha), H^4(\beta)$ on its lower and upper boundaries respectively. Clearly Γ_P must connect β to α through D , and therefore $H^4(\Gamma_P)$ contains a v -segment. \square

We are now ready to establish ergodicity over $\varepsilon_0 < \varepsilon < \varepsilon_2$.

Proof of Proposition 4.4. By the same argument given in the proof of Proposition 4.1, by Lemmas 4.1, 4.7, 4.9, given any $z \in X'$ we can find m such that $H^m(\gamma_u(z))$ contains a v -segment. Similarly by Lemmas 4.1, 4.6, 4.8, given any $z' \in X'$ we can find n such that $H^{-n}(\gamma_s(z'))$ contains a h -segment. It follows that they intersect which, since z and z' were arbitrary, establishes **(M)**. \square

4.2.3 Establishing the Bernoulli property

Proposition 4.5. *Condition **(MR)** holds for H when $\varepsilon_0 < \varepsilon \leq \varepsilon_2$.*

Proof. Follow the same argument given in the proof of Proposition 4.2, replacing η by $\frac{1}{2} - \varepsilon$. \square

We are now ready to prove the main theorem of this section.

Proof of Theorem 4.2. Let $\eta_2 = \frac{1}{2} - \varepsilon_2$ and $\eta_3 = \frac{1}{2} - \varepsilon_0$. Noting that **(KS1)** and **(KS2)** were trivially satisfied, the Bernoulli property holds for H over $\eta_2 \leq \eta < \eta_3$ by Theorem 1.4 and Propositions 4.3, 4.4, and 4.5. \square

4.2.4 Remarks

We remark that the parameter limits given in Theorems 4.1, 4.2 are not optimal. For example, ε_2 is not the highest upper bound on the ε -mixing window that our analysis allows for, but it is very close. By considering a 5-iterate mapping into h - and v -segments, this bound could be increased only very slightly. Improving the bound $\mathcal{B}_1(\varepsilon)$ would increase it further, but would in turn complicate the already lengthy algebraic manipulations.

When following the Katok and Strelcyn approach, it is typical to be left with parameter ranges where hyperbolicity can be established but proving the mixing property is more challenging. See for example the families of maps studied in Przytycki (1983), Wojtkowski (1981). In both of these examples, the strength of the shears is increased to break up elliptic islands and ensure an invariant cone. Indeed, the Wojtkowski (1981), Bullett (1986) map at parameter value $K = 4$ exhibits similar dynamics to a variation of Cerbelli and Giona's map with a double strength non-monotonic shear, i.e taking $H = G \circ F^2$. In contrast, for H_η the shear strength is not varied, in particular integrating the twist functions gives

$$\int_0^1 f(y) dy = \int_0^{1-\eta} \frac{y}{1-\eta} dy + \int_{1-\eta}^1 \frac{1-y}{\eta} dy = \frac{1}{2},$$

independent of η .

We now focus on a new ASM, the map $H_{(\xi,\eta)}$ which limits pointwise onto H_η by taking $\xi \rightarrow 0$.

4.3 Mixing properties of $H_{(\xi,\eta)}$

Analysis of the map $H_{(\xi,\eta)}$ over $0 < \xi, \eta < 1$ was provided in Myers Hill et al. (2022a). We present the same arguments in this section, establishing parameter windows where the dynamics are hyperbolic, mixing, and non-mixing.

Theorem 4.3. *Let $\mathcal{H}, \mathcal{M}, \mathcal{I}_1, \mathcal{I}_2, \mathcal{I}_3$ be the parameter sets shown in Figure 4.11.*

- For $(\xi, \eta) \in \mathcal{H}$, $H_{(\xi,\eta)}$ has non-zero Lyapunov exponents.
- For $(\xi, \eta) \in \mathcal{M}$, $H_{(\xi,\eta)}$ is mixing.
- For $(\xi, \eta) \in \mathcal{I}_1, \mathcal{I}_2, \mathcal{I}_3$ and their reflections in the lines $\eta = \xi$ and $\eta = 1 - \xi$, $H_{(\xi,\eta)}$ is non-mixing.

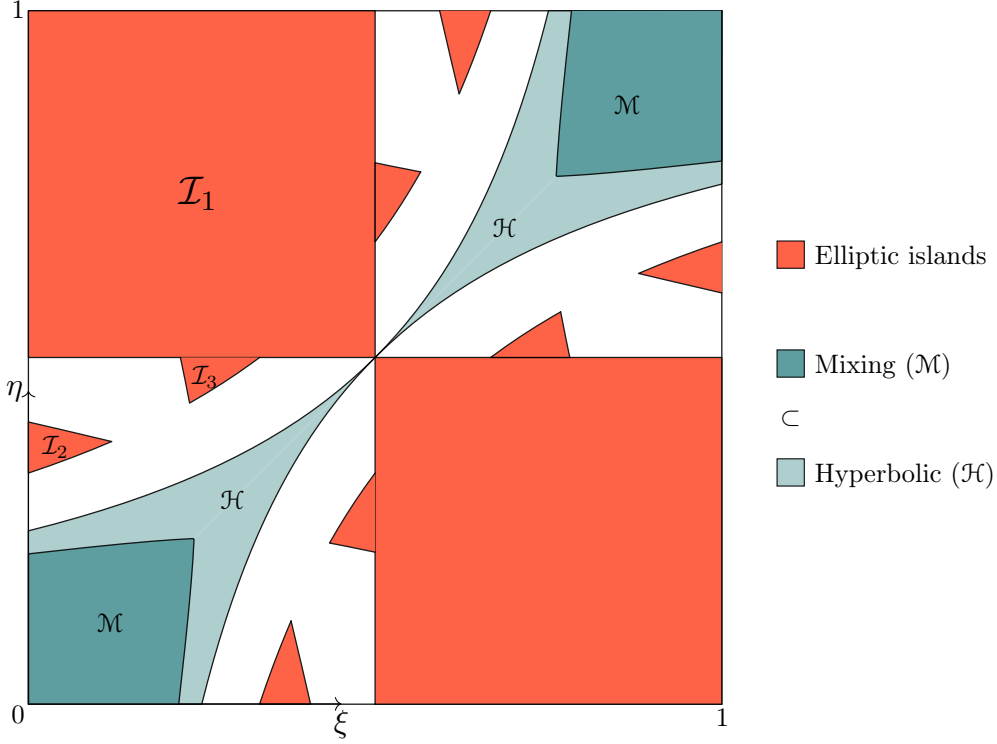


Figure 4.11: Shown behaviour of $H_{(\xi,\eta)}$ over the parameter space $0 < \xi, \eta < 1$.

Explicit definitions for these sets are given later in Proposition 4.10. As in the previous section, our approach is to follow the Katok and Strelcyn scheme.

Lemma 4.10. *For all $0 < \xi, \eta < 1$ the map $H_{(\xi,\eta)}$ satisfies (KS1-2).*

Proof. Write $H = H_{(\xi,\eta)}$ and partition the torus into four rectangles R_j using the lines $x = 0$, $y = 0$, $x = 1 - \xi$, and $y = 1 - \eta$, as shown in Figure 4.12. Letting $A_j = F^{-1}(R_j)$, the Jacobian DH is defined everywhere outside of the set $\mathcal{D} = \cup_j \partial A_j$ and is constant on each of the A_j , given by M_j , where

$$M_1 = \begin{pmatrix} 1 & \frac{1}{1-\eta} \\ \frac{1}{1-\xi} & 1 + \frac{1}{(1-\xi)(1-\eta)} \end{pmatrix}, \quad M_2 = \begin{pmatrix} 1 & \frac{1}{1-\eta} \\ -\frac{1}{\xi} & 1 - \frac{1}{\xi(1-\eta)} \end{pmatrix},$$

$$M_3 = \begin{pmatrix} 1 & -\frac{1}{\eta} \\ \frac{1}{1-\xi} & 1 - \frac{1}{\eta(1-\xi)} \end{pmatrix}, \quad M_4 = \begin{pmatrix} 1 & -\frac{1}{\eta} \\ -\frac{1}{\xi} & 1 + \frac{1}{\eta\xi} \end{pmatrix}.$$

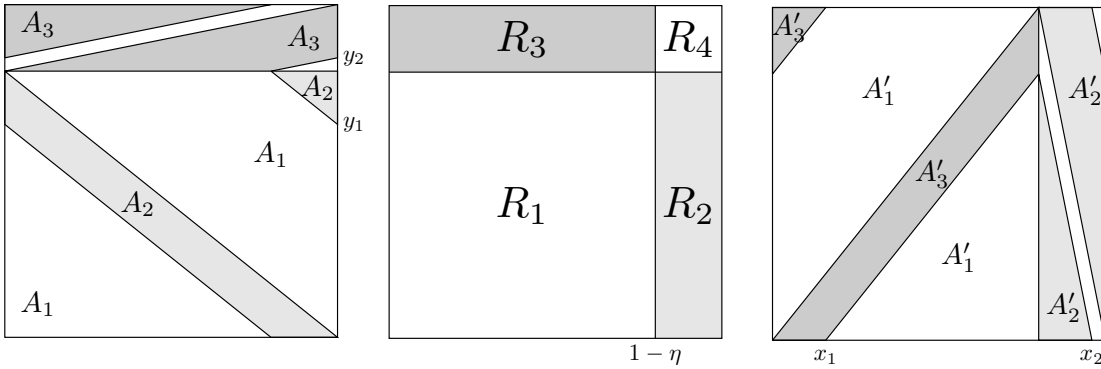


Figure 4.12: A partition of the torus into four rectangles R_j , and their images A_j under F_η^{-1} , A'_j under G_ξ . The smallest partition elements A_4 and A'_4 are left unlabelled. Case illustrated $\xi = \eta = 0.2$.

Letting $A'_j = G(R_j) = H(A_j)$, the derivative of H^{-1} is defined everywhere outside of the set $\mathcal{D}' = \cup_j \partial A'_j$ and is constant on each of the A'_j . The labelled intersections with the axes are $y_1 = (1 - \xi)(1 - \eta)$, $y_2 = 1 - \eta + \xi\eta$, $x_1 = \eta(1 - \xi)$, and $x_2 = 1 - \xi\eta$.

Using the notation of Theorem 1.4, we take our map as $f = H$, our domain as $X = \mathbb{T}^2$, and our singularity set as $S = \mathcal{D}$. Taking μ to be the Lebesgue measure on \mathbb{T}^2 , clearly $\mu(S) = 0$. Since we can cover \mathcal{D} with arbitrarily thin rectangles, **(KS1)** follows for some $C_1 > 0$ with $a = 1$. Since H is piecewise linear, **(KS2)** follows trivially. \square

As in Myers Hill et al. (2022a), we will focus first on the reduced parameter space $\xi = \eta$ for $0 < \eta < 1/2$ and then extend our results to more general parameters (ξ, η) . We begin by establishing non-zero Lyapunov exponents, **(KS3)**.

4.3.1 Hyperbolicity of $H_{(\eta, \eta)}$

Proposition 4.6. *We have non-zero Lyapunov exponents $\chi(z, v) \neq 0$ for almost every $z \in \mathbb{T}^2$, $v \neq 0$, when $0 < \eta < 1/2$.*

Proof. Let $H = H_{(\eta, \eta)}$. We note that each of the matrices M_j , with $\xi = \eta$ and $0 < \eta < 1/2$, are hyperbolic. Write the gradients of their unstable, stable eigenvectors as g_j^u, g_j^s . One can verify that

$$g_4^u(\eta) < g_2^u(\eta) < g_2^s(\eta) < g_1^s(\eta) < g_4^s(\eta) < g_3^s(\eta) < g_3^u(\eta) < g_1^u(\eta) \quad (4.12)$$

across $0 < \eta < 1/2$. This allows us to define a cone region \mathcal{C} in the tangent space, bounded by the unstable eigenvectors of M_2 and M_3 , which includes all of the unstable eigenvectors of the M_j , and none of the stable eigenvectors. For each matrix we define

$$K_j(\eta) = \inf_{v \in \mathcal{C}} \frac{\|M_j v\|}{\|v\|}.$$

Using the $\|\cdot\|_\infty$ norm, these are given as follows:

$$K_1 = \frac{2 - \eta}{1 - \eta}, \quad K_2 = \frac{1 - \eta}{\eta}, \quad K_3 = \frac{1 - \eta}{\eta}, \quad \text{and} \quad K_4 = \frac{1 - \eta + \eta^2}{\eta^2}.$$

All are strictly greater than 1 for $0 < \eta < 1/2$, so \mathcal{C} is invariant and expanding with respect to the matrices M_j over this parameter range. The result then follows from Proposition 3.4. \square

4.3.2 Ergodicity of $H_{(\eta, \eta)}$

In this section we will prove the following:

Proposition 4.7. *Condition **(M)** holds for H when $0 < \eta < \eta_1 \approx 0.2389$.*

The proof consists of three stages. Non-zero Lyapunov exponents a.e implies the existence of local unstable and stable manifolds $\gamma_u(z)$ and $\gamma_s(z)$ at z . The first stage, Lemma 4.11, describes the nature of these local manifolds. In the next stage, Lemmas 4.12 and 4.13, we give an iterative scheme for growing the backwards (forwards) images of any local (un)stable manifold. We then grow the images of these manifolds up until the point where the images connect up certain partition boundaries. This then allows us, by Lemmas 4.14 and 4.15, to establish an intersection in the next several iterates.

Let \mathcal{C}' be the cone bounded by the stable eigenvectors of M_2 and M_3 , including the stable eigenvectors of each of the M_j . It follows that this cone is invariant and expanding under H^{-1} . The cones \mathcal{C} and \mathcal{C}' provide bounds on the gradients of local manifolds:

Lemma 4.11. For a.e. z , $\gamma_u(z)$ is a line segment aligned with some $v \in \mathcal{C}$, and $\gamma_s(z)$ is a line segment aligned with some $v' \in \mathcal{C}'$.

Proof. Analogous to the proof of Lemma 4.1. \mathcal{C} can be described as the cone region bounded by the stable eigenvectors of M_2^{-1} and M_3^{-1} and including the stable eigenvectors of each M_j^{-1} . Clearly v must be aligned in this cone, for if it falls outside of this region, repeatedly applying the M_j^{-1} will pull v towards the invariant expanding cone \mathcal{C}' , resulting in exponential growth in its norm, which contradicts (4.3). □

Lemma 4.12. Let $\eta < \eta_1$. Given a line segment Γ_{p-1} , aligned with some $v \in \mathcal{C}$ and having simple intersection with each A_j , there exists a line segment $\Gamma_p \subset H(\Gamma_{p-1})$ such that

(C1) Γ_p is aligned with some vector in \mathcal{C} ,

(C2) $\ell_v(\Gamma_p) \geq (1 + \delta) \ell_v(\Gamma_{p-1})$ for some $\delta = \delta(\eta) > 0$, independent of Γ_{p-1} .

Proof. Suppose Γ_{p-1} , aligned with some $v \in \mathcal{C}$, has simple intersection with all the A_j and each intersection is non-empty. Write the restriction of Γ_{p-1} to A_j as Γ^j . Now if for some j

$$K_j(\eta, v) \ell_v(\Gamma^j) > \ell_v(\Gamma_{p-1}), \quad (4.13)$$

we can take $\Gamma_p = H(\Gamma^j)$ to satisfy (C2). If Γ_{p-1} was aligned with $v \in \mathcal{C}$, Γ_p is now aligned with $M_j v \in \mathcal{C}$, so (C1) is also satisfied. If (4.13) does not hold, the proportion of Γ^j in Γ_{p-1} is bounded above by K_j^{-1} . Suppose (4.13) does not hold for $j = 2, 3, 4$. Then the proportion of Γ^1 in Γ_{p-1} is bounded below by

$$\frac{\ell_v(\Gamma^1)}{\ell_v(\Gamma_{p-1})} > 1 - \frac{1}{K_2} - \frac{1}{K_3} - \frac{1}{K_4}.$$

Hence taking $\Gamma_p = H(\Gamma^1)$ satisfies (C2) provided that

$$K_1(\eta, v) > \frac{1}{1 - \frac{1}{K_2} - \frac{1}{K_3} - \frac{1}{K_4}},$$

which rearranges to

$$\sum_{j=1}^4 \frac{1}{K_j(\eta, v)} < 1$$

and holds for any $v \in \mathcal{C}$ provided that

$$\sup_{v \in \mathcal{C}} \sum_{j=1}^4 \frac{1}{K_j(\eta, v)} < 1. \quad (4.14)$$

Unit vectors in \mathcal{C} are of the form $(k, 1)^T$ for $k_0 \leq k \leq k_1$ with $k_0 = \eta/(\eta - 1)$, $k_1 = 1$. For each j let $M_j = \begin{pmatrix} a_j & b_j \\ c_j & d_j \end{pmatrix}$, then

$$\begin{aligned} \sum_{j=1}^4 \frac{1}{K_j(\eta, v)} &= \sum_{j=1}^4 \frac{1}{|c_j k + d_j|} \\ &= \frac{1}{c_1 k + d_1} + \frac{1}{-c_2 k - d_2} + \frac{1}{-c_3 k - d_3} + \frac{1}{c_4 k + d_4} \\ &=: \Phi(\eta, k) \end{aligned}$$

where we have used the fact that M_2 and M_3 are orientation reversing. Now

$$\frac{\partial^2 \Phi}{\partial k^2} = \frac{2c_1^2}{(c_1 k + d_1)^3} + \frac{2c_2^2}{(-c_2 k - d_2)^3} + \frac{2c_3^2}{(-c_3 k - d_3)^3} + \frac{2c_4^2}{(c_4 k + d_4)^3}$$

which, by comparing with the terms of $\Phi(\eta, k)$, is clearly positive. Hence for each η , Φ as a function in k is convex, giving

$$\sup_{v \in \mathcal{C}} \sum_{j=1}^4 \frac{1}{K_j(\eta, v)} = \sup_{k_0 \leq k \leq k_1} \Phi(\eta, k) = \max\{\Phi(\eta, k_0), \Phi(\eta, k_1)\}.$$

Over $0 < \eta < \frac{1}{2}$ we have that $\Phi(\eta, k_0) > \Phi(\eta, k_1)$ so that (4.14) holds over $0 < \eta < \eta_1$ where $\eta_1 \approx 0.2389$ solves the equation $\Phi(\eta, k_0) = 1$. So for η in this range, choosing one of $\Gamma_p = H(\Gamma^j)$ will always satisfy (C2). The case where Γ_{p-1} has empty intersection with one or more of the A_j follows as a trivial consequence. \square

The equivalent lemma for the growth of line segments under H^{-1} is as follows. Recall the partition of the torus into four sets A'_j given in Figure 4.12.

Lemma 4.13. *Let $\eta < \eta_1$. Given a line segment Γ_{p-1} , aligned with some $v' \in \mathcal{C}'$ and having simple intersection with each A'_j , there exists a line segment $\Gamma_p \subset H^{-1}(\Gamma_{p-1})$ such that*

(C1') Γ_p is aligned with some vector in \mathcal{C}' ,

(C2') $\ell_h(\Gamma_p) \geq (1 + \delta) \ell_h(\Gamma_{p-1})$ for some $\delta = \delta(\eta) > 0$, independent of Γ_{p-1} .

Proof. The argument is analogous. Parameterise \mathcal{C}' by $(1, m)^T$ for $m_0 \leq m \leq m_1$ with $m_0 = -1$, $m_1 = \eta/(1 - \eta)$. Then the condition on expansion factors equivalent to (4.14) reduces to the bound $\max\{\Psi(\eta, m_0), \Psi(\eta, m_1)\} < 1$ where

$$\Psi(\eta, m) = \frac{1}{-b_1 m + d_1} + \frac{1}{b_2 m - d_2} + \frac{1}{b_3 m - d_3} + \frac{1}{-b_4 m + d_4}.$$

One can verify that $\Psi(\eta, m_0) = \Phi(\eta, k_1)$ and $\Psi(\eta, m_1) = \Phi(\eta, k_0)$ so that the lemma holds over $0 < \eta < \eta_1$. \square

Moving onto the final mapping stage, call any line segment $\Gamma \subset R_1$ which joins the upper and lower boundaries ($y = 0, y = 1 - \eta$) a *v-segment*. Similarly we call any line segment $\Gamma \subset R_1$ which joins the left and right boundaries ($x = 0, x = 1 - \eta$) a *h-segment*. Clearly *v*-segments and *h*-segments must always intersect.

Lemma 4.14. *Let Γ be a line segment contained within some A'_j . If Γ has non-simple intersection with some A_j , then $H^k(\Gamma)$ contains a *v-segment* for some $k \in \{1, 2, 3, 4\}$.*

Proof. Note that the sets A'_1, A'_3 are entirely contained within the strip $\{x \leq 1 - \eta\}$, and the sets A'_2, A'_4 are entirely contained within the strip $\{x \geq 1 - \eta\}$, so Γ lies entirely within one of these strips. Suppose first that it lies in $\{x \leq 1 - \eta\}$, then Γ must have non-simple intersection with A_1 or A_3 . Non-simple intersection with A_2 and A_4 is possible, but involves wrapping vertically around the torus, and in doing so implies non-simple intersection with A_1 or A_3 . Assume Γ has non-simple intersection with A_1 . Then it must either connect the segments 2a and 2b (shown in Figure 4.13) through A_2 or connect the segments 4a and 4b through A_4 , depending which way it connects the two parts of A_1 . The same is true when Γ has non-simple intersection with A_3 .

Equivalent analysis can be applied to the strip $\{x \geq 1 - \eta\}$. For Γ in this strip, it follows that Γ connects 3a to 3b through A_3 or connects 1a to 1b through A_1 . This gives four possible cases. Denote the case where Γ connects ja to jb through A_j by case (j). We will show that all cases reduce to case (3). Suppose first that Γ satisfies case (4), connecting 4a to 4b through A_4 . Then $H(\Gamma)$ connects 4a' to 4b' through A'_4 (see Figure 4.13). To do this, $H(\Gamma)$ must connect the segments 1a and 1b, passing through A_1 . That is, $H(\Gamma)$ satisfies case (1). One can similarly show that if Γ satisfies case (1) then $H(\Gamma)$ satisfies case (2), and that if Γ satisfies case (2) then $H(\Gamma)$ satisfies case (3). This case is illustrated in Figure 4.13.

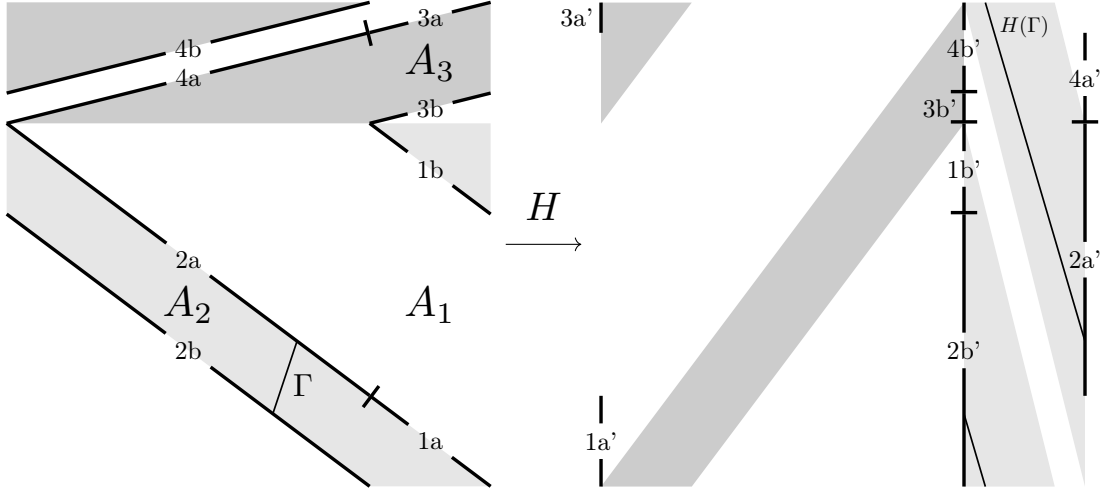


Figure 4.13: Four pairs of line segments ja, jb on the boundaries of A_j , and their images ja', jb' under H on the boundaries of A'_j . A line segment Γ is shown which satisfies case (2). Its image $H(\Gamma) \subset A'_2$ connects $2a'$ to $2b'$, necessarily satisfying case (3).

Looking at the images $3a' = H(3a)$ and $3b' = H(3b)$, we see that any line segment in A'_3 which joins $3a'$ to $3b'$ must pass through $y = 0$ and $y = 1 - \eta$, the lower and upper boundaries of R_1 . It follows that if Γ satisfies case (3), $H(\Gamma)$ contains a v -segment. For any of the four cases (j), $j = 1, 2, 3, 4$, $H^k(\Gamma)$ will contain a v -segment for $k = 3, 2, 1, 4$. \square

Lemma 4.15. *Let Γ be a line segment contained within some A_j . If Γ has non-simple intersection with some A'_j , then $H^{-k}(\Gamma)$ contains a h -segment for some $k \in \{1, 2, 3, 4\}$.*

Proof. The argument is almost entirely analogous, we say that Γ satisfies case (j') if Γ connects jA' to jB' through A'_j (see Figure 4.14 for an illustration of the relevant segments). Γ is entirely contained within one of the strips $\{y \leq 1 - \eta\}$ or $\{y \geq 1 - \eta\}$ which, together with the fact that Γ has non-simple intersection with some A'_j , implies that Γ satisfies case (j') for some j . Again, we have that if Γ satisfies case ($4'$) then $H^{-1}(\Gamma)$ satisfies case ($1'$). This reduces to case ($3'$), and in turn reduces to case ($2'$). Any segment connecting $2A$ to $2B$ through A_2 must pass through the lines $x = 1 - \eta$ and $x = 0$, the right and left boundaries of R_1 . It follows that for Γ satisfying case (j'), $j = 1, 2, 3, 4$, $H^{-k}(\Gamma)$ contains a h -segment for $k = 3, 1, 2, 4$. \square

We are now ready to establish ergodicity.

Proof of Proposition 4.7. For a.e. z , by Lemma 4.11, $\Gamma_0 = \gamma_u(z)$ is a line segment aligned with some vector $v \in \mathcal{C}$. By Lemma 4.12 we can generate a sequence of line segments $(\Gamma_p)_{0 \leq p \leq P}$, with $\Gamma_p \subset H^p(\gamma_u(z))$ and the diameter of Γ_p growing exponentially with p . It follows that after finitely many P steps, Γ_P must have non-simple intersection with one of the partition elements A_j . Since $H^{-1}(\Gamma_P)$ lies entirely within some A_j , Γ_P lies entirely within some A'_j . Now by Lemma 4.14, $H^k(\Gamma_P)$ contains a v -segment for some $k \in \{1, 2, 3, 4\}$. Hence we have found $m = P + k$ such that $H^m(\gamma_u(z))$ contains a v -segment. Similarly for a.e. z , by Lemmas 4.11, 4.13, and 4.15, we can find n such that $H^{-n}(\gamma_s(z'))$ contains a h -segment. It follows that they must intersect. \square

4.3.3 Mixing properties of $H_{(\eta, \eta)}$

Proposition 4.8. *Condition (MR) holds for H when $0 < \eta < \eta_1 \approx 0.2389$.*

Proof. Given $z \in X'$, by Lemmas 5.1, 4.12, 4.14, we have found M_0 such that $H^{M_0}(\gamma_u(z))$ contains a segment Γ which joins $3a'$ to $3b'$ through A'_3 . As shown in the previous section, this means that

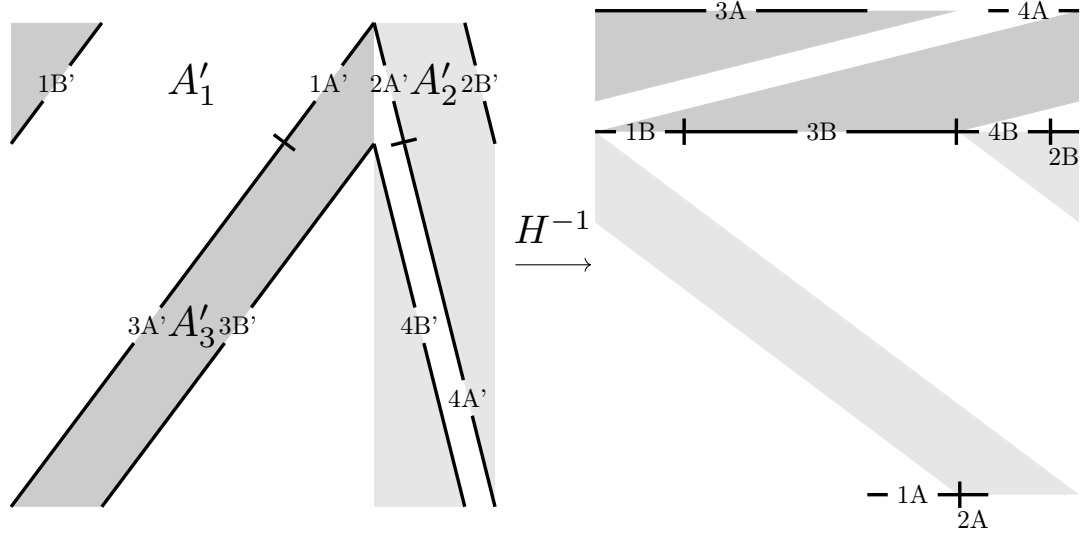


Figure 4.14: Four pairs of line segments jA' , jB' on the boundaries of A'_j , and their images jA , jB under H^{-1} on the boundaries of A_j .

Γ contains a v -segment. It also follows that Γ satisfies case (2) so, by induction, we have that $H^{2k}(\Gamma)$ contains a v -segment for $k \in \mathbb{N}$. Consider the quadrilateral $Q_1 \subset A_1$, defined by its corners

$$q_1 = \left(\frac{(1-\eta)^3}{1+(1-\eta)^2}, 0 \right), \quad q_2 = \left(\frac{(1-\eta)^2}{1+(1-\eta)^2}, 0 \right)$$

$$q_3 = \left(0, \frac{(1-\eta)^3}{1+2(1-\eta)^2} \right), \quad q_4 = \left(0, \frac{(1-\eta)^4}{1+2(1-\eta)^2} \right).$$

An illustration of Q_1 and its image $H(Q_1) \subset A_2$ are shown in Figure 4.15. One can show that each of the points q_i map into the boundary of A_2 so that if Γ joins the dashed boundaries of Q_1 , then $H(\Gamma)$ satisfies case (2). For Γ joining $3a'$ to $3b'$ through A'_3 , Γ must intersect the line $y = 0$ at some point $(x, 0)$ with $0 \leq x \leq x_v = \eta^2(1-\eta)(1-\eta+\eta^2)^{-1}$. Hence our Γ joins the dashed lines of Q_1 as described, provided that $x_v(\eta) \leq q_1(\eta)$. This holds for $\eta \leq \eta_2 \approx 0.4302$. Since $\eta_2 > \eta_1$, this holds in our parameter range so $H(\Gamma)$ satisfies case (2). By the same argument as before, by induction it follows that $H^{1+2k}(\Gamma)$ contains a v -segment for $k \in \mathbb{N}$. Let $M = M_0 + 2$, then $H^m(\gamma_u(z))$ contains a v -segment for all $m \geq M$.

By an entirely analogous argument, showing that h -segments and their images under H^{-1} must satisfy case (3)[§], given any $z' \in X$ we can find $N = N_0 + 2$ such that $H^{-n}(\gamma_s(z'))$ contains a h -segment for any $n \geq N$. Since z and z' are arbitrary, this establishes **(MR)**. \square

We remark that Lemma 4.10 and Propositions 4.6, 4.7, 4.8 give the Bernoulli property over $0 < \eta < \eta_1$ by Theorem 1.4. We now extend our arguments to the wider parameter space $\xi \neq \eta$.

4.3.4 The full parameter space

We begin by establishing some symmetries of the parameter space.

Parameter space symmetries

Note that the system of maps $H_{(\xi, \eta)} = G_\xi \circ F_\eta$ given in the introduction is well defined and incorporates two non-monotonic shears for all $0 < \xi, \eta < 1$. Two symmetries exist which allow us

[§]Showing the equivalent to the $x_v(\eta) < q_1(\eta)$ bound for H^{-1} requires only $\eta < \eta'_2 \approx 0.4643$.

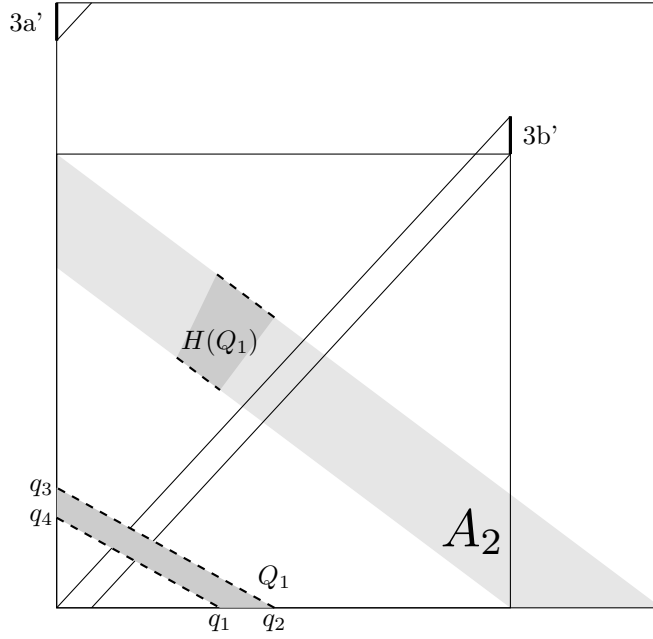


Figure 4.15: Diagram showing that if a segment Γ connects $3a'$ to $3b'$ through A'_3 , then $H(\Gamma)$ must satisfy case (2).

to reduce this parameter space by a factor of four. Firstly consider $\sigma_1(\xi, \eta) = (\eta, \xi)$, reflection in the line $\eta = \xi$. We claim that

$$S_1 \circ G_\xi \circ F_\eta = F_\xi \circ G_\eta \circ S_1$$

where $S_1 : \mathbb{T}^2 \rightarrow \mathbb{T}^2$ maps $(x, y) \mapsto (y, x)$. This follows from the fact that $S_1(A_j) = G_\eta^{-1}(S_1(R_j))$ for $j = 1, \dots, 4$ and the definitions of F, G given in the introduction. Let $\mathcal{H} = F \circ G$ (shearing vertically first instead of horizontally) then it follows that we have a semi-conjugacy between $H_{(\xi, \eta)}$ and $\mathcal{H}_{(\eta, \xi)} = \mathcal{H}_{\sigma_1(\xi, \eta)}$. Clearly H and \mathcal{H} share the same mixing properties, so mixing properties of $H_{\sigma_1(\xi, \eta)}$ follow from those of $H_{(\xi, \eta)}$.

Similarly take $\sigma_2(\xi, \eta) = (1 - \eta, 1 - \xi)$, reflection in the line $\eta = 1 - \xi$. One can verify that

$$S_2 \circ G_\xi \circ F_\eta = F_{1-\xi}^{-1} \circ G_{1-\eta}^{-1} \circ S_2$$

where $S_2 : \mathbb{T}^2 \rightarrow \mathbb{T}^2$ maps $(x, y) \mapsto (1 - y, 1 - x)$, noting that $S_2(A_j) = G_{1-\eta}(S_2(R_j))$. This gives $H_{(\xi, \eta)}$ conjugate to $H_{\sigma_2(\xi, \eta)}^{-1}$, which has the same mixing properties as $H_{\sigma_2(\xi, \eta)}$.

Taking both of these symmetries into account, we need only study the reduced parameter space \mathcal{P} defined by $\xi \leq \eta \leq 1 - \xi$ with $0 < \xi \leq \frac{1}{2}$.

Elliptic islands

Proposition 4.9. *H exhibits elliptic islands of positive measure over the following parameter spaces:*

$$(\mathcal{I}_1): \frac{1}{2} < \eta \leq 1 - \xi \text{ for } 0 \leq \xi < \frac{1}{2},$$

$$(\mathcal{I}_2): 0 < \xi < \min \left\{ 1 - \frac{1}{3\eta}, \frac{8\eta^3 - 22\eta^2 + 18\eta + \sqrt{4\eta^3 - 4\eta^2 + 1 - 5}}{2(4\eta^3 - 9\eta^2 + 7\eta - 2)} \right\},$$

$$(\mathcal{I}_3): \max \left\{ \frac{1}{3-3\xi}, \frac{2\xi^2 - 4\xi + 1}{2\xi^2 - 3\xi + 1} \right\} < \eta < \frac{1}{2}.$$

Proof. This is a straightforward application of Proposition 3.1. Starting with \mathcal{I}_1 , consider the

periodic orbit $\{z_1, z_2\}$ where

$$z_1 = \left(\frac{-2\xi^2\eta + 5\xi\eta - \xi - 3\eta + 1}{4\xi\eta - 4\eta + 1}, \frac{-2\xi\eta^2 + 3\xi\eta + 2\eta^2 - 4\eta + 1}{4\xi\eta - 4\eta + 1} \right)$$

and

$$z_2 = \left(\frac{\eta(2\xi^2 - 3\xi + 1)}{4\xi\eta - 4\eta + 1}, \frac{-2\xi\eta^2 + 5\xi\eta + 2\eta^2 - 5\eta + 1}{4\xi\eta - 4\eta + 1} \right).$$

We claim that for $(\xi, \eta) \in \mathcal{I}_1$ both $z_1 = (x_1, y_1)$ and $z_2 = (x_2, y_2)$ are contained in the interior of A_3 , i.e. both $F(z_k)$ are in R_3 . Now $F(x_1, y_1) = (x_2, y_1)$ and $F(x_2, y_2) = (x_1, y_2)$ so we require $0 < x_k < 1 - \xi$ and $1 - \eta < y_k < 1$, which is easily verified for $(\xi, \eta) \in \mathcal{I}_1$. It follows that $\text{dist}(z_k, \mathcal{D}) > 0$ and the associated cocycle is $M_3 M_3$. We remark that $\text{tr}(M^2) = (\text{tr}M)^2 - 2\det M$ so that for area preserving matrices M , we have $|\text{tr}(M^2)| < 2 \iff |\text{tr}M| < 2$. Hence the conditions listed in Proposition 3.1 are verified provided that $|2 - 1/(\eta - \eta\xi)| < 2$, i.e. $4\eta(1 - \xi) > 1$, which clearly holds over \mathcal{I}_1 .

The analysis for \mathcal{I}_2 and \mathcal{I}_3 is analogous. They correspond to islands around period 6 orbits with itinerary $A_3, A_3, A_1, A_3, A_3, A_1$. The condition on the trace of the associated cocycle gives $\xi < 1 - 1/(3\eta)$, equivalently $\eta > 1/(3 - 3\xi)$. The other bounds on $\mathcal{I}_2, \mathcal{I}_3$ come from requiring $\text{dist}(z_k, \mathcal{D}) > 0$. \square

The parameter regions \mathcal{I}_n and their symmetries under σ_1, σ_2 are shown in Figure 4.11. These are the three largest (in terms of proportion of the parameter space) elliptic island families over \mathcal{P} but do not constitute an exhaustive list. We encountered the straight side of $\partial\mathcal{I}_2$ in Proposition 3.2. The period 3 elliptic periodic orbit seen there bifurcates to give the above period 6 orbit upon taking a second non-monotonic shear ($\xi > 0$).

Mixing properties

In this section we generalise our approach for proving mixing properties over the line $\eta = \xi$ to subsets of \mathcal{P} . Inequalities on generalised expansion factors dictate where in \mathcal{P} we can establish hyperbolicity and **(MR)**. Starting with hyperbolicity, across \mathcal{P} the traces of the $M_j(\xi, \eta)$ satisfy $|\text{tr}M_j| > 2$ for $j = 1, 2, 4$. For M_3 we have $\text{tr}M_2(\xi, \eta) = 2 - 1/(\eta - \eta\xi)$ which has absolute value greater than 2 provided that $1/(\eta - \eta\xi) > 4$, i.e. for $\eta < 1/(4 - 4\xi)$. Let \mathcal{P}' denote the points in \mathcal{P} for which this inequality is satisfied. We remark that the cone \mathcal{C} bounded by the unstable eigenvectors of M_2 and M_3 , containing those of M_1 and M_4 , is invariant and expanding for parameter values in \mathcal{P}' . The cone \mathcal{C}' for H^{-1} is similar, bounded by the stable eigenvectors of M_2 and M_3 . Under the $\|\cdot\|_\infty$ norm, the cone boundaries of \mathcal{C} are given by the unit vectors $(k_0, 1)^T$ and $(k_1, 1)^T$, where

$$k_0(\xi, \eta) = \frac{-2\xi}{1 + \sqrt{1 - 4\xi + 4\xi\eta}} < 0 \quad \text{and} \quad k_1(\xi, \eta) = \frac{2 - 2\xi}{1 + \sqrt{1 - 4\eta + 4\xi\eta}} > 0.$$

The cone boundaries of \mathcal{C}' are given by the unit vectors $(1, m_0)^T$ and $(1, m_1)^T$, where

$$m_0(\xi, \eta) = \frac{\sqrt{4\xi\eta - 4\xi + 1} - 1}{2\xi} \quad \text{and} \quad m_1(\xi, \eta) = \frac{\sqrt{4\xi\eta - 4\eta + 1} - 1}{2\xi - 2}.$$

As before, write the components of M_j as a_j, \dots, d_j then the expansion factor $K_j(\xi, \eta, k)$ of the matrix M_j in the direction $(k, 1)^T \in \mathcal{C}$ is given by $|c_j k + d_j|$. Noting that each matrix has determinant 1, the expansion factor $\mathcal{K}_j(\xi, \eta, m)$ of the matrix M_j^{-1} in the direction $(1, m)^T \in \mathcal{C}'$

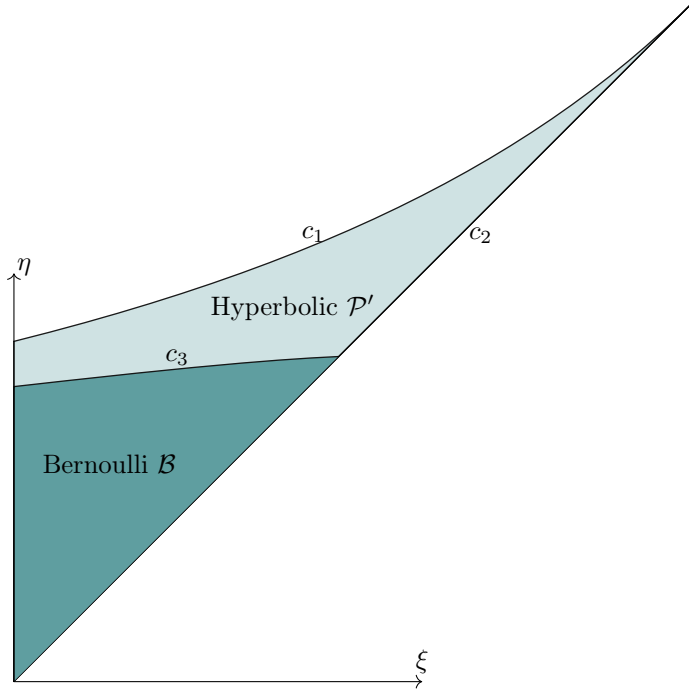


Figure 4.16: Plot of analytical results over \mathcal{P} . The curves c_1 and c_2 define \mathcal{P}' , c_3 defines $\mathcal{B} \subset \mathcal{P}'$, on which H is respectively hyperbolic, mixing. Note that c_3 meets c_2 at the point (η_1, η_1) .

is given by $|d_j - b_j m|$. Let

$$\Phi(\xi, \eta, k) = \sum_{j=1}^4 \frac{1}{K_j(\xi, \eta, k)} \quad \text{and} \quad \Psi(\xi, \eta, m) = \sum_{j=1}^4 \frac{1}{\mathcal{K}_j(\xi, \eta, m)},$$

then by the same reasoning as before, the growth lemmas for H and H^{-1} require

$$\max\{\Phi(\xi, \eta, k_0), \Phi(\xi, \eta, k_1)\} < 1 \quad \text{and} \quad \max\{\Psi(\xi, \eta, m_0), \Psi(\xi, \eta, m_1)\} < 1$$

respectively. We may now give our derived mixing windows:

Proposition 4.10. *Let H be defined by parameter values $(\xi, \eta) \in \mathcal{P}$.*

- For $(\xi, \eta) \in \mathcal{P}'$, H is non-uniformly hyperbolic.
- For (ξ, η) satisfying $\max\{\Phi(k_0), \Phi(k_1), \Psi(m_0), \Psi(m_1)\} < 1$, shown as the set \mathcal{B} in Figure 4.16, H is Bernoulli.

Proof. We adjust the argument given for the case $\xi = \eta$. One can verify that the chain of inequalities (4.12) holds for all $(\xi, \eta) \in \mathcal{P}'$ so that \mathcal{C} is invariant. Similarly one can verify that each of the M_j expands vectors parallel to the cone boundaries, so \mathcal{C} is expanding. Existence of this invariant expanding cone implies non-zero Lyapunov exponents over a full measure set, so H is hyperbolic for parameter values in \mathcal{P}' . Moving onto proving **(M)**, Lemmas 4.11, 4.14, and 4.15 are entirely analogous. Lemma 4.12 follows from $\max\{\Phi(\xi, \eta, k_0), \Phi(\xi, \eta, k_1)\} < 1$ and Lemma 4.13 follows from $\max\{\Psi(\xi, \eta, m_0), \Psi(\xi, \eta, m_1)\} < 1$. One can verify that this reduces to $\Psi(\xi, \eta, m_1) < 1$, shown as the region $\mathcal{B} \subset \mathcal{P}'$ bounded by $\xi = 0$, c_2 , and the curve c_3 given by $\Psi(\xi, \eta, m_1) = 1$ (see Figure 4.16). Condition **(MR)** follows from adapting the $x_v(\eta) < q_1(\eta)$ inequality. Solving line

intersection equations gives

$$x_v(\xi, \eta) = \frac{\eta\xi(1-\xi)}{1-\eta(1-\xi)} \quad \text{and} \quad q_1(\xi, \eta) = \frac{(1-\eta)(1-\xi)^2}{1+(1-\eta)(1-\xi)}$$

so that $x_v(\xi, \eta) < q_1(\xi, \eta)$ reduces to

$$\xi < \frac{(1-\eta)^2}{1-\eta+\eta^2}$$

which holds over \mathcal{B} . Again, the equivalent inequality to $x_v(\xi, \eta) < q_1(\xi, \eta)$ for H^{-1} results in a less stringent condition on the parameter space, hence also holds over \mathcal{B} . It follows, then, that H is Bernoulli over parameter values $(\xi, \eta) \in \mathcal{B}$. \square

We now prove our main theorem.

Proof of Theorem 4.3. Given a parameter set $P \subset (0, 1) \times (0, 1)$, define

$$\Sigma(P) = P \cup \sigma_1(P) \cup \sigma_2(P) \cup (\sigma_2 \circ \sigma_1)(P).$$

Letting $\mathcal{H} = \Sigma(\mathcal{P}')$, $\mathcal{M} = \Sigma(\mathcal{B})$, the first two statements in Theorem 4.3 follow from Proposition 4.10 and the semi-conjugacies established in section 4.3.4. The statement on elliptic islands is similar, following from the semi-conjugacies and Proposition 4.9. \square

4.4 Summary

For both systems H_η , $H_{(\xi, \eta)}$ considered in this chapter, the derived mixing windows are suboptimal. Note that we could use the same convexity argument used in the proof of Lemma 5.9 to improve the mixing window $\eta < \eta_1$ for H_η , but not by much. It cannot be used to improve the mixing window of H_ε as there we are growing piecewise linear curves, made of up line segments of varying gradients, so we cannot minimise expansion over a single vector $v \in \mathcal{C}$. Similarly we cannot use the method of growing piecewise linear curves for $H_{(\xi, \eta)}$ as the Jacobians M_i, M_j over neighbouring partition elements A_i, A_j always have opposite orientation preserving/reversing effects on vectors $v \in \mathcal{C}$.

In general, if we rely on a matrix M_i for expansion and that matrix loses hyperbolicity at a parameter value $\eta = \eta_0$, using the methods described in this chapter the mixing window will necessarily be bounded away from this parameter value. Essentially near η_0 we have $K_i(\eta) \approx 1$ so that $\sum_j 1/K_j < 1$ is satisfied only when the other expansion factors K_j , $j \neq i$ are very large. Similar to the method of dealing with non-hyperbolic regions, this can potentially be overcome by considering expansion over more and more iterates, avoiding using M_i itself. In practice this greatly increases the total number of matrices M_j we must consider. Indeed, if A_i contains a periodic orbit then this number is infinite. Establishing growth conditions in this fashion may be tractable at single parameter values (we will see such an example in the next chapter) but it is much harder to show over large parameter spaces, e.g. for $H_{(\xi, \eta)}$ the rest of the region \mathcal{P}' and beyond.

Figure 4.17 compares a numerical evaluation of the dynamics over the parameter space \mathcal{P} with the results of this chapter. The tighter mixing windows established for the map H_η (i.e. with $\xi = 0$) appear to extend out some distance into the two dimensional $\xi > 0$ parameter space. Chains of island structures persist between the two large island windows $\mathcal{I}_2, \mathcal{I}_3$ identified in Proposition 4.9. These islands fall in the strip

$$\frac{1}{3-3\xi} < \eta < \frac{4\xi - 9 + \sqrt{16\xi^2 - 40\xi + 33}}{8\xi - 8}$$

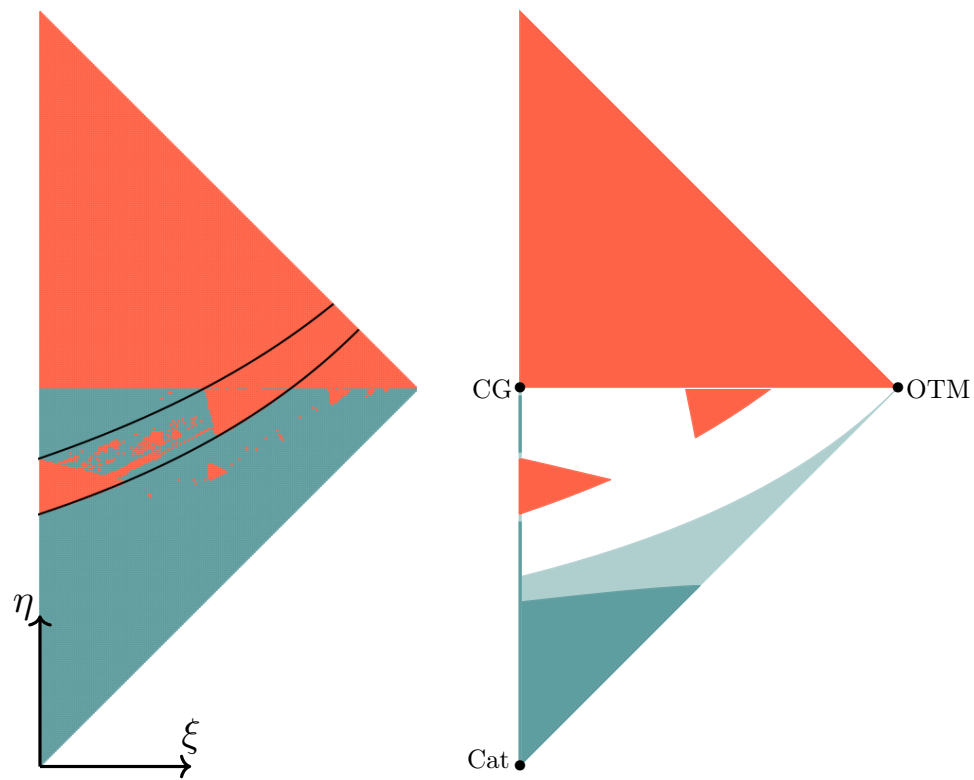


Figure 4.17: Left: a discretised parameter space \mathcal{P} . FTLE fields are calculated at each parameter value (pixel), coloured red in the case of elliptic islands, blue where the dynamics appear ergodic. The black lines highlight a strip where a key matrix is non-hyperbolic. Right: proven behaviour over \mathcal{P} in this chapter; islands (red), hyperbolicity (light blue), Bernoulli (blue). Notable maps on the periphery are also labelled.

on which the matrix $M = M_1 M_3 M_3$ is non-hyperbolic. It is essentially the extension of the matrix $M_3 = \mathcal{M}_1 \mathcal{M}_0 \mathcal{M}_0$ from the proof of Proposition 3.5 (hyperbolicity of H_η) into the full (ξ, η) parameter space. Comparing with proven results to the right, note that the curve $\eta = 1/(3 - 3\xi)$ also bounds the regions $\mathcal{I}_2, \mathcal{I}_3$. Whether $H_{(\xi, \eta)}$ is hyperbolic in this strip depends on the precise location its periodic orbits. If the cocycle associated with an orbit is some power of M and the orbit is bounded away from \mathcal{D} , elliptic islands form.

Like the Cat Map and Cerbelli and Giona's map, the rightmost corner of \mathcal{P} (labelled at the OTM) appears hyperbolic and mixing in numerical tests. Proving this will be subject of the next chapter, requiring a modification of the methods employed in this chapter to deal with the situation of unbounded return times.

Chapter 5

Proving Mixing Results - Unbounded Return Times

5.1 Introduction

In the examples examined in Chapters 3 and 4, return times to a hyperbolic region A were bounded above by some $N \in \mathbb{N}$. For H_η we had $N = 3$ and for $H_{(\xi,\eta)}$ we only considered the case $N = 1$. Unbounded N is not a fundamental barrier to analysis. Linked twist maps, for example, have established mixing properties despite return times diverging as we approach the boundaries. Proving this, however, either relies on monotonicity (co-rotating case, see Wojtkowski, 1980) or periodic behaviour specific to LTMs (counter-rotating case, see Przytycki, 1983). In the more general non-monotonic piecewise linear setting, there is an inherent challenge to establishing growth lemmas. We sketch the details here. If N is unbounded, since $\mu(A)$ is finite, elements of the return time partition $A = \bigcup_{n \geq 1} A_n$ must have measures decaying to 0, typically accumulating at some point p . Any line segment Γ near p may then intersect arbitrarily many partition elements A_j . Due to non-monotonicity we must restrict to a single partition element to grow our line segment forwards, which, following an approach similar to section 4.3.2 involves the expansion factors K_j satisfying $S = \sum_j 1/K_j < 1$. These expansion factors typically grow with return time n as $K_n \sim cn$ so for Γ arbitrarily close to p , the sum S is potentially unbounded, likely greater than 1. We note that this is entirely analogous to the problem with the older one-step expansion condition (2.4) from Chernov and Zhang (2005).

Roughly speaking, our method for getting around the problem outlined above is to leverage the geometric properties of any line segment Γ for which the condition $S < 1$ fails. Assuming it fails the growth lemma, the self similar structure of the partition elements accumulating to p then allows for an inductive argument, implying that Γ must intersect fewer and fewer A_j and giving a contradiction. Our primary aim in this chapter is to show that $H_{(\xi,\eta)}$ at $\xi = \eta = 1/2$ is Bernoulli. The partition of the return map we construct to achieve this is quite complicated so we show our method for establishing growth lemmas in a simpler example, a non-monotonic linked twist map.

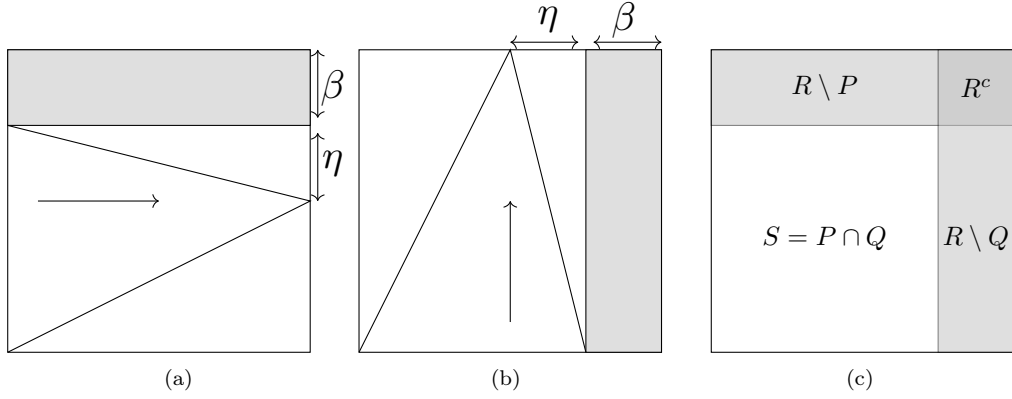


Figure 5.1: A pair of orthogonal non-monotonic shears F (a) and G (b), parameterised by $0 < \beta < 1$ and $0 < \eta < 1 - \beta$, which act on the annuli P and Q respectively. Their composition leaves the complement R^c of $R = P \cup Q$ invariant.

5.2 Mixing properties of non-monotonic LTMs

5.2.1 Map definition

Let H be the map $G \circ F$, acting on the torus \mathbb{T}^2 . Taking local coordinates $(x, y) \in (\mathbb{R}/\mathbb{Z})^2$, F maps

$$(x, y) \mapsto \begin{cases} (x + f_1(y, \eta), y) \bmod 1 & \text{for } y \leq 1 - \beta - \eta, \\ (x + f_2(y, \eta), y) \bmod 1 & \text{for } 1 - \beta - \eta \leq y \leq 1 - \beta, \\ (x, y) \bmod 1 & \text{for } y \geq 1 - \beta, \end{cases}$$

and G maps

$$(x, y) \mapsto \begin{cases} (x, y + f_1(x, \eta)) \bmod 1 & \text{for } x \leq 1 - \beta - \eta, \\ (x, y + f_2(x, \eta)) \bmod 1 & \text{for } 1 - \beta - \eta \leq x \leq 1 - \beta, \\ (x, y) \bmod 1 & \text{for } x \geq 1 - \beta, \end{cases}$$

where $f_1(t, \eta) = t/(1 - \beta - \eta)$ and $f_2(t, \eta) = (1 - \beta - t)/\eta$.

We remark that taking the pointwise limit $\beta \rightarrow 0$ gives the single parameter family of maps $H_{(\eta, \eta)}$ studied in section 4.3. Taking the other limit $\eta \rightarrow 0$ gives a family of co-rotating linked twist maps with known mixing properties (Sturman et al., 2006; Wojtkowski, 1980) over $0 < \beta < 1$. Taking both limits gives the Cat Map. Letting μ be the normalised Lebesgue measure on $R = P \cup Q$, see Figure 5.1(c), we remark that $H : R \rightarrow R$ is measure preserving and invertible. The main theorem of this section is the following:

Theorem 5.1. *Let $\beta = 1/2$, $\eta = 1/4$. Then $H : R \rightarrow R$ is Bernoulli.*

The first task is to establish non-zero Lyapunov exponents, which we will prove over the full parameter space.

5.2.2 Establishing non-uniform hyperbolicity

Proposition 5.1. *Across parameter values $0 < \beta < 1$ and $0 < \eta < 1 - \beta$, the map $H : R \rightarrow R$ admits non-zero Lyapunov exponents $\chi(z, v) \neq 0$ for almost every point $z \in R$ and vector $v \neq 0$.*

Proof. Let $H_S : S \rightarrow S$ be the return map to S , mapping $z \mapsto H^m(z)$ where $m = \inf\{k > 0 \mid H^k(z) \in S\}$, which is well defined for almost every $z \in S$. By an entirely analogous argument

to that given in Sturman et al. (2006), the orbit of almost every $z \in R$ will hit S with positive frequency. Returns to S serve as a natural way to split up itineraries into blocks, non-zero Lyapunov exponents a.e. follow from the existence of an invariant expanding cone for DH_S . Noting that $H_S = G_S \circ F_S^*$, the cocycle DH_S at $z \in S$ is given by $DG_{z'}^l DF_z^k$, where $z' = F^k(z)$, and $k, l \in \mathbb{N}$. The location of z and z' in S decide whether we shear using f_1 or f_2 when we apply F_S and G_S . Fixing k and l , these two binary choices give 4 possible values for $DG_{z'}^l DF_z^k$. Denote these by $M_{j,k,l}$ for $1 \leq j \leq 4$, explicit expressions are as follows:

$$M_{1,k,l} = \begin{pmatrix} 1 & \frac{k}{1-\beta-\eta} \\ \frac{l}{1-\beta-\eta} & 1 + \frac{kl}{(1-\beta-\eta)^2} \end{pmatrix}, \quad M_{2,k,l} = \begin{pmatrix} 1 & \frac{k}{1-\beta-\eta} \\ -\frac{l}{\eta} & 1 - \frac{kl}{\eta(1-\beta-\eta)} \end{pmatrix},$$

$$M_{3,k,l} = \begin{pmatrix} 1 & -\frac{k}{\eta} \\ \frac{l}{1-\beta-\eta} & 1 - \frac{kl}{\eta(1-\beta-\eta)} \end{pmatrix}, \quad M_{4,k,l} = \begin{pmatrix} 1 & -\frac{k}{\eta} \\ -\frac{l}{\eta} & 1 + \frac{kl}{\eta^2} \end{pmatrix}.$$

One can verify that for all j, k, l and parameter values β, η the matrices $M_{j,k,l}$ are hyperbolic, and therefore admit unstable and stable eigenvectors. Let $\mathcal{C} = \mathcal{C}_{\beta,\eta}$ be the cone bounded by the unstable eigenvectors of $M_{2,1,1}$, $M_{3,1,1}$ and containing the vector $(0, 1)^T$. Let $\|\cdot\|$ be the $\|\cdot\|_\infty$ norm. One can verify, by calculating the gradients of eigenvectors and measuring norm expansion over the cone boundaries (Proposition 3.3), that \mathcal{C} is invariant and expanding. Note that hyperbolicity does not immediately follow from Proposition 3.4 as the block length $N = k + l - 1$ (equivalently the return time to S) is unbounded. Following the approach of Sturman et al. (2006), the fact that (almost every) orbit $H^n(z)$ hits S with some positive frequency $\alpha_z > 0$ allows us to adapt the argument of Proposition 3.4 to the case of unbounded N .

For large n and a.e. z the cardinality of $\{0 \leq i \leq n-1 \mid H^i(z) \in S\}$ is roughly $\alpha_z n$, certainly bounded below by $\alpha_z n/2^\dagger$. Let

$$K = \inf_{\substack{j,k,l \\ v \in \mathcal{C}}} \frac{\|M_{j,k,l} v\|}{\|v\|},$$

strictly greater than 1 since \mathcal{C} is expanding. Then for any $v_0 \in \mathcal{C}$,

$$\begin{aligned} \frac{1}{n} \log \|DH_z^n v_0\| &\geq \frac{1}{n} \log \left(K^{\frac{1}{2}\alpha_z n} \|v_0\| \right) \\ &= \frac{\alpha_z}{2} \log(K) + \frac{1}{n} \log \|v_0\| \end{aligned}$$

so that $\chi(z, v_0) \geq \alpha_z \log(K)/2 > 0$. We may then extend to non-zero Lyapunov exponents for general $v \neq 0$ as before, using Corollary 1.1. \square

Following the argument presented in Sturman et al. (2006), **(KS1-2)** easily hold for H . This, together with Proposition 5.1, allows us to define local stable and unstable manifolds $\gamma_s(z)$ and $\gamma_u(z)$ almost everywhere. Recall that by the Katok and Strelcyn (1986) theorem, ergodicity and the Bernoulli property for H then follow from conditions **(M)** and **(MR)** respectively, where:

(M): For almost any $z, z' \in R$, $\exists m, n$ s.t. $H^m(\gamma_u(z)) \cap H^{-n}(\gamma_s(z')) \neq \emptyset$.

(MR): For almost any $z, z' \in R$ there exists M, N such that for all $m > M$ and $n > N$, $H^m(\gamma_u(z)) \cap H^{-n}(\gamma_s(z')) \neq \emptyset$.

We require some basic properties of the inverse map $H^{-1} : R \rightarrow R$. We remark that the cone region \mathcal{C}' , bounded by the stable eigenvectors of $M_{2,k,l}$, $M_{3,k,l}$ and containing $(1, 0)^T$ is invariant and expanding under each $M_{j,k,l}^{-1}$. The return map H_S^{-1} is well defined, and almost every orbit $H^{-k}(z)$ hits S with positive frequency.

*Where F_S, G_S are the return maps to S under F, G . Unchanged from the case of monotonic LTMs, their composition is H_S (Sturman et al., 2006).

†By a combinatorial argument, see Sturman et al. (2006).

5.2.3 Establishing the Bernoulli property

In this section we will prove **(MR)** at the parameter values $\beta = 1/2$, $\eta = 1/4$. We begin with Lemmas 5.1 and 5.2, which describe the nature of local manifolds when mapped into S . In Lemmas 5.3 and 5.4 we give an iterative scheme for growing the forwards images of any local unstable manifold until they satisfy a geometric property. Growth in the backwards images of any local stable manifold is analogous, establishing an intersection by a simple geometric argument.

Lemma 5.1. *For a.e $z \in R$, there exist $m, n \in \mathbb{N}$ such that $H^m(\gamma_u(z))$ contains a line segment in S aligned with some $v \in \mathcal{C}$, and $H^{-n}(\gamma_s(z))$ contains a line segment in S aligned with some $v' \in \mathcal{C}'$.*

Proof. Since H is piecewise linear, $\gamma_u(z)$ and $\gamma_s(z)$ are line segments, aligned with some vectors u and u' respectively. By definition, for any $\zeta, \zeta' \in \gamma_u(z)$

$$\text{dist}(H^{-n}(\zeta), H^{-n}(\zeta')) \rightarrow 0 \quad (5.1)$$

as $n \rightarrow \infty$. Similarly for any $\zeta, \zeta' \in \gamma_s(z)$

$$\text{dist}(H^n(\zeta), H^n(\zeta')) \rightarrow 0 \quad (5.2)$$

as $n \rightarrow \infty$. Let $m = \inf\{k \geq 0 \mid H^k(z) \in S\}$ and $n = \inf\{k \geq 0 \mid H^{-k}(z) \in S\}$. Provided that DH_z^k are well defined for all $k \in \mathbb{Z}$ (the set of points z for which this does not hold has zero measure) it follows that $H^m(\gamma_u(z))$ contains a line segment in S , aligned with some vector $v = DH_z^m u$. Note that \mathcal{C} can be described at the cone region bounded by the stable eigenvectors of $M_{2,k,l}^{-1}$ and $M_{3,k,l}^{-1}$ and including the stable eigenvectors of each $M_{j,k,l}^{-1}$. Now v lies in \mathcal{C} , for if $v \notin \mathcal{C}$ then repeatedly applying the return map H_S^{-1} (applying the matrices $M_{j,k,l}^{-1}$ in the tangent space) will pull v towards the invariant expanding cone \mathcal{C}' , resulting in exponential growth in its norm, which contradicts (5.1). Similarly v' must lie in \mathcal{C}' to avoid contradicting (5.2). □

Partition S into four squares S_j using the lines $y = 1/4$ and $x = 1/4$ (see Figure 5.2). Note that DF is constant on the strips $S_1 \cup S_2$, $S_3 \cup S_4$, and DG is constant on the strips $S_1 \cup S_3$, $S_2 \cup S_4$. Parameterise the tangent space by $(v_1, v_2)^T \in \mathbb{R}^2$ and consider the cone subspaces $\mathcal{C} = \mathcal{C}_+ \cup \mathcal{C}_-$ defined by $(v_1, v_2)^T \in \mathcal{C}_+$ if $v_1 v_2 \geq 0$, $(v_1, v_2)^T \in \mathcal{C}_-$ if $v_1 v_2 \leq 0$. Similarly define \mathcal{C}'_{\pm} . These cones give stronger bounds on the gradients of the images of local manifolds, depending on their location in S :

Lemma 5.2. *Let Γ, Γ' be line segments in S , aligned with vectors $v \in \mathcal{C}$, $v' \in \mathcal{C}$ respectively. It follows that $H_S(\Gamma)$ contains a line segment:*

(A1) *Contained within $S_1 \cup S_3$, aligned with some vector in \mathcal{C}_+ , and/or*

(A2) *Contained within $S_2 \cup S_4$, aligned with some vector in \mathcal{C}_- .*

Similarly $H_S^{-1}(\Gamma')$ contains a line segment

(B1') *Contained within $S_1 \cup S_2$, aligned with some vector in \mathcal{C}'_- , and/or*

(B2') *Contained within $S_3 \cup S_4$, aligned with some vector in \mathcal{C}'_+ .*

Proof. We will show this for the image of Γ ; the argument for Γ' is analogous. Note that if $H_S(\Gamma)$ contains a line segment in $S_1 \cup S_3$ it must have been mapped there by G using the f_1 type shear. Hence it is aligned with a vector of the form $M_{1,k,l} v$ or $M_{3,k,l} v$, for some $k, l \in \mathbb{N}$. One can verify

that the images of \mathcal{C} under these matrices are contained within \mathcal{C}_+ as required. Similarly $M_{2,k,l}$ and $M_{4,k,l}$ map the cone into \mathcal{C}_- . □

It is useful to define additional potential properties of line segments, similar to those given in the above lemma, but with the signs of the cones reversed:

- (A1') Contained within $S_1 \cup S_3$, aligned with some vector in \mathcal{C}_- , and/or
- (A2') Contained within $S_2 \cup S_4$, aligned with some vector in \mathcal{C}_+ .
- (B1) Contained within $S_1 \cup S_2$, aligned with some vector in \mathcal{C}'_+ , and/or
- (B2) Contained within $S_3 \cup S_4$, aligned with some vector in \mathcal{C}'_- .

Call any line segment in S which joins the lines $y = 0$ and $y = 1/2$ a v -segment. Similarly define h -segments as those which join the line $x = 0, x = 1/2$ across S . We define the horizontal and vertical lengths of a line segment Γ by $\ell_h(\Gamma) = \nu(\{x \mid (x, y) \in \Gamma\})$ and $\ell_v(\Gamma) = \nu(\{y \mid (x, y) \in \Gamma\})$, where ν is the Lebesgue measure on \mathbb{R} . We remark that at the parameter values $\beta = 1/2$ and $\eta = 1/4$, the cones \mathcal{C}_\pm are bounded by the unit vectors (using the $\|\cdot\|_\infty$ norm) $(0, 1)^T$ and $(\pm(2 - \sqrt{3}), 1)^T$. Similarly the cones \mathcal{C}'_\pm are bounded by the unit vectors $(1, 0)^T$ and $(1, \pm(2 - \sqrt{3}))^T$.

Lemma 5.3. *Let $\beta = 1/2, \eta = 1/4$. Let $\Gamma \subset S$ be a line segment satisfying either (A1) or (A2). Then at least one of the following consequences hold:*

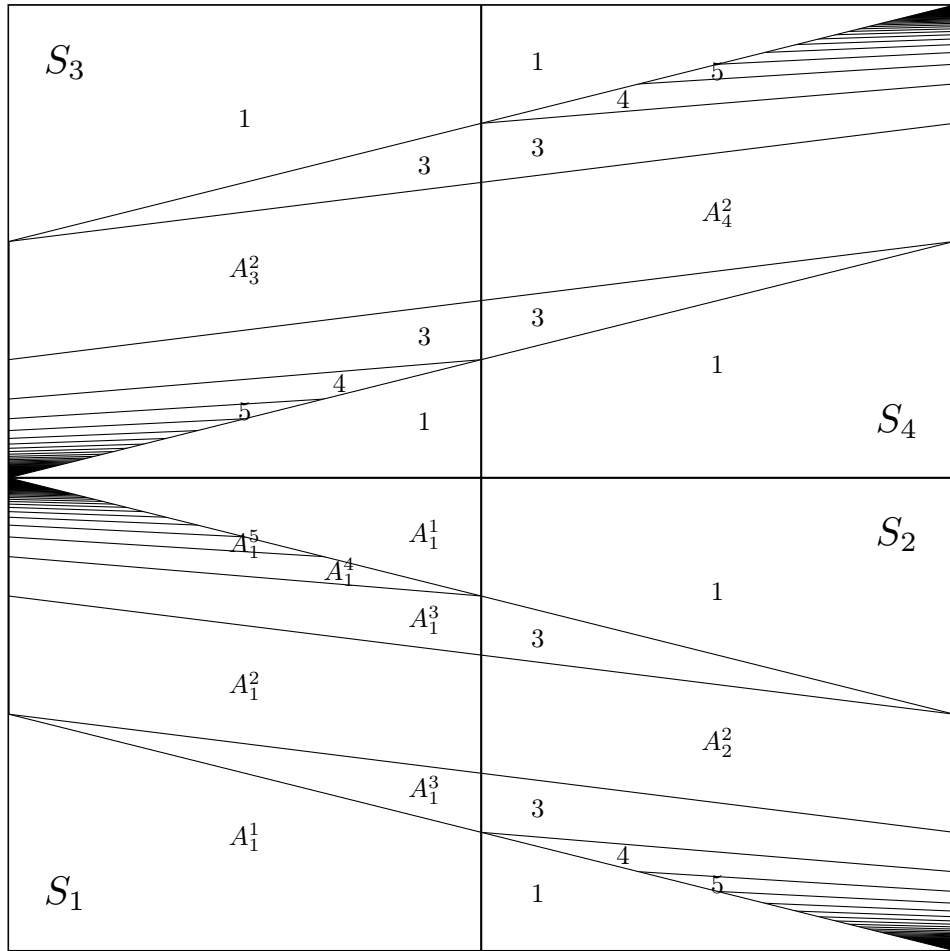
- (C1) $H_S(\Gamma)$ contains a v -segment,
- (C2) $H_S^2(\Gamma)$ contains a v -segment,
- (C3) There exists a line segment $\Lambda \subset F_S(\Gamma)$ satisfying (B1) or (B2) with $\ell_h(\Lambda) \geq (1 + \delta_1)\ell_v(\Gamma)$ for some $\delta_1 > 0$.

Proof. Figure 5.2(a) shows a partition of S into four squares S_j , each in turn partitioned by return time to S under F . Note that each S_j contain similar quadrilaterals A_j^2 within which points have return time 2. We claim that if Γ traverses some A_j^2 , joining its sloping boundaries, it follows that $H_S(\Gamma) \subset H^3(\Gamma)$ contains a v -segment. Let $\Gamma_j^2 = \Gamma \cap A_j^2$, then Γ_j^2 is a line segment with return time 2 to S under F , with endpoints on the two sloping boundaries. These boundaries map into the lines $x = 0$ and $x = \frac{1}{2}$ (the left and right boundaries of S) under F^2 , so $F_S(\Gamma_j^2) = F^2(\Gamma_j^2)$ is a line segment in S which joins its left and right boundaries. That is, $F_S(\Gamma_j^2)$ is a h -segment. Now $F_S(\Gamma_j^2)$ must traverse some B_j^2 , the quadrilaterals which have return time 2 to S under G (see Figure 5.2(b)). By an analogous argument, $G_S(F_S(\Gamma_j^2)) \subset G^2(F_S(\Gamma_j^2))$ contains a v -segment. Hence (C1) is satisfied.

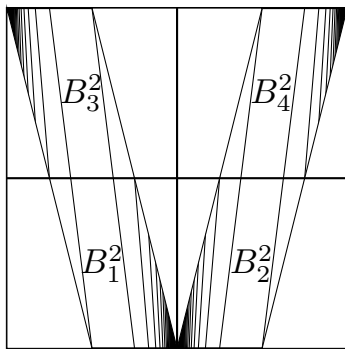
Now suppose Γ traverses none of the A_j^2 and assume Γ satisfies (A1). It follows that Γ satisfies one of the following cases:

- (A1.1) Γ lies entirely below the upper sloping boundary of A_1^2 ,
- (A1.2) Γ lies between the lower sloping boundary of A_1^2 and the upper sloping boundary of A_3^2 ,
- (A1.3) Γ lies entirely above the lower sloping boundary of A_3^2 .

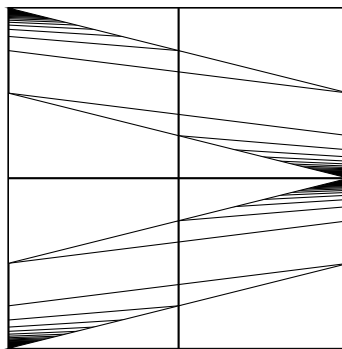
We start with case (A1.1). Let $\Gamma^k = \Gamma \cap A_1^k$ (see Figure 5.2); then the image $F_S(\Gamma)$ is made up of at most 3 line segments $\lambda^k = F^k(\Gamma^k)$, $k = 1, 2, 3$. If $\ell_h(\lambda^k) > \ell_v(\Gamma)$ for k , then we can take $\Lambda = \lambda^k$ to establish (C3). Since Γ is aligned in \mathcal{C}_+ , for each k we have that $\ell_h(\lambda^k) \geq 4k\ell_v(\Gamma^k)$, with equality when Γ is aligned with the cone boundary $(0, 1)^T$. Assume that we cannot satisfy



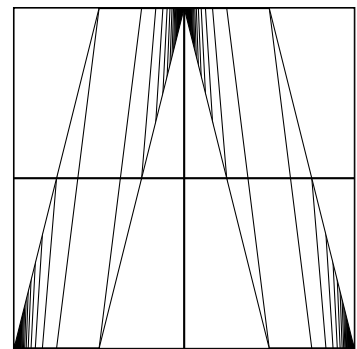
(a)



(b)



(c)



(d)

Figure 5.2: A partition of S into four squares S_j . Each S_j are then partitioned based on return time to S under the map (a) F , (b) G , (c) F^{-1} , (d) G^{-1} . For sets with specific labels (e.g. A_j^k) the subscript j refers to the parent set S_j and the superscript k is the return time.

(C3) by taking Λ to be λ^1 or λ^2 , that is, we have $4(1)\ell_v(\Gamma^1) \leq \ell_v(\Gamma)$ and $4(2)\ell_v(\Gamma^2) \leq \ell_v(\Gamma)$. Now since $\ell_v(\Gamma^1) + \ell_v(\Gamma^2) + \ell_v(\Gamma^3) = \ell_v(\Gamma)$ these two inequalities give

$$\ell_v(\Gamma^3) \geq \left(1 - \frac{1}{4(1)} - \frac{1}{4(2)}\right) \ell_v(\Gamma) = \frac{5}{8} \ell_v(\Gamma)$$

so that

$$\ell_h(\lambda^3) \geq 4(3) \frac{5}{8} \ell_v(\Gamma) > \ell_v(\Gamma).$$

In either case, then, (C3) is satisfied. We remark that this analysis is roughly analogous to deriving the key bound on the reciprocals of expansion factors from the previous chapter, reducing to verifying that

$$\sum_{k=1}^3 \frac{1}{4k} < 1.$$

By an analogous argument, (C3) follows from (A1.3) as

$$\sum_{k=1}^3 \frac{1}{4k - 2 + \sqrt{3}} \approx 0.483 < 1, \quad (5.3)$$

where we have used the fact that within each A_3^k , expansion of F^k is poorest over the other \mathcal{C}_+ boundary $(2 - \sqrt{3}, 1)^T$. For Γ satisfying case (A1.2), let $\Gamma_j = \Gamma \cap S_j$. Clearly for one of the $j = 1, 3$ we have

$$\ell_v(\Gamma_j) \geq \frac{1}{2} \ell_v(\Gamma). \quad (5.4)$$

Assume first that this holds for $j = 1$. As before, label the partition elements with return time k as A_1^k (see Figure 5.3). The set A_1^1 is bounded by ∂S_1 and the line $y = (1 - x)/4$, A_1^2 is as before, and for $k \geq 2$ the line separating A_1^k and A_1^{k+1} has equation $y = (2k - 1 - 2x)/8k$. Note that Γ_1 can intersect arbitrarily many of the A_1^k . Hence we cannot simply apply the previous method of summing the expansion factors as, noting (5.4), we require

$$\sum_{k \geq 1} \frac{1}{4k} < \frac{1}{2}$$

and this sum clearly diverges. Instead, then, suppose that there exists Γ_1 which violates the Lemma and aim for a contradiction. Note that for any three element subset $K = \{k_1, k_2, k_3\} \subset \mathbb{N}$, we have that

$$\sum_{k \in K} \frac{1}{4k} \leq \sum_{k=1}^3 \frac{1}{4k} < \frac{1}{2}$$

so that Γ_1 must intersect four or more of the partition elements A_1^k . By the geometry of the partition, it follows that

(†) Γ_1 traverses A_1^k for some $k \geq 3$, connecting the lines $y = \frac{2k-1-2x}{8k}$ and $y = \frac{2(k-1)-1-2x}{8(k-1)}$.

We state (see Appendix B for proof) that if Γ_1 traverses A_1^k for some $3 \leq k \leq 6$, then $H_S^2(\Gamma_1)$ contains a v -segment, satisfying (C2). The line segment Γ_1 , then, must traverse A_1^k for some $k \geq 7$ and must not traverse A_1^6 . This gives an upper bound $\ell_v(\Gamma_1) \leq L_6 = 1/32$, the height of the segment joining the lower corner of A_1^6 to the upper boundary of S_1 on $y = 1/4$. Suppose first that Γ_1 traverses A_1^7 , let $\Gamma_1^7 = \Gamma_1 \cap A_1^7$. Then since the gradient of the lower boundary of A_1^7 is steeper than that of its upper boundary, and Γ_1^7 is aligned with some vector in \mathcal{C}_+ , we can derive a lower bound $\ell_v(\Gamma_1^7) \geq h_7$ (see Figure 5.3). Specifically $h_7 = y_7 - 11/48$, where y_7 solves the pair

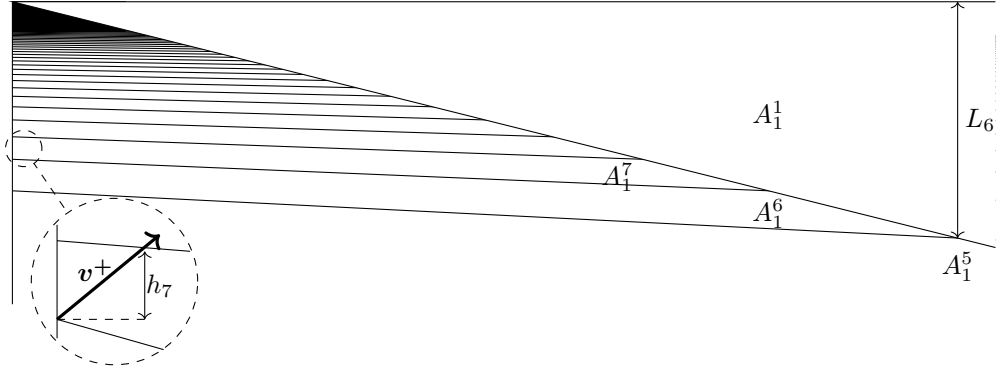


Figure 5.3: The upper section of S_1 with sets of constant return time A_1^k highlighted. The length L_6 shows the maximum height of a line segment satisfying case (A1.2) which does not traverse A_1^6 . The length h_7 is the minimum height of a line segment which traverses A_1^7 , defined using the cone boundary $v^+ = (2 - \sqrt{3}, 1)^T$. The gradients in the magnified region have been altered to ease viewing.

of equations

$$\begin{cases} y = \frac{2(7-1)-1}{8(7-1)} + (2 + \sqrt{3})x, \\ y = \frac{1}{8(7)}(2(7) - 1 - 2x), \end{cases} \quad (5.5)$$

i.e. the intersection of the line passing through the lower left corner of A_1^7 aligned with the cone boundary $(2 - \sqrt{3}, 1)^T$ of C_+ , and the upper boundary of A_1^7 . This gives $h_7 = (30 + \sqrt{3})/10764$ so that, letting $\lambda^7 = F^7(\Gamma_1^7)$,

$$\begin{aligned} \ell_h(\lambda^7) &\geq 4(7)h_7 \approx 0.0825 \\ &> \frac{1}{16} = 2L_6 \geq 2\ell_v(\Gamma_1) \geq \ell_v(\Gamma) \end{aligned}$$

where we have used (5.4). Hence taking $\Lambda = \lambda^7$ satisfies (C3), so that if Γ_1 violates the lemma, it must not traverse A_1^7 , which in turn puts a smaller upper bound on $\ell_v(\Gamma_1)$. We now continue by induction, assume that Γ_1 traverses A_1^k but does not traverse A_1^{k-1} . Then by an analogous argument to the base case $\ell_v(\Gamma_1)$ is bounded from above by $L_{k-1} = 1/(8k - 24)$ and $\ell_v(\Gamma_1^k)$ is bounded from below by

$$h_k = \frac{2 + \sqrt{3}}{2(k-1)(4\sqrt{3}k + 8k + 1)}.$$

Now one can verify that

$$\begin{aligned} \ell_h(\lambda^k) &\geq 4(k)h_k = \frac{2k(2 + \sqrt{3})}{(k-1)(4\sqrt{3}k + 8k + 1)} \\ &> 2L_{k-1} = \frac{1}{4k - 12} \end{aligned}$$

for $k > k_1 \approx 5.0537$, so that $\ell_h(\lambda^k) > 2\ell_v(\Gamma_1) \geq \ell_v(\Gamma)$. It follows by induction that if Γ_1 violates the lemma, it cannot traverse A_1^k for all $k \geq 7$. But this contradicts (\dagger) , so for $j = 1$ the lemma must hold.

For $j = 3$ the argument is analogous, the minimum height of segments traversing the set A_3^k is given by the length of the set's boundary on the line $x = 0$. That is,

$$h_k = \frac{2k-1}{8k} - \frac{2(k-1)-1}{8(k-1)} = \frac{1}{8k(k-1)}.$$

By symmetry, the lengths L_{k-1} remain unchanged, and the expansion factors for each A_3^k are

given by $4k + \sqrt{3} - 2$. Noting that if Γ_3 traverses A_3^k for some $3 \leq k \leq 6$ then $H_S^2(\Gamma_1)$ contains a v -segment (see Appendix B), the induction argument in the case $j = 3$ works for k satisfying:

$$\frac{4k + \sqrt{3} - 2}{8k(k-1)} > \frac{1}{4k-12}.$$

Indeed, the above holds for $k > k_1 \approx 5.0545$, proving the lemma in the case $j = 3$ and completing the case where Γ satisfies (A1).

Let Γ satisfy (A2), as before we split into the following cases:

(A2.1) Γ lies entirely below the upper sloping boundary of A_2^2 ,

(A2.2) Γ lies between the lower sloping boundary of A_2^2 and the upper sloping boundary of A_4^2 ,

(A2.3) Γ lies entirely above the lower sloping boundary of A_4^2 .

Starting with case (A2.2), Γ intersects some collection of the sets A_j^k for $k = 1, 2, 3$, $j = 2, 4$. Noting that the expansion factors for A_3^k and A_4^k are $4k + \sqrt{3} - 2$ and $4k$ respectively, (C3) holds provided that

$$\sum_{k=1}^3 \frac{1}{4k + \sqrt{3} - 2} + \sum_{k=1}^3 \frac{1}{4k} < 1.$$

Comparing with (5.3), this clearly holds. Now for case (A2.1), the induction step[‡] rests on the inequality

$$\frac{4k + \sqrt{3} - 2}{8k(k-1)} > \frac{1}{8k-24},$$

which holds for $k \geq 4$, and the base step $k = 3$ rests on the inequality

$$\frac{4(3) + \sqrt{3} - 2}{8(3)(3-1)} > \frac{5}{32},$$

where $5/32$ is the y -coordinate of the top left corner of A_2^2 . Concluding with case (A2.3), the minimum height of the segment traversing sets with return time $k \geq 3$ is h_k from case (A1.1), so that the induction step rests on $4k h_k > L_{k-1}$ for $k \geq 4$ and the base step rests on $4(3)h_3 > 5/32$. One can verify that these indeed hold. The condition in (C3) that Λ satisfies (B1) or (B2) follows from the fact that for all $k \geq 1$, DF_z^k , $z \in S_1 \cup S_2$, maps \mathcal{C} into \mathcal{C}'_+ and DF_z^k , $z \in S_3 \cup S_4$, maps \mathcal{C} into \mathcal{C}'_- . □

We now give the equivalent lemma for growth under G_S . Let $\mathcal{H} : R \rightarrow R$ be the map $F \circ G$, i.e shearing vertically then horizontally. As before, the return map $\mathcal{H}_S : S \rightarrow S$ is given by $\mathcal{H}_S = F_S \circ G_S$.

Lemma 5.4. *Let $\beta = 1/2$, $\eta = 1/4$. Let $\Lambda \subset S$ be a line segment satisfying either (B1) or (B2). Then at least one of the following consequences hold:*

(C1') $\mathcal{H}_S(\Lambda)$ contains a h -segment,

(C2') $\mathcal{H}_S^2(\Lambda)$ contains a h -segment,

(C3') *There exists a line segment $\Gamma \subset G_S(\Lambda)$ satisfying (A1) or (A2) with $\ell_v(\Gamma) \geq (1 + \delta_2)\ell_h(\Lambda)$ for some $\delta_2 > 0$.*

Proof. By an analogous argument to the proof of Lemma 5.3, after eliminating the cases where $\mathcal{H}_S(\Lambda)$ contains a h -segment, we can split into the following cases:

[‡]In the case $k = 4$, L_3 is actually smaller than $1/8$, but the bound holds nonetheless.

(B1.1) Λ lies entirely left of the right sloping boundary of B_1^2 ,

(B1.2) Λ lies between the left sloping boundary of B_1^2 and the right sloping boundary of B_3^2 ,

(B1.3) Λ lies entirely right of the left sloping boundary of B_3^2 .

(B2.1) Λ lies entirely left of the right sloping boundary of B_2^2 ,

(B2.2) Λ lies between the left sloping boundary of B_2^2 and the right sloping boundary of B_4^2 ,

(B2.3) Λ lies entirely right of the left sloping boundary of B_4^2 .

For $a = 1, 2, 3$, the argument for (B1.a) is then entirely analogous to (A1.a), as is the argument for (B2.a) to (A2.a). \square

We are now ready to prove the main theorem of this section.

Proof of Theorem 5.1. For almost any z , by Lemmas 5.1 and 5.2 we can find m_0 such that $H^{m_0}(\gamma_u(z))$ contains a line segment Γ_0 satisfying (A1) or (A2). Then iteratively apply Lemmas 5.3 and 5.4 to generate a sequence of line segments $(\Gamma_p)_{0 \leq p \leq P}$ with each $\Gamma_p \subset H^{m_p}(\Gamma_{p-1})$ for some $m_p \in \mathbb{N}$ and $\ell_v(\Gamma_p)$ growing exponentially with p . It follows that after finitely many steps P either

- Γ_P satisfies (C1) or (C2), or
- there exists $\Lambda_P \subset F_S(\Gamma_P)$ satisfying (C1') or (C2').

In the first case $H^{m_{P+1}}(\Gamma_P)$ contains a v -segment for some $m_{P+1} \in \mathbb{N}$. Hence $H^{m+m_{P+1}}(\gamma_u(z))$ contains a v -segment where $m = \sum_{i=0}^P m_i$. In the second case we have that $\mathcal{H}_S(\Lambda_P)$ or $\mathcal{H}_S^2(\Lambda_P)$ contains a h -segment. Noting that the images of h -segments under G_S contain v -segments (shown at the start of the proof of Lemma 5.3), $G_S \circ \mathcal{H}_S^n = \mathcal{H}_S^n \circ G_S$, and $\Lambda_P \subset F_S(\Gamma_P)$, we have that $H_S^2(\Gamma_P)$ or $H_S^3(\Gamma_P)$ contains a v -segment. Hence $H^{m+m'_{P+1}}(\gamma_u(z))$ contains a v -segment for some $m'_{P+1} \in \mathbb{N}$.

By the rotational symmetries of both the cone fields and the return time partitions (see Figure 5.2), the argument for growing the backwards images of local stable manifolds is entirely analogous. Hence for almost any z' , we can find $n \in \mathbb{N}$ such that $H^{-n}(\gamma_s(z'))$ contains a h -segment. Clearly h -segments and v -segments must always intersect, establishing **(M)**, so that H is ergodic. By the above, we have found M_1 such that $H^{M_1}(\gamma_u(z))$ contains a v -segment Γ , which lies in $S_1 \cup S_3$ or $S_2 \cup S_4$. Since Γ must traverse some A_j^2 , by the same argument given at the start of the proof of Lemma 5.3, it follows that $H^3(\Gamma)$ contains a v -segment and, by induction, so does $H^{3k}(\Gamma)$ for all $k \in \mathbb{N}$. Now note that $F(\Gamma)$ must connect the left and right boundaries of some S_j , and so $(G \circ F)(\Gamma)$ traverses some A_j^2 . Hence $H^4(\Gamma)$ contains a v -segment, as does $H^{4+3k}(\Gamma)$. Apply this argument once more, so that $H^8(\Gamma)$ and $H^{8+3k}(\Gamma)$ contains a v -segment for all $k \in \mathbb{N}$. These sequences, together with 4 and 8, cover all the naturals $n \geq 6$, so that $H^m(\gamma_u(z))$ contains a v -segment for all $m \geq M = M_1 + 6$. Analogously we can find $N = N_1 + 6$ such that $H^{-n}(\gamma_s(z))$ contains a h -segment for all $n \geq N$, establishing **(MR)**. \square

5.2.4 Remarks

While proving mixing properties of non-monotonic LTMs is worthwhile in its own right, the map $H_{\eta, \beta}$, $\eta = 1/4$, $\beta = 1/2$ above serves as a relatively simple example for showing our method of establishing growth lemmas in non-monotonic systems with unbounded escape times. The symmetrical nature of the shears made this a convenient choice, allowing us to keep calculations to

a minimum. The same method could certainly be used (with perhaps some minor adjustments) to prove mixing properties of $H_{\eta,\beta}$ across much of the hyperbolic parameter range given in Proposition 5.1. This is a purely computational exercise, revealing nothing new about the dynamics of piecewise linear non-monotonic LTMs, so we omit the details.

Conceivably one could also break the symmetry between the horizontal and vertical shears, introducing a third parameter $\xi \neq \eta$ into G , as we did in section 4.3. Numerical experiments suggest that mixing behaviour persists for small β , and (ξ, η) in the mixing windows found in section 4.3. Similarly the families of elliptic islands would persist, provided that:

- The periodic orbit associated with the island family persists under small β perturbations.
- It remains bounded away from the singularities, including those introduced by the boundary region.
- The associated cocycle remains elliptic.

Numerical tests show that the above conditions do hold for small β , provided that (ξ, η) lies sufficiently far (determined by β) from the parameter boundaries ∂I_j .

In line with Springham and Sturman (2014) we expect correlations of $H_{\eta,\beta}$ to decay polynomially for Hölder continuous observables. Following the Chernov and Zhang (2005) approach (or similar), some steps would be slightly more complicated than for monotonic LTMs, namely the cone constructions and structure of the singularity set for H_S . Other matters may be more straightforward as replacing monotonic shears by non-monotonic profiles of equal strength necessarily makes them steeper. This is generally beneficial to hyperbolicity and increases expansion factors, to the extent that it may be possible to show a one-step expansion for H_S , rather than the two-step necessary for the LTM of Springham and Sturman (2014). Again, proving this would likely be a computational exercise, revealing little more about the dynamics of non-monotonic LTMs. Indeed, the phenomenon which gives rise to polynomial mixing, fluid shearing in just one direction near boundaries, is unchanged from the monotonic setting.

5.3 Mixing properties of the OTM

5.3.1 Introduction

Recall the map $H_{(\xi,\eta)}$ studied in section 4.3. Here we study the special case $H = H_{(1/2,1/2)}$, which sits on the cusp of the open hyperbolic parameter space \mathcal{P}' . As the composition of two orthogonal symmetric ‘tent’ shaped shears, we refer to this map as the *Orthogonal Tents Map* (OTM). It is the natural extension to the CG Map, replacing its linear shear by a 90° rotation of its nonlinear horizontal shear.

Several unique features separate it from the rest of the (ξ, η) parameter space. Firstly since both $1/\eta$ and $1/(1-\eta)$ are integer valued over $0 < \eta < 1$ if and only if $\eta = 1/2$, H is the only map in the $0 < \xi, \eta < 1$ parameter space with all integer valued derivative matrices and can be expressed as $H(x, y) = DH_z \cdot (x, y)^T \bmod 1$, where $z = (x, y)$. Before any further analysis this immediately implies that periodic orbits are dense on \mathbb{T}^2 , as the cardinality of any orbit containing a rational point $(s/q, p/q) \in \mathbb{T}^2$ with $s, p, q \in \mathbb{N}$ is bounded above by q^2 (see Cerbelli and Giona, 2005).

Periodicity underlies another fundamental feature of H . Consider the four line segments l_j shown in Figure 5.4. Each has gradient ± 1 and have endpoints $(s/4, p/4)$ for some $s, p = 0, 1, 2, 3, 4$. One can verify that $H(l_1) = l_2$, $H(l_2) = l_1$, $H(l_3) = l_4$, $H(l_4) = l_3$ so that each are periodic with period 2 and their union $l = \cup_j l_j$ is invariant under H . A comparison with linked twist maps is useful here. In those maps the boundary ∂R forms an invariant set, similarly of positive length,

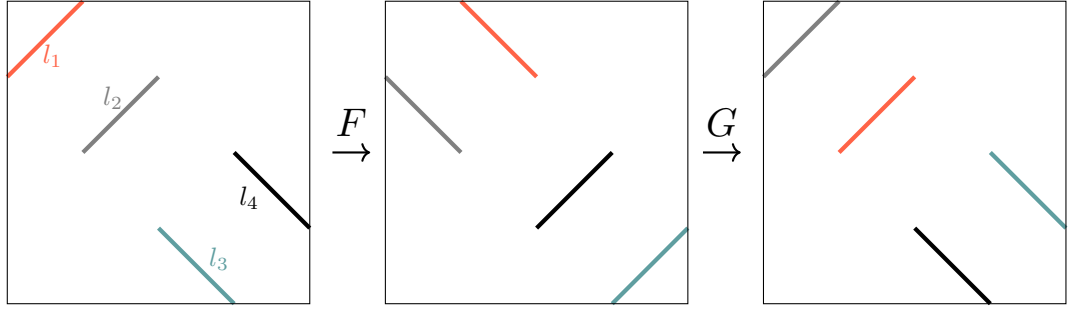


Figure 5.4: Line segments l_j satisfying $H : l_1 \leftrightarrow l_2, l_3 \leftrightarrow l_4$. Each are periodic with period 2, their union is invariant under H .

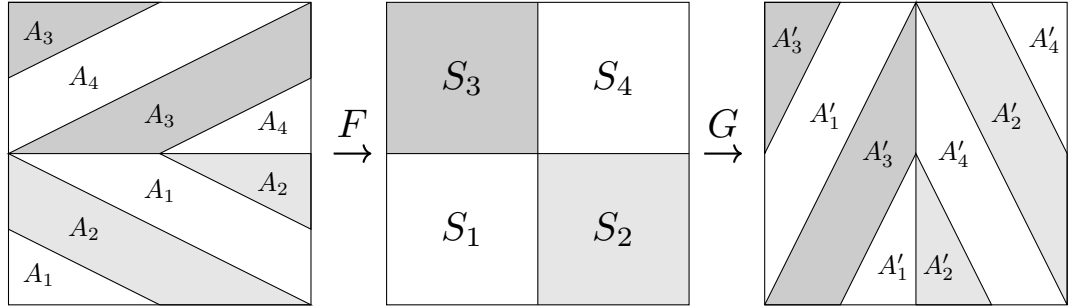


Figure 5.5: A partition of the torus into four rectangles S_j , and their preimages A_j, A'_j under F, G^{-1} .

which is imposed on the system to model ‘slow moving fluid near walls’. In contrast, the invariant set l of the OTM is not *imposed*, rather it arises from the specific dynamics of H . Informally we may treat the l_j as ‘ghost boundaries’, $n - 1$ dimensional manifolds which are advected back and forth, around which we see poor stretching and slowed mixing, akin to the boundary behaviour of LTMs. As an aside, noting that the l_j together span the full length and width of the torus, thinking of these segments as ‘stirrers’ following a periodic protocol gives an alternate way of driving the underlying flow (under idealised Stokes flow conditions). In this section we will show that the slowed stretching near these ghost boundaries / stirrers do not prevent us from establishing mixing results. Our main theorem is as follows:

Theorem 5.2. *The map $H : \mathbb{T}^2 \rightarrow \mathbb{T}^2$ is Bernoulli with respect to the Lebesgue measure.*

As before we begin by establishing hyperbolicity.

5.3.2 Establishing non-uniform hyperbolicity

Proposition 5.2. *H is non-uniformly hyperbolic.*

Partition the torus into the four squares S_j shown in Figure 5.5. The Jacobian DH is then constant on the preimages $A_j = F^{-1}(S_j)$, given by the matrix M_j where

$$M_1 = \begin{pmatrix} 1 & 2 \\ 2 & 5 \end{pmatrix}, \quad M_2 = \begin{pmatrix} 1 & 2 \\ -2 & -3 \end{pmatrix}, \quad M_3 = \begin{pmatrix} 1 & -2 \\ 2 & -3 \end{pmatrix}, \quad M_4 = \begin{pmatrix} 1 & -2 \\ -2 & 5 \end{pmatrix}.$$

For any $z \in X'$ with n -step itinerary

$$A_{j_1}, A_{j_2}, A_{j_3}, \dots, A_{j_n},$$

the cocycle DH_z^n is given by

$$DH_z^n = M_{j_n} \dots M_{j_3} M_{j_2} M_{j_1}$$

with each $j_k \in \{1, 2, 3, 4\}$. Our aim is to decompose any cocycle into hyperbolic matrices which share an invariant expanding cone. Note that while M_1 and M_4 are hyperbolic, M_2 and M_3 are not. Hence when M_2 or M_3 appear in a cocycle at M_{j_k} , we must combine them with its neighbouring matrices $M_{j_{k+1}}, \dots, M_{j_{k+2}}, M_{j_{k+1}}$ for some $l \in \mathbb{N}$.

Consider the countable family of matrices

$$\mathcal{M} = \{M_1, M_4, M_1 M_2^n, M_3 M_2^n, M_4 M_2^n, M_1 M_3^n, M_2 M_3^n, M_4 M_3^n\}$$

with $n \in \mathbb{N}$. Similarly define

$$\mathcal{M}' = \{M_1^{-1}, M_4^{-1}, M_1^{-1} M_2^{-n}, \dots, M_4^{-1} M_3^{-n}\}.$$

Our method for establishing non-uniform hyperbolicity mirrors that employed to show Proposition 5.1. We first show (Lemma 5.5) that \mathcal{M} and \mathcal{M}' give sufficient blocks for a decomposition of the cocycles DH_z^n and DH_z^{-n} . Lemma 5.6 then shows that these families admit invariant expanding cones. For non-monotonic LTMs, the matrix blocks described the behaviour in the tangent space under returns to a subset S . That almost every orbit hit S with positive frequency then implied that we complete blocks with positive frequency and non-zero Lyapunov exponents followed. We will show that blocks from \mathcal{M} may similarly be linked with recurrence to a positive measure subset σ and non-zero Lyapunov exponents follow as a result.

Lemma 5.5. *At almost every z , the cocycle DH_z^n can be decomposed into blocks from \mathcal{M} . At almost every z , the cocycle DH_z^{-n} can be decomposed into blocks from \mathcal{M}' .*

Proof. This argument was presented in Myers Hill et al. (2022a); for completeness we replicate it here.

It is sufficient to show that itineraries cannot get *trapped* in A_2 or A_3 , barring some set of zero measure. We will consider the set A_3 , with the argument for A_2 being entirely analogous. In particular we will show that $\mu(B_n) \rightarrow 0$ as $n \rightarrow \infty$ where $B_n = \{z' \in A_3 \mid H^k(z') \in A_3 \text{ for all } 1 \leq k \leq n\}$.

Let $\mathcal{H} = F \circ G$. For any $z' \in A_3$,

$$\begin{aligned} H^k(z') \in A_3 \text{ for all } 1 \leq k \leq n &\iff (G \circ F)^k(z') \in A_3 \text{ for all } 1 \leq k \leq n \\ &\iff [F \circ (G \circ F)^k](z') \in S_3 \text{ for all } 1 \leq k \leq n \\ &\iff [(F \circ G)^k \circ F](z') \in S_3 \text{ for all } 1 \leq k \leq n \\ &\iff \mathcal{H}^k(z) \in S_3 \text{ for all } 1 \leq k \leq n \end{aligned}$$

where $z = F(z') \in S_3$. Hence recurrence in A_3 under H can be understood by instead studying recurrence in S_3 under \mathcal{H} . Letting $\mathcal{B}_n = \{z \in S_3 \mid \mathcal{H}^k(z) \in S_3 \text{ for all } 1 \leq k \leq n\}$, by the above we have $\mathcal{B}_n = F(B_n)$ and $\mu(B_n) = \mu(\mathcal{B}_n)$ since F preserves μ . The simpler geometry of S_3 makes this a convenient choice. Iteratively define $U_1 = \mathcal{H}(S_3) \cap S_3$, $U_n = \mathcal{H}(U_{n-1}) \cap S_3$ so that $\mathcal{B}_n = \mathcal{H}^{-n}(U_n)$. Since \mathcal{H} preserves μ , we have $\mu(\mathcal{B}_n) = \mu(U_n)$. Let $V = \mathcal{H}^{-1}(S_3) \cap S_3$ be the set of points in S_3 which stay in S_3 . An equivalent definition for the U_n is $U_1 = \mathcal{H}(V)$, $U_n = \mathcal{H}(U_{n-1} \cap V)$. Restricting to V in this way is beneficial as $\mathcal{H}|_V : V \rightarrow S_3$ is an affine transformation, mapping quadrilaterals to quadrilaterals. The sets $V = V_1 \cup V_2$ and $U_1 = P_1 \cup Q_1$ are shown in Figure 5.6, both composed of two quadrilaterals with corners on ∂S_3 . Note that V_1, P_1 share the corners $p_1^1 = (1/4, 1/2)$, $p_1^3 = (0, 3/4)$ and V_2, Q_1 share the corners $q_1^1 = (1/4, 1)$, $q_1^3 = (1/2, 3/4)$, all of which are periodic with period 2.

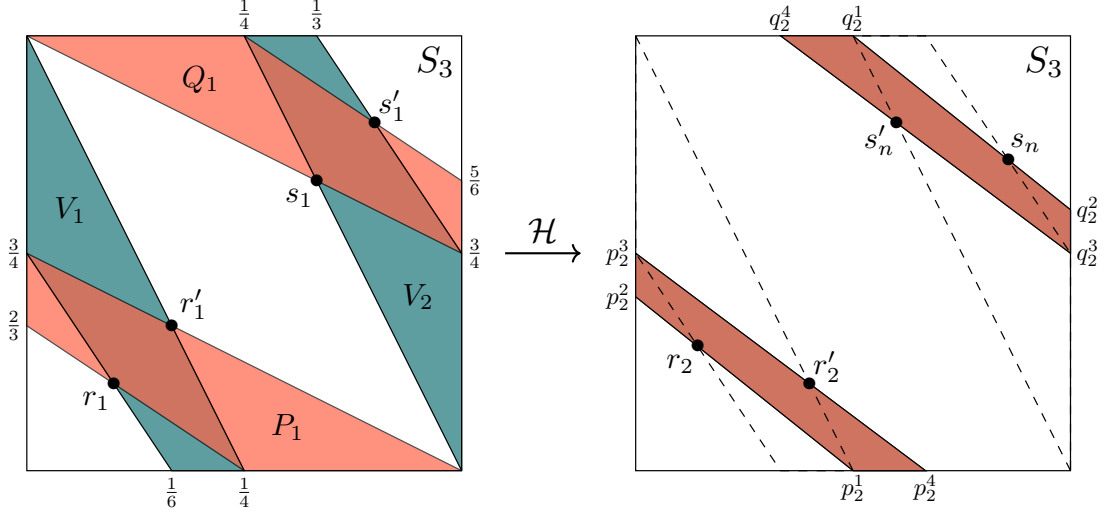


Figure 5.6: Left: Two subsets V (blue) and U_1 (red) of S_3 , each composed of two quadrilaterals. Right: The image $U_2 = \mathcal{H}(U_1 \cap V)$ in S_3 , the dashed lines show the boundary of V .

The intersection $U_1 \cap V$ is made up of two quadrilaterals $P_1 \cap V_1$ and $Q_1 \cap V_2$ with corners on the period 2 points and the points $r_1 = (1/10, 3/5)$, $r'_1 = (1/6, 2/3)$, $s_1 = (1/3, 5/6)$, and $s'_1 = (2/5, 9/10)$. Mapping these quadrilaterals forward under \mathcal{H} gives $U_2 = P_2 \cup Q_2$ where $P_2 = \mathcal{H}(Q_1 \cap V_2)$ and $Q_2 = \mathcal{H}(P_1 \cap V_1)$. Label the corners of these quadrilaterals by p_2^i and q_2^i , $i = 1, 2, 3, 4$, as shown in Figure 5.6.

We claim that for general $n \in \mathbb{N}$, U_n is made up of two quadrilaterals P_n, Q_n with corners

$$p_n^1 = \left(\frac{1}{4}, \frac{1}{2}\right), \quad p_n^2 = \left(0, \frac{3n+1}{4n+2}\right), \quad p_n^3 = \left(0, \frac{3}{4}\right), \quad p_n^4 = \left(\frac{n}{4n-2}, \frac{1}{2}\right),$$

$$q_n^1 = \left(\frac{1}{4}, 1\right), \quad q_n^2 = \left(\frac{1}{2}, \frac{3n+2}{4n+2}\right), \quad q_n^3 = \left(\frac{1}{2}, \frac{3}{4}\right), \quad q_n^4 = \left(\frac{n-1}{4n-2}, 1\right),$$

labelled in the same way as the case $n = 2$. The intersection $P_n \cap V_1$ will be a quadrilateral with corners p_n^1, r_n, p_n^3, r'_n , and $Q_n \cap V_2$ will be a quadrilateral with corners q_n^1, s_n, q_n^3, s'_n , where

$$r_n = \left(\frac{1}{4n+6}, \frac{3n+3}{4n+6}\right), \quad r'_n = \left(\frac{n}{4n+2}, \frac{2n+2}{4n+2}\right),$$

$$s_n = \left(\frac{2n+2}{4n+6}, \frac{3n+6}{4n+6}\right), \quad s'_n = \left(\frac{n+1}{4n+2}, \frac{4n+1}{4n+2}\right)$$

can be obtained by solving the line intersection equations. One can verify that $\mathcal{H}(p_n^1) = q_{n+1}^1$, $\mathcal{H}(r_n) = q_{n+1}^2$, $\mathcal{H}(p_n^3) = q_{n+1}^3$, $\mathcal{H}(r'_n) = q_{n+1}^4$, and $\mathcal{H}(q_n^1) = p_{n+1}^1$, $\mathcal{H}(s_n) = p_{n+1}^2$, $\mathcal{H}(q_n^3) = p_{n+1}^3$, $\mathcal{H}(s'_n) = p_{n+1}^4$, so that $\mathcal{H}(P_n \cap V_1) = Q_{n+1}$ and $\mathcal{H}(Q_n \cap V_2) = P_{n+1}$. Hence

$$\begin{aligned} \mathcal{H}(U_n \cap V) &= \mathcal{H}((P_n \cap V_1) \cup (Q_n \cap V_2)) \\ &= \mathcal{H}(P_n \cap V_1) \cup \mathcal{H}(Q_n \cap V_2) \\ &= Q_{n+1} \cup P_{n+1} \\ &= U_{n+1} \end{aligned}$$

and the claim follows by induction. Now in the limit $n \rightarrow \infty$, P_n limits onto the line segment $F(l_2)$ joining $(0, 3/4)$ to $(1/4, 1/2)$ and Q_n limits onto the line segment $F(l_1)$ joining $(1/4, 1)$ to $(1/2, 3/4)$. This give $\mu(U_n) \rightarrow 0$ as required.

The argument for dividing up DH_z^{-n} into blocks from \mathcal{M}' is entirely analogous, instead studying

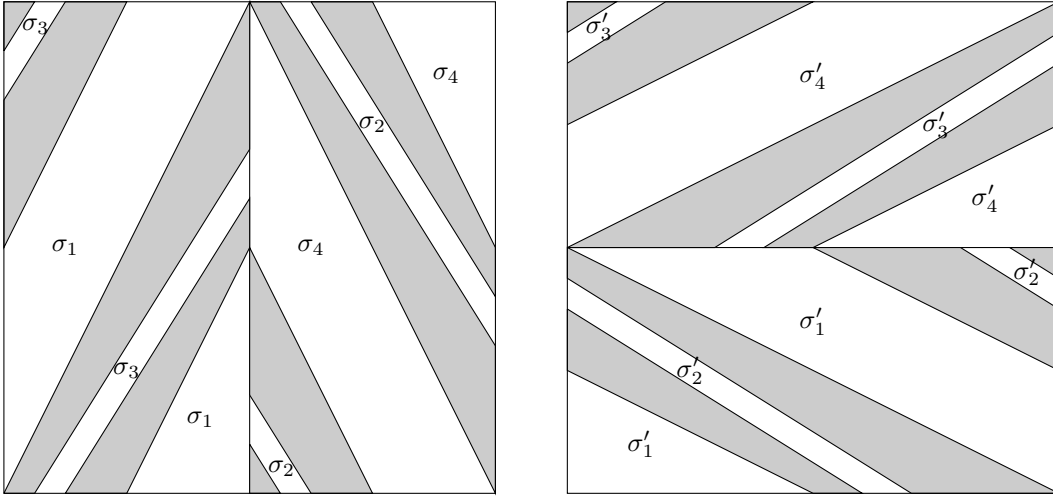


Figure 5.7: Partitions of the return sets σ, σ' (white) for H, H^{-1} into four sets $\sigma_j \subset H(A_j)$, $\sigma'_j \subset H^{-1}(A'_j)$.

the escape behaviour from A'_2 and A'_3 under H^{-1} .

□

Lemma 5.6. *The matrices in \mathcal{M} admit an invariant expanding cone \mathcal{C} . The matrices in \mathcal{M}' admit an invariant expanding cone \mathcal{C}' .*

Proof. Parameterise the tangent space by $(u, v)^T \in \mathbb{R}^2$. The first claim was shown in Myers Hill et al. (2022a) using the cone $\mathcal{C} = \{(v_1, v_2) \neq 0 \mid |v_2| \geq \phi |v_1|\}$ where ϕ is the golden ratio $(1 + \sqrt{5})/2$. Here we define a slightly wider cone $\mathcal{C} = \{(v_1, v_2) \neq 0 \mid |v_2| \geq \varphi |v_1|\}$, $\varphi = 21/13$, which still contains all the unstable eigenvectors of matrices in \mathcal{M} and none of the stable eigenvectors. Hence \mathcal{C} is invariant and one can verify that it is also expanding (minimum expansion factors are calculated later in Table 5.1, in particular the minimum expansion of a matrix M over \mathcal{C} under the $\|\cdot\|_\infty$ norm is given by $\min_\pm K_\pm(M)$). Defining $\mathcal{C}' = \{(v_1, v_2) \neq 0 \mid |v_1| \geq \varphi |v_2|\}$, the second claim follows by an entirely analogous argument. □

Recurrence to σ

Define σ as the union of the sets $\sigma_1 = H(A_1)$, $\sigma_2 = H(A_2 \cap H(A_3))$, $\sigma_3 = H(A_3 \cap H(A_2))$, $\sigma_4 = H(A_4)$. By construction, any orbit escaping A_2, A_3 or passing through A_1, A_4 must pass through σ . By the proof of Lemma 5.5, the return map $H_\sigma : \sigma \rightarrow \sigma$ is well defined at μ -almost every $z \in \sigma$. Similarly define $\sigma' = \cup_j \sigma'_j$ using the A'_j and the return map $H_{\sigma'}^{-1} : \sigma' \rightarrow \sigma'$ for H^{-1} . The sets σ, σ' are shown as the unshaded regions in Figure 5.7.

We begin by identifying the points in σ with return time 1, i.e. $H^{-1}(\sigma) \cap \sigma$. The preimages of σ_1, σ_4 are simply A_1, A_4 and by definition we have $H^{-1}(\sigma_2) = A_2 \cap H(A_3)$ so that $H^{-1}(\sigma_2) \cap \sigma = A_2 \cap \sigma_3 := \varsigma_3$ and similarly $H^{-1}(\sigma_3) \cap \sigma = A_3 \cap \sigma_2 := \varsigma_2$. See Figure 5.8(a) for an illustration.

Now consider recurrence to σ with return times greater than 1, the white regions of Figure 5.8(a). Starting with $z \in A_3$, by the definition of σ , the return time $r_\sigma(z) = \inf\{n \geq 1 \mid H^n(z) \in \sigma\}$ is $k + 1$ where k is the escape time $\inf\{n \geq 1 \mid H^n(z) \notin A_3\}$. Figure 5.9(a) shows a partition of A_3 into sets A^k of constant escape time, bounded by the boundary preimages $H^{-k}(\partial A_3)$. Points in A^k spend k iterates in A_3 then escape via A_1, A_2 , or A_4 and consequently return to σ . We partition each A^k based on this escape path, shown as the red lines in Figure 5.9(b). The labelling $A_{j,i}^k$ is such that $A_{j,i}^k \subset A^k \subset A_i$ and $H^k(A_{j,i}^k) \subset A_j$. It transpires that when points escape after spending 4 or more iterates in A_3 , they can only do so via A_1 or A_4 . Similarly partitioning A_2 and combining with Figure 5.8(a) gives a partition of σ into sets on which DH_σ is constant. The

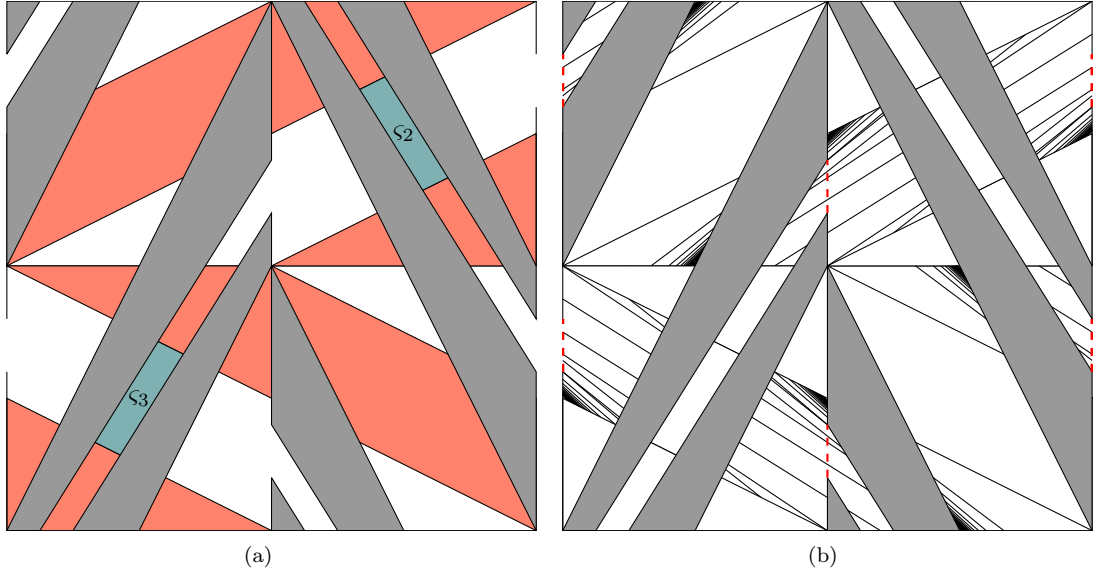


Figure 5.8: Part (a) shows the portions of σ (red, blue) with return time 1 to σ . Points in the white region have return times of 2 or more. Part (b) shows the singularity set \mathcal{S} for the return map H_σ . Red dashed lines denote the shared boundaries of the σ_j .

boundaries of these partition elements are shown in Figure 5.8(b) and constitutes, together with $\partial\sigma$, the singularity set \mathcal{S} for H_σ . We remark that outside of the sets ς_2, ς_3 the Jacobian DH_σ takes values in \mathcal{M} . Noting $H_\sigma(\varsigma_2) = H(\varsigma_2) \subset \sigma_3$ and $H_\sigma(\varsigma_3) = H(\varsigma_3) \subset \sigma_2$ we have that within ς_2 the Jacobian of H_σ^2 is given by MM_3 for some $M \in \mathcal{M} \cup \{M_2\}$ and within ς_3 it is given by MM_2 for some $M \in \mathcal{M} \cup \{M_3\}$. Hence, at almost every $z \in \sigma$ the Jacobian of H_σ or H_σ^2 is some matrix from \mathcal{M} .

We are now ready to establish non-uniform hyperbolicity.

Proof of Proposition 5.2. The proof of Lemma 5.5 shows that almost every orbit $H^n(z)$ hits σ . Similar to LTMs, we can show that almost all of those then continue to return to σ with some positive frequency α_z . This follows straightforwardly from the fact that H preserves the Lebesgue measure on \mathbb{T}^2 , a compact metric space, and σ is measurable. A proof is given in Lemma 6.3.3 of Sturman et al. (2006), originally from Burton and Easton (1980). As in the proof of Proposition 5.1, for large enough n we can guarantee that we hit σ at least $\alpha_z n/2$ times and the cocycle DH_z^n then contains as many applications of DH_σ . By the above, applying DH_σ either completes a block from \mathcal{M} or does so over the next iterate (the case where we land in ς_2, ς_3). At worst, then, we have roughly half as many blocks from \mathcal{M} in DH_z^n as we have returns to σ . Certainly this proportion is greater than a quarter, so DH_z^n contains at least $\alpha_z n/8$ blocks from \mathcal{M} . We may now argue as in Proposition 5.1. Letting

$$K = \inf_{\substack{M \in \mathcal{M} \\ v \in \mathcal{C}}} \frac{\|Mv\|}{\|v\|},$$

Lemma 5.6 gives $K > 1$. By the above, for any $v_0 \in \mathcal{C}$,

$$\begin{aligned} \frac{1}{n} \log \|DH_z^n v_0\| &\geq \frac{1}{n} \log \left(K^{\frac{1}{8} \alpha_z n} \|v_0\| \right) \\ &= \frac{\alpha_z}{8} \log(K) + \frac{1}{n} \log \|v_0\| \end{aligned}$$

so that $\chi(z, v_0) \geq \alpha_z \log(K)/8 > 0$. We may then extend to non-zero Lyapunov exponents for general $v \neq 0$ as before, using Corollary 1.1. \square

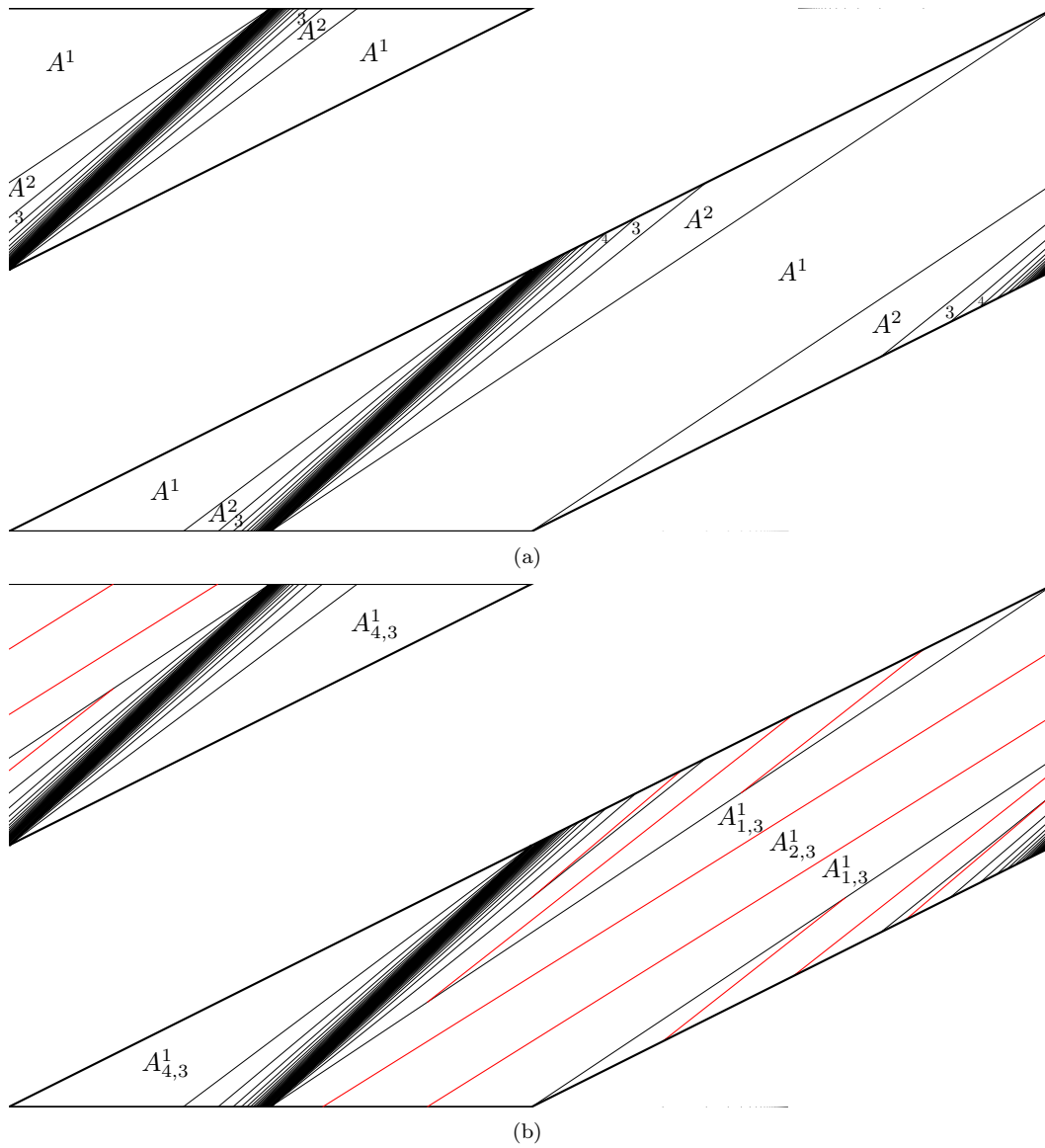


Figure 5.9: Partitions of the region A_3 . Part (a) shows a partition into sets A^k where k is the escape time. Part (b) shows a subdivision into sets $A_{j,3}^k \subset A^k$ where j is such that $H^k(A_{j,3}^k) \subset A_j$. Red lines in each A^k are the preimages of the A_1A_2 boundary under H^k .

5.3.3 Nature of local manifolds

Noting that **(KS1-2)** were shown in section 4.3, by Theorem 1.4, local unstable and stable manifolds $\gamma_u(z), \gamma_s(z)$ exist at a.e. z . Recall the conditions (5.1), (5.2) from section 5.2.3 which points on these manifolds must satisfy. Piecewise linearity of H ensures that these local manifolds are line segments containing z , aligned with some vector v . Our first task is to find bounds on the gradient of v based on the location of $z \in \mathbb{T}^2$.

Lemma 5.7. *For almost every z , there exists $m, n \in \mathbb{N}$ such that $H^m(\gamma_u(z))$ contains a line segment in σ aligned with some $v \in \mathcal{C}$, and $H^{-n}(\gamma_s(z))$ contains a line segment in σ' aligned with some $v' \in \mathcal{C}'$.*

Proof. By definition of the σ_j, σ'_j , we have that $\sigma_j = H(\sigma'_j)$ for $j = 1, 4$, and $\sigma_j = H^2(\sigma'_j)$ for $j = 2, 3$. For almost every z the number $m = \min\{k \geq 1 \mid H^k(z) \in \sigma\}$ is well defined, as is the cocycle DH_z^m . On some portion of $\gamma_u(z)$ around z , the cocycle DH_z^m will be constant and maps to some line segment Γ under H^m . Hence $H^m(\gamma_u(z))$ contains a segment Γ in σ , aligned with some vector v . Now if Γ lies in σ_1 , its preimage is a segment in σ'_1 aligned with the vector $M_1^{-1}v$. Now to satisfy (5.1), $M_1^{-1}v$ must lie in some stable cone \mathcal{C}'_s which contains all the stable eigenvectors of matrices in \mathcal{M}' and none of the unstable eigenvectors. Hence $v \in M_1\mathcal{C}'_s$. Similarly if $z \in \sigma_4$ then $v \in M_4\mathcal{C}'_s$, if $z \in \sigma_2$ then $v \in M_2M_3\mathcal{C}'_s$, and if $z \in \sigma_3$ then $v \in M_3M_2\mathcal{C}'_s$. Such a stable cone \mathcal{C}'_s is given by $\{(v_1, v_2) \neq 0 \mid |v_2| \geq |v_1|\}$; one can verify that $M\mathcal{C}'_s \subset \mathcal{C}$ for each $M \in \{M_1, M_4, M_2M_3, M_3M_2\}$, verifying $v \in \mathcal{C}$. The argument for $v' \in \mathcal{C}'$ is entirely analogous. \square

The expanding and invariance properties of the cone \mathcal{C} formed from \mathcal{M} will be key to growing the images of unstable manifolds. We can ensure stronger expansion by refining the cone, defining $\mathcal{C}_+, \mathcal{C}_- \subset \mathcal{C}$ by

$$(\mathcal{C}_+) \quad 3|v_1| \geq |v_2| \geq \varphi|v_1|, v_1v_2 > 0,$$

$$(\mathcal{C}_-) \quad 3|v_1| \geq |v_2| \geq \varphi|v_1|, v_1v_2 < 0.$$

Lemma 5.8. *Let Γ be a line segment in σ , aligned with some $v \in \mathcal{C}$. It follows that $H_\sigma(\Gamma)$ or $H_\sigma^2(\Gamma)$ contains a line segment:*

(A1) *Contained within $\sigma_1 \cup \sigma_3$, aligned with some vector in \mathcal{C}_+ , or*

(A2) *Contained within $\sigma_2 \cup \sigma_4$, aligned with some vector in \mathcal{C}_- .*

Proof. Suppose first that Γ does not lie entirely within σ_2 or σ_3 . Then Γ contains a component $\tilde{\Gamma}$ (possibly the whole of Γ) on which DH_σ is a matrix from \mathcal{M} . If $H_\sigma(\tilde{\Gamma})$ lands in $\sigma_1 \cup \sigma_3$, then this Jacobian is in the subset $\{M_1, M_1M_2^n, M_3M_2^n, M_1M_3^n\} \subset \mathcal{M}$. Case (A1) then follows from verifying that $M\mathcal{C} \subset \mathcal{C}_+$ for each M in this subset. Case (A2) can be argued similarly. If $\Gamma \subset \sigma_2 \cup \sigma_3$ then it contains a component on which the Jacobian of H_σ^2 is in \mathcal{M} and we can follow a similar argument. \square

5.3.4 Growth lemma

Lemma 5.9. *Let $\Gamma \subset \sigma$ be a line segment which satisfies either (A1) or (A2) and has simple intersection with each of the A_j . Then at least one of the following consequences hold:*

(C1) *There exists k such that $H^k(\Gamma)$ contains a line segment having non-simple intersection with some A_j ,*

(C2) *There exists k such that $H^k(\Gamma)$ contains a line segment Λ satisfying (A1) or (A2) with $\ell_v(\Lambda) \geq (1 + \delta)\ell_v(\Gamma)$ for some $\delta > 0$, independent of Γ .*

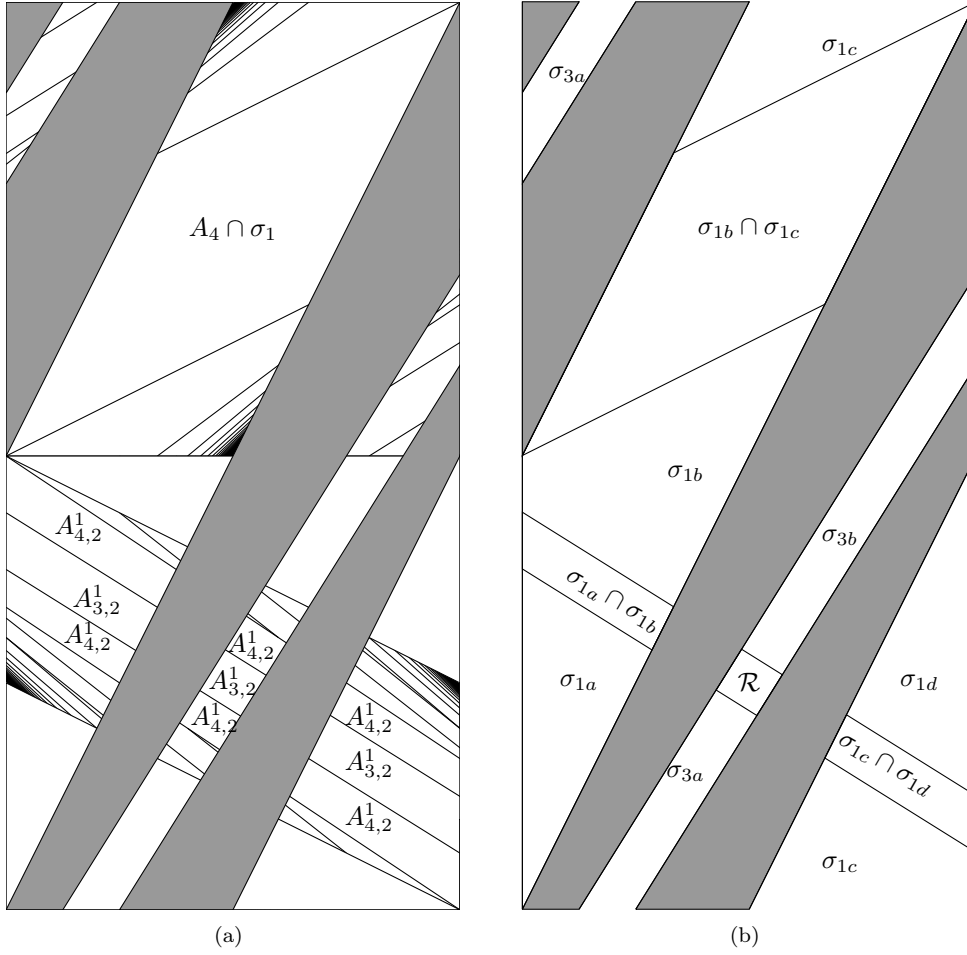


Figure 5.10: Part (a) shows the singularity curves dividing up $\sigma_1 \cup \sigma_3$ with some key partition elements labelled. The elements $A_{3,2}^1, A_4 \cap \sigma$ split $\sigma_1 \cup \sigma_3$ into six subsets $\sigma_{1a}, \dots, \sigma_{3b}$, any two of which are either disjoint or have intersection given by $A_4 \cap \sigma$ or one of the three subsets which make up $A_{3,2}^1$, see part (b). \mathcal{R} denotes the set $\sigma_{3a} \cap \sigma_{3b}$.

Proof. Figure 5.10(a) shows the singularity set for the return map H_σ over $\sigma_1 \cup \sigma_3 \setminus \varsigma_3$, and the singularity set of H_σ^2 over ς_3 . The singularity lines partition $\sigma_1 \cup \sigma_3$ into sets $A_{j,i}^k$ with the same labelling scheme as Figure 5.9(b).

Let Γ satisfy case (A1) and suppose it has non-simple intersection with $A_{4,2}^1$. Now since Γ has simple intersection with A_3 , observing Figure 5.10(a) it is clear that Γ must traverse $A_{3,2}^1$. Restricting $\Gamma^2 = \Gamma \cap A_2$, $H(\Gamma^2) \subset H(\Gamma)$ is a line segment which has non-simple intersection with A_4 , i.e. (C1) is satisfied with $k = 1$. Assume, then, that Γ has simple intersection with $A_{4,2}^1$ and therefore does not traverse $A_{3,2}^1$. If $\Gamma \subset \sigma_3$ then Γ lies entirely within one of two sets σ_{3a}, σ_{3b} (shown in Figure 5.10(b)) whose union is σ_3 , intersection is $\mathcal{R} = A_{3,2}^1 \cap \sigma_3$. For $\Gamma \subset \sigma_1$, simple intersection with A_3 implies that Γ does not traverse $A_4 \cap \sigma_1$. This, together with the two disjoint sets which make up $A_{3,2}^1 \cap \sigma_1$, implies that Γ lies entirely within one of four subsets $\sigma_{1a}, \dots, \sigma_{1d}$, shown in Figure 5.10(b). The behaviour of H_σ over the sets σ_{1a}, σ_{1b} is shown explicitly in Figures 5.11, 5.12.

Let $\|\cdot\|$ denote the $\|\cdot\|_\infty$ norm. Starting with σ_{1a} , the derivative of H_σ takes values in $\mathcal{M}_{1a} = \{M_1, M_4 M_2^k, M_3 M_2^l \mid k \in \mathbb{N}, l = 1, 2, 3\}$. The unlabelled sets in Figure 5.11 are the partition elements $A_{4,2}^k$ for $k \geq 5$, limiting onto the point $(0, 1/4)$ as $k \rightarrow \infty$ in the obvious fashion. We remark that any $\Gamma \subset \sigma_{1a}$ has simple intersection with all of the partition elements $A_{i,j}^k \subset \sigma_{1a}$. If Γ is entirely contained within some partition element A corresponding to $M \in \mathcal{M}_{1a}$, and is aligned with some unit vector $v \in \mathcal{C}_+$, then $\ell_v(H_\sigma(\Gamma)) = \|Mv\| \ell_v(\Gamma)$. Minimum expansion factors are

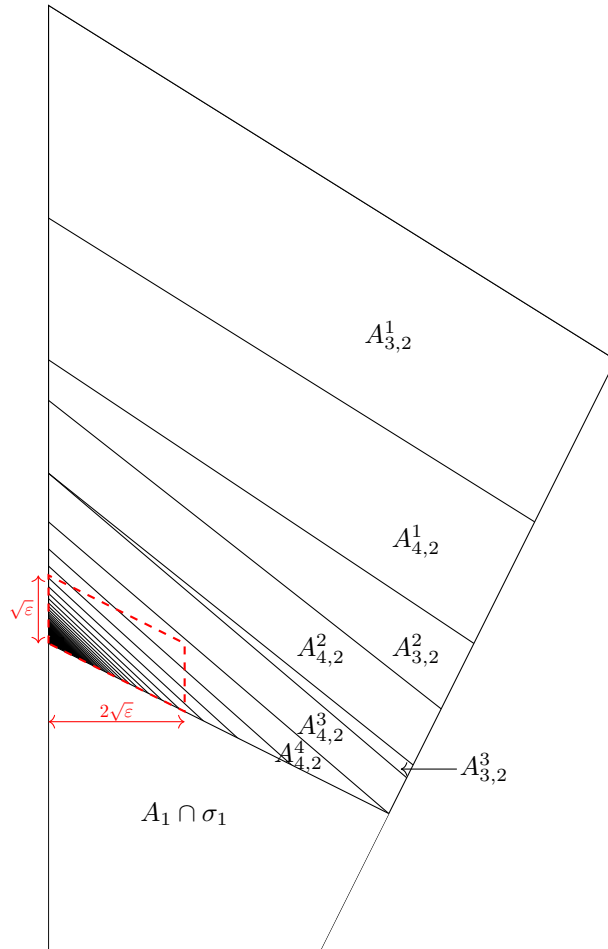


Figure 5.11: The singularity set of H_σ over σ_{1a} . Unlabelled sets are given by $A_{4,2}^k$ for $k \geq 5$ which limit onto the point $(0, 1/4)$ in the obvious fashion. The dashed red line is $\partial P(\varepsilon)$, useful for establishing **(KS1)** for H_σ .

straightforward to calculate. Parameterise unit vectors in \mathcal{C} by $(v_1, 1)^T$ where $1/3 \leq v_1 \leq 13/21$ and write the components of matrices $M \in \mathcal{M}$ as $\begin{pmatrix} a & b \\ c & d \end{pmatrix}$. Then by cone invariance and the fact that vectors $(v_1, v_2)^T \in \mathcal{C}$ have norm $|v_2|$, we have that $\|Mv\| = |cv_1 + d|$. This is monotone increasing in v_1 if $\text{sgn}(c) = \text{sgn}(d)$, monotone decreasing if $\text{sgn}(c) \neq \text{sgn}(d)$, so that $\|Mv\|$ is minimal on $(1/3, 1)^T$ or $(13/21, 1)^T$ in these respective cases. Table 5.1 shows the components of matrices $M \in \mathcal{M}$ and the minimum expansion factors $K_+(M)$ which follow.

M	Components	$K_+(M)$	$K_-(M)$
M_1	$\begin{pmatrix} 1 & 2 \\ 2 & 5 \end{pmatrix}$	$\frac{17}{3}$	$\frac{79}{21}$
M_4	$\begin{pmatrix} 1 & -2 \\ -2 & 5 \end{pmatrix}$	$\frac{79}{21}$	$\frac{17}{3}$
$M_1 M_2^n$	$(-1)^n \begin{pmatrix} 2n+1 & 2n+2 \\ 6n+2 & 6n+5 \end{pmatrix}$	$8n + \frac{17}{3}$	$\frac{16n}{7} + \frac{79}{21}$
$M_1 M_3^n$	$(-1)^n \begin{pmatrix} 1-6n & 6n+2 \\ 2-14n & 14n+5 \end{pmatrix}$	$\frac{16n}{3} + \frac{131}{21}$	$\frac{56n}{3} + \frac{13}{3}$
$M_2 M_3^n$	$(-1)^n \begin{pmatrix} 1-6n & 6n+2 \\ 10n-2 & -10n-3 \end{pmatrix}$	$\frac{80n}{21} + \frac{89}{21}$	$\frac{40n}{3} + \frac{7}{3}$
$M_3 M_2^n$	$(-1)^n \begin{pmatrix} 1-6n & -6n-2 \\ 2-10n & -10n-3 \end{pmatrix}$	$\frac{40n}{3} + \frac{7}{3}$	$\frac{80n}{21} + \frac{89}{21}$
$M_4 M_2^n$	$(-1)^n \begin{pmatrix} 1-6n & -6n-2 \\ 14n-2 & 14n+5 \end{pmatrix}$	$\frac{56n}{3} + \frac{13}{3}$	$\frac{16n}{3} + \frac{131}{21}$
$M_4 M_3^n$	$(-1)^n \begin{pmatrix} 2n+1 & -2n-2 \\ -6n-2 & 6n+5 \end{pmatrix}$	$\frac{16n}{7} + \frac{79}{21}$	$8n + \frac{17}{3}$

Table 5.1: Minimum expansion factors $K_{\pm}(M) = \inf_{v \in \mathcal{C}_{\pm}} \|Mv\|/\|v\|$ for each $M \in \mathcal{M}$ over the cones \mathcal{C}_{\pm} .

If Γ intersects $A_{4,2}^4$ and $A_{3,2}^3$ (traversing $A_{4,2}^3$) then $H^3(\Gamma \cap A_{4,2}^3)$ is a line segment in $A_2' \cap A_4$, connecting the A_3, A_4 boundary to the A_2, A_4 boundary. Noting that $A_2' \cap A_4$ is made up of two quadrilaterals, see Figure 5.5, there are two possible ways this can occur. Firstly, it can connect points $(x, 1)$ to $(2y - 1, y)$ with $1/2 \leq x \leq 3/4$. Its image under F then connects $(x, 1)$ to $(1, y)$ so that then, shearing vertically by G , its image under H connects $(x, 2 - 2x)$ to $(1, y)$, passing through $y = 0$. Since $x \leq 3/4$, we have $2 - 2x \geq 1/2$ so that $H^4(\Gamma \cap A_{4,2}^3)$ must have non-simple intersection with A_2 . The second case, where $H^3(\Gamma \cap A_{4,2}^3)$ connects points $(x, 1/2)$ and $(2y - 1/2, y)$, is similar so that (C1) is satisfied.

Assume, then, that Γ does not traverse $A_{4,2}^3$. Two possible cases follow; either Γ lies entirely below the upper boundary of $A_{4,2}^3$, or Γ lies entirely above the lower boundary of $A_{4,2}^3$. In the first case let $\Gamma_1 = \Gamma \cap A_1$. If $K_+(M_1) \ell_v(\Gamma_1) > \ell_v(\Gamma)$, then we may take $\Lambda = H(\Gamma_1) \subset H_{\sigma}(\Gamma)$ to satisfy (C2). Taking $K_+(M_1) = 17/3$ from Table 5.1, this holds provided that $\ell_v(\Gamma_1)/\ell_v(\Gamma) > 3/17$. Noting that $\Gamma \subset A_1 \cup A_2$, if the above inequality does not hold, then the proportion of Γ in A_2 satisfies $\ell_v(\Gamma_2)/\ell_v(\Gamma) > 14/17$. Observing Figure 5.11, Γ_2 intersects some collection of sets $A_{4,2}^k$, indexed by a consecutive subset $\{k_0, k_0 + 1, \dots\} \subset \mathbb{N}$ with $k_0 \geq 3$. Assume that Γ_2 intersects just two of these sets $\Gamma_2 = \Gamma_{k_0} \cup \Gamma_{k_0+1}$. As we saw in Chapter 4, if

$$\frac{1}{K_+(M_4 M_2^{k_0})} + \frac{1}{K_+(M_4 M_2^{k_0+1})} < 1$$

then at least one of $\Gamma_k = \Gamma_{k_0}, \Gamma_{k_0+1}$ satisfies $\ell_v(H^{k+1}(\Gamma_k)) > \ell_v(\Gamma_2)$ and by extension if

$$\frac{1}{K_+(M_4 M_2^{k_0})} + \frac{1}{K_+(M_4 M_2^{k_0+1})} < \frac{1}{\alpha}$$

then $\ell_v(H^{k+1}(\Gamma_k)) > \alpha \ell_v(\Gamma_2)$. Now noting that $K_+(M_4 M_2^k)$ is monotonic increasing in k we

have

$$\sum_{k=k_0}^{k_0+1} \frac{1}{K_+(M_4M_2^k)} \leq \sum_{k=3}^4 \frac{1}{K_+(M_4M_2^k)} = \frac{3}{181} + \frac{3}{237} < \frac{14}{17}$$

so that, together with $\ell_v(\Gamma_2)/\ell_v(\Gamma) > 14/17$, for some k condition (C2) follows by taking $\Lambda = H^{k+1}(\Gamma \cap A_{4,2}^k)$. The case where Γ intersects just one of the $A_{4,2}^k$ follows as a trivial consequence.

Suppose $\Gamma \subset \sigma_{1a}$ violates the lemma, by the above we have that Γ intersects three or more of the $A_{4,2}^k$, which by the geometry of the partition (see Figure 5.11) implies

$$(\dagger) \Gamma \text{ traverses } A_{4,2}^k \text{ for some } k \geq 4, \text{ connecting the lines } \mathcal{L}_k : y = \frac{k+1-4kx}{4k+2} \text{ and } \mathcal{L}_{k-1} : y = \frac{k-4(k-1)x}{4k-2}.$$

We will show that this leads to a contradiction through an inductive argument. If Γ intersects $A_{4,2}^3$, it must traverse $A_{4,2}^4$. Let $y_k = (k+1)/(4k+2)$ be the sequence of points where \mathcal{L}_k meets $x=0$. Since the gradients of \mathcal{L}_k are monotone decreasing in k , a lower bound $h_4 \leq \ell_v(\Gamma \cap A_{4,2}^4)$ is given by $y'_4 - y_4$ where (x'_4, y'_4) is the intersection of the lines $y = y_4 + \varphi x$ and $\mathcal{L}_3 : y = (4-12x)/14$. Specifically

$$h_4 = \frac{191}{675} - \frac{5}{18} = \frac{7}{1350}. \quad (5.6)$$

As before let $\Gamma_2 = \Gamma \cap A_2$. Observing Figure 5.11, since \mathcal{L}_3 meets the boundary of A_1 and A_2 at the point $(1/10, 1/5)$, the height of Γ_2 is bounded by $\ell_v(\Gamma_2) \leq L_3 = y_2 - 1/5 = 1/10$. Letting $\Lambda = H^5(\Gamma \cap A_{4,2}^4)$, we have that

$$\ell_v(\Lambda) \geq K_+(M_4M_2^4) h_4 = \frac{56(4)+13}{3} \frac{7}{1350} = \frac{553}{1350} \approx 0.4096$$

and $\ell_v(\Gamma) < (17/14)\ell_v(\Gamma_2) \leq 17/140 \approx 0.1214$, so that (C2) is satisfied. For the inductive step, assume that Γ traverses $A_{4,2}^k$, but does not traverse $A_{4,2}^{k-1}$. Using the same method as before we calculate

$$h_k = \frac{21}{2(2k+1)(68k-47)} \quad (5.7)$$

and

$$L_{k-1} = \frac{k-1}{4k-6} - \frac{k-1}{4k-2} \frac{(k-1)}{(2k-3)(2k-1)}. \quad (5.8)$$

Then (C2) is satisfied with $\Lambda = H^{k+1}(\Gamma \cap A_{4,2}^k)$ provided that $K_+(M_4M_2^k) h_k > (17/14)L_{k-1}$, i.e.

$$\frac{56k+13}{3} \frac{21}{2(2k+1)(68k-47)} - \frac{17}{14} \frac{(k-1)}{(2k-3)(2k-1)} > 0, \quad (5.9)$$

which holds for all $k > 4$ as required. It follows by induction that if Γ violates the lemma it must not traverse any $A_{4,2}^k$ for $k \geq 3$, contradicting (\dagger) , so that the lemma must hold when $\Gamma \subset \sigma_{1a}$ lies entirely below the upper boundary of $A_{4,2}^3$. The case where $\Gamma \subset \sigma_{1a}$ lies entirely above the lower boundary of $A_{4,2}^3$ is more straightforward, with (C2) following from the inequality

$$\sum_{k=1}^3 \frac{1}{K_+(M_3M_2^k)} + \frac{1}{K_+(M_4M_2^k)} = \sum_{k=1}^3 \frac{3}{56n+13} + \frac{3}{40n+7} \approx 0.206 < 1. \quad (5.10)$$

The lemma holds, then, for general $\Gamma \subset \sigma_{1a}$.

Moving onto the case $\Gamma \subset \sigma_{1b}$, write its intersections with the lower and upper regions $y \leq 1/2$ and $y \geq 1/2$ as Γ_L and Γ_U respectively. Observing Figure 5.12, Γ_L can intersect up to 5 partition elements from $\mathcal{A}_L = \{A_{3,2}^1, \dots, A_1 \cap \sigma\}$, on which DH_σ takes a value in $\mathcal{M}_L = \{M_1, M_3M_2^k, M_4M_2^k \mid k=1, 2\}$. Let

$$\alpha = \sum_{M \in \mathcal{M}_L} \frac{1}{K_+(M)} = \frac{3}{17} + \sum_{k=1}^2 \left(\frac{3}{40k+7} + \frac{3}{56k+13} \right) \approx 0.342.$$

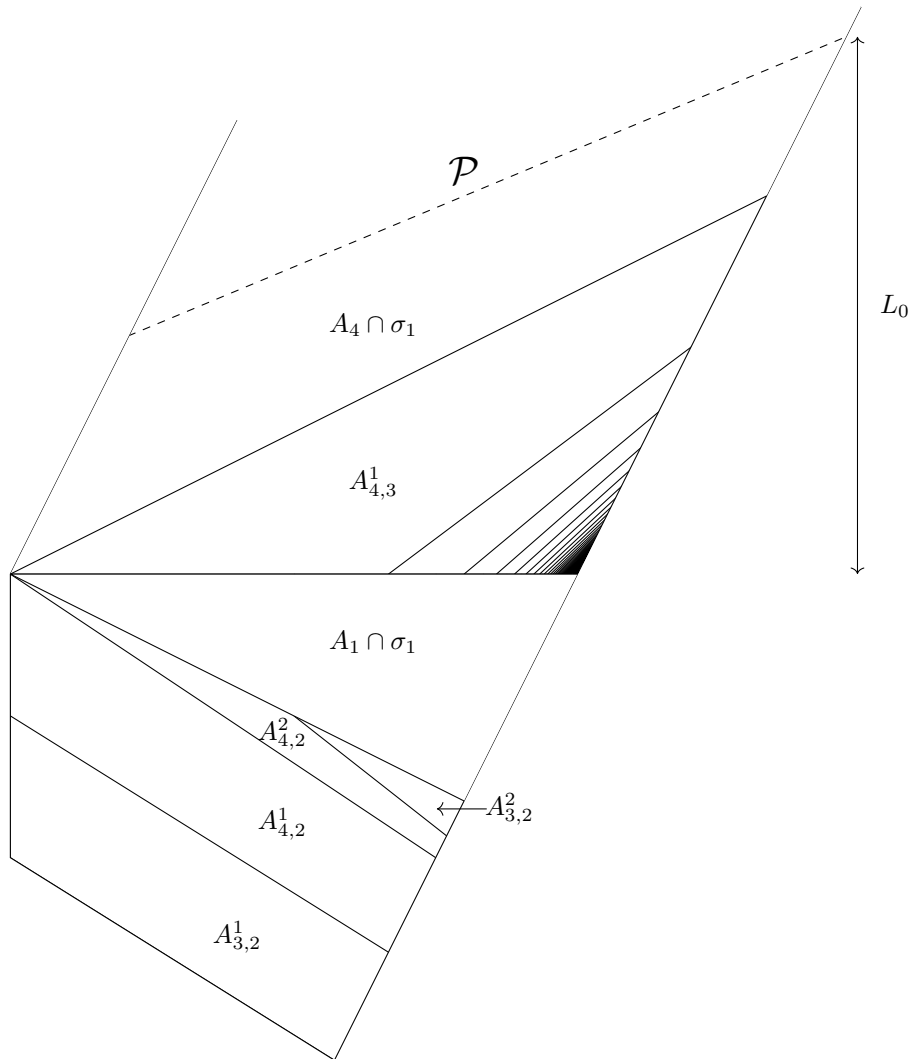


Figure 5.12: The singularity set of H_σ over the lower part of σ_{1b} with the top portion of $A_4 \cap \sigma_1$ omitted. Unlabelled sets are given by $A_{4,3}^k$ for $k \geq 2$ which limit onto the point $(1/4, 1/2)$ in the obvious fashion. The segment \mathcal{P} is the preimage under H of the segment joining $(1/2, 3/4)$ to $(1, 1)$ in S_4 . The length L_0 denotes maximum height of any segment in σ_{1b} bounded by \mathcal{P} and $y = 1/2$.

Dividing through by α , for any subset $\mathcal{N} \subset \mathcal{M}_L$ (including \emptyset and \mathcal{M}_L) we have

$$\sum_{M \in \mathcal{N}} \frac{1}{\alpha K_+(M)} \leq 1.$$

Hence we may always expand from some $A \in \mathcal{A}_L$, taking $\Lambda = H_\sigma(\Gamma \cap A)$, which by the above inequality satisfies $\alpha \ell_v(\Lambda) \geq \ell_v(\Gamma_L)$. Hence (C2) is satisfied when $\ell_v(\Gamma_L) > \alpha \ell_v(\Gamma)$. It remains to show the case $\ell_v(\Gamma_L) \leq \alpha \ell_v(\Gamma)$, i.e.

$$\ell_v(\Gamma_U) \geq (1 - \alpha) \ell_v(\Gamma). \quad (5.11)$$

Observing Figure 5.12, the set of partition elements which Γ_U can intersect is given by $\mathcal{A}_U = \{A_4 \cap \sigma_1, A_{4,3}^k \mid k \geq 1\}$, so $\mathcal{M}_U = \{M_4, M_4 M_3^k \mid k \geq 1\}$. Note that any two element subset $\mathcal{N} \subset \mathcal{M}_U$ satisfies

$$\begin{aligned} \sum_{M \in \mathcal{N}} \frac{1}{K_+(M)} &\leq \frac{1}{K_+(M_4)} + \frac{1}{K_+(M_4 M_3)} \\ &= \frac{21}{79} + \frac{21}{127} = \beta \approx 0.431 \end{aligned} \quad (5.12)$$

and $\alpha + \beta < 1$. It follows that if Γ_U intersects two or fewer of the elements of \mathcal{A}_U , we can guarantee (C2) by the standard method, summing the reciprocals of expansion factors. Assume, then, that Γ_U intersects three or more elements from \mathcal{A}_U . It follows that

$$\begin{aligned} (\dagger) \quad \Gamma_U \text{ traverses } A_{4,3}^k \text{ for some } k \geq 1, \text{ connecting the lines } \mathcal{L}_k : y &= \frac{(4k+2)x+k+2}{4k+4} \text{ and } \mathcal{L}_{k-1} : \\ y &= \frac{(4k-2)x+k+1}{4k}. \end{aligned}$$

We now follow a similar inductive argument to before, assuming that Γ violates the lemma and aiming to contradict (\dagger) . Let $(x_k, y_k) = \left(\frac{k+2}{4k+6}, \frac{k+2}{2k+3}\right)$ denote the intersections of the lines \mathcal{L}_k with the boundary $y = 2x$ of σ . Assume Γ traverses $A_{4,3}^k$, write its restriction to this set as Γ^k . Since the gradients of the \mathcal{L}_k are monotonic increasing in k and vectors in \mathcal{C}_+ have gradients bounded above by 3, a lower bound on $\ell_v(\Gamma^k)$ is given $h_k = y'_k - y_k$, where (x'_k, y'_k) is the intersection of the line $y - y_k = 3(x - x_k)$ and \mathcal{L}_{k-1} , in particular

$$h_k = \frac{8k^2 + 18k + 7}{16k^2 + 28k + 6} - \frac{k+2}{2k+3} = \frac{3}{16k^2 + 28k + 6}. \quad (5.13)$$

For the base case suppose that Γ_U traverses $A_{4,3}^1$. Let (x_U, y_U) be the intersection with $y = 1/2 + x/2$, the boundary between $A_{4,3}^1$ and $A_4 \cap \sigma_1$. Note that this point maps to $(1, y_U)$ under H with $y_U < 2/3$. Figure 5.12 shows the preimage \mathcal{P} in $A_4 \cap \sigma_1$ of the segment joining $(1/2, 3/4)$ to $(1, 1)$ between A_3 and A_4 . Specifically \mathcal{P} lies on the line $y = 7/12 + 5x/12$ and $H(\mathcal{P})$ lies on $y = 1/2 + x/2$. If Γ intersects \mathcal{P} , then $H(\Gamma)$ connects $(1, y_U)$ to a point on the segment joining $(1/2, 3/4)$ to $(1, 1)$. Since $y_U < 3/4$, it follows that $H(\Gamma)$ traverses A_3 , making non-simple intersection with A_4 , so that (C1) is satisfied. Assume, then, that Γ_U does not intersect \mathcal{P} . This gives an upper bound $\ell_v(\Gamma_U) \leq y_0 - 1/2 =: L_0$, where $(x_0, y_0) = (7/19, 14/19)$ is the intersection of \mathcal{P} with the boundary of σ_1 on $y = 2x$ (see Figure 5.12). Noting (5.11), (C2) follows with $\Lambda = H^2(\Gamma^1)$ if the inequality $K_+(M_4 M_3) h_1 > L_0 / (1 - \alpha)$ is satisfied. Indeed

$$\left(\frac{16}{7} + \frac{79}{21}\right) \frac{3}{16 + 28 + 6} - \frac{9}{38(1 - \alpha)} \approx 0.00277 > 0$$

so that the base step of the induction holds. The inductive step is roughly analogous, reducing to checking the inequality

$$K_+(M_4 M_3^k) h_k - \frac{L_{k-1}}{1 - \alpha} > 0, \quad (5.14)$$

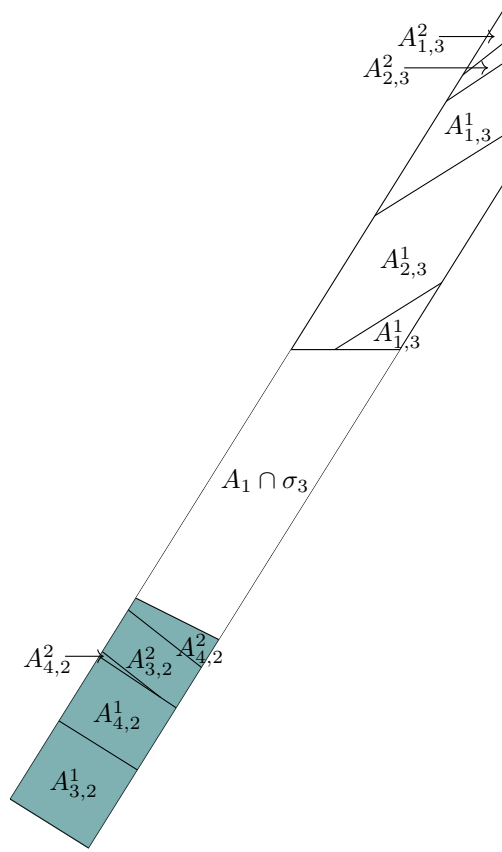


Figure 5.13: Behaviour of H_σ over $\sigma_{3b} \setminus \varsigma_3$ and H_σ^2 over ς_3 , shaded in blue.

where $L_{k-1} = y_{k-2} - 1/2$ is the height of the partition element $A_{4,3}^{k-1}$. One can verify that this inequality holds (the function is monotonic decreasing in $k \geq 2$ with limit 0 as $k \rightarrow \infty$), establishing the lemma for $\Gamma \subset \sigma_{1b}$.

Next consider $\Gamma \subset \sigma_{3b}$, shown in Figure 5.13. Note that outside of ς_3 (shaded in blue) the Jacobian DH_σ is some matrix from \mathcal{M} , but over ς_3 we have $DH_\sigma = M_2 \notin \mathcal{M}$. Therefore if we are to expand from some subset of $\Gamma \cap \varsigma_3$, to ensure that Λ satisfies one of (A1-2) we must map forwards using H_σ^2 , whose Jacobian is always a matrix from \mathcal{M} (analogous to the escape behaviour shown for A_3 , shown in Figure 5.9(b)). The relevant subset of matrices, then, is $\mathcal{M}_{3b} = \{M_1, M_1M_3^k, M_2M_3^k, M_3M_2^k, M_4M_2^k \mid k = 1, 2\}$. Noting that Γ can have non-simple intersection with the sets $A_{4,2}^2$ and $A_{1,3}^1$, the relevant inequality to verify is

$$\left(\sum_{M \in \mathcal{M}_{3b}} \frac{1}{K_+(M)} \right) + \frac{1}{K_+(M_1M_3)} + \frac{1}{K_+(M_4M_2^2)} < 1.$$

Indeed, the above sums to $\delta \approx 0.807 < 1$, so that restricting to one of the partition elements and expanding from there (using H_σ^2 inside of ς_3 , H_σ otherwise) will always satisfy (C2) with some $k \leq 3$. This leaves the cases $\Gamma \subset \sigma_{1c}, \sigma_{1d}, \sigma_{3a}$. Noting that rotating σ_{1c} by 180° about the point $(1/4, 3/4)$ gives σ_{1b} , and \mathcal{C}_+ is invariant under this rotation, the argument is essentially analogous. Similarly the arguments for σ_{1d}, σ_{3a} are equivalent to those for σ_{1a}, σ_{3b} respectively. This concludes the case where Γ satisfies (A1).

Let Γ satisfy (A2). Define the transformation $T : \mathbb{T}^2 \rightarrow \mathbb{T}^2$ given by $T(x, y) = (1 - x, y + 1/2) \bmod 1$. One can verify that $T \circ T = \text{Id}$ and $T \circ H = H \circ T$ so that $H^n = T \circ H^n \circ T$. Now since $T(\sigma_2 \cup \sigma_4) = \sigma_1 \cup \sigma_3$ and $DT\mathcal{C}_+ = \mathcal{C}_-$, the line segment $T(\Gamma)$ satisfies (A1). By our analysis above, $T(\Gamma)$ then satisfies (C1) or (C2). Noting that $T(A_j) = A_{5-j}$, if $T(\Gamma)$ satisfies (C1) then there exists k such that $H^k(\Gamma) = (T \circ H^k \circ T)(\Gamma)$ has non simple intersection with A_{5-j} , so (C1) is

satisfied. Similarly since $\ell_v(\cdot)$ is T -invariant, if $T(\Gamma)$ satisfies (C2) then the same holds for Γ . \square

5.3.5 Establishing the Bernoulli property

We are now ready to establish the mixing property.

Proof of Theorem 5.2. By the Theorem 1.4, since **(KS1-2)** were shown in section 4.3 and **(KS3)** was shown in Proposition 5.2, it suffices to show **(MR)**. By Lemmas 5.7, 5.8, for a.e. z we can find m_0 such that $H^{m_0}(\gamma_u(z))$ contains a line segment Γ_0 satisfying (A1) or (A2). Now iteratively apply Lemma 5.9 until (C1) is satisfied, giving m_1 such that $H^{m_1}(\Gamma_0)$ contains a line segment Γ_1 which has non simple intersection with some A_j . Define a v -segment as any line segment traversing S_1 , connecting its upper and lower boundaries. Similarly define a h -segment as any line segment in S_1 which connects its left and right boundaries. Consider the four parallelograms $Q_j \subset A_j$ given by $Q_1 = A_1 \cap S_2$, $Q_2 = A_2 \cap S_1$, $Q_3 = A_3 \cap S_4$, $Q_4 = A_4 \cap S_3$. It was shown in the proof of Lemma 4.14 that:

- (M1) If Γ_1 has non-simple intersection with some A_{j_1} , it traverses some Q_{j_2} , connecting its sloping boundaries.
- (M2) If Γ_1 traverses Q_{j_2} , $j_2 = 1, 2, 3, 4$, then $H^k(\Gamma_1)$ traverses Q_3 for $k = 2, 1, 0, 3$ respectively.
- (M3) The image of any line segment traversing Q_3 contains a v -segment.

The above gives $m_2 \in \{1, 2, 3, 4\}$ such that $H^{m_2}(\Gamma_1)$ contains a v -segment $\Gamma \subset H(Q_3) \cap S_1$, with this parent set given by the quadrilateral with corners $(0, 0)$, $(1/6, 0)$, $(1/2, 1/2)$, $(1/3, 1/2)$, so that Γ connects points $(x_1, 0)$ and $(x_2, 1/2)$ with $0 \leq x_1 \leq 1/6$ and $1/3 \leq x_2 \leq 1/2$. It follows that Γ traverses Q_2 which, by (M2-3), implies that $H^2(\Gamma)$ contains a v -segment and so does $H^{2+2k}(\Gamma)$ for $k \geq 0$ by induction. Applying F to Γ has no effect on $(x_1, 0)$ and wraps $(x_2, 1/2)$ horizontally around the torus so that $F(\Gamma)$ contains a segment joining $(0, y)$ to $(x_2, 1/2)$ with $y < 1/2$. Now G has no effect on $(0, y)$ and maps $(x_2, 1/2)$ to $(x_2, 1/2 + 2x_2) \bmod 1$. Since $1/2 + 2x_2 \geq 1/2 + 2/3 = 7/6 > 1$, $H(\Gamma)$ contains a segment joining $(0, y)$ to $(x_3, 1)$ with $x_3 \leq x_2 \leq 1/2$. It follows that $H(\Gamma)$ must traverse Q_4 which, by (M2-3), implies that $H^5(\Gamma)$ contains a v -segment. Using the same induction as before we have that $H^{5+2k}(\Gamma)$ contains a v -segment for all $k \geq 0$ which, together with the same result for $H^{2+2k}(\Gamma)$, implies that $H^k(\Gamma)$ contains a v -segment for all $k \geq 4$. Hence there exists $M = m_0 + m_1 + m_2 + 4$ such that $H^m(\gamma_u(z))$ contains a v -segment for all $m \geq M$.

Now for almost any z' , by Lemma 5.7 we can find n_0 such that $H^{-n_0}(\gamma_s(z'))$ contains a line segment $\Gamma' \in \sigma'$, aligned with some $v \in \mathcal{C}'$. Define the transformation $\mathcal{T}(x, y) = (1-y, 1-x) \bmod 1$. One can verify that $\mathcal{T} \circ \mathcal{T} = \text{Id}$ and $\mathcal{T} \circ H^{-1} = H \circ \mathcal{T}$ so that $H^{-k} = \mathcal{T} \circ H^k \circ \mathcal{T}$. Now since $\mathcal{T}(\sigma') = \sigma$ and $D\mathcal{T}\mathcal{C}' = \mathcal{C}$, we have that $\mathcal{T}(\Gamma')$ is a line segment in σ , aligned with some $v = D\mathcal{T}v' \in \mathcal{C}$. We now follow Lemmas 5.8, 5.9 and the argument above to find n_1 such that $(H^m \circ \mathcal{T})(\Gamma')$ contains a v -segment for all $m \geq n_1$. The image of a v -segment under \mathcal{T} is a segment joining the left and right boundaries of S_4 . Noting Figure 5.5, we have that $H^{-m}(\Gamma') = (\mathcal{T} \circ H^m \circ \mathcal{T})(\Gamma')$ traverses the parallelogram $Q'_2 = A'_2 \cap S_4$, connecting its sloping boundaries. It was shown in the proof of Lemma 4.15 that if Γ' traverses Q'_2 then $H^{-1}(\Gamma')$ contains a h -segment, so that $H^{-n}(\gamma_s(z'))$ contains a h -segment for all $n \geq N = n_0 + n_1 + 1$. Since z and z' were arbitrary and h -segments and v -segments must always intersect, **(MR)** holds. \square

Remark 5.1. The v -segments Λ obtained above satisfy $H^{-1}(\Lambda) \subset Q_3$, $H^{-2}(\Lambda) \subset Q_2$ so that $\Lambda \subset H(A_3 \cap H(A_2)) = \sigma_3$. Similarly the h -segments derived from these v -segments can be shown to lie in σ'_2 .

Estimated correlation decay for the OTM

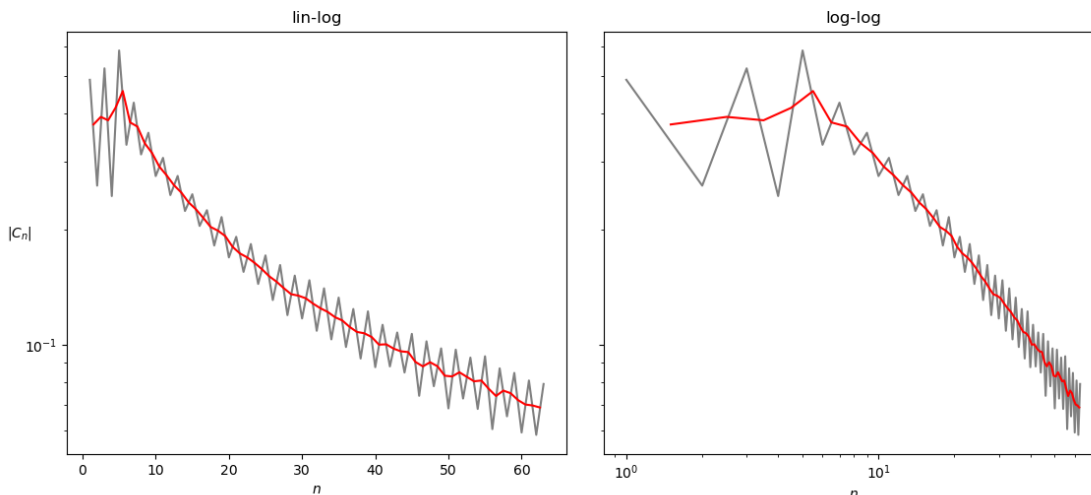


Figure 5.14: Gray: lin-log and log-log plots of the estimated autocorrelation function $|C_n|$ over $n = 1, \dots, 64$ iterates for the OTM. Red: rolling average over two elements.

5.3.6 Remarks

We conclude this chapter comparing the dynamics and analysis of the OTM with maps studied in previous sections. In spirit, the method for establishing the growth lemma was analogous to that seen in the simpler setting of the non-monotonic linked twist map (section 5.2.3). The more complicated geometry of the return set σ and increased variety of accumulation regions obfuscate this relationship but the underlying inductive argument is unchanged. While we have relied on the specific geometry of the OTM and the non-monotonic LTM, we expect a similar method could be used in any system where the partition elements follow a self similar accumulating pattern. Such structure is observed in many return map systems.

The Bernoulli property for the rest of \mathcal{P}' could potentially be proven by an argument adapted from this one. In some sense \mathcal{M} is the widest class of matrices one would ever need to consider, comprising cocycles corresponding to every possible escape from the problematic regions A_2 and A_3 , non-hyperbolic for the OTM, weakly hyperbolic in its vicinity over \mathcal{P}' . In practice, establishing the necessary geometric bounds over such a wide parameter space would be challenging, likely necessitating splitting up the analysis into many cases. The symmetry arguments also would not hold, likely pushing the number of required calculations beyond a manageable (or at least readable) level[§].

The map $H_{(\xi,\eta)}$ over \mathcal{P}' is uniformly hyperbolic with singularities. As such, following the work of Young (1998), one would expect correlations to decay exponentially in this case. In contrast, a straightforward calculation using the sets P_n, Q_n of section 5.3.2 gives $\mu(P_n) = \mu(Q_n) = n / (32n^2 - 8)$ so that $\mu(B_n)$, the measure of the unmixed region in A_3 , is given by $\mu(B_n) = \mu(U_n) = n / (16n^2 - 4)$. This suggests that the mixing rate is at best polynomial and numerical evidence supports this. Figure 5.14 shows the numerically estimated decay of the autocorrelation function $C_n(\varphi, \varphi, H, \mu)$ for the OTM H and observable $\varphi(x, y) = 5 \sin(4\pi x) - 7 \sin(6\pi y)$. The lin-log plot suggests that $|C_n|$ exhibits slower than exponential decay, the log-log plot suggests an algebraic decay rate for the tail end of the distribution. The next chapter attempts to make these predictions rigorous, applying the results covered in section 2.3 to find upper bounds on the correlation decay rate for $H_{(\xi,\eta)}$ at $\xi = \eta = 1/2$ (the OTM) and across the mixing window $(\xi, \eta) \in \mathcal{M}$.

[§]One could argue that our analysis of the OTM already crossed this threshold!

Chapter 6

Rates of Mixing

6.1 Introduction

We begin with the scheme outlined in Chernov and Zhang (2005). It gives conditions under which the distribution of return times to a certain subset Λ decays exponentially and exponential decay of correlations follows by construction of a Young Tower. We first list some basic properties for systems amenable to the scheme, paraphrased from Chernov and Zhang (2005).

Let M be an open domain in a 2D C^∞ compact Riemannian manifold \mathcal{M} with or without boundary, $f : M \rightarrow M$.

(CZ1): Smoothness. The map f is a C^2 diffeomorphism of $M \setminus \mathcal{S}$ onto $f(M \setminus \mathcal{S})$, where \mathcal{S} is a closed set of zero Lebesgue measure.

(CZ2): Hyperbolicity. At any $x \in M' \subset M$ where Df_x exists, there exists two families of cones C_x^u (unstable) and C_x^s (stable) such that $Df_x(C_x^u) \subset C_{f(x)}^u$ and $Df_x(C_x^s) \supset C_{f(x)}^s$. There exists a constant $\lambda > 1$ such that

$$\|Df_x(v)\| \geq \lambda\|v\| \forall v \in C_x^u \quad \text{and} \quad \|Df_x^{-1}(v)\| \geq \lambda\|v\| \forall v \in C_x^s.$$

These families of cones are continuous on M' , and the angle between C_x^u and C_x^s is bounded away from zero. For any f -invariant measure μ' , at almost every $x \in M$ we have non-zero Lyapunov exponents and can define local unstable and stable manifolds $W^u(x)$, $W^s(x)$.

(CZ3): SRB measure. The map f preserves a measure μ whose conditional distributions on unstable manifolds are absolutely continuous, and is mixing.

(CZ4): Distortion bounds. Let $\lambda(x)$ denote the factor of expansion on the unstable manifold $W^u(x)$. If x, y belong to an unstable manifold W^u such that f^n is defined and smooth on W^u , then

$$\log \prod_{i=0}^{n-1} \frac{\lambda(f^i x)}{\lambda(f^i y)} \leq \alpha(\text{dist}(f^n x, f^n y))$$

where $\alpha(\cdot)$ is some function, independent of W^u , with $\alpha(s) \rightarrow 0$ as $s \rightarrow 0$.

(CZ5): Bounded Curvature. The curvature of unstable manifolds is uniformly bounded by a constant $B \geq 0$.

(CZ6): Absolute continuity. If W_1, W_2 are two small unstable manifolds close to each other, then the holonomy map $h : W_1 \rightarrow W_2$ (defined by sliding along stable manifolds) is absolutely continuous with respect to the induced Lebesgue measures ν_{W_1} and ν_{W_2} , and its Jacobian is

bounded:

$$\frac{1}{C'} \leq \frac{\nu_{W_2}(h(W'_1))}{\nu_{W_1}(W'_1)} \leq C'$$

for some $C' > 0$, where $W'_1 \subset W_1$ is the set of points where h is defined.

(CZ7): Structure of the singularity set. For any unstable curve $W \subset M$ (a curve whose tangent vectors lie in unstable cones) the set $W \cap \mathcal{S}$ is finite or countable and...*

Denote the length of a line segment W by $|W|$. Denote the connected components of $W \cap (M \setminus \mathcal{S})$ by W_i . We are now ready to give the result from Chernov and Zhang (2005), specifically their Theorem 10 with $m = 1$.

Theorem 6.1 (Chernov and Zhang). *Let f be defined on a 2D manifold M and satisfy the requirements (CZ1-7). Suppose*

$$\liminf_{\delta \rightarrow 0} \sup_{W: |W| < \delta} \sum_i \lambda_i^{-1} < 1 \quad (6.1)$$

where the supremum is taken over unstable manifolds W and λ_i denotes the minimal expansion factor on W_i . Then the map $f : M \rightarrow M$ enjoys exponential decay of correlations.

Following the analysis of section 4.3, the one step expansion estimate (6.1) may seem familiar. Indeed, its similarity with our growth condition (see Lemma 4.12) allows us to deduce, with minimal further analysis, exponential mixing of $H_{(\xi, \eta)}$ for parameter values (ξ, η) near the Cat Map.

We further state a more recent scheme of Chernov and Zhang (2009), aimed towards proving exponential mixing for systems of type $a < 1$ (see the discussion of section 2.3). Let Ω denote a two dimensional connected compact Riemannian manifold, $f : \Omega \rightarrow \Omega$ preserving a measure μ . Let d denote the distance in Ω induced by the Riemannian metric ρ . For any smooth curve W in Ω , denote by $|W|$ its length, and by m_W the Lebesgue measure on W induced by the Riemannian metric ρ_W restricted to W . Also let $\nu_W = m_W/|W|$ be the normalised (probability) measure on W .

(H1): Hyperbolicity of f (with uniform expansion and contraction). There exist two families of cones C_x^u (unstable) and C_x^s (stable) in the tangent spaces $\mathcal{T}_x\Omega$, for all $x \in \Omega$, and there exists a constant $\Lambda > 1$, with the following properties:

1. $Df(C_x^u) \subset C_{fx}^u$ and $Df(C_x^s) \supset C_{fx}^s$ whenever Df exists.
2. $\|D_x f(v)\| \geq \Lambda \|v\|$, $\forall v \in C_x^u$ and $\|D_x f^{-1}(v)\| \geq \Lambda \|v\|$, $\forall v \in C_x^s$.
3. These families of cones are continuous on Ω and the angle between C_x^u and C_x^s is uniformly bounded away from zero.

We say that a smooth curve $W \subset \Omega$ is an unstable (stable) curve if at every point $x \in W$ the tangent line $\mathcal{T}_x W$ belongs in the unstable (stable) cone C_x^u (C_x^s).

(H2): Singularities and smoothness. Let \mathcal{S}_0 be a closed subset in Ω , such that $M := \Omega \setminus \mathcal{S}_0$ is a dense set in Ω . We put $\mathcal{S}_{\pm 1} = f^{\mp} \mathcal{S}_0$.

1. $f : M \setminus \mathcal{S}_1 \rightarrow M \setminus \mathcal{S}_{-1}$ is a C^2 diffeomorphism.
2. $\mathcal{S}_0 \cup \mathcal{S}_1$ is a finite or countable union of smooth, compact curves in Ω .
3. Curves in \mathcal{S}_0 are transversal to stable and unstable cones. Every smooth curve in \mathcal{S}_1 (resp. \mathcal{S}_{-1}) is a stable (resp. unstable) curve. Every curve in \mathcal{S}_1 terminates either inside another curve of \mathcal{S}_1 or on \mathcal{S}_0 .

*There is an additional requirement in the countable case, irrelevant for use case.

4. There exists $b \in (0, 1)$ and $c > 0$ such that for any $x \in M \setminus \mathcal{S}_1$

$$\|D_x f\| \leq c d(x, \mathcal{S}_1)^{-b}. \quad (6.2)$$

(H3): Regularity of smooth unstable curves. We assume that there is a f -invariant class of unstable curves $W \subset M$ that are *regular* (see Chernov and Zhang, 2009).

(H4): SRB measure. μ is a Sinai-Ruelle-Bowen (SRB) measure which is mixing.

(H5): One-step expansion. There exists $q \in (0, 1]$ such that

$$\liminf_{\delta \rightarrow 0} \sup_{W: |W| < \delta} \sum_i \left(\frac{|W|}{|V_i|} \right)^q \frac{|W_i|}{|W|} < 1, \quad (6.3)$$

where the supremum is taken over all unstable curves, W_i are the components of W split by the singularity set for f , $V_i = f(W_i)$.

Theorem 6.2 (Chernov and Zhang). *Under the conditions (H1)–(H5), the system (f, μ) enjoys exponential decay of correlations.*

Remark 6.1. Condition **(H1.3)** has been relaxed in subsequent schemes (Demers and Zhang, 2014; Wang et al., 2021) and can be replaced by

3'. These families of cones are continuous on components of $\Omega \setminus \mathcal{S}_0$ and the angle between C_x^u and C_x^s is uniformly bounded away from zero.

Theorem 6.2 still follows under this relaxed assumption by applying (for example) Theorem 1 of Wang et al. (2021). Despite the improvement over (6.1), condition **(H5)** still fails for many systems over one iterate. See, for example, the modified stadia considered in Chernov and Zhang (2009). It can be replaced by a multi-step expansion condition, establishing **(H5)** for some higher power f^n of the map f and its singularity set $f^{-n}(\mathcal{S}_0)$.

We apply these schemes to deduce the mixing rates of the map $H_{(\xi, \eta)}$, first for parameters near the Cat Map using Theorem 6.1, then at $\xi = \eta = 1/2$ (the OTM) using Theorem 6.2

6.2 Exponential mixing rates

Recall the map $H_{(\xi, \eta)}$, its derivatives M_j and their shared invariant expanding cone \mathcal{C} , explicitly stated in section 4.3. Letting $\|\cdot\|_2$ denote the Euclidean norm, define expansion factors

$$\mathcal{K}_j(\xi, \eta) = \inf_{v \in \mathcal{C}} \frac{\|M_j v\|_2}{\|v\|_2}.$$

Recall the mixing window \mathcal{B} from Proposition 4.10, plotted in Figure 4.16. In this section we prove:

Theorem 6.3. *For parameter values $(\xi, \eta) \in \mathcal{B}$ further satisfying*

$$\sum_{j=1}^4 \frac{1}{\mathcal{K}_j(\xi, \eta)} < 1, \quad (6.4)$$

the map $H_{(\xi, \eta)}$ enjoys exponential decay of correlations. This window \mathcal{E} is plotted in Figure 6.1.

The argument is presented in Myers Hill et al. (2022a); for completeness we restate it here. In essence, we express our system in the notation of Theorem 6.1 and verify the conditions **(CZ1-7)**.

Proof of Theorem 6.3. Take $M = \mathcal{M} = \mathbb{T}^2$ and $f = H_{(\xi, \eta)}$. Starting with **(CZ1)**, take $\mathcal{S} = \mathcal{D}$ as defined in section 4.3 and let $M' = \mathbb{T}^2 \setminus \mathcal{D}$. Clearly $f : M' \rightarrow f(M')$ is a C^2 diffeomorphism and

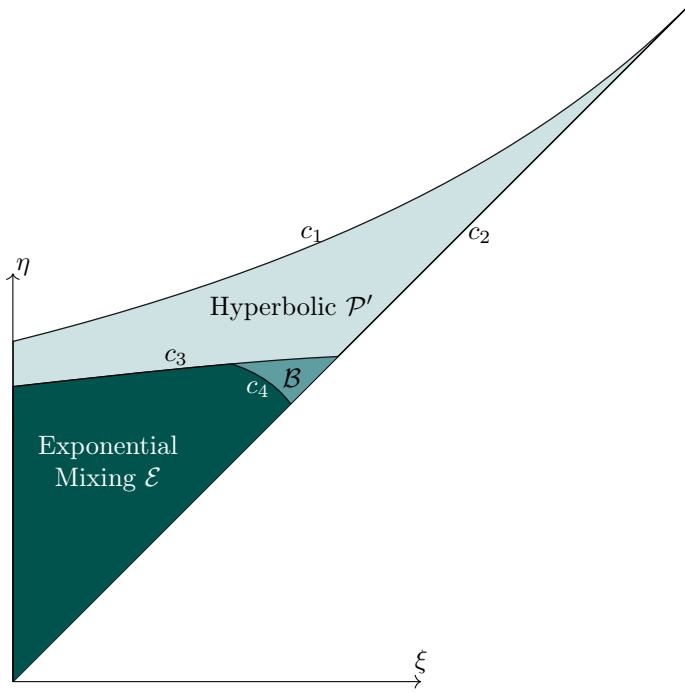


Figure 6.1: Plot of analytical results over \mathcal{P} . The curves c_1 and c_2 define \mathcal{P}' , c_3 defines $\mathcal{B} \subset \mathcal{P}'$, c_3 and c_4 define $\mathcal{E} \subset \mathcal{B}$, on which H is respectively hyperbolic, mixing, and exhibits exponential decay of correlations.

$\mu(\mathcal{D}) = 0$. Moving onto **(CZ2)**, take $C_x^u = \mathcal{C}$ and $C_x^s = \mathcal{C}'$ for all $x \in M'$. These are continuous (constant even) over M' with cone invariance, expansion[†], transversality shown in the proof of Lemma 4.6. **(CZ3)** follows from Theorem 4.3, noting that Bernoulli implies strong mixing in the ergodic hierarchy. Next **(CZ4)**, **(CZ5)** follow from piecewise linearity of H and **(CZ6)** follows from **(KS1-3)**, shown in section 4.3. Finally since vectors tangent to \mathcal{D} lie in \mathcal{C}' , unstable curves W (with tangent vectors in \mathcal{C}) meet \mathcal{D} transversally. Since \mathcal{D} is a finite collection of segments, $W \cap \mathcal{D}$ is finite, satisfying **(CZ7)**.

It remains to show the one step expansion condition (6.1). Note that by inspection of the partition A_i in Figure 4.12, we can pick δ sufficiently small so that any unstable manifold of length δ has at most three intersections with \mathcal{D} , giving four connected components $W_i = W \cap A_i$. Note that each expansion factor λ_i is then bounded from below by $\mathcal{K}(\xi, \eta)$ and the result follows by (6.4). \square

Across $(\xi, \eta) \in \mathcal{B}$ we have that $\mathcal{K}_1(\xi, \eta, v)$ and $\mathcal{K}_2(\xi, \eta, v)$ always attain their infimum over the unstable eigenvector v_2 of M_2 , $\mathcal{K}_3(\xi, \eta, v)$ and $\mathcal{K}_4(\xi, \eta, v)$ always attain their infimum over the unstable eigenvector v_3 of M_3 . Hence (6.4) holds provided that $\Omega(\xi, \eta) < 1$, where

$$\Omega(\xi, \eta) = \frac{1}{\mathcal{K}_1(\xi, \eta, v_2)} + \frac{1}{\mathcal{K}_2(\xi, \eta, v_2)} + \frac{1}{\mathcal{K}_3(\xi, \eta, v_3)} + \frac{1}{\mathcal{K}_4(\xi, \eta, v_3)}.$$

Figure 6.1 shows the curve c_4 given by $\Omega(\xi, \eta) = 1$ in \mathcal{B} , which together with c_3 , c_2 , $\xi = 0$ give the exponential mixing window $\mathcal{E} \subset \mathcal{B}$ where Theorem 6.3 holds.

[†]Expansion in the $\|\cdot\|_2$ norm follows from a similar argument.

6.3 Polynomial mixing rates

Let H denote the OTM, $H_{(\xi, \eta)}$ with $\xi = \eta = 1/2$. The aim of this section is to prove that H enjoys polynomial decay of correlations, in contrast to the exponential mixing rates seen in the previous section. We show:

Theorem 6.4. *Correlations $C_n(\varphi, \psi, H, \mu)$ for H satisfy*

$$|C_n(\varphi, \psi, H, \mu)| \leq c n^{-1}$$

for some constant c and Hölder observables φ, ψ .

Our method follows that outlined in section 2.3, deducing the polynomial decay under H from exponential decay of some induced return map H_A , where returns to A experience ‘strong’ hyperbolic behaviour. The natural choice for A , following the work of section 5.3, is the set σ . We begin by proving the Bernoulli property for H_σ .

6.3.1 Bernoulli property

Proposition 6.1. *The return map H_σ is Bernoulli with respect to the probability measure $\mu_\sigma = \mu(\sigma)^{-1}\mu$.*

We will show the conditions **(KS1-3)** and **(MR)**; the result then follows from Theorem 1.4.

Lemma 6.1. *The return map H_σ satisfies **(KS1-3)**.*

Proof. Starting with **(KS1)** we follow a similar approach to Springham and Sturman (2014), their Lemma 4.1. We show that there exists $a, C_1 > 0$ s.t. $\forall \epsilon > 0, \mu_\sigma(B_\epsilon(S)) \leq C_1 \epsilon^a$ for $S = \mathcal{S} \cap \sigma_{1a}$; the argument for the rest of \mathcal{S} is similar and the result then follows by taking a larger C_1 . Recall the line segments \mathcal{L}_k from (†) which for $k \geq 3$ terminate on the points $(0, (k+1)/(4k+2))$ and $(1/(4k-2), (k-1)/(4k-2))$ on the line $\mathcal{L} : y = 1/4 - x/2$. Let $P(\epsilon)$ denote the parallelogram in σ_{1a} of width $2\sqrt{\epsilon}$, height $\sqrt{\epsilon}$, with sides aligned with $x = 0$ and \mathcal{L} (see Figure 5.11). For small ϵ , $P(\epsilon)$ contains all line segments \mathcal{L}_k where $2\sqrt{\epsilon} \geq 1/(4k-2)$, i.e. $k \geq k_0 = \lceil 1/(8\sqrt{\epsilon}) + 1/2 \rceil$, with

$$\mu(B_\epsilon(P(\epsilon))) = (2\sqrt{\epsilon} + 2\epsilon)(\sqrt{\epsilon} + 2\epsilon) = 2\epsilon + 6\epsilon^{3/2} + 4\epsilon^2 < 12\epsilon.$$

The ball $B_\epsilon(P(\epsilon))$ then covers all of $B_\epsilon(S)$ except the collection $\mathcal{L}_k, 4 \leq k \leq k_0 - 1$ and the seven line segments L_j which terminate on $y = 2x$. The measure of the ball around these latter line segments satisfies

$$\mu(B_\epsilon(\cup_j L_j)) \leq 14\epsilon \left(\max_j |L_j| + 2\epsilon \right) < c_1 \epsilon$$

for some finite c_1 , so it remains to estimate $\sum_{k=4}^{k_0-1} \mu(B_\epsilon(\mathcal{L}_k))$. We can calculate

$$|\mathcal{L}_k| = \sqrt{\left(\frac{1}{4k-2}\right)^2 + \left(\frac{k+1}{4k+2} - \frac{k-1}{4k-2}\right)^2} = \sqrt{\frac{8k^2 + 4k + 1}{4(4k^2 - 1)^2}} < \frac{1}{k} \quad (6.5)$$

so that

$$\sum_{k=4}^{k_0-1} \mu(B_\epsilon(\mathcal{L}_k)) < 2\epsilon \sum_{k=4}^{k_0-1} \frac{1}{k} + 2\epsilon < 4\epsilon^2 k_0 + 2\epsilon \log k_0 < c_2 \epsilon^a$$

for some $0 < a < 1, c_2 > 0$ since $k_0 < \epsilon^{-1/2}$ and there exists finite c such that $c\epsilon^a > \epsilon \log \frac{1}{\epsilon}$ for any $0 < a < 1$.

Since H_σ is piecewise linear, condition **(KS2)** follows trivially and we move onto **(KS3)**. Existence of Lyapunov exponents almost everywhere follows from Oseledets’ theorem (Oseledets,

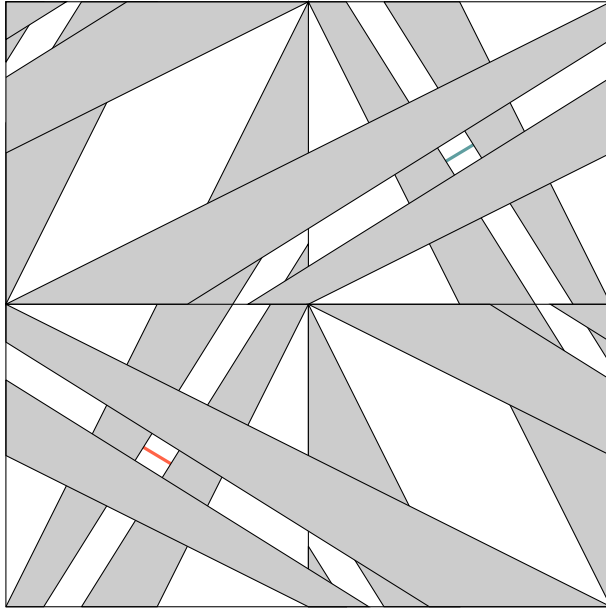


Figure 6.2: The set σ' superimposed on σ , their intersection left white. A \mathfrak{h} -segment (red) and a \mathfrak{h}' -segment (blue) are plotted in \mathcal{R} and \mathcal{R}' respectively.

1968) provided that $\log^+ \|DH_\sigma\|$ is integrable. This follows from the fact that if $z \in \sigma$ has return time $r_\sigma(z) = k$, then the Jacobian of H_σ at z satisfies $\|DH_\sigma\| \leq c_1 k$ for some finite $c_1 > 0$, and that the measure of the sets $\{z \in \sigma \mid r_\sigma(z) = k\}$ are of order k^{-3} . That these Lyapunov exponents are non-zero follows from Lemmas 5.5, 5.6 and an argument similar to that given for H in section 5.3.2.

Lemma 6.2. *The return map H_σ satisfies (MR).*

For a.e $z \in \sigma$, local manifolds $\gamma_u(z)$, $\gamma_s(z)$ under H_σ align with those of H . Note that H_σ does not immediately inherit (MR) from H as while successive images of local manifolds under H contain h -segments and v -segments, these segments may not lie in the successive images under H_σ .

Let \mathcal{R} denote the quadrilateral $\sigma_3 \cap \sigma'_2$ and $\mathcal{R}' = \sigma_2 \cap \sigma'_3$. Define a \mathfrak{h} -segment as a line segment spanning \mathcal{R} with endpoints on $\partial\sigma_3$. Similarly define a \mathfrak{h}' -segment as a line segment spanning \mathcal{R}' with endpoints on $\partial\sigma_2$. Examples are plotted in Figure 6.2. We will show that there exists M, N such that for all $m \geq M$, $n \geq N$, $H_\sigma^m(\gamma_u(z))$ intersects $H_\sigma^{-n}(\gamma_s(z'))$ in either \mathcal{R} or \mathcal{R}' .

By the remark after Theorem 5.2 we can find some n_2 such that $H^{-n_2}(\gamma_s(z'))$ contains a h -segment in σ'_2 , which in turn contains a \mathfrak{h} -segment in \mathcal{R} . As a line segment in σ , this \mathfrak{h} -segment lies in $H_\sigma^{-n_1}(\gamma_s(z'))$ for some $n_1 \leq n_2$. Note that we have a hyperbolic period 2 orbit $(1/4, 1/4) \leftrightarrow (3/4, 3/4)$ under H_σ , alternating between \mathcal{R} and \mathcal{R}' . Any \mathfrak{h} -segment Λ contains a point ζ on the unstable manifold through $(1/4, 1/4)$ so $H_\sigma^{-2}(\Lambda)$ contains a point ζ' on the manifold closer to $(1/4, 1/4)$ and extends beyond the boundaries $\partial\sigma_3$ by the expansion of H_σ^{-2} . Hence $H_\sigma^{-2}(\Lambda)$ contains a \mathfrak{h} -segment and by induction so does $H_\sigma^{-2k}(\Lambda)$ for all $k \geq 1$. The odd iterates $H_\sigma^{-2k+1}(\Lambda)$ similarly span \mathcal{R}' so that

- (†) Given arbitrary $z' \in \sigma$, there exists N such that for all $n \geq N$ the image $H_\sigma^{-n}(\gamma_s(z'))$ contains a \mathfrak{h} -segment or a \mathfrak{h}' -segment.

Define a v' -segment as a line segment vertically spanning $\sigma_2 \cap S_4$. Condition (MR) now follows from establishing

- (‡) Given arbitrary $z \in \sigma$, there exists M such that for all $m \geq M$ the image $H_\sigma^m(\gamma_u(z))$ contains both a v -segment and a v' -segment.

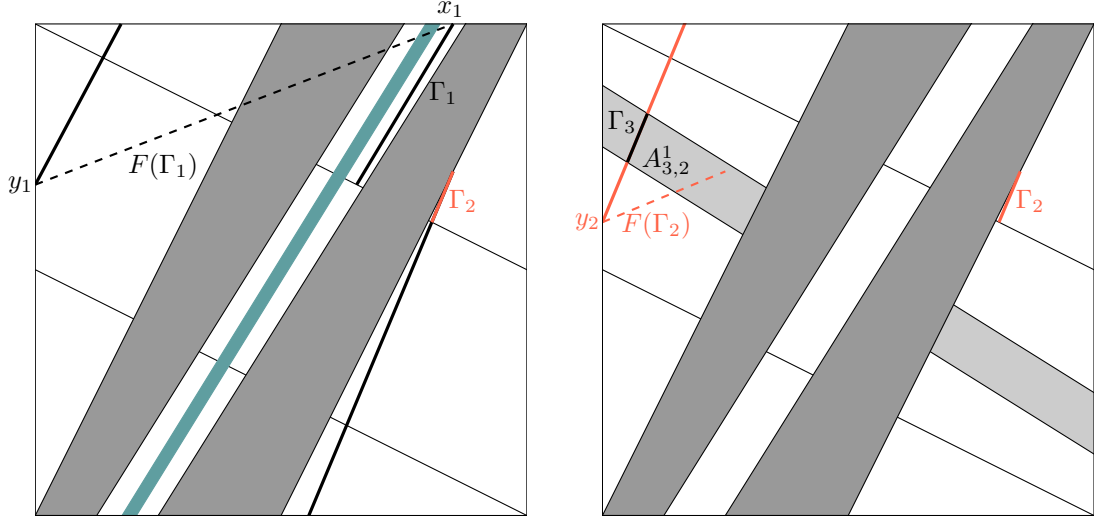


Figure 6.3: Left: The upper part $\Gamma_1 \subset A_1$ of a v -segment in $\sigma_3 \setminus (H(\sigma_2) \cap \sigma_3)$ and its images $F(\Gamma_1)$ (dashed), $H(\Gamma_1) \cap S_1$. Right: A right part $\Gamma_2 \subset A_1$ of $H(\Gamma_1)$ and its images $F(\Gamma_2)$, $H(\Gamma_2) \cap S_1$. This image necessarily contains a line segment Γ_3 traversing $A_{3,2}^1$.

Recall the quadrilaterals $\zeta_j \subset \sigma_j$ of points with return time 1 (see Figure 5.8(a)). It follows from the definitions of the σ_j that $H(\zeta_2) \subset \sigma_3$ and $H(\zeta_3) \subset \sigma_2$. The edges of ζ_3 on the A_1, A_2 boundary map into the lines $x = 1/2$, $x = 1$, in particular onto the red dashed lines on the boundary of S_2 in Figure 5.8(b) so that the image of any line segment in ζ_3 which joins these edges contains a v' -segment. An analogous result holds for lines segments traversing ζ_2 and since this behaviour occurs within the return set σ we have that v -segments map into v' -segments under H_σ and vice versa. It follows that $v^{(\cdot)}$ -segments map into $v^{(\cdot)}$ -segments under H_σ^2 . It suffices to break into the odd iterates to satisfy the ‘and’ condition of (‡).

By following the steps (M1-3) in the proof of Theorem 5.2 we can find m_2 such that $H^{m_2}(\gamma_u(z))$ contains a v -segment $\Gamma \subset \sigma_3 \cap S_1$ with $H^{-1}(\Gamma) \subset A_3$, $H^{-2}(\Gamma) \subset A_2$, $H^{-3}(\Gamma) \subset A_1$, $H^{-4}(\Gamma) \subset A_4$. In particular $H^{-1}(\Gamma)$ lies in $H(A_2 \cap H(A_1))$, i.e. outside of σ_2 , so that Γ lies in $\sigma_3 \setminus (H(\sigma_2) \cap \sigma_3)$. The set $H(\sigma_2) \cap S_1$ (shown in blue in Figure 6.3) is the quadrilateral with corners $(7/68, 0)$, $(3/34, 0)$, $(27/68, 0)$, $(7/17, 0)$, which splits $\sigma_3 \cap S_1$ into left and right parts. We assume first that Γ lies in the right part, intersecting the line $y = 1/2$ at some point $(x_1, 1/2)$ with $x_1 \geq 7/17$ and the A_1, A_2 boundary $y = 1/2 - x/2$ at some point $(1 - 2y_1, y_1)$. These intersections define a line segment $\Gamma_1 \subset \Gamma$, which lies in A_1 shown in Figure 6.3. Applying F maps $(x_1, 1/2)$ to itself (wrapping horizontally around the torus) and maps $(1 - 2y_1, y_1)$ to $(0, y_1)$. Applying G then leaves $(0, y_1)$ invariant and wraps $(x_1, 1/2)$ vertically around the torus to $(x_1, 1/2 + 2x_1) \bmod 1 \equiv (x_1, -1/2 + 2x_1)$. Since $x_1 \geq 7/17$ we have that $-1/2 + 2x_1 \geq 11/34 > 10/24 \geq 1/2 - x_1/2$ so that $(x_1, -1/2 + 2x_1)$ lies above the line $y = 1/2 - x/2$. We restrict again to A_1 , giving $\Gamma_2 \subset H(\Gamma_1)$ with endpoints on $(x_1, -1/2 + 2x_1)$ and some point $(1 - 2y_2, y_2)$ on $y = 1/2 - x/2$. This line meets $y = -1/2 + 2x$ at $(2/5, 3/10)$ so that $y_2 \leq 3/10$ (see Figure 6.3). Now $F(\Gamma_2)$ joins $(0, y_2)$ to $(5x_1 - 2, 2x_1 - 1/2)$ and so $H(\Gamma_2)$ joins $(0, y_2)$ to $(5x_1 - 2, 12x_1 - 9/2)$. The set $A_{3,2}^1$ is bounded by the parallel lines $y = 7/16 - 5x/8$ and $y = 3/8 - 5x/8$. Since $y_2 < 3/8$ and $12x_1 - 9/2 \geq 15/34 > 109/272 \geq 7/16 - 5(5x_1 - 2)/8$ we have that $H(\Gamma_2)$ contains a segment Γ_3 which traverses $A_{3,2}^1$. The image $H(\Gamma_3)$ then traverses Q_3 so that $H^2(\Gamma_3) \subset H^4(\Gamma)$ contains a v -segment in σ_3 . Critically we have that $\Gamma_2, \Gamma_3 \subset H(A_1) \subset \sigma$ but $\Gamma_4 \subset H(A_2 \cap H(A_1))$ which is not in σ . Hence $H_\sigma^3(\Gamma)$ contains a v -segment and we can apply the H_σ^2 result above to show that $H_\sigma^k(\Gamma)$ contains a v -segment for all $k \geq 2$. Similar analysis can be applied to Γ in the left portion of $\sigma_3 \setminus (H(\sigma_2) \cap \sigma_3)$. It follows that $H_\sigma^k(\Gamma)$ contains a v' -segment for all $k \geq 3$, establishing (‡) with $M = m_1 + 3$. □

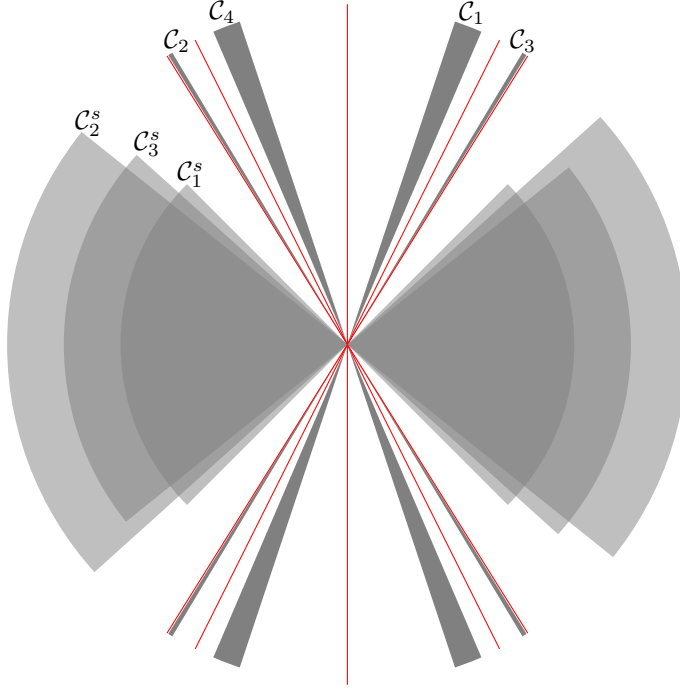


Figure 6.4: Unstable and stable cone fields $\mathcal{C}_j, \mathcal{C}_j^s$ over the subsets $\sigma_j \subset \sigma$ for the return map H_σ . Also shown in red are the gradients of the line segments which make up the boundary $\partial\sigma$ which lie outside of all cone fields.

6.3.2 Invariant cones

We now derive specific unstable and stable cone fields for the return map H_σ , wide enough to ensure invariance **(H1.1)** yet fine enough to produce tight bounds on expansion factors, vital for verifying **(H5)**. Define the cones $\mathcal{C}_1, \dots, \mathcal{C}_4$ by

$$(\mathcal{C}_1) \quad 3|v_1| \geq |v_2| \geq 7|v_1|/3, \quad v_1 v_2 > 0,$$

$$(\mathcal{C}_2) \quad 5|v_1|/3 \geq |v_2| \geq \varphi|v_1|, \quad v_1 v_2 < 0,$$

$$(\mathcal{C}_3) \quad 5|v_1|/3 \geq |v_2| \geq \varphi|v_1|, \quad v_1 v_2 > 0,$$

$$(\mathcal{C}_4) \quad 3|v_1| \geq |v_2| \geq 7|v_1|/3, \quad v_1 v_2 < 0,$$

and the following stable cones

$$(\mathcal{C}_1^s) \quad |v_1| \geq |v_2|,$$

$$(\mathcal{C}_2^s) \quad 9/10 \geq v_2/v_1 \geq -8/10,$$

$$(\mathcal{C}_3^s) \quad 8/10 \geq v_2/v_1 \geq -9/10,$$

$$(\mathcal{C}_4^s) \quad |v_1| \geq |v_2|.$$

In the notation of section 6.1, for general $z \in \sigma$ we take $C_z^u = \mathcal{C}_j$ and $C_z^s = \mathcal{C}_j^s$ for $z \in \sigma_j$. These cone fields are plotted in Figure 6.4.

Lemma 6.3. *The above cones satisfy $DH_\sigma C_z^u \subset C_z^u$, and $DH_\sigma C_z^s \supset C_z^s$, for all $z \in \sigma$ where DH_σ exists, $z' = H_\sigma(z)$.*

Proof. We begin with the unstable cones. Table 6.1 shows the possible values of DH_σ at z if $z \in \sigma_i$ and $z' \in \sigma_j$. The calculations for $z' \in \sigma_1, \sigma_4$ are similar to those made in the proof of Lemma 5.8, noting that each \mathcal{C}_j is contained within \mathcal{C} and, for example, $M_1 M_j^k \mathcal{C} \subset \mathcal{C}_1$ for $j = 2, 3$, and $k \geq 0$.

DH_σ	σ_1	σ_2	σ_3	σ_4
σ_1	M_1	-	$M_3M_2^k$	M_4 $M_4M_2^k$ $M_4M_3^k$
σ_2	-	-	M_3 M_3M_2 $M_3M_2^2$	M_4 M_4M_2 $M_4M_2^2$
σ_3	M_1 M_1M_3 $M_1M_3^2$	M_2 M_2M_3 $M_2M_3^2$	-	-
σ_4	M_1 $M_1M_2^k$ $M_1M_3^k$	$M_2M_3^k$	-	M_4

Table 6.1: Possible values of the Jacobian DH_σ at z if $z \in \sigma_i$ (rows) and $z' = H_\sigma(z) \in \sigma_j$ (columns). Exponent k takes values in \mathbb{N} , dashes are shown if no transition is possible, e.g. $H_\sigma(\sigma_1) \cap \sigma_2 = \emptyset$.

For $z' \in \sigma_2$ we verify that $M_2M_3^k(-1, 3)^T = (-1)^k(-24k+5, -40k-7)^T \in \mathcal{C}_2$ and $M_2M_3^k(-3, 7)^T = (-1)^k(60k+11, -100k-15)^T \in \mathcal{C}_2$ for all $k \geq 1$ so that $DH_\sigma C_z^u \subset C_{z'}^u$ for $z \in \sigma_4$. For $z \in \sigma_3$ we have $M_2(3, 5)^T = (13, -21)^T \in \mathcal{C}_2$ and $M_2(13, 21)^T = (55, -89)^T \in \mathcal{C}_2$, ensuring invariance in this particular case also, despite M_2 being non-hyperbolic. Entirely symmetric calculations can be made for $z' \in \sigma_3$, verifying the result for all unstable cones.

For the stable cones, we remark that taking $C_z^s = \mathcal{C}_1^s$ for all $z \in \sigma$ would satisfy $DH_\sigma C_z^s \supset C_{z'}^s$, but since $M_2^{-1}(1, -1)^T = (-1, 1)^T$ we would be unable to derive sufficient uniform bounds on expansion factors **(H1.2)**. The matrix M_3^{-1} exhibits a similar problem so we must slim down the cones C_z^s when $DH_\sigma^{-1} \in \{M_2^{-1}, M_3^{-1}\}$ which, observing Table 6.1, is for $z \in \sigma_2, \sigma_3$. To remedy this, for such z we slim down the cones C_z^s to $\mathcal{C}_2^s, \mathcal{C}_3^s$ above. As these cones lie in the wider invariant cone $|v_1| \geq |v_2|$, the lemma follows from checking that $DH_\sigma C_z^s \supset C_{z'}^s$ for $z \in \sigma_2, \sigma_3$. This can be verified via direct calculations. \square

6.3.3 Structure of the singularity set

Using the notation of **(H2)** in section 6.1, let $\mathcal{S}_0 = \cup_j \partial\sigma_j$, the union of $\partial\sigma$ and the red dashed lines in Figure 5.8(b). The set $M = \Omega \setminus \mathcal{S}_0$ is clearly dense in Ω and H_σ is a C^2 diffeomorphism from $M \setminus \mathcal{S}_1$ onto $M \setminus \mathcal{S}_{-1}$, being linear on each component.

The set $\mathcal{S}_0 \cup \mathcal{S}_1$ is the countable union of bounded line segments with the endpoints of each segment terminating on another segment, giving **(H2.2)**.

The gradients of the segments in \mathcal{S}_0 take values in $\{\pm 8/5, \pm 2, \infty\}$ which avoid unstable and stable cones C_z^u, C_z^s (see Figure 6.4). The gradients of singularity curves in σ_1 and σ_4 are bounded between -1 and 1 (approaching these limits as we approach the accumulation points) so lie in $\mathcal{C}_1^s, \mathcal{C}_4^s$. The gradients of singularity curves in σ_1 and σ_4 are bounded between -11/14 and 11/14 so lie in $\mathcal{C}_2^s, \mathcal{C}_3^s$ since $11/14 < 8/10$. Similar calculations show that the gradients of segments in \mathcal{S}_{-1} lie in unstable cones.

We conclude this section with showing **(H2.4)**. Condition (6.2) can only fail when $\|DH_\sigma\|$ becomes unbounded, i.e. at points z approaching the accumulation points. We consider the case with $z \in A_{4,2}^k$ near $(0, 1/4)$, the other cases are similar. Recall Figure 5.11 and the lines \mathcal{L}_k from (\dagger) . We note that $d(z, \mathcal{S}_1)$ is bounded above by the length of the segment joining $z = (x, y)$ to $(x, y_k(x))$ on \mathcal{L}_k , which in turn is bounded above by the height of the segment joining $(x, y_k(x))$

to $(x, y_{k-1}(x))$ on \mathcal{L}_{k-1} . This height is

$$y_{k-1}(x) - y_k(x) \leq y_{k-1} \left(\frac{1}{4k-2} \right) - y_k(x) \left(\frac{1}{4k-2} \right) = \frac{1}{2(2k-1)^2} \leq c_1/k^2$$

for some constant $c_1 > 0$. The operator norm of DH_σ over $A_{4,2}^k$ satisfies $\|DH_\sigma\| \leq c_2 k$ for some $c_2 > 0$ so that (6.2) holds for some $c > 0$ whenever we choose $b > 1/2$.

6.3.4 One-step expansion

We will verify (6.3) for the map $f = H_\sigma^2$, $q = 1/2$. We begin with a basic statement on expansion over unstable curves.

Lemma 6.4. *Let M be the constant Jacobian of f over W_i . Then*

$$\lambda^- := \inf_{v \in \mathcal{C}} \frac{\|Mv\|}{\|v\|} \leq \frac{|V_i|}{|W_i|} \leq \sup_{v \in \mathcal{C}} \frac{\|Mv\|}{\|v\|} =: \lambda^+.$$

Proof. Given any $\varepsilon > 0$, consider a piecewise linear approximation \hat{W}_i to W_i such that

$$\left| \frac{|V_i|}{|W_i|} - \frac{|\hat{V}_i|}{|\hat{W}_i|} \right| < \varepsilon$$

where $\hat{V}_i = f(\hat{W}_i)$ gives a piecewise approximation for V_i . Each of the piecewise components will be line segments aligned with vectors in \mathcal{C} so that their expansion factors will be bounded by λ^\pm , giving the result. □

We also derive basic inequalities on the length of a given W_i .

Lemma 6.5. *Let $\mathcal{L}_0, \mathcal{L}_1$ be the singularity curves on which W_i terminates, write these intersections as (x_0, y_0) and (x_1, y_1) . Then*

$$\sqrt{(x_1 - x_0)^2 + (y_1 - y_0)^2} \leq |W_i| \leq |y_1 - y_0| \sqrt{1 + \frac{1}{g^2}}$$

where $g = \inf |v_2/v_1|$ over $(v_1, v_2)^T \in \mathcal{C}$.

Proof. Noting that the lower bound is trivial, we focus on the upper bound. Since $g > 0$ for all unstable cones \mathcal{C} , the projection of W_i to the y -axis is injective. Without loss of generality suppose $y_1 > y_0$, then we can parameterise W_i as a curve $(x(y), y)$ for $y_0 \leq y \leq y_1$. Now

$$\begin{aligned} |W_i| &= \int_{y_0}^{y_1} \sqrt{\left(\frac{dx}{dy}\right)^2 + \left(\frac{dy}{dy}\right)^2} dy \\ &\leq (y_1 - y_0) \sup_{y_0 \leq y \leq y_1} \sqrt{1 + \left(\frac{dx}{dy}\right)^2} \\ &\leq (y_1 - y_0) \sqrt{1 + \frac{1}{g^2}} \end{aligned}$$

as tangent vectors $(x'(y), 1)^T$ to W_i lie in \mathcal{C} . □

Let $P_1 = \{(0, 1/4), (1/2, 1/4), (1/2, 3/4), (1, 3/4)\}$ denote the accumulation points similar to that of σ_{1a} , $P_2 = \{(1/4, 1/2), (1/4, 1), (3/4, 0), (3/4, 1/2)\}$ the accumulation points similar to that of σ_{1b} . Let ε be small. Given a set P , let $B_\varepsilon(P)$ denote the union of the balls $B_\varepsilon(p) \cap \sigma$, centred at $p \in P$ of radius ε . The following describes the images of balls about $P_1 \cup P_2$ under H_σ .

Lemma 6.6. *Given small $\varepsilon > 0$, there exists some $\varepsilon' > 0$ such that $H_\sigma(B_\varepsilon(P_1 \cup P_2))$ covers $B_{\varepsilon'}(P_1 \cup P_2)$.*

Proof. We describe the covering of $B_{\varepsilon'}((1/2, 3/4))$, analysis for the other points in $P_1 \cup P_2$ is analogous. For any $\varepsilon > 0$, $B_\varepsilon(P_1 \cup P_2)$ contains the sets $A_{4,3}^k$ for all $k \geq k_0$ where $k_0 \in \mathbb{N}$ depends on ε . Each $A_{4,3}^k$ consists of two quadrilaterals, one in the ball around $(1/4, 1)$ and the other in the ball around $(1/4, 1/2)$. Figure 6.5(a) shows this latter quadrilateral, with corners on the points

$$r_1 = \left(\frac{k+1}{4k+2}, \frac{k+1}{2k+1} \right), \quad r_2 = \left(\frac{k-1}{4k-2}, \frac{1}{2} \right), \quad r_3 = \left(\frac{k}{4k+2}, \frac{1}{2} \right), \quad r_4 = \left(\frac{k+2}{4k+6}, \frac{k+2}{2k+3} \right).$$

Since DH_σ is constant on $A_{4,3}^k$, given by the integer valued matrix $M_4 M_3^k = (-1)^k \begin{pmatrix} 2k+1 & -2k-2 \\ -6k-2 & 6k+5 \end{pmatrix}$, its image $H_\sigma(A_{4,3}^k)$ is given by the quadrilateral with corners given by $M_4 M_3^k r_j^T \bmod 1$. For odd k we can calculate these corners as

$$r'_1(k) = \left(\frac{1}{2} + \frac{1}{4k+2}, \frac{3}{4} - \frac{5}{8k+4} \right), \quad r'_2(k) = \left(\frac{1}{2} + \frac{1}{4k-2}, \frac{3}{4} - \frac{5}{8k-4} \right),$$

$$r'_3(k) = \left(\frac{1}{2}, \frac{3}{4} + \frac{1}{8k+4} \right), \quad r'_4(k) = \left(\frac{1}{2}, \frac{3}{4} + \frac{1}{8k+12} \right),$$

shown in Figure 6.5(b). For even k the corners of $A_{4,3}^k$ in the ball around $(1/4, 1)$ map into the r'_j . Writing this quadrilateral as $Q(k)$, since $r'_2(k+1) = r'_1(k)$ and $r'_3(k+1) = r'_4(k)$ we have that $\cup_{k \geq k_0} Q(k)$ is the polygon with corners $r'_2(k_0)$, $r'_3(k_0)$, and $\lim_{k \rightarrow \infty} r'_1(k) = \lim_{k \rightarrow \infty} r'_4(k) = (1/2, 3/4)$. Noting that $r'_3(k_0) > 3/4$ and $r'_2(k_0)$ lies on the line $y - \frac{3}{4} = -\frac{5}{2}(x - \frac{1}{2})$, there exists ε' such that $\cup_{k \geq k_0} Q(k)$ covers all points $(x, y) \in B_{\varepsilon'}((1/2, 3/4))$ with $y \geq \frac{3}{4} - \frac{5}{2}(x - \frac{1}{2})$. The image $H_\sigma(B_\varepsilon((1, 3/4)) \cap A_4)$ fills the remaining portion of $B_{\varepsilon'}((1/2, 3/4))$, since $H_\sigma = H$ on A_4 , $H(1, 3/4) = (1/2, 3/4)$, $DH(-2, 1)^T = (0, -1)^T$, and $DH(0, -1)^T = (2, -5)^T$. \square

Proposition 6.2. *Condition (6.3) holds for H_σ^2 when there exists $\varepsilon > 0$ such that $W \cap B_\varepsilon(P_1 \cup P_2) = \emptyset$.*

Proof. We claim that an unstable curve W of vanishing length, bounded away from the accumulation points, is split into at most 9 components W_i by the singularity set for H_σ^2 . The upper bound follows from analysis of the original singularity set for H_σ . Let P_F denote the set of fixed points under H , $P_F = \{(0, 1/2), (1/2, 0), (1/2, 1/2), (1, 1)\}$. Observing Figure 5.8, if $W \cap B_\varepsilon(P_F) \neq \emptyset$ then W is split by \mathcal{S} into at most 5 components W_j , and if $W \cap B_\varepsilon(P_F) = \emptyset$ then the upper bound is 3. We consider these cases separately.

Take, for example, $W \cap B_\varepsilon((0, 1/2)) \neq \emptyset$. Observing Figure 5.12, four of the components W_j map into A'_4 under H_σ , and their images lie in some sector $B_{\varepsilon'}((1, 1/2)) \cap A'_4$. We can take ε small enough that this sector lies entirely in A_4 , so that no further splitting occurs during the next iterate of H_σ . The other component $W \cap A_1$ maps into some sector $B_{\varepsilon'}((0, 1/2)) \cap A'_1$ and is split into at most 5 components, giving at most $N = 9$ components in total. The other cases $W \cap B_\varepsilon(p) \neq \emptyset$, $p \in P_F$, are analogous. Now suppose $W \cap B_\varepsilon(P_F) = \emptyset$. \mathcal{S} splits W into at most 3 components W_j and, by Lemma 6.6 and the above, each $H_\sigma(W_j)$ is bounded away from the accumulation points $P_1 \cup P_2$ and the fixed points P_F . Hence each $H_\sigma(W_j)$ is split into at most 3 components during the next iterate of H_σ , again giving at most $N = 9$ components in total.

The weakest expansion of DH_σ^2 over cones \mathcal{C}_j on σ_j using the euclidean norm is that of $M_1 M_4 = \begin{pmatrix} -3 & 8 \\ -8 & 21 \end{pmatrix}$ on σ_1 (or equivalently $M_4 M_1$ on σ_4), and is given by

$$c = \frac{\|M_1 M_4(3, 7)^T\|}{\|(3, 7)^T\|} \sqrt{\frac{(-9 + 56)^2 + (-24 + 147)^2}{3^2 + 7^2}} = \sqrt{\frac{8669}{29}} \approx 17.29$$

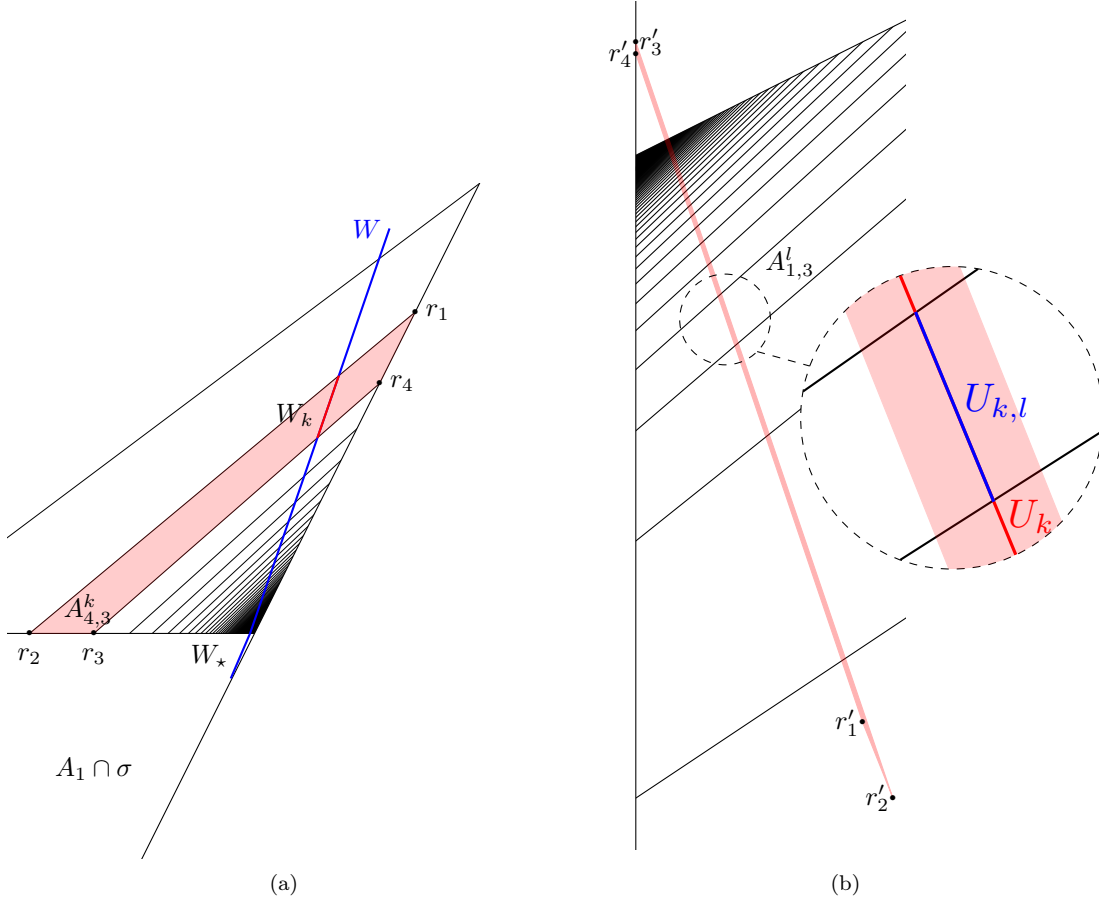


Figure 6.5: Part (a) shows an unstable curve W passing near to the accumulation point $(1/4, 1/2)$, split into W_* below $y = 1/2$ and the collection $W_k \subset A_{4,3}^k$. Part (b) shows the image $U_k = H_\sigma(W_k) \subset H_\sigma(A_{4,3}^k)$, which for odd k lies near the accumulation point $(1/2, 3/4)$ and contains subcurves $U_{k,l} \subset A_{1,3}^l$.

so that, by Lemma 6.4, $|V_i| \geq c|W_i|$ for each component W_i . Now for $q = 1/2$ we have

$$\begin{aligned} \sum_i \left(\frac{|W|}{|V_i|} \right)^q \frac{|W_i|}{|W|} &= \sum_i \sqrt{\frac{|W|}{|V_i|}} \frac{|W_i|}{|W|} \\ &= \sum_i \sqrt{\frac{|W_i|}{|V_i|}} \sqrt{\frac{|W_i|}{|W|}} \\ &\leq \frac{1}{\sqrt{c}} \sum_{i=1}^N \sqrt{\frac{|W_i|}{|W|}}. \end{aligned}$$

Letting $x_i = |W_i|/|W|$ and taking vectors $u = (\sqrt{x_1}, \dots, \sqrt{x_N})$, $v = (1, \dots, 1)$ we have that $\sum_{i=1}^N x_i = 1$ and so $\left(\sum_{i=1}^N \sqrt{x_i} \right)^2 = (u \cdot v)^2 \leq (u \cdot u)(v \cdot v) = \left(\sum_{i=1}^N x_i \right) N = N$ by the Cauchy-Schwarz inequality. Hence

$$\sum_i \left(\frac{|W|}{|V_i|} \right)^q \frac{|W_i|}{|W|} \leq \frac{\sqrt{N}}{\sqrt{c}} < 1$$

since $N \leq 9 < c$.

□

Proposition 6.3. *Condition (6.3) holds for H_σ^2 when $W \cap B_\varepsilon(P_2) \neq \emptyset$ for all $\varepsilon > 0$.*

Proof. We begin with the case $W \cap B_\varepsilon((1/4, 1/2)) \neq \emptyset$ and let $\varepsilon \rightarrow 0$. We may choose δ sufficiently

small so that W intersects $A_1 \cap \sigma$ and some collection of sets $A_{4,3}^k$, $k_0 \leq k \leq k_1$, where $k_1 \rightarrow \infty$ as $\varepsilon \rightarrow 0$, $k_0 \rightarrow \infty$ as $\delta \rightarrow 0$. Therefore, \mathcal{S} splits W into a lower component $W_\star \subset A_1 \cap \sigma$ and upper components $W_k \subset A_{4,3}^k$, illustrated in Figure 6.5(a). We study how the images of these components under H_σ are split up by \mathcal{S} .

Recall the corners $r_j(k)$ which define $A_{4,3}^k$ near $(1/4, 1/2)$. The curve W_k has endpoints on $r_1 r_2$ and $r_3 r_4$, and all tangent vectors to W lie in \mathcal{C}_1 . For odd k the image $U_k = H_\sigma(W_k)$ is a curve joining $r'_1 r'_2$ to $r'_3 r'_4$, with tangent vectors aligned in $M_4 M_3^k \mathcal{C}_1$. This curve is split by \mathcal{S} into an upper portion $U_{k,\star} \subset A_4 \cap \sigma$, and a collection $U_{k,l} \subset A_{1,3}^l$ for some consecutive range $l_0 \leq l \leq l_1$ which depends on k . Each $A_{1,3}^l$ is bounded by the lines

$$\mathcal{L}_l : y - \frac{1}{2} = \frac{2l}{2l+1}(x - 1/4) \quad (6.6)$$

and \mathcal{L}_{l-1} , hence a lower bound on $l_0(k)$ is given by the largest l such that $r'_2(k)$ lies on or above \mathcal{L}_{l-1} . One can verify that $r'_2(k)$ lies on \mathcal{L}_{l-1} when $k = 7l - 4$ and approaches $(1/2, 3/4)$ monotonically in x and y so that $l_0(k) \geq \lfloor \frac{k+4}{7} \rfloor$. To determine an upper bound on l_1 , note that $r'_4 r'_1$ lies on the line

$$y - \frac{3}{4} - \frac{1}{8k+12} = -\frac{6k+8}{2k+3} \left(x - \frac{1}{2}\right), \quad (6.7)$$

meeting the A_4 boundary $\mathcal{L} : y = 1/2 + x/2$ at the point

$$(x_k, y_k) = \left(\frac{7k+10}{14k+19}, \frac{21k+29}{28k+38} \right). \quad (6.8)$$

We similarly calculate that the line \mathcal{L}_l meets $y = 1/2 + x/2$ at the point

$$(X_l, Y_l) = \left(\frac{l}{2l-1}, \frac{1-3l}{2-4l} \right).$$

The intersection of U_k with $y = 1/2 + x/2$ must be some point $(x, 1/2 + x/2)$ with $x \geq x_k$ so that an upper bound on $l_1(k)$ is the smallest l such that $x_k \geq X_l$, which reduces to $l \geq 7k + 10$, hence $l_1(k) \leq \lceil 7k + 10 \rceil = 7k + 10$. For even k the splitting behaviour is entirely analogous, with $H_\sigma(W_k)$ intersecting \mathcal{S} in the neighbourhood of $(1, 1/4)$.

For the lower component W_\star , the image $U_\star = H_\sigma(W_\star) = H(W_\star)$ lies in a neighbourhood of $H(1/4, 1/2) = (1/4, 1)$ and is split by \mathcal{S} into a collection $U_{\star,j} \subset A_{4,3}^j$, $j_0 \leq j \leq j_1$, where $j_1 \rightarrow \infty$ as $\varepsilon \rightarrow 0$, $j_0 \rightarrow \infty$ as $\delta \rightarrow 0$. Write $W_{\star,j} = H_\sigma^{-1}(U_{\star,j})$, $W_{k,\star} = H_\sigma^{-1}(U_{k,\star})$, $W_{k,l} = H_\sigma^{-1}(U_{k,l})$, then W splits into components

$$W = \left(\bigcup_{j \geq j_0} W_{\star,j} \right) \cup \left(\bigcup_{k \geq k_0} W_{k,\star} \right) \cup \left(\bigcup_{k \geq k_0} \bigcup_{l=l_0}^{l_1} W_{k,l} \right) \quad (6.9)$$

on which DH_σ^2 is constant. Let $V_i = H_\sigma(U_i) = H_\sigma^2(W_i)$, then for $q = 1/2$:

$$\begin{aligned} \sum_i \left(\frac{|W|}{|V_i|} \right)^q \frac{|W_i|}{|W|} &= \sum_i \sqrt{\frac{|W_i|}{|V_i|}} \sqrt{\frac{|W_i|}{|W|}} \\ &= \sum_{j \geq j_0} \sqrt{\frac{|W_{\star,j}|}{|V_{\star,j}|}} \sqrt{\frac{|W_{\star,j}|}{|W|}} + \sum_{k \geq k_0} \sqrt{\frac{|W_{k,\star}|}{|V_{k,\star}|}} \sqrt{\frac{|W_{k,\star}|}{|W|}} + \sum_{k \geq k_0} \sum_{l=l_0}^{l_1} \sqrt{\frac{|W_{k,l}|}{|V_{k,l}|}} \sqrt{\frac{|W_{k,l}|}{|W|}} \\ &\leq \sum_{j \geq j_0} \sqrt{\frac{1}{\Lambda_{\star,j}}} \sqrt{\frac{|W_{\star,j}|}{|W|}} + \sum_{k \geq k_0} \sqrt{\frac{1}{\Lambda_{k,\star}}} \sqrt{\frac{|W_{k,\star}|}{|W|}} + \sum_{k \geq k_0} \sum_{l=l_0}^{l_1} \sqrt{\frac{1}{\Lambda_{k,l}}} \sqrt{\frac{|W_{k,l}|}{|W|}} \end{aligned}$$

by Lemma 6.4, where Λ_i is the minimum expansion factor of DH_σ^2 on W_i over the cone \mathcal{C}_1 . Define

$W_\diamond = W \setminus W_\star$ and let $0 \leq p \leq 1$ denote the proportion $|W_\diamond| = p|W|$, then

$$\begin{aligned} \liminf_{\delta \rightarrow 0} \sup_{W:|W|<\delta} \sum_i \left(\frac{|W|}{|V_i|} \right)^q \frac{|W_i|}{|W|} &\leq \sup_{0 \leq p \leq 1} \left(\lim_{j_0 \rightarrow \infty} \sum_{j \geq j_0} \sqrt{\frac{1}{\Lambda_{\star,j}}} \sqrt{\frac{(1-p)|W_{\star,j}|}{|W_\star|}} \right. \\ &\quad + \lim_{k_0 \rightarrow \infty} \sum_{k \geq k_0} \sqrt{\frac{1}{\Lambda_{k,\star}}} \sqrt{\frac{p|W_{k,\star}|}{|W_\diamond|}} \\ &\quad \left. + \lim_{k_0 \rightarrow \infty} \sum_{k \geq k_0} \sum_{l=l_0}^{l_1} \sqrt{\frac{1}{\Lambda_{k,l}}} \sqrt{\frac{p|W_{k,l}|}{|W_\diamond|}} \right). \end{aligned}$$

We put upper bounds on each of these sums using lower bounds on the expansion factors Λ_i and geometric bounds on the curves U_i terminating on \mathcal{S} . We use asymptotic notation $f \sim g$ for functions f, g if $f/g \rightarrow 1$, and write $f \lesssim g$ if there is some function h such that $f \leq h \sim g$.

Starting with the first sum, DH_σ^2 is given by $M_4 M_3^j M_1 = (-1)^j \begin{pmatrix} -2j-3 & -6j-8 \\ 6j+8 & 18j+21 \end{pmatrix}$ on each component $W_{\star,j}$ with minimum expansion factors given by

$$\begin{aligned} \Lambda_{\star,j} &= \inf_{7/3 \leq m \leq 3} \sqrt{\frac{(-2j-3-6jm-8m)^2 + (6j+8+18jm+21)^2}{1+m^2}} \\ &\sim \inf_{7/3 \leq m \leq 3} \sqrt{\frac{(2+6m)^2 + (6+18m)^2}{1+m^2}} j = \frac{48\sqrt{145}}{29} j := c_\star j. \end{aligned} \tag{6.10}$$

Each curve $U_{\star,j}$ has tangent vectors in $M_1 \mathcal{C}_1$ satisfying $41/17 \leq |v_2|/|v_1| \leq 17/7$, $v_1 v_2 \geq 0$. For each $j > j_0$, $U_{\star,j}$ traverses $A_{4,3}^j$ so that (making a similar calculation to equation 5.13) Lemma 6.5 gives

$$\frac{a_\star}{j^2} \lesssim |U_{\star,j}| \lesssim \frac{b_\star}{j^2} \tag{6.11}$$

for $a_\star = \frac{13}{80}\sqrt{2}$, $b_\star = \frac{41}{192}\sqrt{1+17^2/41^2}$ (calculated in the appendix, section C.1). The upper bound also trivially holds for $j = j_0$. Let Λ_1^+ , Λ_1^- denote the maximum and minimum expansion factors of M_1 over \mathcal{C}_1 , then

$$|W_\star| = \sum_{j \geq j_0} |W_{\star,j}| \geq \sum_{j \geq j_0} \frac{|U_{\star,j}|}{\Lambda_1^+} \gtrsim \frac{a_\star}{\Lambda_1^+} \sum_{j \geq j_0+1} \frac{1}{j^2} \geq \frac{a_\star}{\Lambda_1^+(j_0+1)} \sim \frac{a_\star}{\Lambda_1^+ j_0}$$

where we have used the fact that

$$\frac{1}{j^2} \geq \frac{1}{j(j+1)} = \frac{1}{j} - \frac{1}{j+1}$$

and considered the telescoping sum. Similarly $|W_{\star,j}| \lesssim b_\star / (\Lambda_1^- j^2)$ so that

$$\frac{|W_{\star,j}|}{|W_\star|} \lesssim \frac{b_\star \Lambda_1^+ j_0}{a_\star \Lambda_1^-} \frac{1}{j^2}.$$

Hence

$$\begin{aligned}
\sum_{j \geq j_0} \sqrt{\frac{1}{\Lambda_{\star, j}}} \sqrt{\frac{(1-p)|W_{\star, j}|}{|W_{\star}|}} &\lesssim \sum_{j \geq j_0} \sqrt{\frac{1}{c_{\star} j}} \sqrt{\frac{(1-p)b_{\star} \Lambda_1^+ j_0}{a_{\star} \Lambda_1^-} \frac{1}{j^2}} \\
&= \sqrt{\frac{(1-p)b_{\star} \Lambda_1^+ j_0}{c_{\star} a_{\star} \Lambda_1^-}} \sum_{j \geq j_0} j^{-3/2} \\
&\leq \sqrt{\frac{(1-p)b_{\star} \Lambda_1^+}{c_{\star} a_{\star} \Lambda_1^-}} 2 \sqrt{\frac{j_0}{j_0 - 1}} \\
&\rightarrow 2 \sqrt{\frac{(1-p)b_{\star} \Lambda_1^+}{c_{\star} a_{\star} \Lambda_1^-}}
\end{aligned} \tag{6.12}$$

as $j_0 \rightarrow \infty$, where we have used $\sum_{j \geq j_0} j^{-3/2} \leq \int_{j_0-1}^{\infty} x^{-3/2} dx$.

Moving onto the next summation, $\Lambda_{k, \star}$ is determined by $M_4^2 M_3^k = (-1)^k \begin{pmatrix} 14k+5 & -14k-12 \\ -34k-12 & 34k+29 \end{pmatrix}$ and satisfies

$$\Lambda_{k, \star} \sim \inf_{7/3 \leq m \leq 3} \sqrt{\frac{(14-14m)^2 + (34-34m)^2}{1+m^2}} k = \frac{104}{\sqrt{29}} k =: c_{\diamond} k.$$

For odd k the curve $U_{k, \star}$ has endpoints $(1/2, y_0)$ on $r'_3 r'_4$ and $(2y_1 - 1, y_1)$ on \mathcal{L} , where y_1 is bounded by the intersections of $r'_4 r'_1$ and $r'_3 r'_2$ with \mathcal{L} (see Figure 6.5(b)). An upper bound on $|y_1 - y_0|$ is given by taking $(1/2, y_0) = r'_3$ and $(2y_1 - 1, y_1) = r'_4 r'_1 \cap \mathcal{L}$. Noting (6.8), this gives

$$|y_1 - y_0| \leq \frac{3}{4} + \frac{1}{8k+4} - \frac{21k+29}{28k+38} = \frac{6k+9}{56k^2+104k+38} \sim \frac{6}{56} k^{-1}.$$

$U_{k, \star}$ has tangent vectors $(v_1, v_2)^T$ in $M_{4,3}^k \mathcal{C}_1 \subset \mathcal{C}_4$, so that $|v_2/v_1| \geq 7/3$. By Lemma 6.5 we then have $|U_{k, \star}| \lesssim b_{\diamond}/k$, where $b_{\diamond} = \frac{6}{56} \sqrt{1 + \frac{9}{49}} \approx 0.117$. The minimum expansion factor of $M_4 M_3^k = (-1)^k \begin{pmatrix} 2k+1 & -2k-2 \\ -6k-2 & 6k+5 \end{pmatrix}$ over \mathcal{C}_1 is given by

$$\inf_{7/3 \leq m \leq 3} \sqrt{\frac{(2-2m)^2 + (6-6m)^2}{1+m^2}} k = \frac{8\sqrt{145}}{29} k =: \gamma k$$

which gives $|W_{k, \star}| \lesssim b_{\diamond}/(\gamma k^2)$. The analysis for even k is analogous and gives the same upper bound. We next require a lower bound on $|W_{\diamond}|$. For $k > k_0$, W_k is a curve with tangent vectors in \mathcal{C}_1 which traverses $A_{4,3}^k$. Making the same calculation as (5.13), $|W_k|$ is bounded below by the shortest path across $A_{4,3}^k$, the line segment passing through r_4 with gradient 3. That's

$$|W_k| \geq \sqrt{\left(\frac{1}{16k^2+28k+6}\right)^2 + \left(\frac{3}{16k^2+28k+6}\right)^2} \sim \frac{\sqrt{10}}{16k^2} \tag{6.13}$$

so that

$$|W_{\diamond}| \geq \sum_{k \geq k_0+1} |W_k| \gtrsim \frac{a}{k_0} \tag{6.14}$$

with $a := \sqrt{10}/16$. Hence

$$\sum_{k \geq k_0} \sqrt{\frac{1}{\Lambda_{k, \star}}} \sqrt{\frac{p|W_{k, \star}|}{|W_{\diamond}|}} \lesssim \sum_{k \geq k_0} \sqrt{\frac{1}{c_{\diamond} k}} \sqrt{\frac{pb_{\diamond} k_0}{a\gamma} \frac{1}{k^2}} \rightarrow 2 \sqrt{\frac{pb_{\diamond}}{c_{\diamond} a\gamma}}$$

as $k_0 \rightarrow \infty$, by a similar argument to (6.12).

For the third summation, $\Lambda_{k,l}$ is determined by the matrix

$$M_1 M_3^l M_4 M_3^k = (-1)^{k+l} \begin{pmatrix} -48kl - 10k - 18l - 3 & 48kl + 10k + 42l + 8 \\ -112kl - 26k - 42l - 8 & 112kl + 26k + 98l + 21 \end{pmatrix}$$

and satisfies (for large k, l)

$$\Lambda_{k,l} \sim \inf_{7/3 \leq m \leq 3} \sqrt{\frac{(48 - 48m)^2 + (112 - 112m)^2}{1 + m^2}} kl = 64kl =: ckl.$$

We can show an upper bound $|U_{k,l}| \lesssim b/l^2$ where $b = \frac{3}{32} \sqrt{1 + \frac{9}{49}} \approx 0.102$ (see section C.1) so that $|W_{k,l}| \lesssim b/(\gamma kl^2)$. Now by (6.14),

$$\begin{aligned} \sum_{l=l_0}^{l_1} \sqrt{\frac{1}{\Lambda_{k,l}}} \sqrt{\frac{p|W_{k,l}|}{|W_\diamond|}} &\lesssim \sum_{l=l_0}^{l_1} \sqrt{\frac{1}{ckl}} \sqrt{\frac{pbk_0}{a\gamma kl^2}} \\ &\leq \sqrt{\frac{1}{ck}} \sqrt{\frac{pbk_0}{a\gamma k}} \sum_{l=\lfloor \frac{k+4}{7} \rfloor}^{7k+10} l^{-3/2} \\ &\leq 2\sqrt{\frac{1}{ck}} \sqrt{\frac{pbk_0}{a\gamma k}} \left(\frac{1}{\sqrt{\lfloor \frac{k+4}{7} \rfloor - 1}} - \frac{1}{\sqrt{7k+10}} \right) \\ &\sim 2\sqrt{\frac{1}{ck}} \sqrt{\frac{pbk_0}{a\gamma k}} \left(\sqrt{7} - \frac{1}{\sqrt{7}} \right) \frac{1}{\sqrt{k}}. \end{aligned}$$

Letting $h = (\sqrt{7} - 1/\sqrt{7})^2 = 36/7$, we have that

$$\begin{aligned} \sum_{k \geq k_0} \sum_{l=l_0}^{l_1} \sqrt{\frac{1}{\Lambda_{k,l}}} \sqrt{\frac{p|W_{k,l}|}{|W_\diamond|}} &\lesssim 2\sqrt{\frac{pbhk_0}{ca\gamma}} \sum_{k \geq k_0} k^{-3/2} \\ &\rightarrow 4\sqrt{\frac{pbh}{ca\gamma}} \end{aligned}$$

as $k_0 \rightarrow \infty$. Hence for $q = 1/2$

$$\liminf_{\delta \rightarrow 0} \sup_{W: |W| < \delta} \sum_i \left(\frac{|W|}{|V_i|} \right)^q \frac{|W_i|}{|W|} \leq \sup_{0 \leq p \leq 1} \left(2\sqrt{\frac{(1-p)b_*\Lambda_1^+}{c_*a_*\Lambda_1^-}} + 2\sqrt{\frac{pb_\diamond}{c_\diamond a\gamma}} + 4\sqrt{\frac{pbh}{ca\gamma}} \right). \quad (6.15)$$

It is simple to show that for $s, t > 0$ the function $f(p) = s\sqrt{1-p} + t\sqrt{p}$ always attains its maximum value at $p = t^2/(s^2 + t^2)$. Hence letting

$$s = 2\sqrt{\frac{b_*\Lambda_1^+}{c_*a_*\Lambda_1^-}} \approx 0.450, \quad t = 2\sqrt{\frac{b_\diamond}{c_\diamond a\gamma}} + 4\sqrt{\frac{bh}{ca\gamma}} \approx 0.639$$

gives

$$\liminf_{\delta \rightarrow 0} \sup_{W: |W| < \delta} \sum_i \left(\frac{|W|}{|V_i|} \right)^q \frac{|W_i|}{|W|} \leq s\sqrt{\frac{s^2}{s^2 + t^2}} + t\sqrt{\frac{t^2}{s^2 + t^2}} \approx 0.781 < 1$$

as required. The analysis is analogous for W near $(1/4, 1)$ and extends to W near $(3/4, 0)$ and $(3/4, 1/2)$ using the symmetry $T(x, y) = (1 - x, y + 1/2)$ which commutes with H_σ (as seen in the proof of Lemma 5.9). \square

Equivalent analysis verifies the two step expansion for curves near the other accumulation points $p \in P_1$. We provide the relevant calculations to the appendix, Proposition C.1. We are now ready

to apply Theorem 6.2.

6.3.5 Decay of correlations

Theorem 6.5. *The return map $H_\sigma : \sigma \rightarrow \sigma$ enjoys exponential decay of correlations. In particular it admits a Young tower with base Δ_0 satisfying the exponential tail bound*

$$\mu(\{z \in \sigma \mid R(z, H_\sigma, \Delta_0) > n\}) \leq \text{const } \theta^n \quad (6.16)$$

for all $n \geq 1$ where $\theta < 1$ is some constant.

Proof. We run through the conditions for applying Theorem 6.2. Invariance of the unstable and stable cone fields C_z^u, C_z^s was the subject of section 6.3.2, satisfying **(H1.1)**. Condition **(H1.2)** follows by taking $\Lambda = \sqrt{85/41}$, with this lower bound attained by considering the expansion of M_2^{-1} over the cone boundary of \mathcal{C}_2^s with gradient $-8/10$. Noting Remark 6.1, we next show **(H1.3')**. The cone fields are continuous over the components σ_j of $\Omega \setminus \mathcal{S}_0$, indeed they are constant. Noting that all of the stable cones lie within \mathcal{C}_1^s and all of the unstable cones lie in \mathcal{C} , a positive angle between stable and unstable cone fields follows from $\mathcal{C}_1^s \cap \mathcal{C} = \emptyset$. **(H2)** was the subject of section 6.3.3. Unstable manifolds provide a class of H_σ invariant unstable curves which satisfy the regularity conditions listed in Chernov and Zhang (2009). Piecewise linearity of the map trivially implies their bounded curvature and bounds on distortion; absolute continuity follows from Lemma 6.1. **(H4)** follows from Proposition 6.1, where we showed that H_σ is Bernoulli with respect to the normalised Lebesgue measure on σ . Noting Remark 6.1, **(H5)** follows for the map H_σ^2 by Propositions 6.2, 6.3, C.1. □

We follow the approach outlined in Chernov and Zhang (2008) to infer the polynomial mixing rate of H from the exponential mixing rate of H_σ . For reference, their \mathcal{M} and $M \subset \mathcal{M}$ are our \mathbb{T}^2 and $\sigma \subset \mathbb{T}^2$, their $\mathcal{F} : \mathcal{M} \rightarrow \mathcal{M}$ and $F : M \rightarrow M$ are our H and H_σ respectively. With Δ_0 above, define

$$A_n = \{z \in \mathbb{T}^2 \mid R(z, H, \Delta_0 > n)\}.$$

We will show

Proposition 6.4. $\mu(A_n) = \mathcal{O}(n^{-1})$.

Theorem 6.4 then follows from the work of Young (1999). Proving Proposition 6.4 involves treating separately a set of infrequently returning points. For each $z \in \mathbb{T}^2$ and $n \geq 1$ define

$$r(z; n, \sigma) = \#\{1 \leq i \leq n \mid H^i(z) \in \sigma\},$$

counting the number of times the orbit of z hits σ over n iterates of H . Define

$$B_{n,b} = \{z \in \mathbb{T}^2 \mid r(z; n, \sigma) > b \ln n\}$$

where b is a constant to be chosen shortly.

Lemma 6.7. $\mu(A_n \cap B_{n,b}) = \mathcal{O}(n^{-1})$.

Proof. This follows from (6.16), choosing b large enough so that $n \theta^{b \ln n} < n^{-1}$. See Chernov and Zhang (2008), or Springham and Sturman (2014) for a detailed proof. □

Proposition 6.4 then follows from similarly establishing

Lemma 6.8. $\mu(A_n \setminus B_{n,b}) = \mathcal{O}(n^{-1})$.

Analysis of the set $A_n \setminus B_{n,b}$ is the focus of Chernov and Zhang (2008). It consists, for large n , of points which take many iterates to hit Δ_0 and hit σ infrequently during these iterates. Chernov and Zhang define m -cells

$$M_m = \{z \in \sigma \mid R(z; H, \sigma) = m + 1\}$$

for $m \geq 0$. For the OTM the coloured regions of Figure 5.8(a) form M_0 and for $m > 0$ each set M_m is the union $\cup_{i,j} A_{i,j}^m$. For these latter sets, the authors assume that their measures decrease polynomially

$$\mu(M_m) \leq C_1/m^r, \quad (6.17)$$

where $r \geq 3$. Further they assume that if $z \in M_m$ then $F(z) \in M_k$ with

$$\beta^{-1}m - C_2 \leq k \leq \beta m + C_3 \quad (6.18)$$

for some $\beta > 1$ and unimportant constants $C_i > 0$. It is straightforward to verify that (6.17) holds for $r = 3$: each $A_{i,j}^m$ has length similar to $|\mathcal{L}_m| = \mathcal{O}(m^{-1})$, see (6.5) and width similar to $|W_m| = \mathcal{O}(m^{-2})$, see (6.13). Recalling the bounds l_0 and l_1 found in the proof of Proposition 6.3, we see that for our map H_σ , condition (6.18) holds with $\beta = 7$. In §4 of Chernov and Zhang (2008) the authors describe an ‘ideal situation’ under which the action of F on the cells M_m is equivalent to a discrete Markov chain. This requires:

- (I1) The components of each M_m and their images under F are exact trapezoids which shrink homotetically as m grows,
- (I2) The measure μ has constant density,
- (I3) F is linear over each component,
- (I4) Condition (6.18) holds with $C_2 = C_3 = 0$ (no irregular intersections).

These conditions, together with:

$$\frac{\mu(F(M_m) \cap M_k)}{\mu(F(M_m))} = C_4 \frac{m}{k^2} + \mathcal{O}\left(\frac{1}{m^2}\right) \quad (6.19)$$

for some $C_4 > 0$ and k satisfying (6.18), are sufficient to establish the lemma. The authors show that their cells admit good linear approximations and the irregular intersections are of relative measure $\mathcal{O}(1/k)$ so that (I1) and (I4) are essentially satisfied, removing some portion of negligible measure from each cell. They then go on to estimate the effect of nonlinearity and nonuniform density of μ to address (I2) and (I3), requiring a more sophisticated approach. For our system (I2) and (I3) are already satisfied by H_σ , so it remains to verify (6.19) for H_σ , show that our $A_{i,j}^k$ are well approximated by exact trapezoids, and calculate the relative measure of the irregular intersections. For (6.19), areas of the regular intersections can be calculated using the shoelace formula on the corner coordinates $p_{k,l}$, $\bar{p}_{k,l}$, given explicitly in the appendix, section C.1 and Proposition C.1. Our cells are near exact trapezoids, unlike the billiards systems considered in Chernov and Zhang (2008) whose cell sides are curvilinear, our cell boundaries are linear with the sides (e.g. \mathcal{L}_m , \mathcal{L}_{m-1}) near parallel for large m . For the irregular intersections, (6.19) still gives an upper bound on their measure and there are some constant $C_2 + C_3$ of them. The total number of intersections scales with m by (6.18) so they have negligible measure compared to $\mu(H_\sigma(M_m))$.

6.4 Summary

Akin to Cerbelli and Giona’s map, where precise mapping behaviour gave rise to its atypical[‡] pseudo-Anosov dynamics, precise mapping behaviour of the OTM on the segments l_j gives rise to more atypical behaviour, global mixing but at a reduced rate. This is in contrast to the exponential mixing rate proven in \mathcal{E} and expected across \mathcal{P}' (maps over this parameter set are uniformly hyperbolic with singularities). One could argue that since the dynamics are entirely contingent on this behaviour, not preserved under small perturbations, it has minimal relevance to applications. We argue, however, that the OTM serves as a simple model for two key phenomena in laminar mixing.

The first of these is the ‘stirrers’ analogy mentioned in section 5.3.1. Defining our map as the change after each stir, i.e. one cycle of the stirrers’ periodic protocol, the space the stirrers occupy forms a natural invariant set. Imposing no-slip boundaries on the stirrers influences the neighbouring fluid bulk, spawning trajectories which ‘stick’ to them for arbitrarily many stirs. The way in which orbits under the OTM escape the partition elements A_2, A_3 containing the l_j mirrors this sticking behaviour. While linked twist maps (like the non-monotonic example studied in section 5.2) provide a paradigm for mixing in the presence of a static boundary, the OTM perhaps addresses the situation of moving boundaries (i.e. stirrers). Realistic mixing devices may exhibit both phenomena, stretching and folding using interspersed stirrers, with slowed mixing near the vessel walls. Constructing an ASM which captures both of these is not trivial. By the analysis of section 5.1, introducing a boundary means we must vary the non-monotonic shears (e.g. their strength) to maintain parabolic Jacobians, but this has to be balanced against preserving the precise periodic structure of the l_j .

Its second use is as a rough description of non-ergodic ASMs restricted to their chaotic sea. Like the OTM, the tail end of their correlation decay is determined by escapes from non-hyperbolic regions, with points arbitrarily close to island boundaries experiencing non-hyperbolic behaviour for arbitrarily many iterates. Recalling Figure 2.4, showing mixing dynamics of a non-ergodic counter-rotating LTM, accumulating behaviour onto the outer invariant ellipses (equivalently the boundary of the chaotic region) is observed, analogous to the accumulation onto l_j for the OTM. For comparison, see the similar visualisation for the OTM given later in Figure 7.5(a). Elliptic island and ghost boundaries, then, influence the surrounding chaotic dynamics in a similar fashion, trapping nearby orbits for long time periods and thus slowing mixing to a polynomial rate. The OTM then forms a watershed between global mixing at an exponential rate (e.g. across \mathcal{P}') and polynomial mixing alongside islands, the zero measure of the ghost boundaries permitting global mixing at these precise parameters.

The analysis presented in this chapter is restricted to *asymptotic* mixing rates inherent to the ergodic theory approach. Naturally, realistic mixing devices are not run for infinite time, rather just until some mixing threshold has been met, i.e. sufficiently thin striation widths for diffusion to dominate. The asymptotic description is appropriate when the tail end of the distribution is representative of the whole, see e.g. the estimated correlation decay of the OTM (Figure 5.14). In other systems, like those with perhaps long but bounded return times to a hyperbolic region, the (presumably exponential) tail end may be less relevant. A future extension to this work could include relating the rate of escapes from non-hyperbolic regions to the finite time decay rates of correlations. Depending on the specifics of the systems and the threshold for mixing, it may be preferable to optimise for fast polynomial decay over initially slow but eventually exponential decay.

[‡]In the context of the wider $H_{(\xi, \eta)}$ parameter space.

Chapter 7

Wider Protocols, Summary & Outlook

7.1 Mixing protocols

7.1.1 Introduction

Recall the system of two orthogonal non-monotonic shears $H = H_{(\xi, \eta)}$ from section 4.3. Repeated application of H amounts to alternating between the two shears F and G , where F maps

$$(x, y) \mapsto \begin{cases} (x + f_1(y, \eta), y) \bmod 1 & \text{for } y \leq 1 - \eta, \\ (x + f_2(y, \eta), y) \bmod 1 & \text{for } y \geq 1 - \eta, \end{cases}$$

and G maps

$$(x, y) \mapsto \begin{cases} (x, y + f_1(x, \xi)) \bmod 1 & \text{for } x \leq 1 - \xi, \\ (x, y + f_2(x, \xi)) \bmod 1 & \text{for } x \geq 1 - \xi, \end{cases}$$

where $f_1(t, \alpha) = t/(1 - \alpha)$ and $f_2(t, \alpha) = (1 - t)/\alpha$.

This is an example of a *periodic protocol*, which we define as any map of the form $H_P = G^{l_p} \circ F^{k_p} \circ \dots \circ G^{l_1} \circ F^{k_1}$, represented as the $2p$ -tuple $P = (k_1, l_1, \dots, k_p, l_p)$, where p and each entry k_i, l_i are in \mathbb{N} . Using this notation, H is the periodic protocol with $P = (1, 1)$. We remark that by periodicity we can rearrange protocols such as $F \circ G^3 \circ F$ to $G^3 \circ F^2$ i.e. $P = (2, 3)$, so any periodic binary sequence in F and G^* can be represented by some $2p$ -tuple P .

The aim of this section is to test the mixing efficiency of various protocols. To do this we will compare Lyapunov exponents normalised by the *energy* required to complete a protocol. Noting that for any $0 < \alpha < 1$

$$\int_0^{1-\alpha} f_1(t, \alpha) dt + \int_{1-\alpha}^1 f_2(t, \alpha) dt = \frac{1}{2},$$

an appropriate measure of energy expenditure for a periodic protocol $P = (k_1, l_1, \dots, k_p, l_p)$ is $E(P) = \frac{1}{2} \sum_{i=1}^p k_i + l_i$. The original protocol then satisfies $E((1, 1)) = 1$.

The metric we have chosen to test mixing efficiency essentially follows that of D'Alessandro et al. (1999), where a similar analysis was performed for the Sawtooth Maps studied in section 2.2. In that setting the Jacobian DH_P is constant a.e. and therefore the variation in protocol performance is entirely determined by its trace. For our map $H_{(\xi, \eta)}$ the analysis is less straightforward, owing to the wider variety of possible cocycles over $z \in \mathbb{T}^2$. To make the data visualisation easier, we will restrict to the one dimensional parameter space $\xi = \eta$ with $0 < \eta < \eta_3 \approx 0.2389$. The latter

*Other than all F or all G , which results in a fully integrable, non-mixing system.

restriction ensures that we can derive rigorous bounds on Lyapunov exponents, in particular it ensures that all systems resulting from periodic protocols P are ergodic. We will cover this in the following section.

7.1.2 Ergodic properties

In this section we will show the following:

Theorem 7.1. *Let $P = (k_1, l_1, \dots, k_p, l_p)$ be a $2p$ -tuple with values in \mathbb{N} . Then for parameter values $\xi = \eta$, $0 < \eta < \eta_3$, the map $H_P = G^{l_p} \circ F^{k_p} \circ \dots \circ G^{l_1} \circ F^{k_1}$ is ergodic, mixing with respect to the Lebesgue measure.*

The proof is largely adapted from that of the (1,1) protocol. We will use the Katok and Strelcyn (1986) scheme, and give a brief account of the alterations that are necessary.

Proof. Starting with hyperbolicity, it is sufficient to show that given P and η there exists a cone \mathcal{C} such that $DH_P \mathcal{C} \subset \mathcal{C}$ (invariance) and $\|DH_P v\|/\|v\| > 1$ for all $v \in \mathcal{C}$ (expansion). For simplicity we will use the $\|\cdot\|_\infty$ norm and the original cone \mathcal{C} , bounded by the unit vectors $v_2 = (\eta/(\eta-1), 1)^T$ and $v_3 = (1, 1)^T$.

Let $H_i = G^{l_i} \circ F^{k_i}$. Clearly if for each $1 \leq i \leq p$ the cone \mathcal{C} is invariant and expanding under DH_i , the same holds for DH_P . Parameterise the torus by $(x, y) \bmod 1$, and split it into four rectangles R_j such that $0 < x < 1 - \eta$ in R_1 and R_3 , $1 - \eta < x < 1$ in R_2 and R_4 , $0 < y < 1 - \eta$ in R_1 and R_2 , $1 - \eta < y < 1$ in R_3 and R_4 . To simplify the notation drop the subscripts from k_i, l_i then DH_i is constant on each of the four $A_{j,k} = F^{-k}(R_j)$. Write its restriction to $A_{j,k}$ as $M_{j,k,l}$, each of which are hyperbolic for all $k, l \in \mathbb{N}$ and therefore admit stable and unstable eigenvectors. One can verify that for each $k, l \in \mathbb{N}$ the unstable vectors all lie in \mathcal{C} and the stable vectors all lie outside of \mathcal{C} , so that the cone is invariant under each of the matrices $M_{j,k,l}$. It follows that each of these matrices see their minimum expansion $K_{j,k,l}$ over the cone boundaries v_2 and v_3 :

$$K_{j,k,l} = \inf_{v \in \mathcal{C}} \frac{\|M_{j,k,l} v\|}{\|v\|} = \min\{\|M_{j,k,l} v_2\|, \|M_{j,k,l} v_3\|\}.$$

For each j the expansions of v_2 and v_3 under $M_{j,k,l}$ are straightforward to calculate and can be shown to be monotonic increasing in k and l . Hence for each j we have

$$\|M_{j,k,l} v_2\| \geq \|M_{j,1,1} v_2\| \quad \text{and} \quad \|M_{j,k,l} v_3\| \geq \|M_{j,1,1} v_3\|, \quad (7.1)$$

so that cone expansion of each DH_i follows from cone expansion of DH_P with the original protocol (1,1).

Moving onto establishing **(MR)**, non-zero Lyapunov exponents a.e. implies the existence of local stable and unstable manifolds $\gamma_s(z), \gamma_u(z)$ at a.e. point $z \in \mathbb{T}^2$. Decompose H_P as $H_P = H_p \circ \dots \circ H_1$, then rather than establishing the growth lemma for H_P , we show it for each of the H_i . In forwards time, the inequalities (7.1) together with the explicit calculation for the (1,1) protocol establish

$$\min \left\{ \sum_{j=1}^4 \frac{1}{\|M_{j,k,l} v_2\|}, \sum_{j=1}^4 \frac{1}{\|M_{j,k,l} v_3\|} \right\} < 1 \quad (7.2)$$

for all $k, l \in \mathbb{N}$. In backwards time we remark that the cone \mathcal{C}' bounded by the unit vectors $u_2 = (1, -1)^T$ and $u_3 = (1, \eta/(1-\eta))^T$ is invariant and expanding under DH_P^{-1} . Letting $s : \{1, 2, 3, 4\} \mapsto \{1, 3, 2, 4\}$, one can show that for each j

$$\|M_{j,k,l}^{-1} u_2\| = \|M_{s(j),l,k} v_3\| \quad \text{and} \quad \|M_{j,k,l}^{-1} u_3\| = \|M_{s(j),l,k} v_2\|$$

so that the inequality which underpins the growth lemma in backwards time,

$$\min \left\{ \sum_{j=1}^4 \frac{1}{\|M_{j,k,l}^{-1} u_2\|}, \sum_{j=1}^4 \frac{1}{\|M_{j,k,l}^{-1} u_3\|} \right\} < 1, \quad (7.3)$$

also follows from (7.1).

By an analogous argument to that given for the (1,1) protocol, for a.e. $z \in \mathbb{T}^2$ there exists some finite $r_1 = m_1 p + i$ such that $(H_i \circ \dots \circ H_1 \circ H_P^{m_1})(\gamma_u(z))$ has non-simple intersection with $A_{j,k'}$, for some j , where $k' = k_{i+1}$ with the subscript calculated modulo p . The case (j) analysis and the geometric bound $x_v(\eta) \leq q_1(\eta)$ still hold when mapping under H_i , so that **(MR)** follows when mapping under each H_i . That is, there exists finite $r_2 = m_2 p + i'$ such that $(H_{i'} \circ \dots \circ H_1 \circ H_P^{m_2})(\gamma_u(z))$ contains a v -segment and so too do its forward images under $H_{i'+1}, H_{i'+2}, \dots$. It follows that $H_P^m(\gamma_u(z))$ contains a v -segment for all $m \geq m_2 + 1$. The argument for backwards time mapping into h -segments is entirely analogous. \square

By the Katok and Strelcyn scheme, the system defined by the map protocol map H_P is Bernoulli, hence strong mixing and ergodic by the ergodic hierarchy. We will now use ergodicity to establish rigorous bounds on their normalised Lyapunov exponents.

7.1.3 Bounds on Lyapunov exponents

A basic corollary of Birkhoff's ergodic theorem, see (1.1) in Proposition 1.1, is that for an ergodic (w.r.t μ) map $f : X \rightarrow X$, the proportion of time any typical orbit spends in a set A is given by $\mu(A)/\mu(X)$. Suppose that $f : \mathbb{T}^2 \rightarrow \mathbb{T}^2$ is piecewise linear, with a partition $\{A_j\}_{j \in J}$ such that each matrix M_j , given by Df restricted to A_j , is constant. Then for a.e. $z \in \mathbb{T}^2$, out of the n matrices which multiply to give the cocycle Df_z^n , the proportion of these that are M_j will approach $\mu(A_j)$ in the limit $n \rightarrow \infty$. Note that this does not allow for a direct calculation of Lyapunov exponents,

$$\chi(z, v) = \lim_{n \rightarrow \infty} \frac{1}{n} \log \|Df_z^n v\|,$$

since matrix multiplication is generally non-commutative. We can, however, leverage this limiting behaviour to derive upper and lower bounds on $\chi(z, v)$ whenever we have an invariant cone \mathcal{C} . For an orbit $z_k = f^k(z)$, define the sequence (j_k) with elements in J by $j_k = j$ s.t. $z_k \in A_j$. For unit vectors $v_0 \in \mathcal{C}$ we can write

$$\begin{aligned} \|Df_z^n v_0\| &= \prod_{k=1}^n \frac{\|Df_{z_k}^k v_0\|}{\|Df_{z_k}^{k-1} v_0\|} \\ &= \prod_{k=1}^n \frac{\|M_{j_{k-1}} v_{k-1}\|}{\|v_{k-1}\|} \end{aligned}$$

where $v_k := Df_{z_k}^k v_0$. By cone invariance, the vectors v_k lie in \mathcal{C} so that we can bound each factor by

$$\frac{\|M_{j_{k-1}} v_{k-1}\|}{\|v_{k-1}\|} \geq \inf_{v \in \mathcal{C}} \frac{\|M_{j_{k-1}} v\|}{\|v\|} =: K_{j_{k-1}}. \quad (7.4)$$

Now since $\log(\cdot)$ is monotone increasing we have

$$\begin{aligned}\log \|Df_z^n v_0\| &\geq \log \left(\prod_{k=1}^n K_{j_{k-1}} \right) \\ &= \sum_{k=1}^n \log K_{j_{k-1}}\end{aligned}$$

so that

$$\chi(z, v) \geq \lim_{n \rightarrow \infty} \frac{1}{n} \sum_{k=1}^n \log K_{j_{k-1}}.$$

Out of the n terms in the above summation, the proportion of these with subscript j will approach $\mu(A_j)$ in the limit $n \rightarrow \infty$. Hence

$$\chi(z, v) \geq \sum_{j \in J} \mu(A_j) \log K_j. \quad (7.5)$$

for a.e. $z \in \mathbb{T}^2$. We remark that by Theorem 1.1, this bound holds for generic $v \neq 0$, not necessarily in \mathcal{C} , barring vectors parallel to the local stable manifold $\gamma_s(z)$.

Upper bounds of the form

$$\chi(z, v) \leq \sum_{j \in J} \mu(A_j) \log L_j \quad (7.6)$$

can be derived by the same argument, where $L_j = \sup_{v \in \mathcal{C}} \|M_j v\|/\|v\|$. The inequalities (7.5) and (7.6) give a variety of bounds for the Lyapunov exponent as K_j, L_j depend on the choice of invariant cone and norm. For the sharpest bounds one should always take the smallest invariant cone possible, but the choice of norm is less clear cut.

7.1.4 Analysis of $E = 3$ protocols

Consider protocols P of energy $E = 3$. Omitting protocols which are equivalent to others by periodicity, e.g. $(1, 2, 2, 1)$ and $(2, 1, 1, 2)$, there are 12 in total. They fall into the categories of completing one ‘stir’:

$$(1, 5) \quad (2, 4) \quad (3, 3) \quad (4, 2) \quad (5, 1)$$

two stirs:

$$(1, 1, 1, 3) \quad (1, 1, 2, 2) \quad (1, 1, 3, 1) \quad (1, 2, 1, 2) \quad (2, 1, 2, 1) \quad (1, 2, 2, 1)$$

or three stirs:

$$(1, 1, 1, 1, 1, 1)$$

within the $E = 3$ energy budget. All of these protocols P can be expressed in the form $P = (k_1, l_1, k_2, l_2)$. Protocols such as $(1, 1, 1, 3)$ are already in this form, others such as $(1, 5)$ can be doubled up to give $(1, 5, 1, 5)$ with the change in the energy normalising factor noted[†]. Writing each protocol in this consistent fashion will allow us to estimate Lyapunov exponents using a single algorithm and normalise as necessary for comparison at the end. Since by periodicity (k_1, l_1, k_2, l_2) is equivalent to (k_2, l_2, k_1, l_1) , we can always flip the order of the pairs so that $l_2 \geq l_1$ and, in the case $l_2 = l_1$, $k_2 \geq k_1$. Fix a protocol P and write $H_i = G^{l_i} \circ F^{k_i}$ so that $H_P = H_2 \circ H_1$. As in the proof of Theorem 7.1 the Jacobian DH_1 of H_1 is constant over each A_{j, k_1} and is given by M_{j, k_1, l_1} . These four matrices form an invariant cone $\mathcal{C}(k_1, l_1)$ which, for k_2, l_2 satisfying the inequalities above, also serves as an invariant cone for DH_2 as $\mathcal{C}(k_2, l_2) \subset \mathcal{C}(k_1, l_1)$. By extension, $\mathcal{C}(k_1, l_1)$ is an invariant cone for the entire protocol H_P . Its Jacobian takes one of $4^2 = 16$ values, with DH_P

[†]Similarly we contract $(1, 1, 1, 1, 1, 1)$ to $(1, 1, 1, 1)$ and note the energy change.

at z equal to $M_{j',k_2,l_2}M_{j,k_1,l_1}$ if $z \in A_{j,k_1}$ and $(G^{l_1} \circ F^{k_1})(z) \in A_{j',k_2}$.

To estimate Lyapunov exponents, we require the weights

$$\begin{aligned}
\mu(\{z \mid DHP = M_{j',k_2,l_2}M_{j,k_1,l_1}\}) &= \mu(A_{j,k_1} \cap (G^{l_1} \circ F^{k_1})^{-1}(A_{j',k_2})) \\
&= \mu(F^{k_1}(A_{j,k_1}) \cap G^{-l_1}(A_{j',k_2})) \\
&= \mu(R_j \cap G^{-l_1}(A_{j',k_2})) \\
&= \mu(G^{l_1}(R_j) \cap (A_{j',k_2})) \\
&= \mu((F^{k_2} \circ G^{l_1})(R_j) \cap R_{j'}),
\end{aligned} \tag{7.7}$$

where we have used the area preserving properties of shears F^{k_1} , G^{l_1} , F^{k_2} and the definitions $A_{j,k} = F^{-k}(R_j)$. This clarifies that $\mu(\{z \mid DHP = M_{j',k_2,l_2}M_{j,k_1,l_1}\})$ is independent of k_1, l_2 and can be calculated by studying the transitions between the rectangles R_j under $F^{k_2} \circ G^{l_1}$. Straightforward (yet lengthy) calculations yield a transition matrix

$$T = \begin{pmatrix} -\frac{(\eta-1)^4(-kl+2\eta-1)}{kl+\eta^2-2\eta+1} & \frac{\eta(\eta-1)^3(-kl+\eta-1)}{kl+\eta^2-2\eta+1} & \frac{\eta(\eta-1)^3(-kl+\eta)}{kl+\eta^2-\eta} & \frac{kl\eta^2(\eta-1)^2}{kl+\eta^2-\eta} \\ \frac{\eta(\eta-1)^3(-kl+\eta)}{kl+\eta^2-\eta} & \frac{kl\eta^2(\eta-1)^2}{kl+\eta^2-\eta} & \frac{kl\eta^2(\eta-1)^2}{kl+\eta^2} & -\frac{\eta^3(\eta-1)(kl+\eta)}{kl+\eta^2} \\ \frac{\eta(\eta-1)^3(-kl+\eta-1)}{kl+\eta^2-2\eta+1} & \frac{kl\eta^2(\eta-1)^2}{kl+\eta^2-2\eta+1} & \frac{kl\eta^2(\eta-1)^2}{kl+\eta^2-\eta} & -\frac{\eta^3(\eta-1)(kl+\eta-1)}{kl+\eta^2-\eta} \\ \frac{kl\eta^2(\eta-1)^2}{kl+\eta^2-\eta} & -\frac{\eta^3(\eta-1)(kl+\eta-1)}{kl+\eta^2-\eta} & -\frac{\eta^3(\eta-1)(kl+\eta)}{kl+\eta^2} & \frac{\eta^4(kl+2\eta-1)}{kl+\eta^2} \end{pmatrix}$$

where the quantity (7.7) is given by the entry $T_{j,j'}$ on j th row and j' th column. To ease viewing we have dropped the subscripts $k_2, l_1 \rightarrow k, l$.

Given a protocol map H_P , by (7.5), (7.6) its positive Lyapunov exponent χ_P satisfies

$$\sum_{j,j'=1}^4 T_{j,j'} \log K_{j,j'} \leq \chi_P \leq \sum_{j,j'=1}^4 T_{j,j'} \log L_{j,j'} \tag{7.8}$$

where $K_{j,j'}, L_{j,j'}$ denote the minimum, maximum expansion factors of the matrix $M_{j',k_2,l_2}M_{j,k_1,l_1}$ over the invariant cone $\mathcal{C}(k_1, l_1)$. It remains to specify a norm under which these expansion factors are calculated. Various $\|\cdot\|_p$ norms were tested; the $p = 1$ norm appeared to give the largest lower bounds and the $p = 2$ norm appeared to give the smallest upper bounds. Under the $p = 1$ norm, minimum expansion factors over $\mathcal{C}(k_1, l_1)$ are attained on one of the cone boundaries, i.e. either the unstable eigenvector of M_{2,k_1,l_1} or M_{3,k_1,l_1} . Maximum expansion factors are bounded above by the operator norm of each matrix M , which under the $p = 2$ norm is $\sqrt{\lambda}$ where λ is the largest eigenvalue of the symmetric matrix $M^T M$. The vector giving this maximal expansion often lies in the invariant cone so this upper bound (on $L_{j,j'}$) is optimal. Even if it didn't, $L_{j,j'}$ calculated in this fashion still provides the upper bound (7.8).

Figure 7.1 shows a comparison of Lyapunov exponents, normalised by energy, for 6 of the 12 protocols listed above. Similarly performing protocols are omitted for ease of viewing, e.g. (5, 1) and (1, 5). The analytical upper and lower bounds are shaded in the relevant colour. There is a notable disparity in the tightness of the bounds (7.8). Starting with the original protocol (1, 1), when η is very small the dynamics are dominated by repeated stretching by the matrix M_1 . This pulls tangent vectors very close to its unstable eigenvector and stretches them with expansion factor roughly equal to λ^+ , its larger eigenvalue. As a consequence, the $p = 2$ norm upper bound provides an excellent approximation as $L_{1,1}$ is precisely λ^+ (the matrix M_1 is symmetric). The $p = 1$ norm lower bound fares worse, calculating expansion at the boundaries of the very wide cone \mathcal{C} , where vectors are rarely aligned. The (1, 1, 1, 3) protocol is similar, hindered by the same wide cone \mathcal{C} . The $p = 1$ lower bound more closely mirrors the numerically evaluated $\hat{\chi}$ as the cones

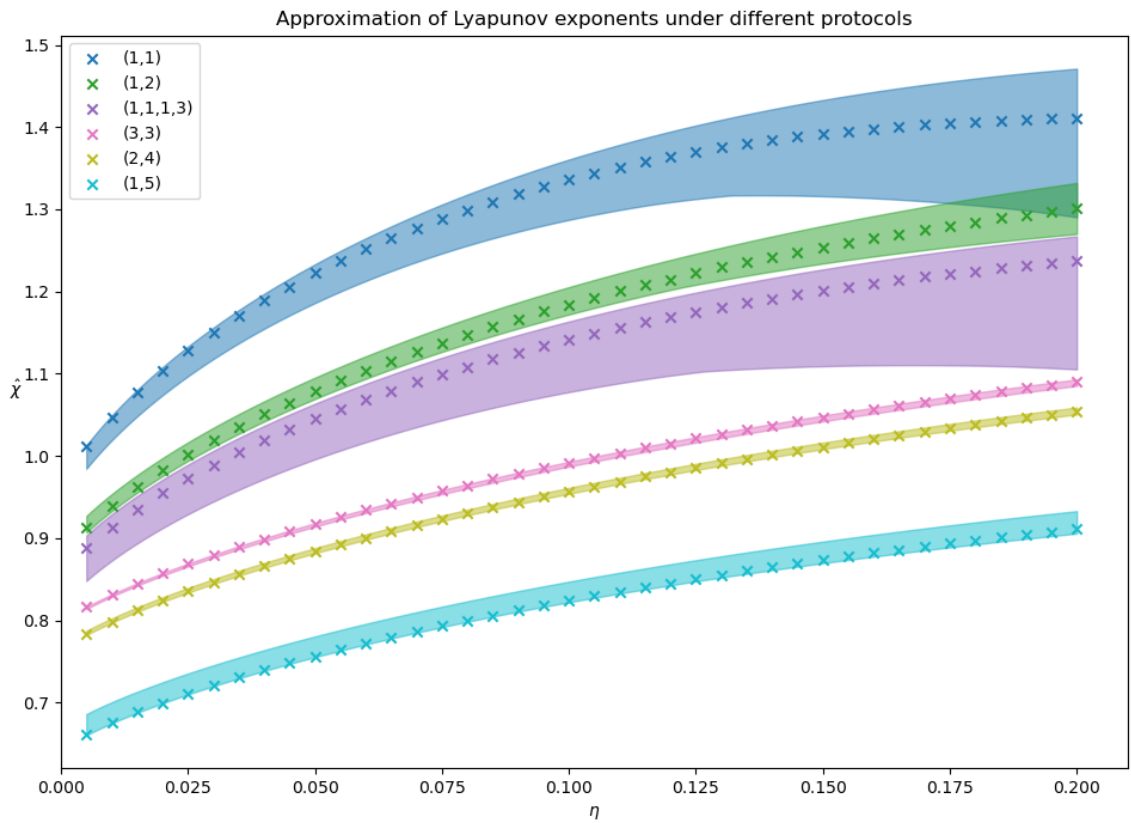


Figure 7.1: Comparison of normalised Lyapunov exponents $\hat{\chi}$ for a selection of $E = 3$ protocols over the ergodic parameter space $0 < \eta < 1/5$. Crosses show numerically estimated $\hat{\chi}$, shaded region shows analytical upper and lower bounds. Order of protocols in the legend matches that of the plot.

become narrower, see e.g. (1, 5).

Comparing the relative performance of each protocol, we see that the protocols which completed more stirs within the energy budget achieved larger values of $\hat{\chi}$, and this behaviour is consistent across the entire parameter range. We also note, however, a clear performance gap between protocols such as (3, 3) and (1, 5) which both complete one stir but have allocated their energy budget to each shear in a balanced and less balanced way respectively. The same is true comparing (1, 2, 1, 2) and (1, 1, 1, 3). This suggests the following ranking system:

- (A) Sort protocols P into groups \mathcal{P}_p by number of stirs completed p - more is better.
- (B) Within each group, sort the $P \in \mathcal{P}_p$ by variance - lower is better.

Here we define the variance of each tuple $P = (k_1, \dots, l_p)$ is in the standard way,

$$\text{Var}(P) = \frac{1}{2p} \sum_{i=1}^p \left(k_i - \frac{E}{p} \right)^2 + \left(l_i - \frac{E}{p} \right)^2,$$

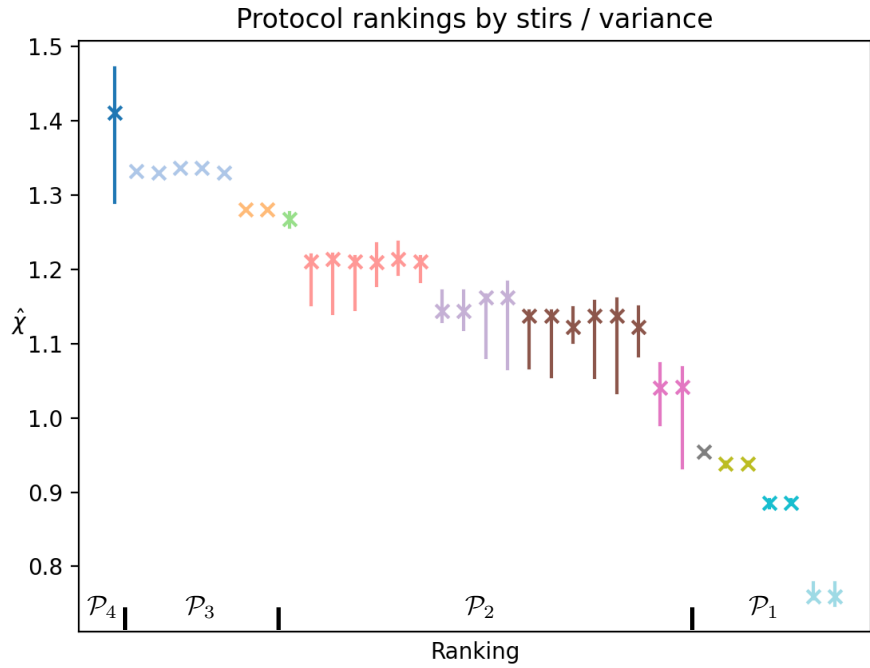
noting that the mean strength of each shear in a protocol of energy E is E/p . Ordering the $E = 3$ protocols of Figure 7.1 based on (A), the *primary ranking*, then (B), the *secondary ranking*, gives a predicted ranking in agreement with the numerically evaluated $\hat{\chi}$ and the analytical bounds. We now turn to $E = 4$ protocols to test this ranking algorithm across a broader range of protocols.

7.1.5 Analysis of $E = 4$ protocols

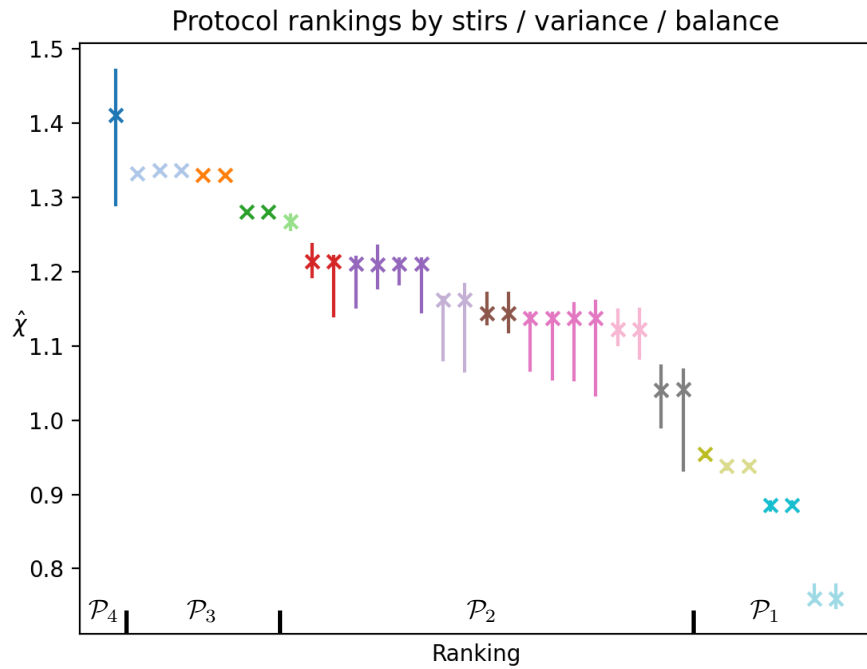
Combinatorial calculations, similar to those employed for the $E = 3$ setting, are employed to show that there are 34 protocols of energy $E = 4$, unique in the sense that they cannot be rearranged by periodicity to give one another. For ease of comparison over this larger set of protocols, we restrict to a single parameter value $\eta = 1/5$. Other parameter values were tested and, similar to the $E = 3$ study, gave the same rankings under changes in η . Since $\eta = 1/5$ lies in the proven ergodic parameter space, we can still derive analytical upper and lower bounds for the majority of protocols. The exceptions to this being the protocols which complete three stirs over each periodic cycle, e.g. (1, 2, 1, 1, 2, 1), which cannot be expressed as a 4-tuple (k_1, l_1, k_2, l_2) . Extending our analytical work to these protocols would necessitate a larger $4 \times 4 \times 4$ transition array T , each element of which would be far more complicated to calculate. Protocols which complete two stirs are already in the necessary form, protocols which complete one can be doubled up, and finally the single protocol which completes four stirs (1, 1, 1, 1, 1, 1, 1, 1) can be compressed to (1, 1, 1, 1).

Figure 7.2(a) plots the performance of each of the 34 protocols, organised by (A) into groups \mathcal{P}_p then further subdivided by the secondary ranking (B). The same colour is used when two protocols have the same predicted ranking, the order within each colour grouping is random. Error bars show the analytical bounds when they can be calculated, again using the $\|\cdot\|_1$ and $\|\cdot\|_2$ norms. Our first observation is that maximising the number of stirs within an energy budget still appears to maximise the normalised Lyapunov exponent. Numerically evaluated $\hat{\chi}$ for the (1, 1) protocol (dark blue) is clearly larger than that of any other protocol considered. We remark, though, that this is purely an observation. To *prove* this, analytical bounds for the (1, 1) protocol would need to be improved and bounds for the 7 protocols which complete three stirs in the energy budget would need to be derived. We see similar sharp jumps in $\hat{\chi}$ moving between \mathcal{P}_2 and \mathcal{P}_1 but a less stark change moving between \mathcal{P}_3 and \mathcal{P}_2 , the (2, 2, 2, 2) protocol performing almost as well as (3, 1, 1, 1, 1, 1).

We now study the capability of our ranking method to categorise each protocol from the tuple data alone. Performance is overall good, the consistent negative trend over the rankings of Figure 7.2(a) showing that no protocol has been incorrectly categorised. The method entirely predicts



(a)



(b)

Figure 7.2: Part (a) shows ranking of all $E = 4$ protocols into groups \mathcal{P}_p by (A), then further ranked by variance (B). Same colour signifies equivalent ranking, error bars show analytical bounds where available. Part (b) considers a tertiary ranking (C).

the variation over protocols in \mathcal{P}_1 , identifying the symmetric protocol $(4, 4)$ as optimum and $\hat{\chi}$ decreasing over the pairs $(4 \pm n, 4 \mp n)$, $n = 1, 2, 3$. Protocols in \mathcal{P}_3 are similarly correctly split into the two obvious groupings, the two which contain a strength 3 shear and the five which do not. The suggested groupings for the \mathcal{P}_2 protocols are reasonable with the best and worst protocols clearly identified. The performance is somewhat weaker over the mid-ranking protocols (purple and brown) with notable variation within each grouping. For the purple grouping we observe that protocols $(3, 3, 1, 1)$ and $(3, 1, 1, 3)$ outperform $(3, 1, 3, 1)$ and $(1, 3, 1, 3)$. The obvious distinction between these pairs is the balance between horizontal and vertical shears, the former protocols evenly sharing its shears between the two orthogonal directions. The latter protocols significantly bias a certain direction and $\hat{\chi}$ suffers as a result, almost to the level of the brown protocols of greater variance. This suggests a *tertiary ranking*:

(C) Sort by $|\sum k_i - l_i|$ - lower is better,

which rewards protocols which maximise ‘balance’ between the orthogonal directions. Figure 7.2(b) shows all $E = 4$ protocols, grouped by (A), (B), and then (C). Including this tertiary ranking appears to capture well the sub-grouping variation observed previously and even suggests subdivisions, e.g. in \mathcal{P}_3 , that were not obvious at first glance but hold true upon closer inspection of the numerically estimated $\hat{\chi}$. While further rankings levels may provide an even finer classification, with expected limit being that of pairs (and self pairs) of the form $(k_1, l_1, \dots, k_p, l_p) \leftrightarrow (l_1, k_1, \dots, l_p, k_p)$, the three level method considered here strikes a good balance between ease of computation and quality of the final ranking.

7.1.6 Remarks

Our analysis above aligns with the findings of D’Alessandro et al. (1999), but in the non-monotonic (uniformly hyperbolic) setting. To maximise chaotic mixing over a given energy budget, the best approach is to alternate between orthogonal shears of similar strength, weak enough to maximise the number of stirs completed. Naturally this cannot be taken to an extreme. Taking very weak shears may produce island structures, detrimental to overall mixing quality, however strong stretching rates may be in the chaotic sea. In the above we mitigated this possibility by specifying a minimum shear strength, allowing us to establish mixing properties using the results of section 4.3. To use these results we have also restricted ourselves to a fairly limited parameter space. An interesting extension to the study would be to take F and G as the symmetric shears of the OTM. Here the original protocol F, G, F, G, \dots is presumably not the optimal choice. While the shears are (just) strong enough to achieve global mixing, the weak stretching near the ghost boundaries gives a reduced $\hat{\chi}$ and polynomial tail on mixing rates (Theorem 6.4). A better choice may be to alternate between F^2 and G^2 , see Cheng et al. (2021)[‡] for a numerical study of mixing rates in such systems.

Aperiodic mixing protocols may provide a means to utilise many weak shears and avoid islands, destroying the symmetries of the flows intrinsically linked to their structure (Franjione et al., 1989; Franjione and Ottino, 1992). Such *random* protocols show potential as efficient mixers (Liu et al., 1994) but equally may give rise to poor mixing and be difficult to implement in an industrial context (Franjione and Ottino, 1992). Fixing η in the mixing window of $H_{(\eta, \eta)}$ and some $0 < p < 1$, we remark that shearing horizontally (applying F) with probability p and shearing vertically with probability $1 - p$ generates an aperiodic mixing protocol with straightforward to prove mixing statistics. Indeed, with p bounded away from 0 and 1 we may split the protocol into blocks of the form $G^l \circ F^k$ and employ a similar argument to section 7.1.2.

[‡]Unpublished at the time of writing.

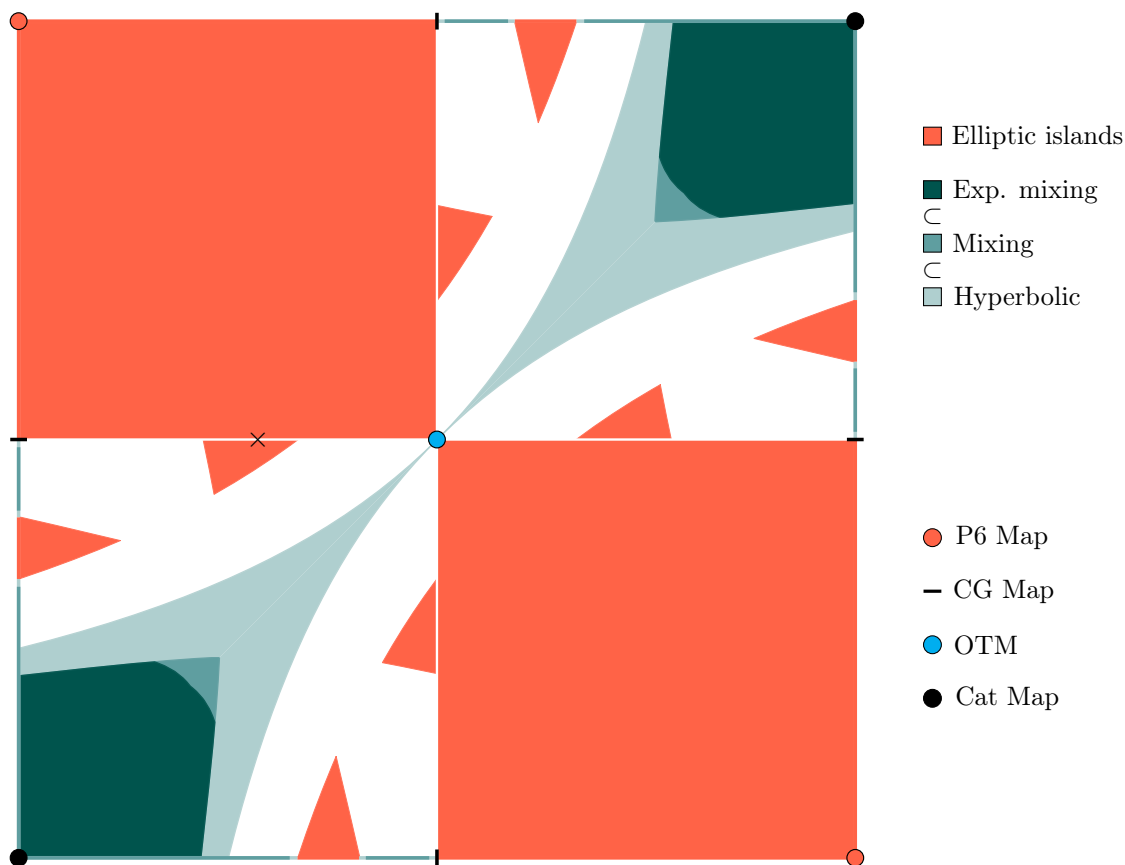


Figure 7.3: Plot of proven mixing behaviour over the full $0 \leq \xi, \eta \leq 1$ parameter space for $H_{(\xi, \eta)}$, i.e. including the limiting maps H_η and its symmetries. Notable maps are highlighted, alongside an atypical example marked with \times .

7.2 Summary & outlook

We conclude this chapter with a summary of our findings and some natural avenues for further analysis. We begin with the effect of non-monotonicity in the piecewise linear systems analysed. The spread of gradients inherent to non-monotonic shears necessarily realigns tangent vectors and, by extension, curves defining the interface between two mixing fluids. This can be detrimental to mixing, allowing stretching under one stir to be subsequently undone, opening up the potential for persistent regions of non-stretching behaviour. We made this idea precise in Proposition 3.1, showing that ellipticity over a periodic orbit precludes global mixing. Sometimes, however, vector realignment is strong enough to map relevant vectors v close to their antipodes $-v$. By linearity, stretching can then continue as normal. Cerbelli and Giona’s map can be thought of as the most extreme example of this, where passing through the non-hyperbolic upper plane gives an exact sign change $v \rightarrow -v$. We showed, see Chapters 3 and 4, that such precise realignment is not necessary, existence of an invariant cone suffices to establish global stretching behaviour (Proposition 3.4). This orientation reversing behaviour did complicate establishing mixing results, however. The ‘doubling back’ effect in the images of local manifolds forced us to discard portions of the image and focus on the growth of a single line segment, leading to suboptimal mixing windows.

Recalling our research questions at the end of section 2.2, we are ready to answer **(Q1)**. The mixing property can indeed persist under certain perturbations to the CG Map, see Theorems 4.1 and 4.2, despite loss of the pseudo-Anosov property. The same is not true for all perturbations, though, with the CG map sitting at the very edge of the hyperbolicity window for H_η . Taking

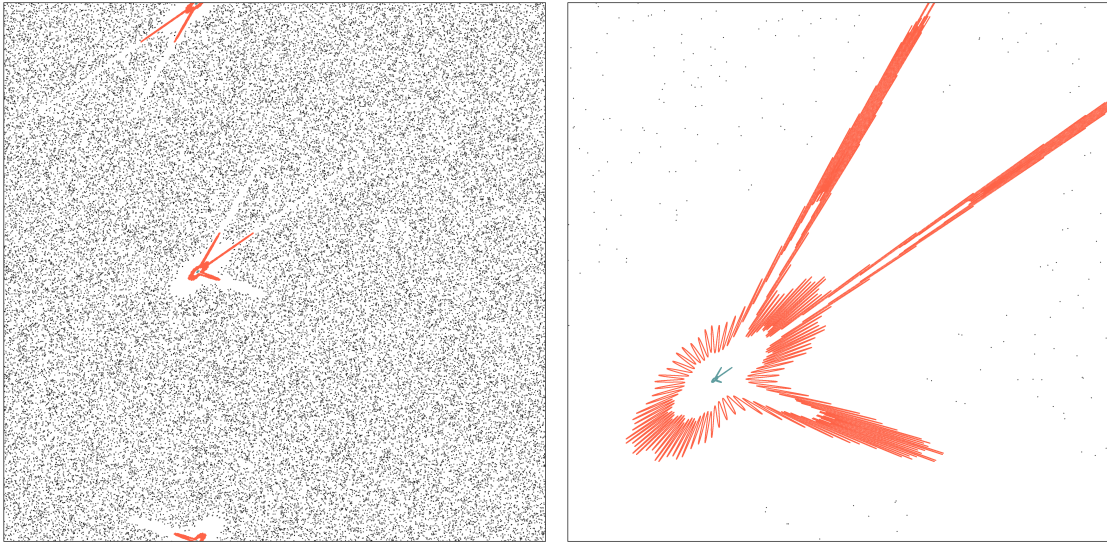


Figure 7.4: Three trajectories, one chaotic (black) and two elliptic (red, blue) for the map $H_{(\xi,\eta)}$ at $\xi = 0.286$, $\eta = 1/2$. Zoomed image shows a closeup on the ‘island’ centred at a period two point on the singularity set.

any $\eta > 1/2$ births island structures around a period two orbit[§] which grow to envelop the entire domain as $\eta \rightarrow 1$. This limiting map, essentially a counter-rotating Cat Map defined by the single matrix

$$M = \begin{pmatrix} 1 & 0 \\ 1 & 1 \end{pmatrix} \begin{pmatrix} 1 & -1 \\ 0 & 1 \end{pmatrix} = \begin{pmatrix} 1 & -1 \\ 1 & 0 \end{pmatrix},$$

is entirely periodic with period 6.

Including a second non-monotonic shear parameterised by $\xi > 0$ gives a further way of perturbing the CG Map. Numerical results (see Figure 4.17) suggest that mixing behaviour persists under small such perturbations (small ξ with $\eta < 1/2$). Too large a perturbation, however, may give the right conditions for islands to form, hitting e.g. the parameter sets \mathcal{I}_2 and \mathcal{I}_3 of Proposition 4.9, also sketched in Figure 7.3. Keeping $\eta = 1/2$ fixed and varying ξ (exploring the parameter space between the CG Map and the OTM) may similarly produce island structures, but whose internal dynamics differ substantially from the situation examined in Proposition 3.1. Here, the period 2 orbit which seeds the pair of islands,

$$z_1 = \left(\frac{1-\xi}{2}, \frac{1}{2} \right) \leftrightarrow z_2 = \left(\frac{1-\xi}{2}, 0 \right),$$

lies on the singularity set \mathcal{D} marking the boundary between the partition elements A_1 and A_3 . Consequently, there no longer exists a neighbourhood about each point obeying the same itinerary (the cocycle is not even well defined on the periodic orbit). Orbits within these islands, if they form, no longer trace out concentric ellipses. Figure 7.4 plots such an example at $\xi = 0.286$, marked with a \times on Figure 7.3. Three orbits are plotted, two elliptic in nature and one hyperbolic, the latter filling in the chaotic sea enclosing the island pair. The red and blue orbits trace out pairs of similar closed curves about the z_i , the radial distance to these points governed by the orbit’s cocycle, a binary sequence between the matrices M_1 and M_3 . Numerically observed to be aperiodic, why this cocycle gives rise to such wildly oscillatory behaviour requires a more detailed analysis, beyond the scope of this thesis.

Moving onto more typical behaviour (that exists beyond atypical parameter sets of negligible measure) we address **(Q2)**. Global mixing can indeed be achieved by composing orthogonal non-

[§]In particular the same orbit given in the proof of Proposition 4.9, taking $\xi = 0$.

monotonic shears, proven in a wide neighbourhood of the Cat Map (Theorem 4.3, sketched in Figure 7.3) and observed numerically beyond (Figure 4.17). For certain parameters (ξ, η) however, formation of elliptic islands precludes ergodicity. Indeed this situation occurs at *most* parameters, the set \mathcal{I}_1 (see Proposition 4.9) and its reflections alone covering half the parameter space $0 < \xi, \eta < 1$. Considering the wider parameter space $0 \leq \xi, \eta \leq 1$, we observe unique dynamics for H whenever its Jacobians are integer valued. From the uniformly hyperbolic Cat Map to the entirely periodic ‘P6 Map’ and the pseudo-Anosov CG Map half way in between, a rich variety of dynamics is possible from such a simply defined family of maps. A new example to add to this list is the OTM whose ghost boundaries permit only non-uniform hyperbolicity and necessitate a far more involved approach to proving mixing statistics. We arrive at an interesting, perhaps unexpected conclusion to **(Q3)**. Despite not imposing physical boundaries, a polynomial mixing rate may still emerge, in contrast to the exponential mixing rate proven elsewhere and observed across the hyperbolic parameter space (see Figure 7.3) of which the OTM lies at the cusp.

Whether the boundaries are imposed or arise as periodic structures, the reduced rate of mixing in LTM and the OTM follow from the same fundamental dynamical feature: *parabolic*[¶] invariant sets near which hyperbolic orbits are trapped for arbitrarily long periods. For ergodicity to hold, these sets necessarily have measure 0. In the piecewise linear setting we have considered, they are line segments of positive length. For general nonlinear maps, a single parabolic point can influence its neighbourhood and slow the mixing to a polynomial rate, the Katok Map (Katok, 1979) being a canonical example.

Another example, with a more straightforward definition and clearer relevance to laminar mixing applications, comes from taking horizontal and vertical twists $f(y) = 4y(1 - y)$ and $g = f$. A sketch was given earlier in Table 3.1. Composing two parabolic shape shears, modelling the Poiseuille flow profile of Figure 1.1(a), we refer to this map as the *parabolic shears map* (PSM) and denote it by H . It can be thought of as a smoothed version of the OTM, much closer to the eggbeater type systems considered in section 2.1. While the peak of the shear is smoothed: $f'(1/2) = 0$, each shear still possesses singularities over the no-slip boundaries. As such H fits the definition of a ‘smooth map with singularities’ in the sense of section 1.5. The fixed points of H match those of the OTM, namely $(0, 0)$, $(0, 1/2)$, $(1/2, 0)$, and $p = (1/2, 1/2)$. The behaviour of H near p is crucial to its mixing dynamics. A simple calculation yields $DH_p = \text{Id}$ so H has a parabolic fixed point at the centre of the domain.

The substantial influence of p on its surroundings is illustrated in Figure 7.5, comparing the effect of the OTM and PSM on two initially segregated regions. In (b), while certain regions exhibit stronger stretching behaviour, the shear gradients are twice as strong as one approaches the singularity lines and ghost boundaries are absent, the slow stretching behaviour near p adversely affects the overall mixing quality. Although no neighbourhood around p appears to form an invariant set, any finite time measure of mixing captures a sort of *transient* or *parabolic island*. The plots of finite time Lyapunov exponents in Figure 7.6 provide a clearer picture of its evolving boundary, demarcating a shrinking region of poor stretching (near zero χ_n) against a convergent backdrop. Its measure appears to decay to zero, the expected limit being the local manifold terminating on p . We can estimate this decay numerically, fixing some low threshold $c = 1/10$ and approximating $\mu(\{z | \chi_n(z) < c\})$ for increasing n . Figure 7.7 plots this approximation, the roughly linear decay under log-log scaling suggesting a polynomial law for the shrinking island.

It also provides a rough approximation for the distribution of escape times away from p . If such escapes are followed by strong stretching (as the numerics suggest) then we arrive at a similar situation to the OTM, where return times to some region of ‘good hyperbolicity’ can be inferred from escape times and a similar distribution holds. By the work of Young (1999), polynomial decay

[¶]Equivalently ‘neutral’ in the language of section 2.2. For our purposes characterised by a Jacobian with trace equal to 2.

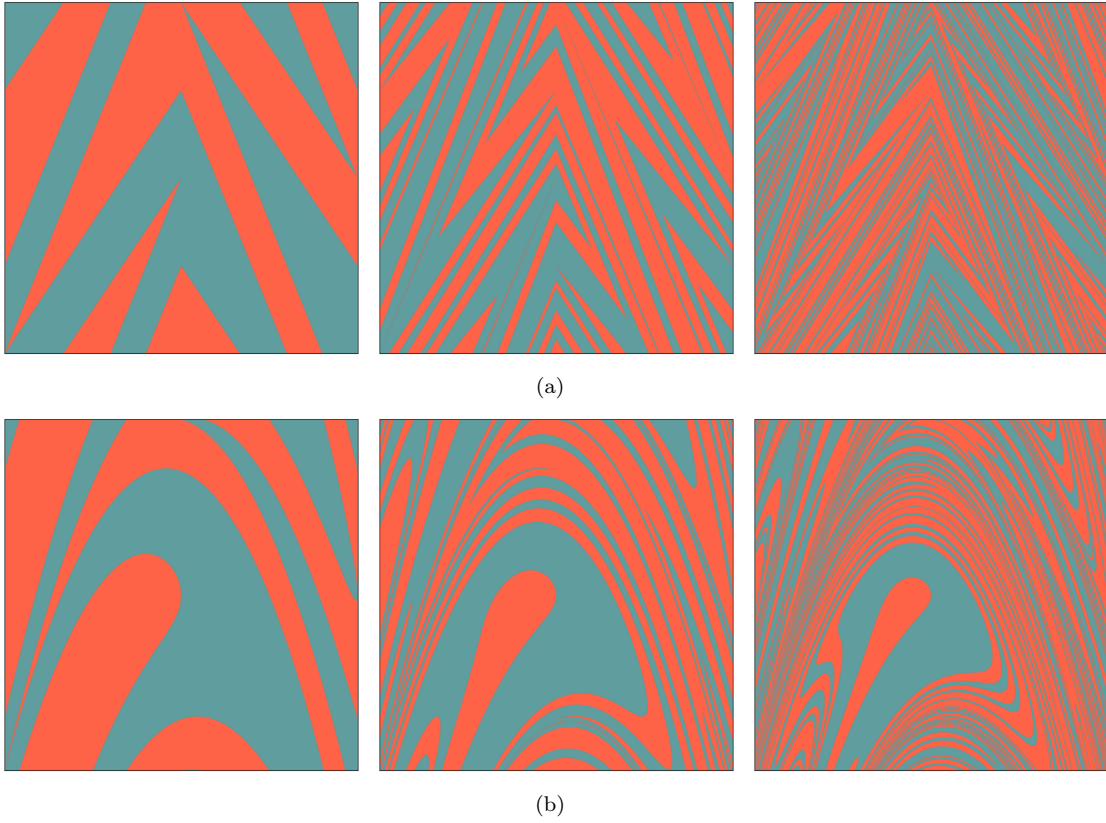


Figure 7.5: Comparison of mixing dynamics between (a) the OTM and (b) the PSM on two initially segregated regions coloured red and blue.

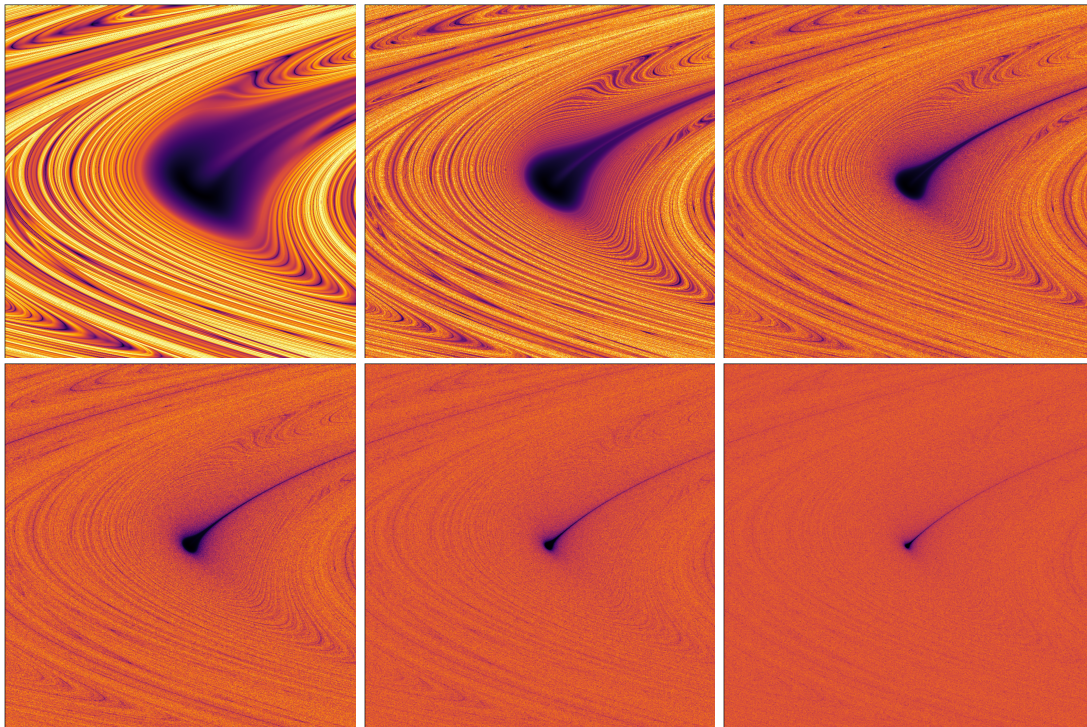


Figure 7.6: Convergence of FTLEs $\chi_n(z)$ for the PSM, iterates shown: $n = 2^2, \dots, 2^7$. Lighter colour corresponds to higher values of $\chi_n(z)$.

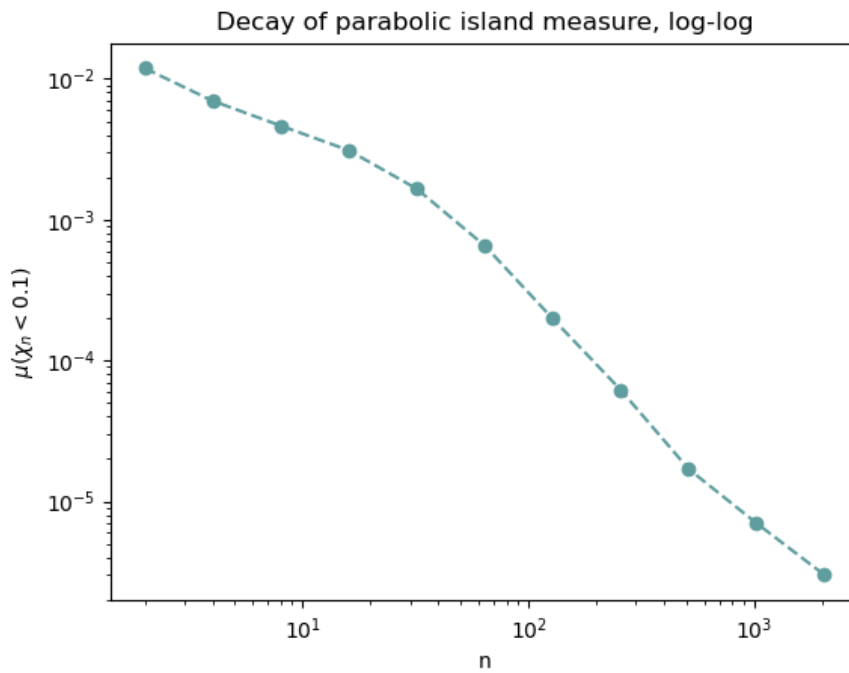


Figure 7.7: Shrinking of the region exhibiting low FTLEs. Noting the log-log scaling, the decay appears polynomial in nature.

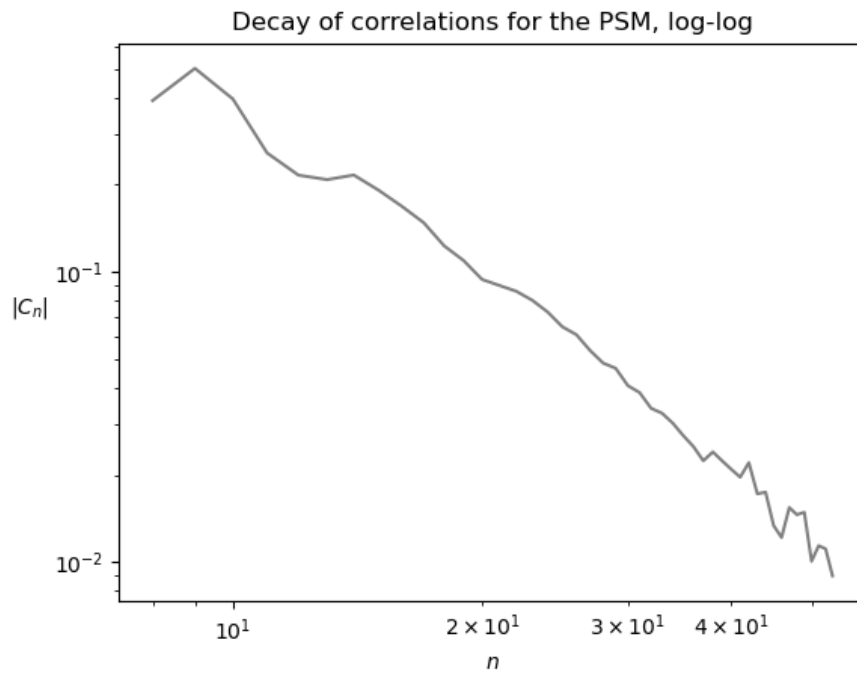


Figure 7.8: Tail end of the (estimated) autocorrelations $|C_n|$ for the PSM, same observable as Figure 5.14. Log-log scaling suggests a polynomial law.

of correlations would presumably follow. Figure 7.8 supports this hypothesis, showing estimated decay of the autocorrelation function $|C_n|$ for the observable $\varphi(x, y) = 5 \sin(4\pi x) - 7 \sin(6\pi y)$. Proving such statements about the PSM (or even plain hyperbolicity) is certainly more challenging than the piecewise linear examples we have considered. The smooth non-monotonic nature of the dynamics near the point p necessarily dilate cone fields and its non-linear nature aggravates analysis of escape and return times.

We conclude with the observation that in every ASM we have considered, ergodicity and hyperbolicity appear to go hand in hand. While our proven mixing windows do not extend right across those of hyperbolicity, this is an artefact of our method (see the discussion of section 4.4) and does not signify absence of the property. A natural question is whether it is possible to construct an ASM with non-vanishing Lyapunov exponents a.e. but whose ergodic partition cannot be reduced to a full measure component. Else, is hyperbolicity of an aperiodic point incompatible with confinement to an invariant set of positive, non-full measure? Other types of hyperbolic systems admit such counterexamples, see e.g. the billiards example given in Wojtkowski (1986). Does the restricted structure of ASMs, specifically continuous ASMs, permit such counterexamples?

Appendices

Appendix A

Bounds from the proof of Lemma 4.6

A.1 Establishing the lower bound $\mathcal{B}_1(\varepsilon)$

Following the argument presented in Myers Hill et al. (2022b), in this section we derive a lower bound

$$\frac{\ell_h(\Gamma^4)}{\ell_h(\Gamma^4) + \ell_h(\Gamma^5)} > \mathcal{B}_1(\varepsilon)$$

on the proportions of a piecewise linear curve Γ_{p-1} , constrained by the invariant cone, in the regions A_4 and A_5 . We do this by maximising $\ell_h(\Gamma^5)$ and minimising $\ell_h(\Gamma^4)$, i.e we assume that Γ_{p-1} takes the longest possible path (in diameter) across A_5 , and the shortest possible path across A_4 . These are straight line segments, each aligned with one of the cone boundaries. Write the gradient of segments across A_4 and A_5 as k_4 and k_5 respectively. We now have to choose where on the L_1 (boundary between A_4 and A_5) Γ_{p-1} intersects so that the proportion in A_4 is minimal. The lines where each segment terminates are shown in Figure A.1(a). Note that L_2 is the line $y = k_2x$, and L_3 is the line $y = x - (\frac{1}{2} - \varepsilon)$. The diameter of the A_4 segment passing through $(x_1, y_1) \in L_1$ is given by

$$\ell_h(\Gamma^4) = x_1 - \frac{y_1 - k_4x_1}{k_2 - k_4} \quad (\text{A.1})$$

and the diameter of the A_5 segment passing through $(x_1, y_1) \in L_1$ is given by

$$\ell_h(\Gamma^5) = \frac{y_1 + (\frac{1}{2} - \varepsilon) - k_5x_1}{1 - k_5} - x_1, \quad (\text{A.2})$$

valid for $(x_1, y_1) \in L_1$ above a certain threshold. This is the point Q_3 , defined as the intersection of L_1 with the line $y = k_5(x - \frac{1}{2} + \varepsilon)$, the lowest point on L_1 such that the segment in A_5 still intersects $L_3 \cap A$. We claim that Q_3 is the point where the proportion (4.10) is minimal. To see this, note that as we move along L_1 from Q_2 to Q_3 , both diameters grow linearly. Parameterise the path as $Q_2(1 - z) + Q_3z$ for $z \in [0, 1]$. Now, at each ε , $\ell_h(\Gamma^4)(z)$ grows like $m_4z + c_4$ for some $m_4 > 0$, and $c_4 > 0$ the diameter of the segment in A_4 passing through Q_2 . Next, $\ell_h(\Gamma^5)(z)$ grows like m_5z for some $m_5 > 0$ since it grows from 0. Now

$$\begin{aligned} \frac{\ell_h(\Gamma^4)}{\ell_h(\Gamma^4) + \ell_h(\Gamma^5)}(z) &= 1 - \frac{\ell_h(\Gamma^5)}{\ell_h(\Gamma^4) + \ell_h(\Gamma^5)}(z) \\ &= 1 - \frac{m_5z}{m_4z + c_4 + m_5z} \\ &= 1 - \frac{1}{\frac{c_4}{m_5z} + \frac{m_4}{m_5} + 1} \end{aligned}$$

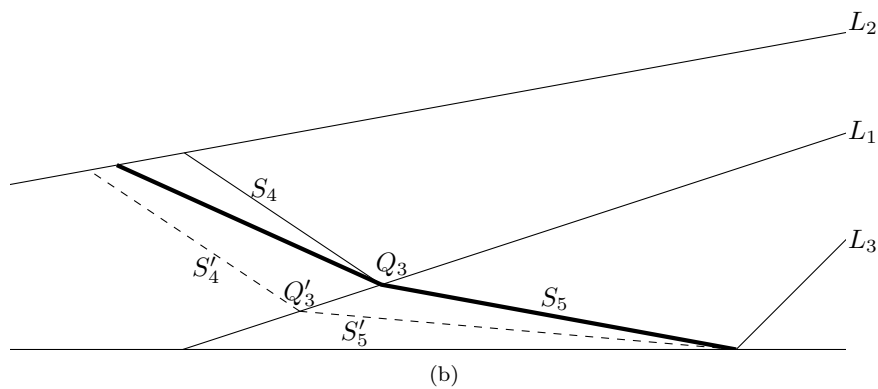
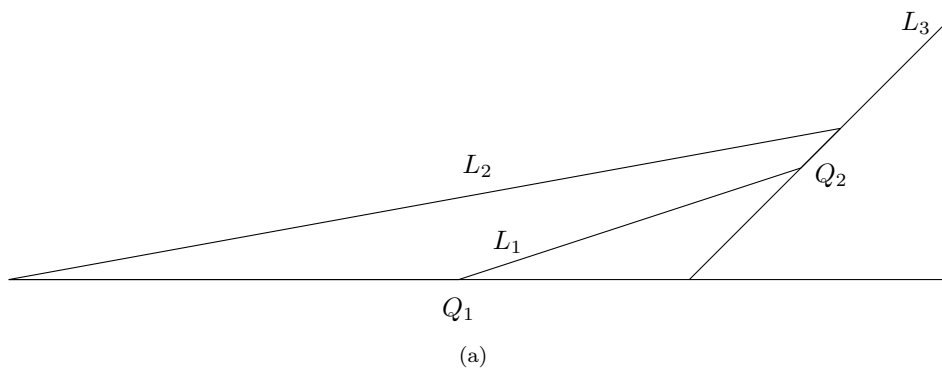


Figure A.1: A close-up on the lower portion of A_2 , $\varepsilon = 0.05$. Part (a) shows the lines which bound the regions A_4 and A_5 . Part (b) shows the curve (thickest line) across A_2 which minimises (4.10), crossing L_1 at Q_3 . Also shown is the segments S_4 which provides a lower bound for its diameter in A_4 . Segments S'_4 and S'_5 are defined to give further bound on (4.10) with minimal ε dependence.

which is minimal at $z = 1$, so (4.10) is minimal at Q_3 . We will now derive a lower bound on (4.10) which has weaker ε dependence.

Figure A.1(b) shows the path through Q_3 in bold. Its gradient in A_5 is given by $k_5(\varepsilon)$, aligned with the unstable eigenvector of \mathfrak{M}_2 . Its gradient in A_4 is given by $k_4(\varepsilon)$, aligned with the unstable eigenvector of \mathfrak{M}_3 . Writing the segment in A_5 as S_5 , note that

$$\frac{\ell_h(\Gamma^4)}{\ell_h(\Gamma^4) + \ell_h(\Gamma^5)} \geq \frac{\ell_h(S_4)}{\ell_h(S_4) + \ell_h(S_5)}$$

where S_4 is the segment in A_4 connecting Q_3 with L_2 , with gradient aligned with the steepest possible $k_4(\varepsilon)$ over the parameter range, $k_4^- = \inf_\varepsilon k_4(\varepsilon) \approx -0.6688^*$. We have equality at $\varepsilon = \varepsilon_2$.

Now define S'_5 as we did S_5 , but aligned with the least steep gradient in the parameter range, $k_5^+ = \sup_\varepsilon k_5(\varepsilon) = k_5(\varepsilon_0) \approx -0.08750$. Write its point of intersection with L_1 as Q'_3 . Note that $Q_3 = Q'_3$ when $\varepsilon = \varepsilon_0$. Define S'_4 as having the same gradient as S_4 , but passing through Q'_3 .

We claim that

$$\frac{\ell_h(S_4)}{\ell_h(S_4) + \ell_h(S_5)} \geq \frac{\ell_h(S'_4)}{\ell_h(S'_4) + \ell_h(S'_5)} \quad (\text{A.3})$$

with equality at $\varepsilon = \varepsilon_0$. Barring this case, note that the inequality is not immediate as both $\ell_h(S'_4) > \ell_h(S_4)$ and $\ell_h(S'_5) > \ell_h(S_5)$. Assume the non-trivial case $\varepsilon > \varepsilon_0$ and rewrite (A.3) as

$$\frac{1}{1 + \frac{\ell_h(S_5)}{\ell_h(S_4)}} > \frac{1}{1 + \frac{\ell_h(S'_5)}{\ell_h(S'_4)}},$$

which is equivalent to

$$\frac{\ell_h(S_5)}{\ell_h(S_4)} < \frac{\ell_h(S'_5)}{\ell_h(S'_4)}. \quad (\text{A.4})$$

Define the diameter differences $\Delta_i = \ell_h(S'_i) - \ell_h(S_i)$ and write Q_3 as (x_1, y_1) , Q'_3 as (x'_1, y'_1) , and Q_1 as $(x_0, 0)$. Then $\Delta_5 = x_1 - x'_1$. We can solve the line intersection equations to show that

$$\begin{aligned} \ell_h(S_4) &= x_1 - \frac{y_1 - k_4^- x_1}{k_2 - k_4} \\ &= \frac{k_2 x_1 - y_1}{k_2 - k_4^-} \end{aligned} \quad (\text{A.5})$$

so that

$$\begin{aligned} \Delta_4 &= x_1 - \frac{k_2 x'_1 - y'_1 - k_2 x_1 + y_1}{k_2 - k_4^-} \\ &= \frac{k_2(x'_1 - x_1) + k_1(x_1 - x'_1)}{k_2 - k_4^-} \\ &= \frac{k_1 - k_2}{k_2 - k_4^-} \Delta_5. \end{aligned} \quad (\text{A.6})$$

We can rewrite (A.4) as

$$\frac{\ell_h(S'_5) - \Delta_5}{\ell_h(S'_4) - \Delta_4} < \frac{\ell_h(S'_5)}{\ell_h(S'_4)},$$

which rearranges to

$$\frac{\Delta_4}{\Delta_5} < \frac{\ell_h(S'_4)}{\ell_h(S'_5)}.$$

*The minus sign in k_4^- refers to it being the clockwise bound on the invariant cone

By (A.6), (A.5), and $y'_1 = k_1(x'_1 - x_0)$ this is

$$\frac{k_1 - k_2}{k_2 - k_4^-} < \frac{\frac{k_2 x'_1 - k_1(x'_1 - x_0)}{k_2 - k_4^-}}{\frac{1}{2} - \varepsilon - x'_1},$$

which can be simplified to $(k_1 - k_2) \left(\frac{1}{2} - \varepsilon\right) < k_1 x_0$. So (A.4) holds, provided that

$$\frac{12\varepsilon^2 + 16\varepsilon + 1}{(2\varepsilon + 1)(2\varepsilon + 5)} - \frac{4\varepsilon}{2\varepsilon + 1} < \frac{12\varepsilon^2 + 16\varepsilon + 1}{(2\varepsilon + 1)(2\varepsilon + 5)} \cdot \frac{-4\varepsilon^3 - 2\varepsilon^2 + \varepsilon + \frac{1}{2}}{12\varepsilon^2 + 16\varepsilon + 1},$$

which reduces to $1 - 4\varepsilon + 4\varepsilon^2 < (1 + 2\varepsilon)^2$, valid for all $\varepsilon > 0$. This verifies the claim, giving us a lower bound

$$\frac{\ell_h(\Gamma^4)}{\ell_h(\Gamma^4) + \ell_h(\Gamma^5)} \geq \frac{\ell_h(S'_4)}{\ell_h(S'_4) + \ell_h(S'_5)} = \frac{k_2 x'_1 - y'_1}{\left(\frac{1}{2} - \varepsilon\right)(k_2 - k_4^-) - y'_1 + k_4^- x'_1}.$$

Noting that y'_1 is very small and positive[†], removing it from the denominator gives a new bound

$$\frac{\ell_h(\Gamma^4)}{\ell_h(\Gamma^4) + \ell_h(\Gamma^5)} > \frac{k_2 x'_1 - y'_1}{\left(\frac{1}{2} - \varepsilon\right)(k_2 - k_4^-) + k_4^- x'_1} := \mathcal{B}_1(\varepsilon)$$

which has fewer terms to consider and is still a sufficiently strong bound for our purposes.

A.2 Expanding the expression for $\mathcal{B}_1(\varepsilon)$

We will now show the expanded form of $\mathcal{B}_1(\varepsilon)$,

$$\frac{k_2 x'_1 - y'_1}{\left(\frac{1}{2} - \varepsilon\right)(k_2 - k_4^-) + k_4^- x'_1} = \frac{(2\varepsilon + 1)(2\varepsilon + 1 - 2k_5^+)}{(2\varepsilon + 1)(-k_4^-(2\varepsilon + 3) - k_5^+(2\varepsilon + 5)) + 12\varepsilon^2 + 16\varepsilon + 1}. \quad (\text{A.7})$$

To simplify the notation, let $x = x'_1$, $k_4 = k_4^-$ and $k_5 = k_5^+$. Then $y'_1 = k_1(x - x_0)$ and we can write

$$\mathcal{B}_1(\varepsilon) = \frac{(k_2 - k_1)x + k_1 x_0}{k_4 x + \left(\frac{1}{2} - \varepsilon\right)(k_2 - k_4)} \quad (\text{A.8})$$

Let $\varphi = 2(1 + 2\varepsilon)(5 + 2\varepsilon)$. Then $\varphi k_1 = 24\varepsilon^2 + 32\varepsilon + 2$, $\varphi k_1 x_0 = -8\varepsilon^3 - 4\varepsilon^2 + 2\varepsilon + 1$, and $\varepsilon k_2 = 8\varepsilon(2\varepsilon + 5)$ so that multiplying (A.8) by φ/φ yields

$$\begin{aligned} \mathcal{B}_1(\varepsilon) &= \frac{(8\varepsilon(2\varepsilon + 5) - (24\varepsilon^2 + 32\varepsilon + 2))x - 8\varepsilon^3 - 4\varepsilon^2 + 2\varepsilon + 1}{k_4 \varphi x + \left(\frac{1}{2} - \varepsilon\right)(8\varepsilon(2\varepsilon + 5) - k_4 \varphi)} \\ &= \frac{(-8\varepsilon^2 + 8\varepsilon - 2)x + (1 - 2\varepsilon)(2\varepsilon + 1)^2}{k_4 \varphi x + (1 - 2\varepsilon)(2\varepsilon + 5)(4\varepsilon - k_4(2\varepsilon + 1))} \\ &= \frac{-2(1 - 2\varepsilon)^2 x + (1 - 2\varepsilon)(2\varepsilon + 1)^2}{k_4 \varphi x + (1 - 2\varepsilon)(2\varepsilon + 5)(4\varepsilon - k_4(2\varepsilon + 1))} \\ &= \frac{-2(1 - 2\varepsilon)x + (2\varepsilon + 1)^2}{\frac{k_4 \varphi x}{1 - 2\varepsilon} + (2\varepsilon + 5)(4\varepsilon - k_4(2\varepsilon + 1))}. \end{aligned}$$

Now by

$$\begin{aligned} x &= \frac{k_5(\varepsilon - \frac{1}{2}) + k_1 x_0}{k_1 - k_5} \\ &= \frac{-k_5(2\varepsilon + 5)(1 - 2\varepsilon) + (1 - 2\varepsilon)(1 + 2\varepsilon)}{2(2\varepsilon + 5)(k_1 - k_5)}, \end{aligned}$$

[†]Also noting that the numerator and denominator are both positive.

we have that

$$\frac{k_4 \varphi x}{1-2\varepsilon} = k_4(2\varepsilon+1) \frac{-k_5(2\varepsilon+5)+1+2\varepsilon}{k_1-k_5} \quad (\text{A.9})$$

and

$$-2(1-2\varepsilon)x = \frac{k_5(1-2\varepsilon)^2}{k_1-k_5} - \frac{(1-2\varepsilon)^2(1+2\varepsilon)}{(2\varepsilon+5)(k_1-k_5)} \quad (\text{A.10})$$

so that

$$\mathcal{B}_1(\varepsilon) = \frac{k_5(2\varepsilon-1)^2(2\varepsilon+5) - (1-2\varepsilon)^2(1+2\varepsilon) + (2\varepsilon+1)^2(2\varepsilon+5)(k_1-k_5)}{k_4(2\varepsilon+1)(2\varepsilon+5)(-k_5(2\varepsilon+5)+1+2\varepsilon) + (2\varepsilon+5)^2(k_1-k_5)(4\varepsilon-k_4(2\varepsilon+1))},$$

where we have substituted in (A.9), (A.10) and multiplied top and bottom by $(2\varepsilon+5)(k_1-k_5)$. Write its numerator and denominator as $N(\varepsilon)$ and $D(\varepsilon)$. Expanding the k_1 term,

$$\begin{aligned} N(\varepsilon) &= k_5(2\varepsilon+5) \left((2\varepsilon-1)^2 - (2\varepsilon+1)^2 \right) + (2\varepsilon+1)(12\varepsilon^2+16\varepsilon+1 - (1-2\varepsilon)^2) \\ &= -8\varepsilon k_5(2\varepsilon+5) + (2\varepsilon+1)(8\varepsilon^2+20\varepsilon) \\ &= (2\varepsilon+5)(4\varepsilon(2\varepsilon+1) - 8\varepsilon k_5(2\varepsilon+5)) \end{aligned}$$

and

$$\begin{aligned} D(\varepsilon) &= k_4(2\varepsilon+1)(2\varepsilon+5) \left(-k_5(2\varepsilon+5)+1+2\varepsilon \right) - k_5(2\varepsilon+5)^2(4\varepsilon-k_4(2\varepsilon+1)) \\ &\quad + \frac{12\varepsilon^2+16\varepsilon+1}{2\varepsilon+1} (2\varepsilon+5)(4\varepsilon-k_4(2\varepsilon+1)) \\ &= (2\varepsilon+5) \left(k_4 \left[(2\varepsilon+1)(-k_5(2\varepsilon+5)+1+2\varepsilon) + k_5(2\varepsilon+5)(2\varepsilon+1) - (12\varepsilon^2+16\varepsilon+1) \right] \right. \\ &\quad \left. - 4\varepsilon k_5(2\varepsilon+5) + \frac{4\varepsilon}{2\varepsilon+1}(12\varepsilon+16\varepsilon+1) \right). \end{aligned}$$

Noting that the $k_4 k_5$ terms cancel and $(1+2\varepsilon)^2 - (12\varepsilon^2+16\varepsilon+1) = -4\varepsilon(2\varepsilon+3)$,

$$\mathcal{B}_1(\varepsilon) = \frac{4\varepsilon(2\varepsilon+1) - 8\varepsilon k_5}{-4\varepsilon k_4(2\varepsilon+3) - 4\varepsilon k_5(2\varepsilon+5) + \frac{4\varepsilon}{2\varepsilon+1}(12\varepsilon^2+16\varepsilon+1)}.$$

Multiplying top and bottom by $\frac{2\varepsilon+1}{4\varepsilon}$ establishes (A.7).

A.3 $\mathcal{B}_1(\varepsilon)\mathcal{B}_2(\varepsilon)$ is monotone increasing

Starting with the bound on $K_4(\varepsilon)$,

$$\begin{aligned} \mathcal{B}_2(\varepsilon) &= \frac{3+46\varepsilon+52\varepsilon^2+8\varepsilon^3}{1+2\varepsilon-4\varepsilon^2-8\varepsilon^3} - \frac{12\varepsilon+14}{1-4\varepsilon^2} L(\varepsilon) \\ &= \frac{3+46\varepsilon+52\varepsilon^2+8\varepsilon^3}{(1-2\varepsilon)(1+2\varepsilon)^2} - \frac{12\varepsilon+14}{(1-2\varepsilon)(1+2\varepsilon)} L(\varepsilon) \\ &= \frac{3+46\varepsilon+52\varepsilon^2+8\varepsilon^3 - (1+2\varepsilon)(12\varepsilon+14)L(\varepsilon)}{(1-2\varepsilon)(1+2\varepsilon)^2}. \end{aligned}$$

Combining with our expanded expression for $\mathcal{B}_1(\varepsilon)$,

$$\mathcal{B}_1(\varepsilon)\mathcal{B}_2(\varepsilon) = \frac{(2\varepsilon+1-2k_5^+)(3+46\varepsilon+52\varepsilon^2+8\varepsilon^3 - (1+2\varepsilon)(12\varepsilon+14)L(\varepsilon))}{(1-2\varepsilon)(1+2\varepsilon)^2(-k_4^-(2\varepsilon+3) - k_5^+(2\varepsilon+5)) + (1-2\varepsilon)(1+2\varepsilon)(12\varepsilon^2+16\varepsilon+1)}$$

where we have divided through by $(1+2\varepsilon)/(1+2\varepsilon)$. Write its numerator and denominator as $P(\varepsilon)$ and $Q(\varepsilon)$, then $\mathcal{B}_1(\varepsilon)\mathcal{B}_2(\varepsilon)$ is monotone increasing if $P'Q - PQ' > 0$. Note that as a linear

function, $L'(\varepsilon) = k_6 \approx -1.85175$ is constant. The factors derived from P are then

$$\begin{aligned} P(\varepsilon) &= (2\varepsilon + 1 - 2k_5^+)(3 + 46\varepsilon + 52\varepsilon^2 + 8\varepsilon^3 - (24\varepsilon^2 + 40\varepsilon + 14)L(\varepsilon)), \\ P'(\varepsilon) &= 6 + 92\varepsilon + 104\varepsilon^2 + 16\varepsilon^3 - (48\varepsilon^2 + 80\varepsilon + 28)L(\varepsilon) \\ &\quad + (2\varepsilon + 1 - 2k_5^+)(46 + 104\varepsilon + 24\varepsilon^2 - (48\varepsilon + 40)L(\varepsilon) - k_6(24\varepsilon^2 + 40\varepsilon + 14)) \end{aligned}$$

which, since $(2\varepsilon + 1 - 2k_5^+) > 0$, $L(\varepsilon) < 0$, and $k_6 < 0$, are both positive for $\varepsilon > 0$. Hence over the parameter range $\varepsilon_0 < \varepsilon \leq \varepsilon_2$, P is maximal at ε_2 . Differentiating again, one can verify that $P'' > 0$, so that P' is bounded below by $P'(\varepsilon_0)$. Now for the factors derived from the denominator,

$$\begin{aligned} Q(\varepsilon) &= (8\varepsilon^3 + 4\varepsilon^2 - 2\varepsilon_1)(k_4^-(2\varepsilon + 3) + k_5^+(2\varepsilon + 5)) + (1 - 4\varepsilon^2)(12\varepsilon^2 + 16\varepsilon + 1), \\ Q'(\varepsilon) &= (24\varepsilon^2 + 8\varepsilon - 2)(k_4^-(2\varepsilon + 3) + k_5^+(2\varepsilon + 5)) + (8\varepsilon^3 + 4\varepsilon^2 - 2\varepsilon_1)(2k_4^- + 2k_5^+) \\ &\quad - 8\varepsilon(12\varepsilon^2 + 16\varepsilon + 1) + (1 - 4\varepsilon^2)(24\varepsilon + 16) \end{aligned}$$

which, since $8\varepsilon^3 + 4\varepsilon^2 - 2\varepsilon_1 < 0$ and $-8\varepsilon(12\varepsilon^2 + 16\varepsilon + 1) + (1 - 4\varepsilon^2)(24\varepsilon + 16) = 16 + 16\varepsilon + \dots > 0$ over the parameter range, are also both positive. Hence Q bounded below by $Q(\varepsilon_0)$. Again, one can verify that $Q'' < 0$ so that Q' is bounded above by $Q'(\varepsilon_0)$.

Hence $P'Q - PQ' > P'(\varepsilon_0)Q(\varepsilon_0) - P(\varepsilon_2)Q'(\varepsilon_0) \approx 29.853$, positive as required.

Appendix B

Mapping behaviour of a non-monotonic LTM

Lemma B.1. *For any line segment Γ which satisfies case (A1.2) and traverses A_1^k or A_3^k for some $3 \leq k \leq 6$, the image $H_S^2(\Gamma)$ contains a v -segment.*

Proof. Let Γ traverse A_1^k , intersecting the boundaries of A_1^k given in (†) at the points $z_k = (x_k, y_k)$ and $z_{k-1} = (x_{k-1}, y_{k-1})$. Calculating intersections with the lines $y = (1-x)/4$ and $x = 0$ gives

$$\frac{2k-5}{8k-16} < y_{k-1} < \frac{2k-3}{8k-8},$$

which together with $3 \leq k \leq 6$ gives

$$\frac{1}{8} < y_{k-1} < \frac{9}{40}. \quad (\text{B.1})$$

Letting $\Gamma^k = \Gamma \cap A_1^k$, we have that $F^k(z_k) = (1/2, y_k)$ and $F^{k-1}(z_{k-1}) = (1/2, y_{k-1})$ so that $F_S(\Gamma^k) = F^k(\Gamma^k)$ is a line segment joining $(1/2, y_k)$ to $F(1/2, y_{k-1}) = (1/2 + 4y_{k-1}, y_{k-1}) \bmod 1$. By (B.1) we have that $1 < 1/2 + 4y_{k-1} < 7/5$ so that $F_S(\Gamma^k)$ passes through $(1/2, y_k)$ and some point $(2/5, y)$ with $y_{k-1} < y < y_k$. This first point is invariant under G and the latter maps into $G(2/5, y) = (2/5, y + 2 - 8/5) = (2/5, y + 2/5)$. By (B.1) we have $y + 2/5 > y_{k-1} + 2/5 > 1/2$ so that $(G \circ F_S)(\Gamma)$ contains a line segment passing through $(1/2, y_k)$ and $(x, 1/2)$ for some $2/5 < x < 1/2$. This line segment lies in S and must traverse A_4^2 by $y_k < 1/4$, so that $H_S(\Gamma) = (G_S \circ F_S)(\Gamma)$ contains a segment traversing A_4^2 . It follows from a previous argument that $H_S^2(\Gamma)$ contains a v -segment.

For Γ traversing A_3^k , by the symmetry of F_S in the line $y = 1/4$ and the argument above we have that $F_S(\Gamma)$ contains a line segment connecting the points $(1/2, 1/2 - y_k)$ and $(4/5, y')$ for some $1/2 - y_k < y' < 1/2 - y_{k-1}$. Again, it follows that $(G \circ F_S)(\Gamma)$ traverses A_4^2 and the result follows. □

Appendix C

Two-step expansion calculations from section 6.3.4

C.1 Calculations for Proposition 6.3

We begin by showing the bounds (6.11). Note that $U_{\star,j}$ is a curve traversing $A_{4,3}^j$ near $(1/4, 1)$ with tangent vectors $(v_1, v_2)^T$ in the cone $M_1\mathcal{C}_1$ satisfying $41/17 \leq |v_2|/|v_1| \leq 17/7$. Noting that the geometry of $A_{4,3}^j$ near $(1/4, 1)$ is a 180° rotation of $A_{4,3}^j$ near $(1/4, 1/2)$ and the cone is invariant under this rotation, we can follow an analogous argument to (6.14) to calculate a_\star . In particular $|U_{\star,j}|$ is bounded below by the length of the segment passing through r_4 with gradient $17/7$, which gives $a_\star = 13\sqrt{2}/80$ as required. For the upper bound, the height of $|U_{\star,j}|$ is bounded above by the height of the line segment with endpoints on $r_3(j)$ and \mathcal{L}_{j-1} with gradient $41/17$. In particular

$$\ell_v(U_{\star,j}) \leq \frac{48j^2 + 41j + 29}{(2j+1)(48j+17)} - \frac{1}{2} = \frac{41}{2(96j^2 + 82j + 17)} \sim \frac{41}{192j^2}$$

so that, by Lemma 6.5 and $|v_2/v_1| \geq 41/17$, $|U_{\star,j}| \geq b_\star/j^2$ with $b_\star = \frac{41}{192}\sqrt{1 + 17^2/41^2}$ as required.

We move onto calculating b such that $|U_{k,l}| \lesssim b/l^2$. Define a (k, l) -cell as the intersection $H_\sigma(A_{4,3}^k) \cap A_{1,3}^l$ near the accumulation point $(1/2, 3/4)$, shown as the magnified region in Figure 6.5(b), the quadrilateral bounded by the lines $\mathcal{L}_l, \mathcal{L}_{l-1}$ (as defined in equation 6.6) on $\partial A_{1,3}^l$ and $\mathcal{L}_k, \mathcal{L}_{k-1}$ on $\partial H_\sigma(A_{4,3}^k)$. The explicit equation for \mathcal{L}_k is given in (6.7), letting us calculate the corner coordinates $p_{k,l} \in \mathcal{L}_k \cap \mathcal{L}_l$ as

$$p_{k,l} = (x_{k,l}, y_{k,l}) = \left(\frac{16kl + 7k + 23l + 10}{32kl + 12k + 44l + 16}, \frac{12kl + 3k + 17l + 4}{16kl + 6k + 22l + 8} \right). \quad (\text{C.1})$$

The curve $U_{k,l}$ traverses the (k, l) -cell with endpoints on the segments $p_{k,l}p_{k-1,l}$ and $p_{k,l-1}p_{k-1,l-1}$ and has tangent vectors in the cone $M_4M_3^k\mathcal{C}_1$. Roughly speaking, for large k the vectors in this cone are essentially parallel to the cell boundaries $\mathcal{L}_k, \mathcal{L}_{k-1}$ with gradient approaching -3 , so that $\ell_v(U_{k,l})$ is given to leading order by $y_{k,l} - y_{k,l-1} \sim \frac{3}{32}l^{-2}$. Noting that $M_4M_3^k\mathcal{C}_1 \subset \mathcal{C}_4$ for any k , we can bound the gradient of vectors as $|v_2/v_1| \geq 7/3$ so that by Lemma 6.5 we have $|U_{k,l}| \lesssim b/l^2$ with $b = \frac{3}{32}\sqrt{1 + \frac{9}{49}}$. A more careful calculation similar to that of b_\star above gives the same bound to leading order.

C.2 Two-step expansion near P_1

We will follow similar analysis to the proof of Proposition 6.3 to show:

Proposition C.1. *Condition (6.3) holds for H_σ^2 when $W \cap B_\varepsilon(P_1) \neq \emptyset$ for all $\varepsilon > 0$.*

Proof. We consider the case where W lies near the accumulation point $(0, 1/4)$, split by \mathcal{S} into subcurves $\overline{W}_\star = W \cap A_1$ and $\overline{W}_k = W \cap A_{4,2}^k$. The image of the lower subcurve $\overline{U}_\star = H_\sigma(\overline{W}_\star)$ lies near the accumulation point $(1/2, 1/4) = H(0, 1/4)$ and is split by \mathcal{S} into curves $\overline{U}_{\star,j} \subset A_{4,2}^j$. The image of each upper subcurve $\overline{U}_k = \overline{W}_k$ maps close to $(3/4, 1/2)$ for k odd, $(3/4, 0)$ for k even. Analysis for both of these cases is analogous, as before we take k to be odd and consider the geometry of \mathcal{S} near the accumulation point $(3/4, 1/2)$. We calculate the corners of $A_{4,2}^k$ near $(0, 1/4)$ as

$$\bar{r}_1 = \left(0, \frac{k}{4k-2}\right), \quad \bar{r}_2 = \left(\frac{1}{4k-6}, \frac{k-2}{4k-6}\right), \quad \bar{r}_3 = \left(\frac{1}{4k-2}, \frac{k-1}{4k-2}\right), \quad \bar{r}_4 = \left(0, \frac{k+1}{4k+2}\right).$$

so that, using the integer valued matrix $M_4 M_2^k = (-1)^k \begin{pmatrix} 1-6k & -6k-2 \\ 14k-2 & 14k+5 \end{pmatrix}$, its image $H_\sigma(A_{4,2}^k)$ is the quadrilateral with corners

$$\begin{aligned} \bar{r}'_1 &= \left(\frac{3k+1}{4k-2}, \frac{2k-7}{4k-1}\right), & \bar{r}'_2 &= \left(\frac{3k-2}{4k-6}, \frac{2k-9}{4k-6}\right), \\ \bar{r}'_3 &= \left(\frac{3k-2}{4k-2}, \frac{k}{2k-1}\right), & \bar{r}'_4 &= \left(\frac{3k+1}{4k+2}, \frac{k+1}{2k+1}\right). \end{aligned}$$

The curve \overline{U}_k has endpoints on the segments $\bar{r}'_1 \bar{r}'_2$ and $\bar{r}'_3 \bar{r}'_4$ and is split by \mathcal{S} into an upper portion $\overline{U}_{k,\star}$ in A_4 above $y = 1/2$ and subcurves $\overline{U}_{k,l} \subset A_{1,2}^l$ where $l_0 \leq l \leq l_1$. Comparison of the point \bar{r}'_2 with the lines $\bar{\mathcal{L}}_l : y - 1/4 = -\frac{2l+1}{2l+2}(x-1)$ and $\bar{\mathcal{L}}_{l-1}$ on $\partial A_{1,2}^l$ yields $l_0(k) \geq \lfloor \frac{k-4}{7} \rfloor$, intersecting $\bar{r}'_1 \bar{r}'_4$ with $y = 1/2$ yields $l_1(k) \leq 7k+2$. Let $W_i = H_\sigma^{-1}(\overline{U}_i)$ then W splits in an analogous fashion to (6.9) with DH_σ^2 constant on each component. It follows that for $q = 1/2$,

$$\liminf_{\delta \rightarrow 0} \sup_{W: |W| < \delta} \sum_i \left(\frac{|W|}{|V_i|} \right)^q \frac{|W_i|}{|W|} \leq \sup_{0 \leq p \leq 1} \left(2\sqrt{\frac{(1-p)\bar{b}_\star \Lambda_1^+}{\bar{c}_\star \bar{a}_\star \Lambda_1^-}} + 2\sqrt{\frac{p\bar{b}_\diamond}{\bar{c}_\diamond \bar{a}_\diamond \bar{\gamma}}} + 4\sqrt{\frac{p\bar{b}h}{\bar{c}a\bar{\gamma}}} \right)$$

where the new constants satisfy (letting $K(M)$ denote the minimum expansion of M over \mathcal{C}_1)

- $K(M_4 M_2^j M_1) \sim \bar{c}_\star j$
- $K(M_4^2 M_2^k) \sim \bar{c}_\diamond k$
- $K(M_1 M_2^l M_4 M_2^k) \sim \bar{c}kl$
- $K(M_4 M_2^k) \sim \bar{\gamma}k$
- $\bar{a}_\star/j^2 \lesssim |\overline{U}_{\star,j}| \leq \bar{b}_\star/j^2$
- $|\overline{U}_{k,\star}| \lesssim \bar{b}_\diamond/k$
- $|\overline{W}_k| \gtrsim \bar{a}/k^2$
- $|\overline{U}_{k,l}| \lesssim \bar{b}/l^2$

and Λ_1^\pm , h are unchanged from (6.15). The expansion factors can be calculated in the same fashion as (6.10), in particular

$$\bar{c}_\star = \frac{48\sqrt{145}}{5}, \quad \bar{c}_\diamond = 8\sqrt{197}, \quad \bar{c} = 64, \quad \bar{\gamma} = \frac{8\sqrt{145}}{5}.$$

The constant \bar{a}_\star is obtained by considering the shortest path across $A_{4,2}^j$ with tangent vectors aligned in the cone $M_1 \mathcal{C}_1$, bounded by the length of the segment with endpoints on $r_4(j)$ and

\mathcal{L}_{j-1} (as defined in (†), proof of Lemma 5.9) with gradient 41/17. The constant \bar{b}_* is obtained by considering the maximum height of a segment joining \mathcal{L}_{j-1} to \mathcal{L}_j , given by the segment passing through $r_3(j) \in \mathcal{L}_j$ with gradient 17/17, and applying Lemma 6.5. In particular $\bar{a}_* = \sqrt{1970}/464$ and $\bar{b}_* = \frac{17}{192} \sqrt{1 + \frac{17^2}{41^2}}$. Similar analysis to the calculation of \bar{a}_* but using the wider cone \mathcal{C}_1 yields $\bar{a} = \sqrt{55}/80$. We again apply Lemma 6.5 to find \bar{b}_\diamond , with $\ell_v(\bar{U}_{k,*})$ bounded above by the height $1/(4k-2) \sim 1/(4k)$ of $r'_3(k)$ above $y = 1/2$. Tangent vectors of $\bar{U}_{k,*}$ lie in the cone $M_4 M_2^k \mathcal{C}_1 \subset \mathcal{C}_4$ so that $\bar{b}_\diamond = \frac{1}{4} \sqrt{1 + 9/49}$ provides the upper bound. Finally we calculate \bar{b} , following a similar approach to section C.1. For each k the segments $\bar{r}'_1 \bar{r}'_4$ and $\bar{r}'_2 \bar{r}'_3$ lie on the lines $\bar{\mathcal{L}}_k$ and $\bar{\mathcal{L}}_{k-1}$ respectively, with

$$\bar{\mathcal{L}}_k : y - \frac{k+1}{2k+1} = -\frac{14k+5}{6k+2} \left(x - \frac{3k+1}{4k+2} \right).$$

Define a (k, l) cell as the intersection of $H_\sigma(A_{4,2}^k) \cap A_{1,2}^l$, given the by quadrilateral bounded by the lines $\bar{\mathcal{L}}_k, \bar{\mathcal{L}}_{k-1}, \bar{\mathcal{L}}_l, \bar{\mathcal{L}}_{l-1}$. Its corners $\bar{p}_{k,l}, \dots, \bar{p}_{k-1,l-1}$ are given by

$$\bar{p}_{k,l} = \left(\frac{(3k+1)(2l+3)}{8kl+11k+3l+4}, \frac{16kl+15k+7l+6}{4(8kl+11k+3l+4)} \right)$$

with (as before, to leading order terms for k large) $\ell_v(\bar{U}_{k,l})$ bounded above by the height of the segment $\ell_v(\bar{p}_{k-1,l} \bar{p}_{k-1,l-1}) \sim 7/32l^{-2}$. Again, tangent vectors to $\bar{U}_{k,l}$ lie in \mathcal{C}_4 so that $\bar{b} = \frac{7}{32} \sqrt{1 + 9/49}$ gives an upper bound $|\bar{U}_{k,l}| \lesssim \bar{b}/l^2$ by Lemma 6.5.

As before we take

$$\bar{s} = 2\sqrt{\frac{\bar{b}_* \Lambda_1^+}{\bar{c}_* \bar{a}_* \Lambda_1^-}} \approx 0.186, \quad \bar{t} = 2\sqrt{\frac{\bar{b}_\diamond}{\bar{c}_\diamond \bar{a} \gamma}} + 4\sqrt{\frac{\bar{b} h}{\bar{c} \bar{a} \gamma}} \approx 0.488,$$

giving

$$\liminf_{\delta \rightarrow 0} \sup_{W: |W| < \delta} \sum_i \left(\frac{|W|}{|V_i|} \right)^q \frac{|W_i|}{|W|} \leq \bar{s} \sqrt{\frac{\bar{s}^2}{\bar{s}^2 + \bar{t}^2}} + \bar{t} \sqrt{\frac{\bar{t}^2}{\bar{s}^2 + \bar{t}^2}} \approx 0.522 < 1$$

as required. □

Bibliography

- Alekseev, V. M. (1969). Quasirandom Dynamical Systems. *Mathematics of the USSR-Sbornik*, 7(1):1.
- Aref, H. (1984). Stirring by chaotic advection. *Journal of Fluid Mechanics*, 143:1–21.
- Aref, H., Blake, J. R., Budišić, M., Cardoso, S. S., Cartwright, J. H., Clercx, H. J., El Omari, K., Feudel, U., Golestanian, R., Gouillart, E., van Heijst, G. F., Krasnopolskaya, T. S., Le Guer, Y., MacKay, R. S., Meleshko, V. V., Metcalfe, G., Mezić, I., de Moura, A. P., Piro, O., Speetjens, M. F., Sturman, R., Thiffeault, J.-L., and Tuval, I. (2017). Frontiers of chaotic advection. *Reviews of Modern Physics*, 89(2):025007.
- Arnol'd, V. I. and Avez, A. (1968). *Ergodic Problems of Classical Mechanics*. Benjamin.
- Baladi, V. (2001). Decay of correlations. In *Smooth ergodic theory and its applications*, number 69 in Proceedings of symposia in pure mathematics. American Mathematical Society.
- Barreira, L. and Pesin, Y. B. (2002). *Lyapunov Exponents and Smooth Ergodic Theory*. American Mathematical Soc.
- Beigie, D., Leonard, A., and Wiggins, S. (1994). Invariant manifold templates for chaotic advection. *Chaos, Solitons & Fractals*, 4(6):749–868.
- Bowen, R. (1975). *Equilibrium states and the ergodic theory of Anosov diffeomorphisms*. Lecture notes in mathematics. Springer-Verlag.
- Boyland, P. (1994). Topological methods in surface dynamics. *Topology and its Applications*, 58(3):223–298.
- Brin, M. and Stuck, G. (2002). *Introduction to Dynamical Systems*. Cambridge University Press, Cambridge.
- Bullett, S. (1986). Invariant circles for the piecewise linear standard map. *Communications in Mathematical Physics*, 107(2):241–262.
- Bunimovich, L. A. (1974). On ergodic properties of certain billiards. *Functional Analysis and Its Applications*, 8(3):254–255.
- Bunimovich, L. A., Sinai, Y. G., and Chernov, N. I. (1991). Statistical properties of two-dimensional hyperbolic billiards. *Russian Mathematical Surveys*, 46(4):47.
- Burton, R. and Easton, R. W. (1980). Ergodicity of linked twist maps. In Nitecki, Z. and Robinson, C., editors, *Global Theory of Dynamical Systems*, Lecture Notes in Mathematics, pages 35–49, Berlin, Heidelberg. Springer.
- Cerbelli, S. and Giona, M. (2005). A Continuous Archetype of Nonuniform Chaos in Area-Preserving Dynamical Systems. *Journal of Nonlinear Science*, 15(6):387–421.

- Cerbelli, S. and Giona, M. (2008). Characterization of nonuniform chaos in area-preserving nonlinear maps through a continuous archetype. *Chaos, Solitons & Fractals*, 35(1):13–37.
- Cheng, L.-T., Rajasekaran, F., Wong, K. Y. J., and Zlatos, A. (2021). Numerical Evidence of Exponential Mixing by Alternating Shear Flows. arXiv:2111.00093 [nlin].
- Chernov, N. (1999). Decay of Correlations and Dispersing Billiards. *Journal of Statistical Physics*, 94(3):513–556.
- Chernov, N. and Markarian, R. (2006). *Chaotic Billiards*, volume 127 of *Mathematical Surveys and Monographs*. American Mathematical Society.
- Chernov, N. and Young, L. S. (2000). Decay of Correlations for Lorentz Gases and Hard Balls. In Szász, D., editor, *Hard Ball Systems and the Lorentz Gas*, Encyclopaedia of Mathematical Sciences, pages 89–120. Springer, Berlin, Heidelberg.
- Chernov, N. and Zhang, H.-K. (2005). Billiards with polynomial mixing rates. *Nonlinearity*, 18:1527.
- Chernov, N. and Zhang, H.-K. (2008). Improved Estimates for Correlations in Billiards. *Communications in Mathematical Physics*, 277:305–321.
- Chernov, N. and Zhang, H.-K. (2009). On Statistical Properties of Hyperbolic Systems with Singularities. *Journal of Statistical Physics*, 136(4):615–642.
- Chernov, N. I. and Haskell, C. (1996). Nonuniformly hyperbolic K-systems are Bernoulli. *Ergodic Theory and Dynamical Systems*, 16(1):19–44.
- Chirikov, B. V. (1971). Research concerning the theory of non-linear resonance and stochasticity. Technical Report CERN-Trans-71-40, CM-P00100691.
- Coudène, Y. (2016). The Hopf Argument. In Coudène, Y., editor, *Ergodic Theory and Dynamical Systems*, Universitext, pages 35–46. Springer, London.
- D’Alessandro, D., Dahleh, M., and Mezic, I. (1999). Control of mixing in fluid flow: a maximum entropy approach. *IEEE Transactions on Automatic Control*, 44(10):1852–1863.
- Demers, M. F. and Wojtkowski, M. P. (2009). A family of pseudo-Anosov maps. *Nonlinearity*, 22(7):1743–1760.
- Demers, M. F. and Zhang, H.-K. (2014). Spectral analysis of hyperbolic systems with singularities. *Nonlinearity*, 27(3):379–433.
- Franjone, J. G., Leong, C., and Ottino, J. M. (1989). Symmetries within chaos: A route to effective mixing. *Physics of Fluids A: Fluid Dynamics*, 1(11):1772–1783.
- Franjone, J. G. and Ottino, J. M. (1992). Symmetry concepts for the geometric analysis of mixing flows. *Philosophical Transactions of the Royal Society of London. Series A: Physical and Engineering Sciences*, 338(1650):301–323.
- Galaktionov, O. S., Anderson, P. D., Peters, G. W. M., and Meijer, H. E. H. (2003). Analysis and Optimization of Kenics Static Mixers. *International Polymer Processing*, 18(2):138–150.
- Gidea, M., Meiss, J. D., Ugarcovici, I., and Weiss, H. (2011). Applications of KAM theory to population dynamics. *Journal of Biological Dynamics*, 5(1):44–63.
- Giona, M. and Adrover, A. (1998). Nonuniform Stationary Measure of the Invariant Unstable Foliation in Hamiltonian and Fluid Mixing Systems. *Physical Review Letters*, 81(18):3864–3867.

- Giorgilli, A. and Lazutkin, V. F. (2000). Some remarks on the problem of ergodicity of the Standard Map. *Physics Letters A*, 272(5):359–367.
- Gouillart, E., Dauchot, O., Dubrulle, B., Roux, S., and Thiffeault, J.-L. (2008). Slow decay of concentration variance due to no-slip walls in chaotic mixing. *Physical Review E*, 78(2):026211.
- Gouillart, E., Kuncio, N., Dauchot, O., Dubrulle, B., Roux, S., and Thiffeault, J.-L. (2007). Walls Inhibit Chaotic Mixing. *Physical Review Letters*, 99(11):114501.
- Halmos, P. R. (1976). *Measure Theory*. Springer New York.
- Hertzsch, J.-M., Sturman, R., and Wiggins, S. (2007). DNA Microarrays: Design Principles for Maximizing Ergodic, Chaotic Mixing. *Small*, 3(2):202–218.
- Hopf, E. (1939). *Statistik der geodätischen Linien in Mannigfaltigkeiten negativer Krümmung*. Ber. Verh. Akad. Wiss. Leipzig, 91 edition.
- Hopf, E. (1940). Statistik der Lösungen geodätischer Probleme vom unstabilen Typus. II. *Mathematische Annalen*, 117(1):590–608.
- Hu, H. (2001). Statistical properties of some almost hyperbolic systems. In *Smooth ergodic theory and its applications*, number 69 in Proceedings of symposia in pure mathematics. American Mathematical Society.
- Katok, A. (1979). Bernoulli Diffeomorphisms on Surfaces. *Annals of Mathematics*, 110(3):529–547.
- Katok, A. and Strelcyn, J.-M. (1986). *Invariant Manifolds, Entropy and Billiards. Smooth Maps with Singularities*. Lecture Notes in Mathematics. Springer-Verlag, Berlin Heidelberg.
- Khakhar, D. V., Franjione, J. G., and Ottino, J. M. (1987). A case study of chaotic mixing in deterministic flows: The partitioned-pipe mixer. *Chemical Engineering Science*, 42(12):2909–2926.
- Kreczak, H. E. (2019). *Rates of mixing in models of fluid devices with discontinuities*. PhD thesis, University of Leeds.
- Liu, M., Muzzio, F. J., and Peskin, R. L. (1994). Quantification of mixing in aperiodic chaotic flows. *Chaos, Solitons & Fractals*, 4(6):869–893.
- Liverani, C. (2004). Birth of an elliptic island in a chaotic sea. *Mathematical Physics Electronic Journal*, 10.
- Liverani, C. and Wojtkowski, M. P. (1995). Ergodicity in Hamiltonian Systems. In Jones, C. K. R. T., Kirchgraber, U., and Walther, H. O., editors, *Dynamics Reported: Expositions in Dynamical Systems*, Dynamics Reported, pages 130–202. Springer, Berlin, Heidelberg.
- MacKay, R. (2006). Cerbelli and Giona’s Map Is Pseudo-Anosov and Nine Consequences. *Journal of Nonlinear Science*, 16(4):415–434.
- Markarian, R. (2004). Billiards with polynomial decay of correlations. *Ergodic Theory and Dynamical Systems*, 24(1):177–197.
- Mezić, I., Wiggins, S., and Betz, D. (1999). Residence-time distributions for chaotic flows in pipes. *Chaos: An Interdisciplinary Journal of Nonlinear Science*, 9(1):173–182.
- Myers Hill, J., Sturman, R., and Wilson, M. C. T. (2022a). Exponential mixing by orthogonal non-monotonic shears. *Physica D: Nonlinear Phenomena*, 434:133224.

- Myers Hill, J., Sturman, R., and Wilson, M. C. T. (2022b). A Family of Non-Monotonic Toral Mixing Maps. *Journal of Nonlinear Science*, 32(3):31.
- Oseledets, V. I. (1968). A multiplicative ergodic theorem. Lyapunov characteristic numbers for dynamical systems. *Transactions of the Moscow Mathematical Society*, 19:197–231.
- Ottino, J. (1989a). The mixing of fluids. *Scientific American*, 260:56–67.
- Ottino, J. M. (1989b). *The Kinematics of Mixing: Stretching, Chaos, and Transport*. Cambridge University Press.
- Pesin, Y. B. (1977). Characteristic Lyapunov Exponents and Smooth Ergodic Theory. *Russian Mathematical Surveys*, 32(4):55.
- Petersen, K. E. (1983). *Ergodic Theory*. Cambridge Studies in Advanced Mathematics. Cambridge University Press, Cambridge.
- Przytycki, F. (1983). Ergodicity of toral linked twist mappings. *Annales scientifiques de l'École Normale Supérieure*, 16(3):345–354.
- Robinson, C. (1995). *Dynamical Systems: Stability, Symbolic Dynamics and Chaos*. CRC-Press.
- Ruelle, D. (1978). *Thermodynamic Formalism: The Mathematical Structures of Classical Equilibrium Statistical Mechanics*. Addison-Wesley.
- Springham, J. (2008). *Ergodic properties of linked-twist maps*. PhD thesis, University of Bristol.
- Springham, J. and Sturman, R. (2014). Polynomial decay of correlations in linked-twist maps. *Ergodic Theory and Dynamical Systems*, 34(5):1724–1746.
- Springham, J. and Wiggins, S. (2010). Bernoulli linked-twist maps in the plane. *Dynamical Systems*, 25:483–499.
- Sturman, R. (2012). The Role of Discontinuities in Mixing. In van der Giessen, E. and Aref, H., editors, *Advances in Applied Mechanics*, volume 45, pages 51–90. Elsevier.
- Sturman, R., Ottino, J. M., and Wiggins, S. (2006). *The Mathematical Foundations of Mixing: The Linked Twist Map as a Paradigm in Applications: Micro to Macro, Fluids to Solids*. Cambridge University Press.
- Sturman, R. and Springham, J. (2013). Rate of chaotic mixing and boundary behavior. *Physical review. E, Statistical, nonlinear, and soft matter physics*, 87:012906.
- Thurston, W. P. (1988). On the geometry and dynamics of diffeomorphisms of surfaces. *Bulletin of the American Mathematical Society*, 19(2):417–431.
- Vaianti, S. (1992). Ergodic properties of the discontinuous sawtooth map. *Journal of Statistical Physics*, 67(1):251–269.
- Viana, M. (2014). *Lectures on Lyapunov Exponents*. Cambridge Studies in Advanced Mathematics. Cambridge University Press, Cambridge.
- Wang, F., Zhang, H.-K., and Zhang, P. (2021). Decay of correlations for unbounded observables. *Nonlinearity*, 34(4):2402–2429.
- Wilkinson, A. (2009). Smooth Ergodic Theory. In Meyers, R. A., editor, *Encyclopedia of Complexity and Systems Science*, pages 8168–8183. Springer, New York, NY.

- Wojtkowski, M. (1980). Linked Twist Mappings Have the K-Property. *Annals of the New York Academy of Sciences*, 357(1):65–76.
- Wojtkowski, M. (1981). A model problem with the coexistence of stochastic and integrable behaviour. *Communications in Mathematical Physics*, 80(4):453–464.
- Wojtkowski, M. (1982). On the ergodic properties of piecewise linear perturbations of the twist map. *Ergodic Theory and Dynamical Systems*, 2(3-4):525–542.
- Wojtkowski, M. (1986). Principles for the design of billiards with nonvanishing Lyapunov exponents. *Communications in Mathematical Physics*, 105(3):391–414.
- Wright, P. J. (2018). *Bounds on Lyapunov exponents in non-Anosov systems*. PhD thesis, University of Leeds.
- Young, L.-S. (1998). Statistical Properties of Dynamical Systems with Some Hyperbolicity. *Annals of Mathematics*, 147(3):585–650.
- Young, L.-S. (1999). Recurrence times and rates of mixing. *Israel Journal of Mathematics*, 110(1):153–188.